Antiviral activity of human hepatocytes and its regulation by cellular antioxidant systems

Trinity College Dublin
Coláiste na Tríonóide, Baile Átha Cliath
The University of Dublin

Thesis submitted to the University of Dublin for the degree of

Doctor of Philosophy (Ph.D.)

By

Vasile Mihai Sularea

B.Sc., M.Sc.

School of Biochemistry and Immunology

Trinity College Dublin

2023

Supervisor: Professor Cliona O'Farrelly

This project has received funding from the European Union's Horizon 2020 research and innovation programme under grant agreement No 813343.

Declaration

I declare that this thesis has not been submitted as an exercise for a degree at this or any other university and it is entirely my own work, except where duly acknowledged.

I agree to deposit this thesis in the University's open access institutional repository or allow the Library to do so on my behalf, subject to Irish Copyright Legislation and Trinity College Library conditions of use and acknowledgement.

I consent to the examiner retaining a copy of the thesis beyond the examining period, should they so wish (EU GDPR May 2018).

Vasile Mihai Sularea

General abstract

Although several antiviral strategies have been developed in the last decade, hepatotropic viruses are still a significant public health burden, with more than 300 million people being affected worldwide. Hepatocytes, the primary cells of the liver, are the primary targets of hepatotropic viruses. Moreover, hepatotropic viruses, in particular hepatitis B and C viruses, can persist causing chronic viral hepatitis, where hepatocellular carcinoma is a common outcome.

While research on the liver antiviral response has focused on immune cell involvement, less is known about the intrinsic antiviral activity of hepatocytes, the primary target of hepatotropic viruses. Development of antiviral strategies focusing on hepatocyte antiviral activity might, as shown by clinical trials using type III interferons, increase the efficacy of antiviral therapies. Therefore, studying and characterising the molecular mechanisms behind antiviral activity of hepatocytes can potentially lead to development of new antiviral therapies.

Pathogen detection and activation of innate antiviral activity is required for the clearance of the virus. In this case, evolutionary conserved pathogen-associated molecular patterns (PAMPs) are recognised by germline encoded pattern recognition receptors (PRRs). Virus-derived RNA, which acts as a potent PRR in hepatotropic viral infections, is recognised by different PRRs, such as Toll-Like Receptor 3 (TLR3), Retinoic Acid-inducible Gene I-like receptors (RLRs) and double-stranded RNA-activated protein kinase (PKR). In our study, using human hepatoma cell lines and induced pluripotent stem cell (iPSC)-derived hepatocytes as primary human hepatocyte models, we first aimed to identify the PRRs activated by viral-like RNA. In this case, using double stranded RNA (dsRNA) such as polyinosinic:polycytidylic acid (poly I:C) which mimics viral RNA, we observed that RLRs and PKR, but not TLR3, are the main receptors involved in recognition of immunogenic RNA by hepatocytes.

Immune response-dependent metabolism has been extensively studied in immune cells. Whether cellular metabolism is involved in the innate antiviral response in hepatocytes,

which have demanding metabolic roles when compared to other cell types, is subject of this thesis. In our study, we observed that stimulation with transfected dsRNA decreased mitochondrial respiration and increased reactive oxygen species (ROS) production while inducing an antiviral state. ROS homeostasis, regulated by ROS production and antioxidant enzymes, is crucial for modulating cell signaling and avoiding cell damage during viral infection. However, the molecular mechanisms through which antioxidant enzymes are involved in the innate antiviral response are not fully understood.

Therefore, we went on to explore how cellular antioxidants involved in controlling ROS and oxidative stress might influence the antiviral activity of the hepatocyte. Analysing publicly available datasets, we identified the antioxidant enzyme peroxiredoxin 4 (PRDX4) as a potential regulator of innate antiviral activity in hepatocytes. Decreasing PRDX4 expression resulted in increased IFN-mediated antiviral activity and pro-inflammatory cytokine production following dsRNA stimulation or hepatotropic viral infection in human hepatic models. These results were confirmed in other cell types, suggesting that the mechanism observed is conserved among different cell types. Cytoplasmic dsRNA activates RLRs and the downstream mitochondrial antiviral protein (MAVS), which aggregates and functions as a hub for the activation of transcriptional factors involved in inducing the antiviral state. In this case, we observed that PRDX4 silencing increased MAVS aggregation upon dsRNA stimulation.

Taken together, our results highlight and explore the intimate link between innate antiviral activity and the cellular redox system in hepatocytes. We identified a novel role for PRDX4 in modulating the innate antiviral response. The molecular mechanisms through which PRDX4 deficiency increase innate antiviral activity remain to be defined.

Acknowledgements

Firstly, I would like to thank my supervisor Cliona O'Farrelly. I've never met such an enthusiastic and full of energy person. Thank you for all your scientific and non-scientific inputs. You taught me a lot, as a scientist and as a human being.

I've been really lucky to end up in such a diverse and interesting lab. Mag, thank you for all your help and patience during these years. I will make sure to have always some sweets in the little drawer for you. And Marie, you are among the most supportive person I've ever met. I'm glad we work in the same lab. Sarah, thank you for all your technical knowledge, it was really helpful. I hope you are enjoying your new job. To the new people in the lab, Cian, Evita, Valeria, and Ziyu, thank you for your help. To all the bachelor and master students I've had in the last four years. You guys have taught me more than you think.

Fede and Jamie, I don't really know from where to start… Federica, thank you for your emotional and technical support. It has been a pleasure to work with you, we recreated a Little Italy in 4.11. Just make sure Cliona will not catch you eating bananas again. Jamie, I can't really express the gratitude towards you. You've been way more than a colleague. You've been always helping me, whether writing an abstract for a conference or designing an experiment. I'm always grateful to you, guys.

To the past Sheedy lab members, Emer, Hugo, and Sarah. Emer, I miss your laugh and jokes; Hugo, since you left our lab is not the most handsome in TBSI anymore; and Sarah, I can't believe you won't be here anymore. To the current Sheedy lab members, and especially to Anna, Cian, Hannah, and John. I will better bring some good Italian wine for you, Anna. Cian, you are probably one of the most science enthusiast I've ever met, keep it like that and you will do great. And Hannah, thank for the TMRM, I brought it back, I hope you won't kill me (joking). John, to be honest with you, I envy you a lot, not only for your science but also for your running times.

I'm extremely grateful to be part of such an amazing network as INITIATE has been for the last four years. Firstly, I want to thank my co-supervisors from Trinity, Andrew and Luke. Thank you for all your ideas and inputs, they have been really helpful. A huge thanks to Hauke and Coralie, for being always supportive and down for pints and pizzas. Hauke, I'm looking forward to having a nice barbecue at your place. And Coralie, thank you so much for being in the lab in the weekends, it made my work easier. Thank you for all the reagents I've "borrowed" from you and all the western blot tricks you taught me. You are a great person before being an amazing scientist. But I won't stop trying to convince you to do a post doc.

Thank you to all the PIs from INITIATE outside Ireland. In particular Andreas Bergthaler, Roland Zahn, and John Hiscott. It has been a honour to work in your labs. And to all the INITIATE students. Zsofia, I hope you enjoyed your Dublin secondment more than I did in Vienna, and thanks for your help with the experiments! And Sonia, thank you for hosting me at Janssen. A huge thanks to Xavier, I'm in debt for hosting me in Leiden and for the plasmids. You have a place where to stay in Dublin! A massive thanks to the people at Pasteur in Rome. Enrico, Daniele, and Michela for their help in the lab. And Magda and Julija for their company during the long hours in the lab. Magda, thank you so much for your help, it really gave a boost to the project. I hope to see you in Athens in October.

To all my friend in Rome, I know I'm not the best at coming back to Italy often, but I'm extremely grateful for your support. Even though we haven't met that often during these four years, every time I come back I feel as I've never left. To the people from the previous lab I was working in, and especially Dr. Anna Barile. Without you I wouldn't be here.

Finally, a huge thanks to my relatives, from Romania and from Rome, for their support and motivation. My mom for being such a strong woman and an inspiration. And to my dad, the most supportive, calm, and bright person I've met; I still have to learn a lot from you. I could not have bare all of this without you.

Table of Contents

List of figures

List of tables

Abbreviations

AIM2:	Absent in melanoma 2
AP-1:	Activator protein 1
APS:	Ammonium persulfate
BIR:	Baculovirus inhibitor of apoptosis protein repeat
BSA:	Bovine serum albumin
CARD:	Caspase activation and recruitment domain
CAT:	Catalase
cGAS:	Cyclic GMP-AMP synthase
Chr:	Chromosome
CoA:	Coenzyme A
CXCL10:	C-X-C motif chemokine ligand 10, also known as interferon gamma-induced protein 10 (IP-10)
CYP450:	Cytochrome P450
DAA:	Direct-acting antiviral
DAI:	DNA-dependent activator of IFN-regulatory factors
DAMP:	Damage associated molecular pattern
DDAH2:	Dimethylarginine dimethylaminohydrolase 2
DDX41:	DEAD-Box Helicase 41
DENV:	Dengue virus
DMEM:	Dulbecco's Modified Eagle's Medium
DMSO:	Dimethyl sulfoxide
dsDNA:	Double-stranded DNA
dsRNA:	Double-stranded RNA
DNA:	Deoxyribonucleic acid
DTT:	Dithiothreitol
ELISA:	Enzyme-linked immunosorbent assay
ER:	Endoplasmic reticulum
ETC:	Electron transport chain
FAD:	Flavin adenine dinucleotide
FBS:	Foetal bovine serum

HAV:	Hepatitis A virus
HBV:	Hepatitis B virus
HCV:	Hepatitis C virus
HK:	Hexokinase
HIF:	Hypoxia-inducible factor
HLC:	Hepatocyte-like cell
GLRX:	Glutaredoxin
GLUT:	Glucose transporter
GSH:	Glutathione (reduced)
GSSG:	Glutathione (oxidised)
GST:	Glutathione S-transferase
IAV:	Influenza A virus
IFI16:	IFN inducible protein 16
IFN:	Interferon
IFNAR:	Type I interferon receptor
IFNLR:	Interferon lambda receptor
IKK:	Inhibitor of nuclear factor-κB (IκB) kinase
IL:	Interleukin
IL1-R:	IL-1 receptor
IMM:	Inner mitochondrial membrane
iPSC:	Induced pluripotent stem cell
IRF:	Interferon regulatory factor
IRG1:	Immune-responsive gene 1
ISG:	Interferon stimulated gene
ISGF3:	IFN-stimulated factor 3
ISRE:	Interferon-stimulated response element
JAK:	Janus kinase
LCMV:	Lymphocytic Choriomeningitis virus
LDH:	Lactate dehydrogenase
LGP2:	Laboratory of Genetics and Physiology 2
LPS:	Lipopolysaccharide
LRR:	Leucine rich repeat

MAL: MyD88-adaptor-like

MAM: Mitochondrial-associated membrane

MAVS: Mitochondrial antiviral-signaling protein

MDA5: Melanoma differentiation associated gene 5

MOI: Multiplicity of infection

mRNA: Messenger RNA

mROS: Mitochondrial reactive oxygen species

MSRA: Methionine sulfoxide reductase A

mtDNA: Mitochondrial DNA

mtRNA: Mitochondrial RNA

MyD88: Myeloid differentiation primary response protein 88

NAD: Nicotinamide adenine dinucleotide

NADP: Nicotinamide adenine dinucleotide phosphate

NAFLD: Non-alcoholic fatty liver disease

NATCH: NAIP, CIITA, HET-E, and TP-1

NEK7: Never in mitosis gene a-related kinase 7

NF-κB: Nuclear factor kappa B

NLR: NOD-like receptor

NLRA: NLR family, acid domain containing

NLRB: NLR family, BIR domain containing

NLRC: NLR family, CARD domain containing

NLRP: NLR family, PYD domain containing

NLRX: NLR family, mitochondrial-addressing sequence containing

NOD: Nucleotide-binding oligomerisation domain

NRF2: Nuclear factor erythroid 2-related factor 2

OAA: Oxaloacetic acid

OAS1: 2’-5’-Oligoadenylate synthase 1

OMM: Outer mitochondrial membrane

OxPhos: Oxidative phosphorylation

PACT: PKR activating protein

PAMP: Pathogen-associated molecular pattern

PBS: Phosphate buffered saline

PGE2: Prostaglandin E2

PHH: Primary human hepatocyte

PKR: Protein kinase R

PMSF: Phenylmethanesulfonylfluoride

Poly I:C: Polyinosine-polycytidylic acid

PRDX: Peroxiredoxin

PRR: Pattern recognition receptor

PYD: Pyrin

RAG2: Recombination activating gene 2

RET: Reverse electron transport

RIG-I: Retinoic acid-inducible gene I

RLR: RIG-I-like receptor

RNA: Ribonucleic acid

ROS: Reactive oxygen species

RSV: Respiratory syncytial virus

SARM: Sterile α- and armadillo-motif-containing protein

SARS-CoV2: Severe acute respiratory syndrome coronavirus 2

SDD-AGE: Semi-denaturating detergent agarose gel electrophoresis

SDH: Succinate dehydrogenase

SDS: Sodium dodecylsufate

SDS-PAGE: SDS-polyacrylamide gel electrophoresis

SEM: Standard error of the mean

shRNA: Short hairpin RNA

siRNA: Small interfering RNA

SIRT: Sirtuin

SLE: Systemic lupus erythematosus

SOD: Superoxide dismutase

ssRNA: Single-stranded RNA

STAT: Signal transducer and activator of transcription

STING: Stimulator of interferon genes

TBK1: TANK-binding kinase 1

TBS: TRIS-buffered saline

TCA:	Tricarboxylic acid
TEMED:	N,N,N’,N’-Tetramethylethylenediamine
TIR:	Toll-interleukin-1 receptor
TLR:	Toll-like receptor
TNF:	Tumor necrosis factor
TRAF:	TNF receptor-associated factor
TRAM:	TRIF-related adaptor molecule
TRIF:	TIR-domain containing adaptor inducing interferon (IFN)-β
TYK2:	Tyrosine kinase 2
T-poly I:C:	Transfected poly I:C
USP18:	Ubiquitin specific peptidase 18
VSV:	Vesicular stomatitis Indiana virus
ZBP1:	Z-DNA binding protein 1
ZIKV:	Zika virus
3-hpRNA	5’ triphosphate hairpin-RNA

Chapter 1: General introduction

Hepatocytes are targeted by different hepatotropic viruses, such as hepatitis viruses (hepatitis B and C viruses, HBV and HCV). Worldwide, more than 360 million people are affected by HBV and HCV. Although type I IFN- and direct acting antiviral (DAAs)-based drugs have been developed, chronic hepatotropic infections are still a common outcome, increasing the risk of liver fibrosis, cirrhosis, and eventual hepatocellular carcinoma. Unravelling the cellular and molecular mechanisms behind hepatic innate antiviral activity is required for developing more efficient and specific pharmacological strategies.

While hepatocytes are responsible for metabolism homeostasis, they are also able to mount an innate antiviral response. Although immune activities have been found to rewire cellular metabolism in myeloid and lymphoid cells, less is known in other cell types, such as hepatocytes. Given the fundamental metabolic role and antiviral response in hepatocytes, studying the link between the two activities may shed light on new mechanisms which can provide tools for developing new therapeutical strategies. This introduction will therefore focus first on innate antiviral response, before introducing the field of immunometabolism and its role in the hepatic antiviral response.

1.1 Innate immunity

The immune system is responsible for protecting the host from harmful pathogens, such as bacteria and viruses, and maintaining a homeostatic balance. The immune response can be divided, based on differences in specificity, memory capacity, and kinetic, into innate and adaptive immunity. Innate immunity is the first line of defence against invading pathogens and sets the basis for a long lasting adaptive immune response [1]. Innate immunity can be divided into two levels itself, physical and chemical barriers including epidermis, mucosal tissues, antimicrobial peptides, acidic pH, and proteins involved in the complement and coagulation systems; and a second level based on innate immune cells activity. Innate immune cells include myeloid cells such as monocyte

subsets, granulocytes, and lymphoid cells such as dendritic cells and Natural Killer cells [2].

Activation of the innate immune system relies on the ability to identify invading pathogens and host-derived molecular danger signals. This is possible due to the recognition of evolutionary conserved pathogen-associated molecular patterns (PAMPs) and damage-associated molecular patterns (DAMPs), respectively, by pattern-recognition receptors (PRRs). PAMPs are specific and highly conserved molecular structures, such as lipids, proteins, and nucleic acids, shared by the same type of pathogens. PAMPs are essential for pathogen survival and usually have molecular characteristics not found in host cells. Thus, providing the basics for recognising the "self" from the "not-self" by PRRs [3]. Conventionally, PRRs can be divided into five families based on their molecular structures: Toll-like receptors (TLRs), nucleotide oligomerization domain (NOD)-like receptors (NLRs), retinoic acid-inducible gene-I (RIG-I)-like receptors (RLRs), C-type lectin receptors (CLRs), and absent in melanoma-2 (AIM2)-like receptors (ALRs) [3]. PRRs are localized in different cellular compartments, in the cytosol or anchored to cellular membranes and facing the extracellular space or the endosome. Innate immune cells are considered the effector cells of innate immunity, due to a higher basal expression of different PRRs and their capacity to recognise and eliminate invading pathogens through phagocytosis. However, innate immune functions are not unique to innate immune cells. PRRs are germline encoded genes, thus they can be expressed by several cell types, such as epithelial cells, which have been shown to display mechanisms of pathogen defence [4].

1.2 Pattern recognition receptors of innate antiviral immunity

PAMPs recognition by PRRs results in signal transduction and activation of different transcription factors (TFs), leading to production of a broad range of molecules involved in the defence mechanism, including proinflammatory cytokines, chemokines, and interferons. Nuclear factor kappa-light-chain-enhancer of activated B cells (NF-κB), interferon regulatory factor 3 and 7 (IRF3 and IRF7), and activator protein 1 (AP-1) are

the main transcription factors orchestrating the innate antiviral immune response [5]. Different viral structures are recognised as PAMPs by PRRs. Among these, envelope glycoproteins and genomic material (nucleic acids, DNA and RNA) are the most characterised viral PAMPs (Table 1.1) [5].

PRR	Class of PRR	Ligand	Location
TLR2-TLR1/6	Toll-like receptor	Glycoproteins [6, 7]	Plasma membrane
TLR3	Toll-like receptor	dsRNA [8]	Endosome
TLR4	Toll-like receptor	Glycoproteins [9, 10]	Plasma membrane
TLR7	Toll-like receptor	ssRNA [11, 12]	Endosome
TLR8	Toll-like receptor	ssRNA [11, 13]	Endosome
TLR9	Toll-like receptor	Non methylated CpG DNA [14]	Endosome
RIG-I	RIG-I-like receptor	5'- 3p hairpin RNA, dsRNA [15]	Cytosol
MDA5	RIG-I-like receptor	dsRNA [16]	Cytosol
NOD2	NOD-like receptor	ssRNA [17]	Cytosol
NLRP1	NOD-like receptor	dsRNA [18]	Cytosol
NLRP6	NOD-like receptor	dsRNA [19]	Cytosol
PKR	Cytosolic receptor	dsRNA [20]	Cytosol
AIM2	AIM2-like receptor	dsDNA [21]	Cytosol
IFI16	Cytosolic receptor	DNA [22]	Cytosol
ZBP1	Cytosolic receptor	DNA [23]	Cytosol, nucleus
DDX41	Cytosolic receptor	DNA [24]	Cytosol
cGAS	Cytosolic receptor	DNA [25]	Cytosol

Table 1.1 PRRs activated by virus-derived PAMPs.

1.2.1 Toll-like receptors involved in the antiviral response

Toll-like receptors (TLRs) were the first class of PRRs to be discovered [26–28]. The TLR family comprises 10 members in humans (TLR1 – TLR10) and 12 in mice (TLR1 – TLR9, TLR11 – TLR13). TLRs are membrane-bound receptors, with a N-terminal leucine-rich repeat-containing ectodomain, involved in PAMP recognition, a single transmembrane

helix, and a cytoplasmic C-terminal Toll-interleukin-1 receptor (IL1-R) homology (TIR) domain, involved in the downstream signaling [29]. TLRs form heterodimers (TLR2/TLR1 and TLR2/TLR6) or homodimers (TLR3, TLR4, TLR5, TLR7, TLR8, TLR9, TLR10), and upon interaction between the ectodomain and the specific PAMP, a conformational change in the receptor bring near the two TIR domains, which can recruit adaptor proteins involved in the downstream signaling. To date, five adaptor proteins have been described to interact with TLRs and mediated the signaling transduction: myeloid differentiation primary response protein 88 (MyD88), MyD88-adaptor-like (MAL, also known as TIRAP), TIR-domain-containing adaptor protein inducing IFN-β (TRIF, also known as TICAM1), TRIF-related adaptor molecule (TRAM, also known as TICAM2), and sterile α- and armadillo-motif-containing protein (SARM) [30]. MyD88 is recruited by all TLRs, with exception for TLR3, which interacts with TRIF. TLR2 and TLR4 signaling depend on the recruitment of MyD88 by MAL. Endocytosed TLR4 can also signal dependently on TRAM and TRIF and MAL/MyD88-independently [30, 31]. SARM is a negative regulator of TRIF-dependent signaling, thus inhibiting TLR3 and TLR4 pathways [32]. Except for SARM, the other four adaptor proteins interact with downstream kinases resulting in activation of transcription factors, among others NF-κB and IRFs (Fig. 1.1). These transcription factors mediate the induction of IFNs, inflammatory cytokines, and chemokines needed for the immune response [30].

Among the TLRs characterised to date, several are implicated in the antiviral immunity. TLR4 was the first PRR identified and studied [27]. Although TLR4 is known as being the lipopolysaccharide (LPS) receptor, different studies have shown that it binds also viral glycoprotein [33]. For instance, severe acute respiratory syndrome coronavirus 2 (SARS-CoV-2) spike protein has been shown to bind TLR4 and activate a downstream immune response [34]. Also TLR2, anchored to the plasma membrane and forming heterodimers with TLR1 or TLR6, is involved in recognising viral PAMPs, such as the SARS-CoV-2 envelope protein [35]. Whether the mechanism relies on TLR2-TLR1, TLR2-TLR6, or both heterodimers is still unclear.

Four different TLRs, TLR3, TLR7, TLR8 and TLR9, are localised in the endosome and recognise viral genetic material. TLR3 binds virus-derived double-stranded RNA (dsRNA)

[8]. While TLR7 and TLR8 recognise single-stranded RNA (ssRNA) [11], TLR9 engages with unmethylated CpG DNA, a PAMP specific for both bacteria and viruses [36]. Although both TLR7 and TLR8 are activated by ssRNA, differences between the two receptors have been reported. TLR7 activation is more effective in inducing type I IFNs compared to TLR8 activation, while TLR8 selective agonists are more effective at inducing pro-inflammatory cytokines [37].

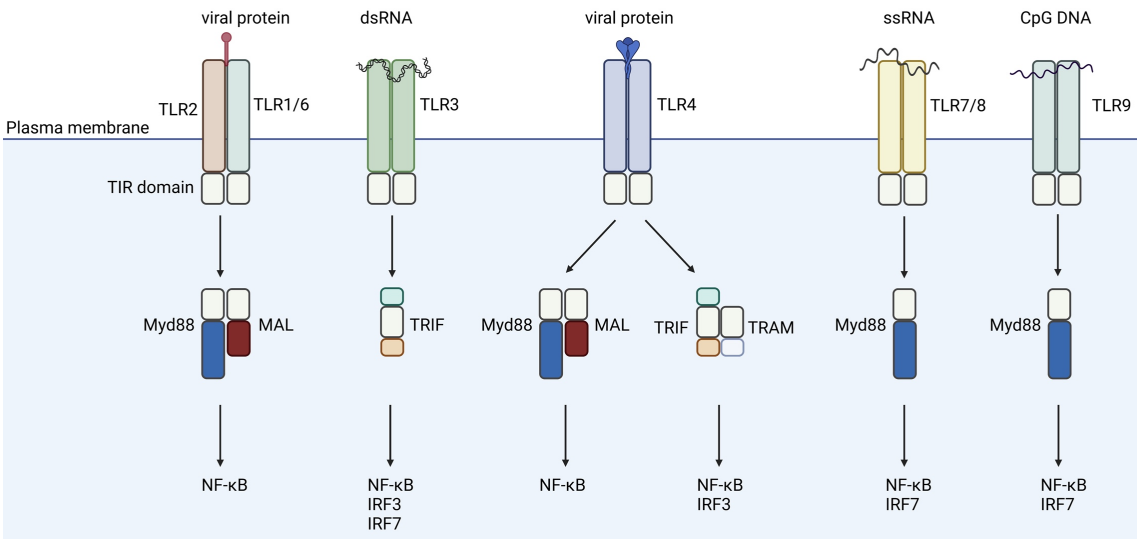

Figure 1.1 Overview of TLRs involved in antiviral response structure and downstream transcription factors.

TLRs dimers change their structure upon ligation with the cognate PAMP(s). This causes the activation of TIR domains which can interact with downstream adaptor proteins. Each adaptor, which contain a TIR domain as well, ultimately leads to activation of specific transcription factors. Figure adapted from [30].

1.2.2 Cytosolic PRRs involved in the antiviral response

While TLRs are localized withing the endosome or facing to extracellular space, different PRRs are cytoplasmic and have a key-role in the innate antiviral response by their ligation with viral nucleic acids.

1.2.2.1 RIG-I like receptors

RIG-I-like receptors (RLRs) are RNA sensors localised in the cytosol. This protein family includes three members: retinoic acid-inducible gene I (RIG-I), melanoma differentiation-associated protein 5 (MDA5), and laboratory of genetics and physiology 2 (LGP2) [38]. All RLRs contain a central DExD/H-Box RNA helicase domain and a carboxy terminal domain, which work together in detecting immunostimulatory RNAs. RIG-I and MDA5, but not LGP2, have also two amino terminal caspase activation and recruitment domains (CARDs) involved in the downstream signaling. LPG2 lacks the N-terminal CARD domain but it contains the central helicase and the C-termina domain. Thus, LPG2 is able to bind RNAs but it cannot activate the downstream signaling. LPG2 function is still unclear. Studies have shown that LPG2 acts as feedback inhibitor of RIG-I signaling [39], in other studies LPG2 was described as promoting MDA5 activation and downstream activation [40], and LPG2 knock-out mice were more susceptible to certain RNA viruses [41].

Although RIG-I and MDA5 belong to the same family receptor and have shared characteristics, they also present structural and functional differences. In its inactive form, RIG-I has a closed conformation mediated by specific interactions between the two CARD domains and the helicase region [42]. While MDA5 adopts a more open conformation in absence of RNA. Moreover, the two receptors recognise different viral RNA structures. The chemical properties of RNAs able to activate RIG-I have been extensively studied. RIG-I is activated by RNA molecules bearing a triphosphate group at their 5' end [43, 44], with the first nucleotide being unmethylated at its 2'-O [45]. These characteristics allow interactions between the immunostimulatory RNA and RIG-I C-terminal domain. Moreover, a double strand region of the RNA is needed for its interaction with the RIG-I helicase domain, causing an interruption in CARD-helicase domains interaction [42]. Less is known about the chemical characteristics needed by RNAs to activate MDA5. Nonetheless it has been shown that long dsRNA binds to MDA5 and activate the antiviral response [46, 47].

Upon RNA binding, RLRs undergo conformational changes which expose their CARD domains. This allows homotypic CARD-CARD interactions with the downstream mitochondrial antiviral signaling protein (MAVS), which serves as scaffold protein for RLR signaling transduction. MAVS is anchored through its carboxy terminal domain to the mitochondrial membrane, although it has been found also at the mitochondrial associated membranes [48] (MAMs, membrane structures connecting endoplasmic reticulum and mitochondria) and anchored to peroxisomes [49]. MAVS CARD domains oligomerization, upon RLR interaction, cause MAVS proteins to form prion-like aggregates. This MAVS aggregation step is essential for the RLR-mediated antiviral response [50]. MAVS aggregates are able to interact with the tumor necrosis factor receptor-related factor (TRAF) family members TRAF2, TRAF3, TRAF5, and TRAF6 [51], and inhibitor of NF-κB kinase (IKK) family members (IKKε, TBK1, and IKKα/β) forming the supramolecular complex known as "MAVS signalosome" [52]. Once recruited and interacting with MAVS, TRAFs and IKKs proteins activate a signaling cascade causing the phosphorylation of the transcription factors IRF3, and NF-κB. Activation of these transcription factors induces an innate antiviral response with an increase in gene expression of type I and III interferons as well as pro-inflammatory cytokines (Fig. 1.2) [50, 52].

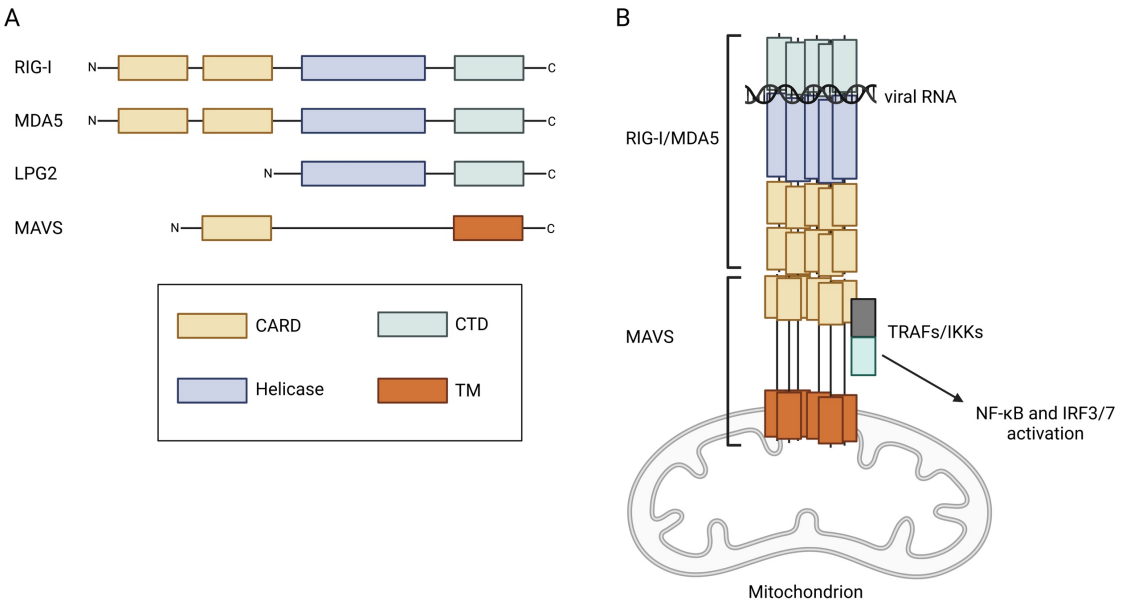

Figure 1.2 RLRs and MAVS share the CARD domain.

Domain architecture of RLRs and MAVS. The three members of the RLRs family contain a helicase domain involved in binding RNA, but only RIG-I and MDA5 have the CARD domain needed for their interaction with MAVS and the further downstream activation of the antiviral response (A). RIG-I and MDA5 interact with MAVS through a CARD-CARD domain interaction. Upon RNA binding, RIG-I and MDA5 oligomerize and interact with MAVS CARD, causing MAVS aggregation. MAVS aggregates form a signalosome platform needed for the downstream signal transduction which culminates in NF-κB, IRF3, and IRF7 activation, responsible for expression of IFNs and cytokines involved in the antiviral response. Figure adapted from [38].

1.2.2.2 NOD-like receptors

Nucleotide oligomerisation domain (NOD)-like receptors (NLRs) are a third class of PRR recognising PAMPs and DAMPs during pathogen infection or cellular stress. The human genome contains 22 genes encoding for NLRs. NLRs are formed by three domains, a central NATCH, a C-terminal leucin-rich repeat shared by almost all the NLRs, and a specific N-terminal effector domain. The central NATCH domain (also known as NOD domain) is common to all NLRs and consists in seven distinct conserved motifs, including an ATP/GTPase-specific P-loop, a Mg^{2+} binding site, and five specific motifs. The C-terminal leucin-rich repeat (LRR) domain is involved in ligand binding, while the N-terminal domain is involved in the effector functions and enables interactions with downstream signaling molecules [53]. NLRs can be divided into five subfamilies, based on the N-terminal domain, namely the acidic transactivation domain (NLRAs), BIR (Baculovirus Inhibitor of apoptosis protein Repeat) domain (NLRBs), CARD domain (NLRCs), PYD (pyrin) domain (NLRPs), and mitochondrial-addressing domain (NLRX) [54].

Several members of NLRs are involved in the innate antiviral response. For instance, NOD2 recognises respiratory syncytial virus (RSV)-derived ssRNA and trigger a MAVS-dependent antiviral response [17], while NLRP1 and NLRP6 have been shown to bind dsRNA and activate a downstream antiviral response [18, 19].

1.2.2.3 Protein kinase RNA-activated

Protein kinase RNA-activated, also known as Protein kinase R (PKR), is a cytosolic serine-threonine kinase. PKR promoter contains an IFN-stimulated response element (ISRE), thus PKR expression is enhanced during an IFN-mediated antiviral response [55]. PKR contains an N-terminal domain through which it binds dsRNA, and a kinase domain at its carboxy terminal [56]. Binding to dsRNA causes conformational changes in PKR, which leads to homodimerization and autophosphorylation [57]. Activated PKR, by phosphorylating and subsequently inhibiting the initiation factor of the translation (eIF2α), block the host protein translation, thus causing arrest of viral protein synthesis [57]. Moreover, PKR activates a NF-κB-dependent innate antiviral response [57], inducing expression of pro-inflammatory cytokines and interferons. Besides its role as a PRR, PKR can be activated by PKR activating protein (PACT) during cellular stress, such as endoplasmic reticulum stress and oxidative stress [58].

1.2.2.4 Cytosolic DNA receptors

In eukaryotic cells, DNA is confined in the nuclei and mitochondria. On the other hand, during infection or cellular stress it can be found in the cytosol, where it is recognised by cytosolic PRRs that activate a downstream immune response. In the last twenty years, several cytosolic DNA sensors have been discovered, among these, absent in melanoma 2 (AIM2, belonging to the ALRs class of PRRs), interferon gamma inducible protein 16 (IFI16), Z-DNA binding protein 1 (ZBP1), DEAD-Box Helicase 41 (DDX41), and cyclic GMP-AMP synthase (cGAS) [59]. Interestingly, many DNA sensors are important also for initiating an antiviral response against RNA viruses, thus highlighting the cross-talk among the various PRRs [60]. For instance the DNA sensor IFI16 has been shown to bind Influenza A virus RNA and cooperate with RIG-I in inducing an IFN-based antiviral response [61].

1.2.3 Pattern recognition receptors in non-immune cells

The mammalian immune system is based on hematopoietic immune cells, which constitute the main components of the innate and adaptive immunity. However immune functions are not restricted to immune cells, and other cell types exhibit mechanisms of pathogen defence [4, 62]. Among others, activation of PRRs in non-immune cells acts as an intrinsic immune mechanism activating expression of pro-inflammatory cytokines and interferons. Different non-immune cells, such as gut and lung epithelial cells, are able to activate PRR-mediated immune activities upon pathogen infection [63, 64]. PRR expression is cell type specific, as shown by studies conducted in intestinal epithelium [64], therefore specific cells are able to induce with a greater magnitude pro-inflammatory cytokines and interferons when challenged by pathogens [4]. Cytosolic PRRs, in particular RLRs, seem to be expressed in most tissues, conferring a first line of defence against viral pathogens [65–67].

1.3 Interferons in innate antiviral immunity

The term cytokine refers to a broad range of small secreted proteins that act in an autocrine, paracrine, or endocrine manner. Cytokines group includes chemokines, interferons, interleukins, and tumor necrosis factors. Cytokines are produced by immune and non-immune cells. Cytokines act through binding to their cognate receptor, which triggers an intracellular signaling transduction. During an antiviral response, activation of NF-κB, IRF3, and IRF7, induce the expression of different cytokines, such as pro-inflammatory cytokines, chemokines involved in recruiting immune cells, and interferons.

Interferons were first described in 1957 by their ability to interfere with influenza A virus propagation [68], today much more is known about them. Interferons (IFNs) play a critical role in orchestrating both innate and adaptive immune responses against bacteria, viruses, tumors and modulating inflammatory processes. IFNs are divided into three different families (type I, II, and III) based on their sequence homology and functional activities. Although at least 20 IFNs have been identified to date, only three

cell surface receptors (one for each family of IFN) are known. Each class of IFN signals through a specific heterodimeric receptor and activates the downstream transduction based on the Janus kinase signal transducer and activator of transcription (JAK-STAT) signaling pathway [69]. In human and mice, IFN I family includes 13 and 14, respectively, IFN-α subtypes, a single IFN-β, IFN-ε, IFN-κ, IFN-ω (in humans), and IFN-ζ (in mice). Type II IFN family comprehends only interferon gamma (IFN-γ), produced mainly by specific immune cells and acting through the widely expressed IFN-γ receptor (IFNγR) [70, 71]. Type III IFNs family is formed by 4 genes in human, IFNλ1 (IL-29), IFNλ2 (IL28-A), IFNλ3 (IL-28B), and IFNλ4 which is a pseudogene in many population and it has been associated with HCV clearance [72].

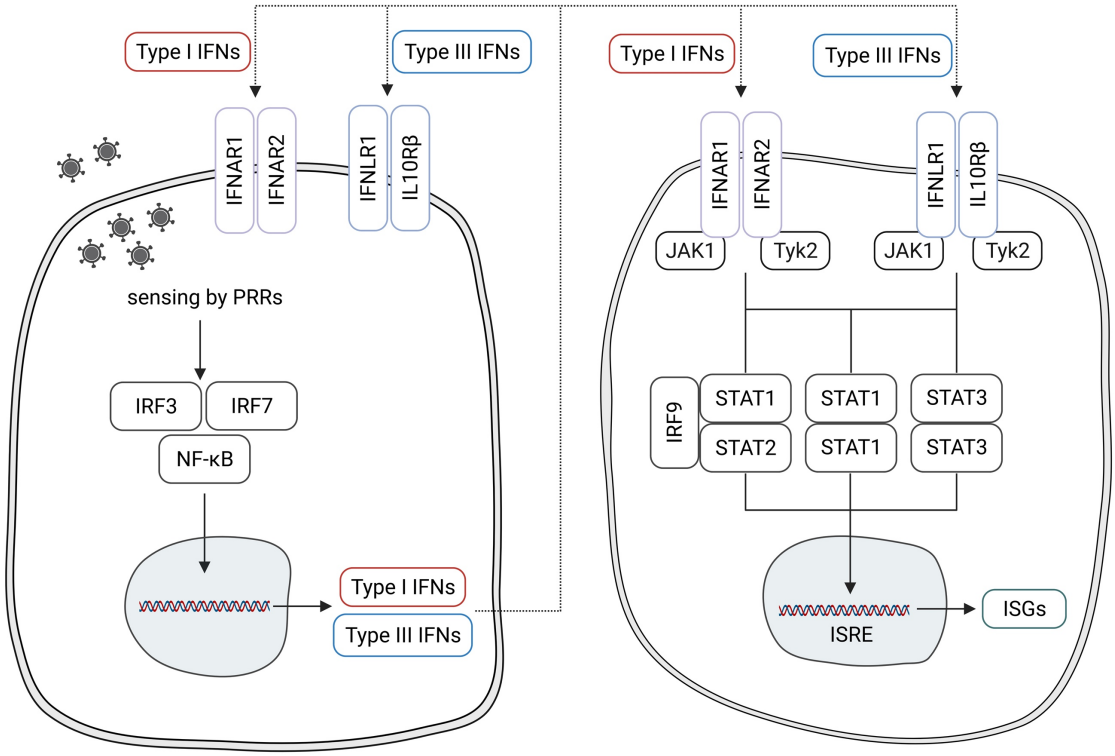

Figure 1.3 Overview of type I and III interferons induction and signaling.

Viral infection induces activation of cytoplasmic and endosomal PRRs resulting in activation of the transcription factors NF-κB, IRF3, and IRF7 and subsequent IFN-I and IFN-III production. IFN-I binds to IFNAR1/IFNAR2 and IFN-III to IFNLR1/IL10Rβ heterodimers and signal both in paracrine and autocrine manners through JAK/STAT

pathway to upregulate interferon stimulated genes which act to protect the host against viral pathogens.

1.3.1 Type I interferon

IFN I signaling exerts antiproliferative and cytotoxic effects as well as modulates innate and adaptive immune responses. IFN I antagonizes a broad range of viruses, such as influenza virus and hepatotropic viruses (hepatitis B virus; HBV, hepatitis C virus; HCV, Dengue virus) [69, 73]. Inhibition of type I IFN signaling is crucial for pathogens to successfully replicate within the host, thus it is not surprising that great majority of viruses developed different strategies to inhibit type I IFN signaling, such as HCV, which causes degradation of the key-component STAT3 [74].

Type I IFN receptor (IFNAR) is a dimeric cell surface receptor composed of the two subunits IFNAR1 and IFNAR2, present on all nucleated cell types [69]. IFNs I bind to the heterodimeric transmembrane IFNAR, which activate JAK1 and the tyrosine kinase 2 (TYK2). Subsequently, JAK1 and TYK2 phosphorylate the transcription factors signal transducers and activator of transcription 1 (STAT1), STAT2, and STAT3. STAT1 and STAT2 can dimerize and assemble with IFN-regulatory factor 9 (IRF9), forming the trimolecular complex called IFN-stimulated gene factor 3 (ISGF3). In the nucleus, ISGF3 binds to IFN-stimulated response elements (ISREs) DNA sequences, thereby inducing the expression of hundreds of interferon-stimulated genes (ISGs). ISG-encoded proteins are considered the effectors of the antiviral response (Fig. 1.3). These proteins restrain pathogens through several mechanisms, such as inhibition of viral transcription, translation and replication, degradation of viral nucleic acids and alteration of the cellular metabolism in order to block viral propagation [75].

How 17 different human IFN I, signaling through the same receptor (IFNAR), are able to produce distinct responses remains elusive [69]. Yet, studies show that a variety of factors, including ligand binding affinity, stability of the ternary receptor complex (IFN I – IFNAR), receptor expression, and positive or negative downstream regulation, might explain differences in IFN signaling [76][77].

1.3.2 Type III interferon family

The third type of IFNs, IFNλ, was discovered in 2003 by two separate groups [78][79]. IFN III receptor is comprised of IFNLR1 (also known IL28Rα) and IL10Rβ. Similarly to IFN I signaling, also type III IFNs, by binding to their cognate receptors activate the JAK/STAT pathway, with the formation of ISGF3 complex, inducing expression of several ISGs. IFN III are induced upon infection by cells constituting barrier surfaces, such as respiratory and gastrointestinal tract epithelial cells, hepatocytes, and subsets of immune cells such as plasmacytoid dendritic cells [80–82].

Whereas all nucleated cells respond to type I interferon by expressing the specific IFNAR receptor, type III interferons are produced by and target mainly mucosal epithelial cells, dendritic cells [83], and hepatocytes [82]. Interestingly, while type III IFN receptor is expressed by human hepatocytes, that is not the case in mice [84, 85].

Although IFN I and III bind different receptors, the downstream signaling and induced genes coincide substantially [82]. Transcriptome studies have shown that IFN I and IFN III signatures overlap [86]. In general, IFN I is more potent in inducing the antiviral response and IFN III-activated ISGs are a subset of those induced by IFN I.

Nonetheless, substantial differences between the two IFN types have emerged. From a signaling transduction prospective, while IFN I uses JAK1 and TYK2 to activate ISGF3, in certain cell types (such as fibroblasts) IFN III signals also through JAK2 [87]. Whether this causes a difference in the kinetic or induced ISGs is not clear yet. Studies in primary cells, such as human vaginal epithelial cells, showed that a subset of ISGs (such as CXCL10, CXCL11, and IFIT3) were uniquely or more potently induced by IFN-λ1 rather than IFN-β [88]. Also the kinetics differs for the two IFN; IFN I-induced ISGs peak early and decline, while IFN III-induced ISGs occurs later and persist for a longer period [89–91]. These differences might be due to negative feed-back mechanisms; for instance the negative

regulatory ISG ubiquitin specific peptidase 18 (USP18) mainly inhibits IFN-α rather than IFN-λ1 signaling [92].

PRRs cellular localization has been demonstrated to be crucial in balancing type I and III IFNs. The RLR-dependent antiviral response relies on MAVS, which can be anchored to membranes of mitochondria, peroxisomes, and mitochondrial-associated membranes of the endoplasmic reticulum. It has been shown that upon viral or bacterial infection (e.g. Dengue virus and *Listeria monocytogens*), signal transduction through mitochondria-anchored MAVS induces type I IFNs, while signal transduction mediated by peroxisome-anchored MAVS induces type III IFNs. Moreover during epithelial cell differentiation and polarization, an increase in IFN III response correlating with increase in peroxisome abundance has been observed, and cells derived from patients with peroxisomal disorder display an aberrant antiviral response [87].

The two most striking differences between IFN I and IFN III signaling are the potency difference and compartmentalized cell responsiveness. These two characteristics highlight the paradigm in which IFN III serves as first-line of defence with a lower magnitude, less inflammatory, and specifically localised at anatomic barriers response. When the initial IFN III-mediated defence is breached, a more potent and inflammatory systemic type I IFN response is activated [82, 91, 93]. An explanatory example is the intestinal tract, where epithelial cells present a high IFNLR and low IFNAR expression, in contrast to lamina propria expressing greater levels of IFNAR. Thus, the intestinal epithelium relies on IFN III to restrict pathogen infection; when this is not possible and the pathogen reach the inner lamina propria, a systemic type I IFN-dependent response is activated [94].

	Type I IFN	Type III IFN
Gene	Single exon, intronless Human Chr. 9 Murine Chr. 4	Multiple exons (5 exons) Human Chr. 19 Murine Chr. 7
Members	Human α1, α2, α4, α5, α6, α7, α8, α10, α13, α14, α16, α17, α21, β, ε, κ, ω Mouse α1, α2, α4, α5, α6, α7, α9, α11, α12, α13, α14, α15, α16, αB, β, ε, κ, ζ	Human λ1, λ2, λ3, λ4 Mouse λ2, λ3
Receptor characteristics	• High-affinity binding to IFNAR2, then low-affinity IFNAR1 is recruited to form ternary complex • Receptor is ubiquitously expressed	• High-affinity binding to IFNLR1, then low-affinity IL10Rβ is recruited to form ternary complex • Receptor is preferentially expressed on epithelial cells, hepatocytes, and some immune cells (e.g. dendritic cells)
Response	• High potency • Rapid kinetics • Systemic • Inflammatory	• Lower potency • Slower kinetics • Anatomic barriers • Less inflammatory

Table 1.2 Comparison of type I and type III IFNs.

Even though IFN-I and IFN-III have signaling and transcriptional similarities, some features distinguish the two IFNs, among others: the majority of type I IFN genes lack introns, while type III IFN genes have 5 exons; type I IFN family (17 members in humans) is much larger compared to type III family (4 members in mice); they also bind distinct receptors. The expression of the two IFNs and their cognate receptors is differently distributed among the tissues; IFNAR is ubiquitously expressed, while IFNLR is preferentially found on epithelial cells, hepatocytes, and dendritic cells. Although the response induced by the two classes of IFN partially overlap, they present differences: (1) IFN-I-mediated response has a higher potency, a more rapid kinetic and is systemic, while IFN-III-mediated response has a lower potency, a slower kinetics, and it is mainly observed at anatomic barriers.

1.4 Cellular metabolism in innate antiviral immunity

In the early '30s of last century, biochemist Hans Krebs described the first metabolic cycle (urea cycle), while physiologist Otto Warburg observed increased glycolysis in tumour cells, process known as Warburg effect. Two decades later, among others, Warburg observed that activated leukocytes also have an increased glycolysis, similar to tumour cells [95]. In the last 25 years, seminal discoveries have highlighted the link between metabolism and immune response, initiating the immunometabolism field [96–98].

Immune response-activated metabolic changes are stimulation-specific [96]. An informative example is macrophage activation by LPS or interleukin 4 (IL-4). LPS stimulation induces macrophages towards a pro-inflammatory phenotype, while IL-4-stimulated macrophages have anti-inflammatory characteristics. These differences are observed also in their metabolism. LPS-stimulated macrophages increase glycolysis [99] and break Krebs cycle in two places – after citrate [100] and after succinate [101], causing accumulation of these two metabolites. Citrate is used for fatty acid synthesis, which in turn are used for membrane biogenesis, nitric oxide and prostaglandins generation as well as itaconic acid production, which has a bactericidal effect [102] and is involved in immunomodulating the response [103]. Succinate accumulation has a direct impact on cytokine production. This metabolite, as discussed in details below, leads to stabilization of hypoxia inducible factor 1 alpha (HIF1α) and sustained production of IL-1β [101]. On the other hand, IL4-activated macrophages, known to have an anti-inflammatory phenotype, have intact Krebs cycle and functional oxidative phosphorylation, coupled with an enhanced fatty acid oxidation [100].

The cross-talk between host metabolism and viral infection can be analysed from different perspectives: (1) metabolism involvement in anti-viral response, (2) virus control of cell metabolism for the subversion of the antiviral response, (3) metabolism and viral replication [104]. Viruses require synthesis of lipid, proteins and nuclei acids by host cells in order to replicate and energy to drive viral particle assembly and release [104]. Thus, it is not surprising that viruses have developed different strategies to take control of the host metabolism. For instance, HCV increases cellular fatty acid

biosynthesis needed for viral replication [105]. Since the pathogen itself alters the host metabolism, deciphering metabolic changes due to innate antiviral activity presents major caveat. In this case, using synthetic PAMPs that mimic viral infection by activating cognate PRRs can be informative about host metabolism. In this section we focus on glucose catabolism (glycolysis, Krebs cycle, and oxidative phosphorylation) and its role in the innate antiviral activity.

1.4.1 Glycolysis in innate antiviral immunity

Glucose catabolism starts with glycolysis. Briefly, this pathway consists of ten reactions which convert glucose to pyruvate through a series of intermediate metabolites. Different studies have analysed the role of glycolysis during innate antiviral activity [106, 107].Studies conducted on dendritic cells showed that stimulation with TLR3 (poly I:C), TLR7/TLR8 (R848), or TLR9 (CpG) agonists induced increase glycolysis, similarly to TLR4 activation with LPS [106]. Whether this is the case also in non-immune cells has not been shown yet.

RLR-dependent antiviral response has also been shown to alter glycolytic flux. Activation of RLR signaling decreases levels of glycolytic intermediates downstream of hexokinase-2 (HK2). HK2 is normally associated with MAVS and voltage-dependent anion channel (VDAC) on the outer mitochondrial membrane. Activation of RLRs disrupts HK2-MAVS interaction, decreasing HK2 activity and the downstream glucose consumption. Moreover the glycolytic by-product lactate has been found to act as natural suppressor of MAVS activation. Lactate, but not other glycolytic metabolites, was found to interact with MAVS transmembrane domain, inhibiting MAVS aggregation. This interaction is abolished during RLR activation (Fig. 1.4). The findings have implications in *in vivo* models. Fasting (which causes decreased lactate levels) or pharmacological lactate reduction showed an increased type I IFN and pro-inflammatory cytokines (such as IL-6) production upon vesicular stomatitis Indiana virus (VSV). This resulted in lower viral titres in mice with decreased lactate levels compared to the control [107].

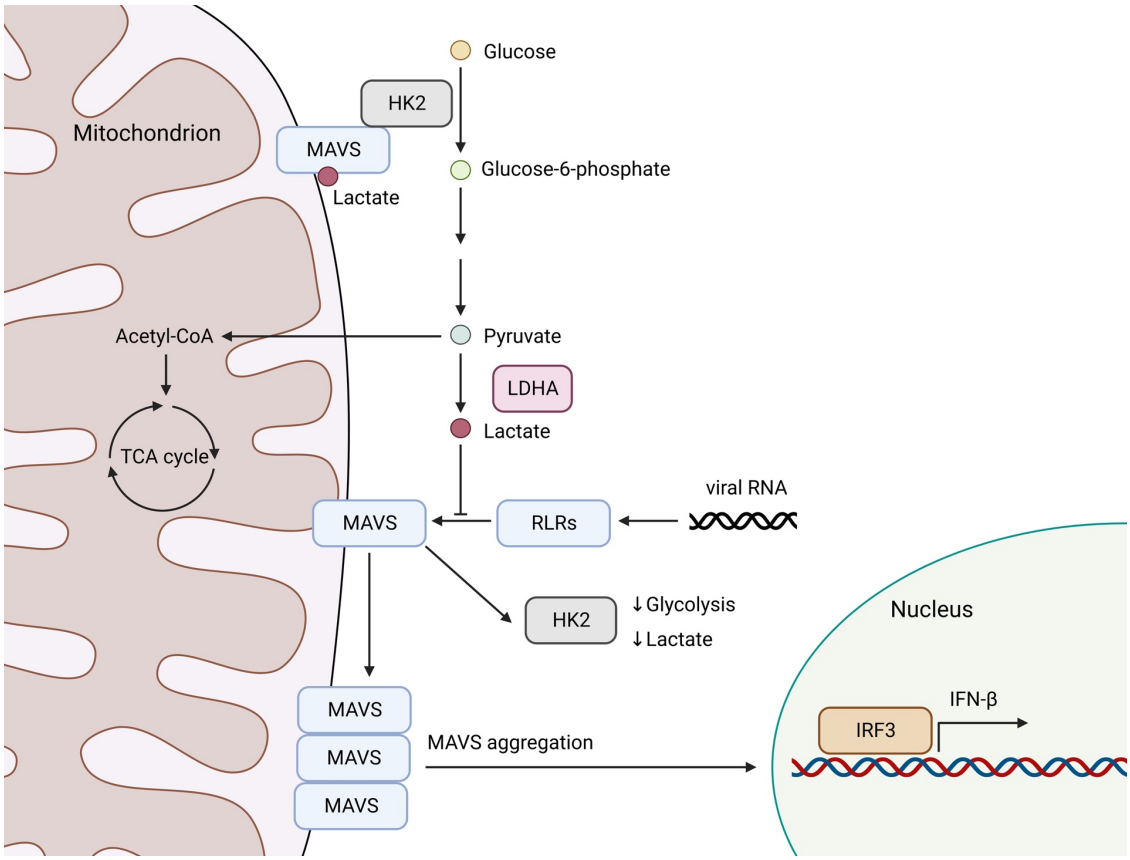

Figure 1.4 Glycolysis-derived lactate suppresses RLR-MAVS-driven antiviral response. *HK2 is localised on the outer mitochondrial membrane and interacts with MAVS in absence of viral RNA. Upon viral RNA exposure, activated RLRs bind MAVS and decrease MAVS-HK2 activation, which diminish HK2 activity therefore the glycolytic flux and lactate production. Lactate inhibits MAVS aggregation which is necessary for IFN-β expression. Thus, RLR activation by viral RNA promotes type I IFN response by decreasing lactate production. Figure adapted from* [108].

1.4.2 Mitochondria in innate antiviral immunity

The mitochondrion is often described as the "powerhouse of eukaryotic cells", since Krebs cycle and oxidative phosphorylation take place in this organelle. With the development of the immunometabolism field, mitochondria have been rediscovered as important signaling organelles. Different findings have shown that mitochondria are key regulators of the innate immune response [109–113].

Mitochondria are surrounded of two lipidic bilayers: an inner mitochondrial membrane (IMM) and an outer mitochondrial membrane (OMM), that define three compartments: the inner compartment also known as mitochondrial matrix, the IMM, and the intermembrane space delimited by the IMM and the OMM. The matrix contains the mitochondrial genetic system, allowing replication and transcription of the mitochondrial DNA, and the enzymes involved in Krebs cycle (also known as tricarboxylic acid cycle, TCA) and fatty acid catabolism. The IMM delimits the mitochondrial matrix. The IMM forms numerous folds (cristae) that invaginate into the mitochondrial matrix and contains the machinery responsible for the oxidative phosphorylation. The IMM is permeable only to oxygen, carbon dioxide, and water. The outer mitochondrial membrane is permeable to different molecules. This is achieved by the lipid composition of the membrane and thanks to proteins – known as porins - that allow the translocation of molecules between the cytosolic and mitochondrial compartments [114, 115]. Mitochondria, together with the endoplasmic reticulum (ER), are responsible for cellular calcium homeostasis. The two organelles are physically interconnected by ER-derived membranes (known as mitochondrial-associated membranes, MAMs) that allow the translocation of different molecules, such as lipids and Ca^{2+}. Mitochondria are able to store and release calcium ions (Ca^{2+}), which regulate energy production and signaling events [116, 117].

1.4.2.1 Krebs cycle and antiviral immunity

The TCA cycle constitute an epicentre in cellular metabolism, since various substrates can feed in. The TCA cycle begins with the condensation of acetyl-CoA, generated from fatty acids, amino acids or pyruvate oxidation, with oxaloacetate (OAA) to generate the six-carbon molecule citrate, the first TCA metabolite. In the second step, citrate is converted into cis-aconitase and further isocitrate by the enzyme aconitase. Through two oxidative decarboxylations, isocitrate is converted in the five-carbon α-ketoglutarate (α-KG, by), which is subsequently used as substrate for the four-carbon succinyl-CoA, thus resulting in the release of two molecules of CO_2 and the reduction of two molecules of nicotinamide adenine dinucleotide (NAD+ reduced to NADH). Next, succinyl-CoA is converted into succinate, with the generation of guanosine-5'-

triphosphate (GTP), which can be converted into ATP. Succinate is oxidized to fumarate by succinate dehydrogenase, which is also part of the OxPhos molecular machinery. This reaction is coupled with transfer of two hydrogen atoms to FAD, producing $FADH_2$. Fumarate is then converted into malate and further into OAA, which can combine with another acetyl-CoA molecule to form again citrate and renter into the cycle [118]. In this series of enzymatic reactions, the TCA cycle generated NADH and $FADH_2$, which are the substrates of OxPhos as discussed below. Metabolites of the TCA cycle can be used as substrates for different anabolic pathways. For instance, citrate is exported to the cytosol where it is converted to OAA or acetyl-CoA that can be used for nucleotide or lipid synthesis, respectively. Different metabolites can also be converted to enter into the TCA cycle. Pyruvate, which is converted to acetyl-CoA by pyruvate dehydrogenase, can also be decarboxylated into mitochondrial OAA by pyruvate decarboxylase. While glutaminolysis converts glutamine to glutamate and subsequently to α-KG. These two reaction, pyruvate decarboxylation and glutaminolysis, are used to replenish the TCA cycle and keep it running when metabolites such as citrate are needed for cytosolic anabolic activity. These processes are also known as anaplerosis [118]. TCA metabolites have been shown to be involved in different aspects of cellular signaling. In specific, citrate, succinate and the isocitrate-derived itaconate are implicated in innate immunity and, to some extent in innate antiviral activities [101, 104, 119, 120].

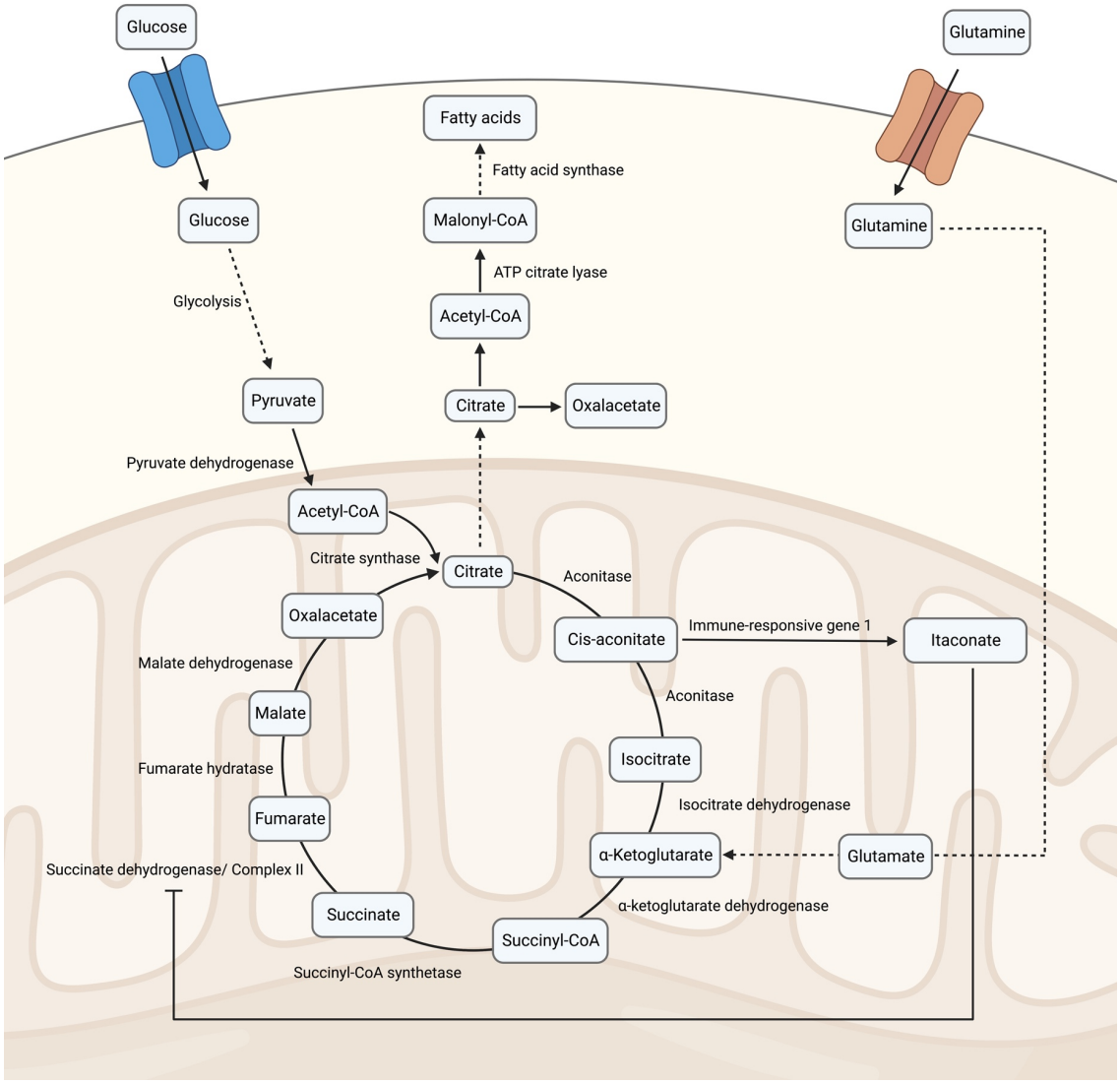

Figure 1. 5 Tricarboxylic acid cycle.

The TCA cycle takes place within mitochondria and its metabolites serve as source for synthesis of molecules required for viral replication. TCA metabolites have also different signaling properties as highlighted in the text. Figure adapted from [104].

Mitochondrial citrate can be transported to the cytosol. Here, it can be converted into acetyl-CoA and oxalacetate. Acetyl-CoA is not only the first substrate in fatty acid synthesis – which is fundamental for viral replication - but it is also utilised for the production of prostaglandins and nitric oxide, involved in inflammation [119, 121]. Moreover, acetyl-CoA is needed by acetyltransferases to catalyse lysin residues

acetylation. Protein acetylation is a fundamental post translational modification (PTM) that regulates protein activity. For instance, acetylation of the NF-κB subunit RelA is needed for its activation and cytokine expression induction. Viruses have developed strategies to inhibit acetylation of host proteins involved in the antiviral response. In this specific case, human papilloma virus blocks NF-kB activation by inhibiting RelA acetylation [122].

Succinate is accumulated in LPS-stimulated macrophages and it is a key player in mediating macrophage polarization towards a proinflammatory phenotype [101]. Whether it is also crucial in antiviral activities is still subject of debate. Dendritic cells have been shown to express the succinate receptor (SUCNR1), and upon stimulation with TLR3 or TLR7 agonists, succinate synergistically increases TNF-α expression [123]. On the other hand, recent studies described a decrease in the antiviral response upon VSV infections in presence of exogenous succinate. In this case succinate was shown to inhibit MAVS aggregation [124]. Thus, succinate seems to regulate specific PRRs activation differently. The molecular mechanism through which succinate modulates TLR3/TLR7 and RLR-dependent antiviral activities is still object of research.

Itaconate is produced in pro-inflammatory macrophages after activation with LPS [100]. This is due to upregulation of immune-responsive gene 1 (Irg1, also known as aconitase decarboxylase 1; Acod1) expression. This enzyme catalyse the conversion of TCA metabolite cis-aconitase to itaconate. Different studies showed the immunoregulatory functions of itaconate, such as inflammasome inhibitor by post-translationally modifying NLRP3 on a cysteine residue [125], and inhibitor of succinate dehydrogenase, which, as described below, is involved in LPS-induced macrophage activation. Irg1 and itaconate increase have also been documented during influenza viral infection in macrophages. In this case, a depletion of itaconate by deletion of Irg1 gene showed higher mortality and increased lung inflammation in *in vivo* model infection. This is probably due to anti-inflammatory functions held by itaconate [126]. Although Irg1 expression has been extensively studied in macrophages, recent insights have shown that also other cell types are able to induce this enzyme and produce itaconate. This is the case for neurons infected with Zika virus (ZIKV). In neurons, ZIKV activates the nucleotide sensor Z-DNA-

binding protein 1 (ZBP1, also known as DNA-dependent activator of IFN-regulatory factors, DAI) and the kinases RIPK1 and RIPK3, components of virus-induced necroptotic cell death signaling. However, activation of this signaling pathway by ZIKV does not induce cellular death. RIPK signaling activates Irg1 expression which catalyses itaconate synthesis. In this scenario, itaconate blocks succinate dehydrogenase activity, which supports ZIKV replication. Thus itaconate is responsible for altering the cellular metabolism and protecting against specific viral infections [127].

1.4.2.2 Oxidative phosphorylation in innate antiviral immunity

Oxidative phosphorylation is the last step in glucose catabolism (after glycolysis and Krebs cycle) and the main source of energy in eukaryotic cells. OxPhos involves electron flow along four enzymes (complex I – IV) collectively called electron transport chain (ETC). These enzymes are localised in the IMM, facing the mitochondrial matrix. Three of them (complex I, III, and IV) are proton (H^+) pumps and couple their electron transport activity with translocation of H^+ from the mitochondrial matrix to the mitochondrial intermembrane space. This causes an electrochemical gradient used by the complex V (also known as ATP synthase) to phosphorylate ADP into ATP [114][128]. Two electron carriers shuttle the electrons from one complex to the next. The first is coenzyme Q (also known as ubiquinone since is a ubiquitous quinone). Ubiquinone is hydrophobic and it diffuses rapidly within the inner mitochondrial membrane, it is involved in transporting electrons from the two first complexes to the third. The second electron carrier is cytochrome C, which transports electrons form complex III to complex IV, the final component of the ETC.

Complex I, also known as NADH dehydrogenase in the largest complex of the ETC. It receives two electrons from NADH and translocates four protons across the membrane into the IMM. Complex II, also known as succinate dehydrogenase, is involved in both, Krebs cycle and OxPhos. It mediates the oxidation of succinate to fumarate. The electrons derived from this reaction are used for reduction of FAD to FADH2, which subsequently is used for ubiquinone reduction. Complex II is not a proton pump. Complex III, also known as cytochrome c oxidoreductase, receives electrons from

ubiquinone, which is oxidised to ubiquinol. This results in translocation of two protons in the IMM. The last enzyme of the ETC, also known as cytochrome c oxidase, accepts electrons from cytochrome c and delivers them to an oxygen molecule, converting into two molecules of water. In this instance four protons are pumped to the IMM. Complexes I, III, and IV couple electron flux with translocation of protons across the IMM, creating an H^+ electrochemical gradient also known as proton motive force (Δp). The proton motive force consists of two parts; the chemical gradient due to difference in solute concentration across the IMM, and an electrical gradient due to difference in charge across the IMM (the electrical gradient is responsible for the mitochondrial membrane potential, MMP). This electrochemical gradient is used by the last enzyme of the OxPhos to generate ATP, the ATP synthase (or complex V). ATP synthase is constituted by two subunits, F_0 and F_1. F_0 is embedded in the inner mitochondrial membrane and contains the proton channel of the complex, which allows the proton flow from the IMM to the mitochondrial matrix. F_1 protrudes into the mitochondrial matrix and is the catalytic part of the complex [114].

Oxygen is the terminal electron acceptor of the ETC. However, electron leak from the ETC is not uncommon – during a steady-state 0.2 to 2% of electrons leak from the ETC and reduce oxygen [129]. Alteration in ETC activity causes an increase in electron leaking from ETC, thus an increase in reduction of oxygen. In these circumstances, differently from its fully reduction by complex IV to water, O_2 is partially reduced by accepting one electron. This reaction generates the superoxide radical anion ($O_2^{\bullet -}$) (Fig. 1.6). This highly reactive molecule can non-specifically oxidise different macromolecules, such as carbohydrates, lipids, and proteins. Cells have evolved mechanisms to avoid superoxide-induced damage; mitochondrial superoxide dismutases are a class of enzymes involved in catalysing the conversion of $O_2^{\bullet -}$ to H_2O_2 (hydrogen peroxide). Hydrogen peroxide can be subsequently detoxified by different antioxidant enzymes, such as catalases, which convert H_2O_2 into water. $O_2^{\bullet -}$ and H_2O_2 are generically called reactive oxygen species (ROS). This broad term comprehends a wide variety of oxygen-derived molecules which, because of their chemical properties, are more reactive than oxygen itself [130].

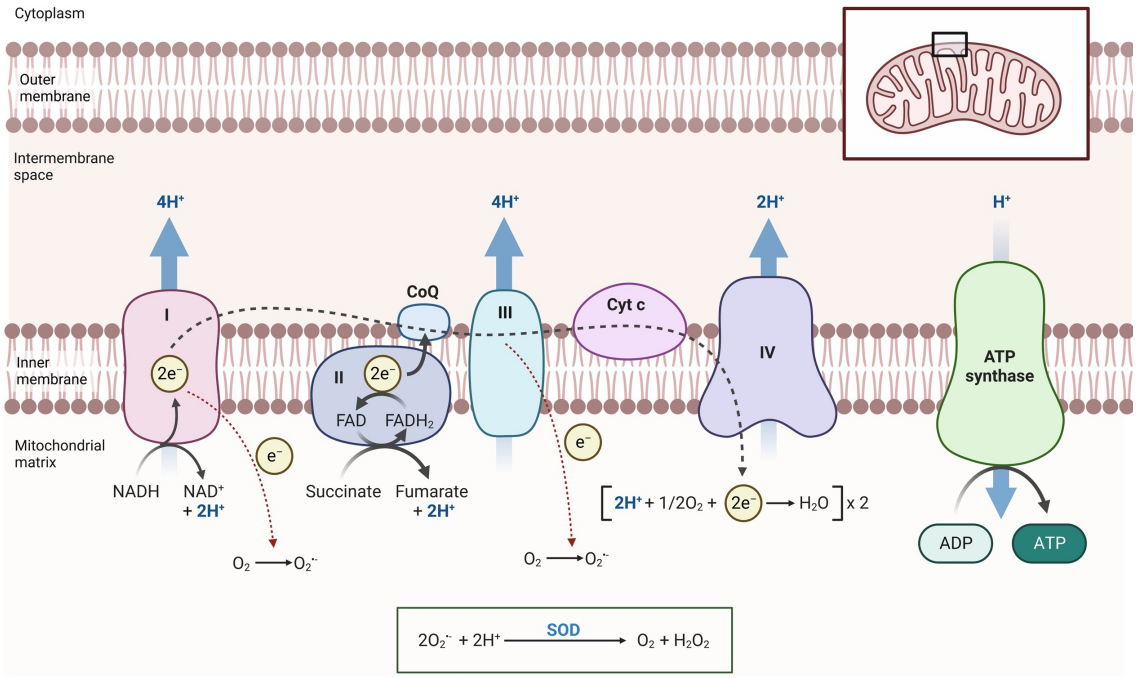

Figure 1.6 Overview of the oxidative phosphorylation and superoxide generation by the electron transport chain.

Complex I and III of the electron transport chain are the two main sources of $O_2^{\bullet-}$ within the cell. $O_2^{\bullet-}$ is converted into H_2O_2 by superoxide dismutases (SODs). H_2O_2 is then converted to H_2O by different antioxidant enzymes, such as catalases.

Generation of mitochondrial $O_2^{\bullet-}$ depends on Δp, NADH/NAD^+, coenzyme Q state (ratio between reduced and oxidised coenzyme Q), and O_2 concentration. The two main sources of mROS are complex I and III [129]. Although mROS can be produced through different mechanisms, one in particular – reverse electron transport (RET) - has been shown to be important in innate immunity and inflammation [111, 131]. In this case, succinate dehydrogenase activity, which causes overreduction of coenzyme Q, in concomitance with increased mitochondrial membraned potential, lead to mROS production. In this instance, mitochondrial ROS stabilise the transcription factor HIF-1α, which induces expression of IL-1β and glycolytic genes, promoting a proinflammatory phenotype [111].

OxPhos and mROS functions are critical also in innate antiviral activity. Surprisingly, macrophage stimulation with TLR3, TLR7/8, or TLR9 agonists does not increase mROS [132], whereas RLR activation decreases OxPhos and upregulates mROS in different cellular models, such as macrophages and fibroblasts [133, 134]. The biochemical mechanism through which RLR activation inhibits Oxphos and increases mROS is still not clear. On the other hand, mROS enhance the RLR-mediated antiviral activity. Mitochondrial ROS lead to increased MAVS aggregation and enhanced interferon levels, while pharmacological depletion of mROS decreases interferon-dependent antiviral response by blocking MAVS aggregation and downstream signaling activation [134].

Although mROS trigger host antiviral response, *in vitro* and *in vivo* studies show that increased mROS can favour replication of specific viruses, such as hepatotropic viruses belonging to the Flaviviridae family (among others HCV, Dengue virus and West Nile virus) [115]. Flaviviruses are known to decrease mitochondrial membrane polarization and increase mROS, thus inducing an oxidant environment. The flavivirus non-structural protein 5 (NS5) capping enzyme is necessary for viral replication and oxidation of a conserved methionine residue (Met 219), which is increased by ROS, is necessary for its activity [135]. But the cross-talk between viral infection, mitochondrial activity, and mROS generation is much more complex. Viruses can benefit from ROS but excess levels of ROS can damage the viral proteins and nucleic acids as well as cause cell death, which, in certain instances can be disadvantageous for viral replication itself. In this case, viruses have also developed strategies to limit mROS production [115]. From these observations, it is clear that the interplay between mitochondrial activity and viral infection is really complex. Nonetheless, understanding these mechanisms is crucial for the development of new antiviral strategies.

1.5 The liver as a metabolic and immunological organ

The liver mediates and regulates whole body metabolism, detoxifies harmful substances, and is constantly absorbing and processing nutrients carried by the portal vein from the gastro-intestinal (GI) tract [136]. The liver functions as a hub metabolically connecting various tissues, including skeletal muscle, adipose, and nervous tissue. These different

functions are mediated by hepatocytes, which account for almost 70% of the mass of the liver. Hepatocytes express nutrient transporters that enable uptake of glucose, amino acids, and fatty acids as well as enzymes required for their metabolism. Diet-derived glucose and amino acids reach the bloodstream in the GI tract and are transported to the liver through the portal vein circulatory system. During a fed state, excess glucose is condensed into glycogen and/or converted into fatty acids by hepatocytes. Here, fatty acids are esterified with glycerol-3-phosphate generating triacylglycerol (TAG). TAG molecules are stored within hepatocytes as lipid droplets (LDs) or can be secreted in the circulation as lipoprotein particles. Also diet derived aminoacids are metabolised within hepatocytes, where they can provide energy or be used to synthesize proteins, glucose, and/or other molecules. In a fasted state, glucose and TAGs are released from the liver into the circulation in order to be utilised by extrahepatic tissues as sources of energy [137]. Hepatic metabolism is regulated by multiple nutrient, hormonal, and neuronal signals. Dysfunctions in the hepatic regulation causes or predisposes to metabolic diseases, including non-alcoholic fatty liver disease (NAFLD) and type 2 diabetes [137].

The liver also has important roles in defence, being determinant in driving systemic inflammation. It is capable of mediating powerful local innate and adaptive immune responses against hepatic infections and malignancy [138]. However, most antigens in gut-derived blood originate from the diet or are products of GI microbiota and are not pathogenic. Thus, the liver maintains a unique tolerogenic environment while also remaining poised to respond to hepatotropic infections, inflammatory signals and malignancies. The unique immune cell repertoire of the liver, which includes diverse populations of liver resident macrophages [139, 140] and lymphoid populations, supplemented by circulating myeloid and lymphoid cells, is a key determinant of the tolerogenic hepatic environment [141–144]. Hepatocytes play a key role in local hepatic tolerance and defence as well, being able to modulate T cell activation [145–148].

1.5.1 Acute phase response

The acute phase response (APR) is a systemic reaction to local or systemic disruption of organism homeostasis caused by infection, tissue injury, neoplasia, or immunological disorders [149]. Innate immune cells, such as macrophages and neutrophils, are recruited at the damaged site and produce proinflammatory cytokines, among others IL-1β, IL-6, and TNF-α. In response to PRR stimulations, pro-inflammatory cytokines are released in the bloodstream and reach different organs responsible for the acute phase response. Proinflammatory cytokines responsible for the APR act mainly on: (1) the hypothalamic-pituitary-adrenal axis, causing fever and sickness behaviour, (2) bone barrow, increasing haematopoiesis, (3) hepatocytes, inducing expression of acute phase proteins (APPs) (Fig. 1.7) [149].

IL-6 is the major mediator of the hepatic APR [150]. Acute phase proteins include several proteins whose hepatic synthesis and plasma concentration increases (positive acute phase proteins) or decreases (negative acute phase proteins) during the acute phase response. The changes in concentration vary, from a 50% increase in the case of ceruloplasmin (copper-carrying protein) to 1000-fold in the case of serum amyloid A and C-reactive proteins (CRP) [151]. APPs are involved in different aspects of the acute phase response, from inflammation and elimination of the pathogen (in the case of an infection), to resolution of inflammatory processes. For instance, CRP binds to bacterial phosphocholines, activating the complement system and phagocytotic capacity of innate immune cells, while fibrinogen and haptoglobin are involved in the later stage of wound repair [151]. Although the mechanisms behind induction of APR and the APPs have been widely described, the metabolic requirements needed by hepatocytes to achieve such a rapid protein synthesis are still poorly understood.

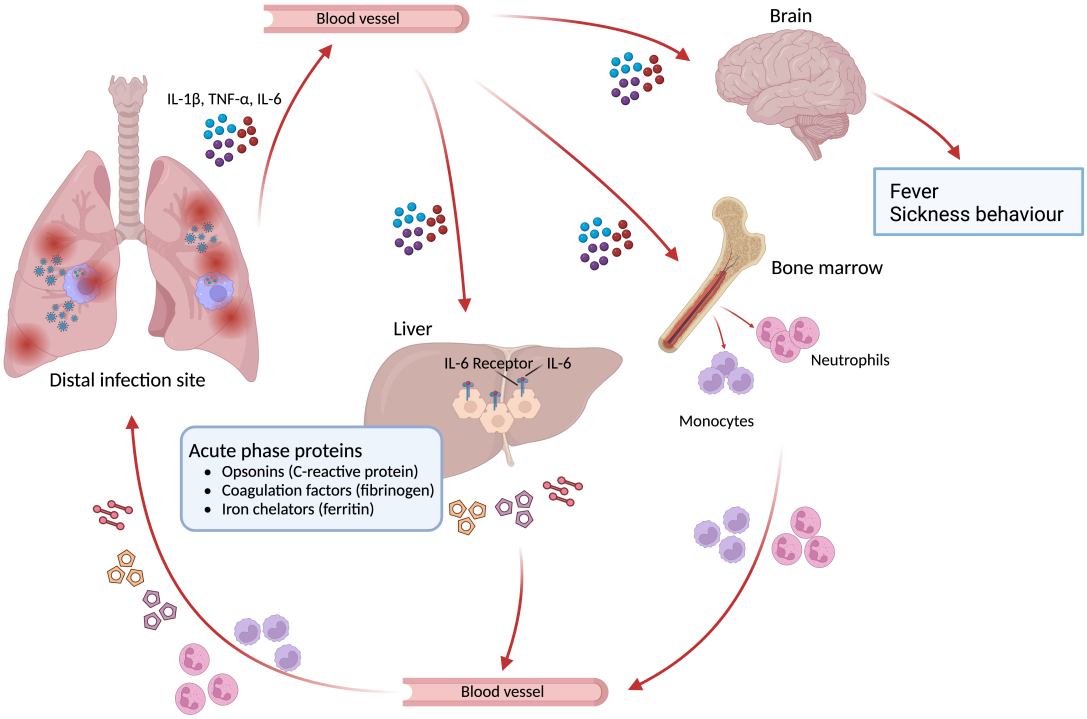

Figure 1.7 The liver mediates pathogen-induced acute phase response.

IL-1β, IL-6, and TNF-α produced at the site of infection or damage are released in the systemic circulation. They reach the brain, bone marrow, and liver, which are the main mediators of systemic inflammation. Hepatocytes in the liver, detect IL-6 through its cognate IL-6 receptor. This interaction leads to an increase in the expression of acute phase proteins (APPs). Opsonins, including C-reactive protein, coagulation factors such as fibrinogen, and metal chelators such as ferritin are among hundreds of APPs involved in the inflammatory response.

Protein	Function	Regulation
C3	Complement system	Positive
C4	Complement system	Positive
C9	Complement system	Positive
Factor B	Complement system	Positive
C1-inhibitor	Complement system	Positive
C4b-binding protein	Complement system	Positive
Mannose binding lectin	Complement system	Positive
Fibrinogen	Coagulation	Positive
Plasminogen	Coagulation	Positive
Tissue plasminogen activator	Coagulation	Positive
Urokinase	Coagulation	Positive
Protein S	Coagulation	Positive
Vitronectin	Coagulation	Positive
α_1-protease inhibitor	Antiprotease	Positive
α_1-antichymotrypsin	Antiprotease	Positive
Pancreatic secretory trypsin inhibitor	Antiprotease	Positive
Ceruloplasmin	Transport protein	Positive
Haptoglobin	Transport protein	Positive
C-reactive protein	Opsonin	Positive
Serum amyloid A proteins	Opsonin	Positive
Ferritin	Iron chelant	Positive
Albumin	Transport protein	Negative
Transferrin	Iron transporter	Negative
Alpha-fetoprotein	Transport protein	Negative
Insulin-like growth factor I	Hormone	Negative
Factor XII	Coagulation	Negative

Table 1.3 Overview of the major acute phase proteins.

Positive acute phase proteins (APPs) are upregulated during the acute phase, while negative APPs expression is downregulated. Table adapted from [151].

1.5.2 Viral sensing in hepatocytes

Hepatocytes are targeted by many major pathogenic viruses including hepatitis A-E, Zika, West Nile and Dengue virus. Although hepatocytes are not immune cells, they are capable of mounting an antiviral response. This is possible since hepatocytes express PRRs that can recognise viral PAMPs (such as viral RNA) and activate the downstream signaling pathways which induce expression of IFNs and pro-inflammatory cytokines that activate local hepatic immune populations. Even though basal expression of PRRs is much lower in hepatocytes compared to immune cells, such as macrophages (and the liver resident macrophages, Kupffer cells), hepatocytes are among the first cells encountering and detecting hepatotropic viruses [66, 67, 152, 153]. Therefore activation of an innate antiviral response in hepatocytes is fundamental for controlling and clearing hepatotropic viral infections. Single nucleotide polymorphisms in TLR3, RIG-I and the IFN signalling pathway have been associated with chronic hepatotropic infections, underscoring the importance of these pathways in control of hepatic infections [72, 154].

Research on hepatic cell lines, human and mouse primary hepatocytes showed that hepatocytes express several PRRs involved in the innate antiviral activity. Among the TLRs, TLR3, TLR7, and TLR8 were able to induce innate antiviral immunity upon stimulation with specific agonists or hepatotropic infection. TLR3 agonist polyinosinic-polycytidilic acid (poly I:C) is able to activate IFN-β expression in primary mouse and human hepatocytes [155, 156]. According to literature, the human hepatic cell lines HepG2 and Huh7 – widely used as human hepatic model - express lower levels of TLR3 when compared to primary human hepatocytes (PHH). Thus, while PHHs induce IFNs and ISGs expression upon poly I:C stimulation, this is not the case for HepG2 and Huh7 cells [157, 158].

TLR7 expression has been detected in primary human hepatocytes and at lower levels in human hepatic cell lines [159]. Moreover, TLR7 overexpression and activation in Huh7 cells induces an IFN-mediated antiviral state, which, causing the upregulation of several ISGs, is protective against HCV infection [159]. Whether TLR7 is also activated in hepatocytes in viral infection scenarios has not been investigated yet.

Among the different cytosolic PRRs, RLRs and PKR are expressed in both PHHs and human hepatic cell lines and their activation induces an IFN-mediated antiviral response [155, 157, 160]. Although RIG-I and MDA5 share structural and functional features, they differ in their interaction with viral RNA [65, 161]. RIG-I preferentially interacts with the 5'-triphosphate group of dsRNA, while MDA5 has a greater affinity for longer dsRNA structures. In the context of hepatotropic viral infections, RIG-I recognises the 5' region of HBV-derived pre-genomic RNA [162], or the polyuridine motif of the HCV genome at 3' untranslated region [163]. MDA5 has also been shown to be critical in inducing an innate antiviral response upon HBV or HCV infections and to bind the specific regions of viral RNA [164]. In order to achieve persistent infection, viruses are able to subvert host anti-viral activity. Hepatotropic viruses can block the TLR3 and RLR signalling pathways by several mechanisms, including degradation of adaptor proteins such as MAVS (Fig. 1.8) [74, 165–168].

PRR	Expression	Experimental model	Reference
TLR3	PHHs, iPSC-derived hepatocytes	poly I:C	[157, 169]
TLR7	PHHs, Huh7 cell line	HCV infection	[159]
TLR8	Huh7 cell line	HCV infection	[170]
RIG-I	PHHs, Huh7 and HepG2 cell lines	Transfected poly I:C, HCV, HBV infection	[162, 163]
MDA5	Huh7	HCV infection	[164]
PKR	Huh7	poly I:C	[171]

Table 1.4 Major pattern recognition receptors expressed by human hepatocytes involved in recognition of RNA-derived PAMPs.

While different PRRs have shown to be expressed in primary human hepatocytes and hepatic cell lines (the studies were carried out mainly in Huh7 cells), only RLRs, and in particular RIG-I, have been extensively studied, defining their molecular interaction with hepatotropic virus-derived RNA and their function in inducing an IFN-based antiviral activity. It is also worth noting that PRRs expression levels varies between PHHs and hepatic cell lines [157, 158]. Endosomal PRRs (specifically TLR3, TLR7, and TLR8) seem to be almost absent in human hepatic cell lines, while their expression level is higher in PHHs [157, 159]. On the other hand, cytoplasmic PRRs (RLRs and PKR) have comparable levels of expression between hepatic cell lines and PHHs [66, 67].

1.5.3 Liver metabolism and antiviral response

Although immunometabolism has been extensively studied in immune cells, little is known in non-immune cells. Recent research has begun to unravel the interconnection between cellular metabolism and innate antiviral activity in hepatocytes [172–175]. In this section we highlight the major findings in immunometabolism in hepatocytes, focusing on the interplay between glycolysis and innate antiviral response.

Hepatocytes regulate blood glycemia by balancing the uptake and release of glucose [176]. This process occurs through the hepatic regulation of glycolysis, gluconeogenesis (*de novo* glucose synthesis), glycogen synthesis (glycogenesis) and hydrolysis (glycogenolysis), as well as other secondary pathways [177]. Hepatocytes provide glucose to maintain euglycemia and fuel glucose-dependent cell types, such as neurons and red blood cells [178]. Hepatic glucose metabolism is regulated by several mechanisms, including balancing of hormones such as insulin, glucagon, and corticosteroids [177]. Blood glucose enters the hepatocyte through facilitated transport by the glucose transporters (GLUT), with GLUT2 being the most expressed glucose transporter in hepatocytes [179]. Glucose is phosphorylated to become glucose-6-phosphate (G6P) which serves as substrate for glycogenesis or glycolysis. In this second case, the last glycolytic metabolite, pyruvate can be channelled into the mitochondria or used as substrate for lactate production.

As described previously, lactate negatively modulates RLR-dependent antiviral activity by inhibiting MAVS [107]. This mechanism is exploited by HBV for its immune escape [180]. HBV enhances the formation of a ternary complex composed of HK2, Voltage-dependent anion channel 1 (VDAC1) and MAVS. The complex prevents the RLR-MAVS interaction and increases HK2 enzymatic activity. As glycolysis is upregulated, lactate levels are also increased and act as an inhibitory post-translation modifier of MAVS, blunting the antiviral response [107]. Pharmacologically decreased glycolysis showed enhanced antiviral response and decreased HBV virus titres [175]. Moreover, increased glycolysis due to HBV infection is also fundamental for upregulation of the pentose phosphate pathway needed for viral nucleic acid and protein synthesis [181, 182].

Also other hepatotropic viruses – such as HCV and Dengue virus - are able to rig the host metabolism [183]. The HCV non-structural protein 5A increases hepatic HK2 activity and subsequent lactate production (Fig. 1.8) [184]. Whether the mechanism is used for immune escape as described during HBV infection or exclusively to increase the metabolites needed for the viral replication has not been clarified yet.

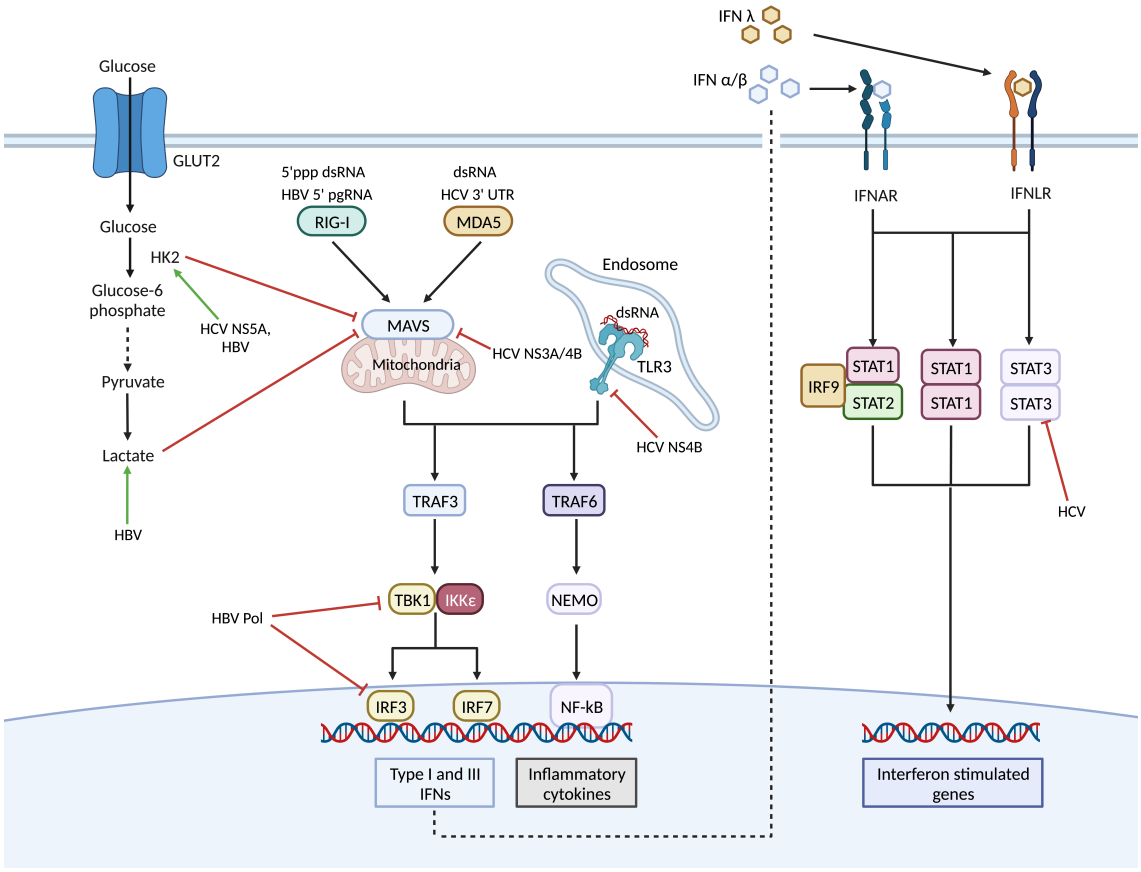

Figure 1.8 Hepatotropic viruses subvert the host antiviral activity by blocking RLR, TLR3, and IFN signaling in human hepatocytes.

Among the different PRRs involved in recognition of pathogen-derived RNA, RLR and TLR3 are critical in hepatocytes. Viruses, such as HCV and HBV have evolved mechanisms to suppress and evade these pathways. Endosomal TLR3 activates downstream signalling through TRIF which can be inhibited by HCV NS4B (non-structural protein 4B). RIG-I and MDA-5 dependent responses can be blunted by the degradation of MAVS by the two HCV proteases NS3A and NS4B. Glucose metabolism is linked to the RLR response; lactate and hexokinase 2 (HK2) inhibit MAVS aggregation and disrupt downstream signalling. This mechanism is exploited by HBV, which increases lactate levels and HK2 activity in order to disrupt the antiviral response. The IFN-based antiviral response is further blocked by hepatotropic viruses that inhibit protein-protein interactions; HBV polymerase blocks the TBK1 - IKKε interaction. Other suppression strategies employed by viruses such as HCV include the ubiquitination and subsequent degradation of signalling proteins such as STAT3, which limits IFN-I signalling.

1.6 Thesis rationale, hypothesis, and objectives

Innate antiviral activity is initiated by recognition of evolutionary conserved pathogen-associated molecular patterns (PAMPs) by host germline encoded pattern recognition receptors (PRRs). Thus, cells expressing PRRs are able to mount an innate antiviral response when in contact with PAMPs, such as viral RNA. Innate immune activity involves significant changes in cellular metabolism. This phenomenon has been extensively described in immune cells. Whether non-immune cells also alter their metabolism upon activation of innate antiviral activity is the focus of this study. Hepatocytes, which present a unique metabolism, express different PRRs and are able to mount an interferon-based innate antiviral response. How innate antiviral response alters cellular metabolism in hepatocytes is still unclear. Here we hypothesise that innate antiviral activity in hepatocytes causes major alterations in glycolysis and mitochondrial metabolism.

1.6.1 Overall objective

To determine the metabolic changes caused by innate antiviral response in human hepatocytes.

1.6.2 Aims

- To identify the PRRs activated in initiation of innate antiviral activity upon stimulation with viral-like PAMPs in different human hepatic models.

- To determine whether innate antiviral activity alters glucose and mitochondrial metabolism in human hepatocytes.

- To determine whether metabolic alterations impact innate antiviral activity in human hepatocytes.

- To investigate potential mechanisms behind metabolic alterations during the antiviral activity in human hepatocytes.

Chapter 2. Materials and methods

2.1 Materials

Target gene	Forward primer (5’ - 3’)	Reverse primer (5’ - 3’)
Hs_Ifnb1	AAACTCATGAGCAGTCTGCA	AGGAGATCTTCAGTTTCGGAGG
Hs_Cxcl10	CCTGCAAGCCAATTTTGTCCA	TGTGGTCCATCCTTGGAAGC
Hs_Isg15	TTTGCCAGTACAGGAGCTTGTG	GGGTGATCTGCGCCTTCA
Hs_Mx1	GGTGGTGGTCCCCAGTAATG	ACCACGTCCACAACCTTGTCT
Hs_Il29	TCCAAGCCCACCACAACTG	TGAGTGACTCTTCCAAGGCGT
Hs_Tnf	TGGCCCAGGCAGTCAGATCA	GTAGGAGACGGCGATGCGGC
Hs_Mavs	GTGCCTACTAGCATGGTGCTC	GACCCAAGGCCCCTATTCT
Hs_Prdx1	CCACGGAGATCATTGCTTTCA	AGGTGTATTGACCCATGCTAGAT
Hs_Prdx2	CGAGCATGGGGAAGTTTGTC	GGCACAAGCTCACTATCCGT
Hs_Prdx4	AGAGGAGTGCCACTTCTACG	GGAAATCTTCGCTTTGCTTAGGT
Hs_Prdx6	GACTCATGGGGCATTCTCTTC	CAAGCTCCCGATTCCTATCATC
Hs_Gsto1	GAACGGCTGGAAGCAATGAAG	TGCCATCCACAGTTTCAGTTT
Hs_Gstp1	CCCTACACCGTGGTCTATTTCC	CAGGAGGCTTTGAGTGAGC
Hs_Rplpo	ACTTGCTGAAAAGGTCAAGGC	CCAAATCCCATATCCTCGTCCG
Hs_Beta actin	ATTGGCAATGAGCGGTTC	TGAAGGTAGTTTCGTGGATGC
Mm_Prdx4	TCCTGTTGCGGACCGAATC	CCACCAGCGTAGAAGTGGC
Mm_Ef1α	GCAAAAACGACCCACCAATG	GGCCTTGGTTCAGGATA
Dengue NS4A	ATCCTCCTATGGTACGCACAAA	CTCCAGTATTATTGAAGCTGCTATCC

Table 2.1 Forward and reverse primer sequences of target genes.

Hs = Homo sapiens, Mm = Mus musculus.

Target gene	Sense strand (5’ - 3’)	Antisense strand (5’ - 3’)
Prdx1	GGGCAGAAGAAUUUAAGAA	UUCUUAAAUUCUUCUGCCC
Prdx2	AGGUGAAGCUGUCGGACUA	UAGUCCGACAGCUUCACCU
Prdx4	CUGGAAAGCUGAAGUAUUU	AAAUACUUCAGCUUUCCAG
Prdx6	CAGAAUUUGCCAAGAGGAA	UUCCUCUUGGCAAAUUCUG
Gsto1	GAGAAAGACUGGCAAGGUU	AACCUUGCCAGUCUUUCUC
Gstp1	CAUCAAUGGCAACGGGAAA	UUUCCCGUUGCCAUUGAUG
Control	UGGUUUACAUGUCGACUAA	UUAGUCGACAUGUAAACCA

Table 2.2 Sense and antisense strand sequences of siRNAs used to knock down target genes.

Target gene	21 bp sense (5’ – 3’)	21 bp antisense (5’ – 3’)
MAVS	GACCTTGGGCAAGGGATTTAT	ATAAATCCCTTGCCCAAGGTC
GFP (control)	GCAAGCTGACCCTGAAGTTCAT	ATGAACTTCAGGGTCAGCTTGC

Table 2.3 Sense and antisense strand sequences used for lentiviral silencing with shRNAs.

Buffer	**Composition**
10X phosphate buffer saline (PBS)	800 g NaCl 20 g KCl 144 Na_2HPO_4 (sodium phosphate monobasic) 24 g KH_2PO_4 (potassium phosphate) Adjust to 10 L in deionized H_2O, pH 7.4
10X tris-buffered saline (TBS)	1.37 M NaCl 250 mM Tris 27 mM KCl pH 7.5
10X running buffer – SDS PAGE	250 mM Tris 1.9 M Glycine 35 mM SDS
1X running buffer SDD-AGE	1X TAE 0.1% SDS
10X transfer buffer – Western blot	250 mM Tris 1.9 M Glycine
1X transfer buffer - Western blot	10 % (v/v) 10X transfer buffer 20 % (v/v) Methanol
Washing buffer - Western blot	TBS/0.1 % (v/v) Tween-20
Washing buffer - ELISA	1X PBS/0.1 % (v/v) Tween-20
RIPA buffer	150 mM NaCl 5 mM EDTA, pH 8.0 50 mM TRIS, pH 8.0 1% NP-40 (IGEPAL CA-630) 0.5% sodium deoxycholate 0.1% SDS

3X loading buffer – SDS PAGE	30 % (v/v) Glycerol 6 % (w/v) SDS 0.3 % (w/v) Bromophenol blue 187.5 mM Tris pH 6.8 150 mM DTT added freshly
Sample buffer mitochondrial isolation	10 mM TRIS-HCl pH 7.5 10 mM KCl 1.5 mM $MgCl_2$ 0.25 mM D-mannitol
1X loading buffer SDD AGE	0.5% TAE 10% glycerol 2% SDS 0.025% bromophenol blue
1X running buffer SDD AGE	1X TAE, 0.1% SDS
Co-immunoprecipitation lysis buffer	50 mM HEPES pH 7.5 200 mM NaCl 1 mM EDTA 10% (v/v) glycerol 1% (v/v) NP-40 (IGEPAL) 10 µl/ml Aprotinin 1 mM PMSF 1 mM sodium orthovanadate

Table 2.4 Buffers used.

Reagent	Supplier	Cat. number
Acetic acid	Sigma-Aldrich	A6283
Acrylamide	National diagnostics	EC-890
Agarose	Sigma-Aldrich	A9539-500G
Ammonium persulfate (APS)	Thermo-Fisher Scientific	17874
Aprotinin	Sigma-Aldrich	A6279
Bovine serum albumin (BSA), Cohn fraction V	Avantor	422371X
Bromophenol blue	Sigma-Aldrich	B8026
Chloroform	Sigma-Aldrich	C2432
Dithiothreitol (DTT)	Sigma-Aldrich	1019777701
D-mannitol	Sigma-Aldrich	M1902
Ethylenediaminetetraacetic acid (EDTA)	Sigma-Aldrich	E5134
Formaldehyde	Sigma-Aldrich	F8775-500ML
Glycerol	Sigma-Aldrich	G5516
Glycine	Thermo-Fisher Scientific	BP381-1
Halt protease phosphatase inhibitor cocktail 100X	Thermo-Fisher Scientific	10137963
Hexadimethrine bromide	Sigma-Aldrich	H9268
High-Capacity cDNA Reverse Transcription Kit	Applied Biosystems	4368814
Isopropanol	Thermo-Fisher Scientific	BP2618-500
Marvel Original Dried Skimmed Milk	Marvel	N/A
Methanol	TCD stores	MET001
MitoSOX Red	Thermo-Fisher Scientific	M36008
Paraformaldehyde	Alfa aesar	J19943

PowerUp™ SYBR™ Green Master Mix	Applied Biosystems	A25742
NP-40 (IGEPAL9	Sigma-Aldrich	I3021
Phenylmethylsulphonyl fluoride (PMSF)	Sigma-Aldrich	T8830
Potassium chloride (KCl)	Sigma-Aldrich	P9541
Protein G Sepharose	Cytiva	17061801
PVDF membrane	Bio-Rad	1620177
Sodium chlroride (NaCl)	Thermo-Fisher Scientific	S3014
Sodium deoxycholate	Sigma-Aldrich	D6750
Sodium dodecyl sulphate	Sigma-Aldrich	L4390
Sodium orthovanadate	Sigma-Aldrich	S6508
Spectra™ Multicolor Broad Range Protein Ladder	Thermo-Fisher Scientific	26623
SYBR™ Safe DNA Gel Stain	Invitrogen	S33102
Sulfuric Acid	Sigma-Aldrich	07208
TMRM	Thermo-Fisher Scientific	T668
Tris base	Thermo-Fisher Scientific	BP152-1
Tris hydrochloride	Sigma-Aldrich	T5941
Triton X	Sigma-Aldrich	X100-500ML
TRIzol™ Reagent	Invitrogen	15596018
Tween-20	Sigma-Aldrich	P1379-500ML
Wizard® SV Gel and PCR Clean-Up System	Promega	A9281
1-Step Ultra TMB-ELISA	Thermo-Fisher Scientific	34029

Table 2.5 General reagents used.

Reagent	Supplier	Cat. number
Antimycin A	Sigma-Aldrich	A8674
Blasticidin	Invivogen	Ant-bl-1
Distilled, sterile, nuclease-free water	Gibco	10977-035
Dimethyl Sulfoxide (DMSO)	Sigma-Aldrich	D2660-100ML
DMEM	Gibco	61965059
Ethanol	Honeywell	E7023-500ML
Carbonyl cyanide-p-trifluoromethoxyphenylhydrazone (FCCP)	Sigma-Aldrich	C2920
Foetal Bovine Serum (FBS)	Gibco	10270106
Human interferon beta	PBL	11415-1
Hepes buffer	Gibco	15630056
Lipofectamine 2000	Invitrogen	11668019
Lipofectamine RNAiMax	Invitrogen	13778030
Oligomycin	Sigma-Aldrich	495455
N-acetyl cysteine	Sigma-Aldrich	A7250
Normocin	Invivogen	ant-nr-1
Opti-MEM reduced serum medium	Gibco	31985062
Penicillin-Streptomycin	Gibco	15070-063
Phosphate buffered saline (PBS)	Gibco	14190094
Poly(I:C)	Invivogen	tlrl-pic
Puromycin dihydrochloride	Gibco	A1113803
Rotenone	Sigma-Aldrich	R-8875
Trypsin-EDTA solution	Sigma-Aldrich	t3924-500ml
Zeocin	Invivogen	Ant-zn-1
5’ triphosphate hairpin RNA	Invivogen	Tlr-hprna-100

Table 2.6 Cell culture reagents.

Cell line	Supplier	Cat. number
HepG2 cell line	ATCC	ATCC-HB8065
Huh7 cell line	Kind gift from Dr. Hante	
HEK-Blue type I IFN cells	Invivogen, kind gift from Prof. Bowie	Hkb-ifnab
HEK293T cells	Kind gift from Prof. Bowie	

Table 2. 7 Cell lines used as experimental models.

Reagent	Supplier	Cat. number
Human IFN-β ELISA	BioTechne	DY814-05
Human IL-29 ELISA	BioTechne	DY7246
Anti-human β actin	Sigma-Aldrich	A5136
Anti-cMyC	Merck	M5546
Anti-human GAPDH	Santa Cruz Biotechnology	sc-47724
Anti-human MAVS	Cell signalling Technology	3993
Anti-human PRDX4	Abcam	Ab59542

Table 2. 8 ELISA and antibodies used in the thesis.

2.2 Methods

2.2.1 Cell culture

Cell culture was carried out according to strict standard operating procedures (SOPs) generated in the O'Farrelly lab based on best practice guidelines [185]. Cell culture was carried out in sterile conditions using laminar air flow hoods and sterile or autoclaved materials and reagents. HepG2, Huh7, and HEK293T cells were grown in Dulbecco's modified Eagle's medium (DMEM) supplemented with 10% (v/v) foetal bovine serum (FBS), 100 Units/mL penicillin, and 100 µg/mL streptomycin. HEK-blue IFN-α/β were grown in DMEM supplemented with 10% (v/v) heat inactivated FBS, 50 U/mL penicillin, 50 µg/mL streptomycin, and 100 µg/mL normocin. For the test medium 30 µg/mL blasticidin and 100 µg/mL zeocin were added to the growth medium.

2.2.2 Differentiation of iPSC-derived hepatocytes

iPSCs were differentiated into iPSC-derived hepatocytes according to an established protocol [186]. The human embryonic stem cell line H9 (WA09, WiCell) and induced pluripotent stem cells obtained from skin biopsies were differentiated into iPSC-derived hepatocytes through 4 different stages (Stemnovate), pluripotent stem cells, definitive endoderm, hepatic progenitors, and hepatocyte-like cells (HLCs) (Stemnovate). Stem cells were cultured on Lamina 521 (5 µg/ml) (Biolamina) in mTESR until reaching 80% confluency. One day prior to differentiation, cells were seeded and treated overnight with 10 µM Rock Inhibitor. The endoderm stage was induced by RPMI 1x supplements with 2% B27, 100 ng/ml Activin A, and 50 ng/ml Wnt3A for 3 days. Subsequently, for the Hepatoblast differentiation, cells were cultured in KO DMEM, serum replacement, 0.5% Glutamax, 1% non-essential amino acids, 0.2% β-mercaptoethanol, and 1% DMSO for 5 days and it was renewed every second day. For the differentiation in hepatocyte-like cells, cells were cultured for further 10 days in HepatoZYME containing 1% Glutamax, 20 ng/ml Hepatocyte Growth Factor, 10 ng/ml oncostatin, and 10 µM hydrocortisone. Media was renewed every second day. Cells were collected on the last day of each stage

and stained for specific markers in order to confirm the differentiation process. Expression of the transcriptional factors FOX2A and GATA4 were used as markers for the definitive endoderm stage. Hepatic progenitors were positive for alpha-fetoprotein (AFP) and hepatic nuclear factor 4-alpha (HNF4A) Albumin and E-cadherin were used to confirm the mature hepatocyte-like cell stage.

2.2.3 Cell viability and enumeration of cells

In order to count cells and assess cell viability, Trypan blue exclusion dye was used. Briefly, cells were diluted in Trypan blue at 1:20. Carefully, 10µl of the cell/Trypan blue solution was mounted to a Neubauer Haemocytometer and visualised using a fluorescence microscope. The numbers of cells in four grid sections were counted and an average for the number of cells in a 0.1mm x 1mm x 1mm section was calculated. Cells touching the top and right borders of each grid section were not counted to avoid counting the same cells twice. The average number of cells in one section is multiplied by 10^4 then by the dilution factor to give the number of cells per ml. Dead cells were unable to exclude the Trypan blue and therefore easily excluded in order to obtain a viable cell count.

2.2.4 Cell plating and stimulation

Cells were allowed to grow to 70-80 % confluency before being either being split or plated out. In order to plate or split the cells, the medium was removed and cells were washed with PBS. Trypsin-EDTA was added and the flask was incubated for 10 minutes at 37°C. Cells were subsequently centrifuged at 400 g for 5 minutes and resuspended in 2 ml of media, before either being counted or split into new T75 flasks. Cells were plated in 6, 12, 24 or 96 well-plate. Cells were left for overnight to adhere. Before adding the stimulation, cells were replaced with fresh media.

2.2.5 DNA and RNA transfection

Small interfering RNA, high molecular poly I:C, 5’ triphosphate hairpin RNA (3p-hRNA), and DNA were transfected using Lipofectamine 2000. 1 µL of Lipofectamine was used

for every μL of DNA/RNA. The mix was prepared starting from 2 tubes, the first one containing 1 μL of Lipofectamine each mL of media in 50 μL of serum-free media (OptiMem) and the second one containing the RNA in 50 μL of serum-free media. The 2 tubes were left for 5 minutes at room temperature. After, the content of the second tube was transferred into the first tube and it was left for at least 20 min to form the complex RNA-Lipofectamine. The RNA-lipofectamine was subsequently added to the cells with fresh media.

In order to achieve the knock-down of target genes, cells were transfected with 20 μM of the specific siRNA. Cells were left between 48 and 72h in order to achieve the downregulation, which was confirmed either by qPCR or western blot.

2.2.6 RNA extraction

Total RNA was extracted using a phenol-chloroform extraction protocol. The growth media was removed and 0.5 or 1 mL of TriZol was added every well in a 24 or 12 well plate respectively. The content was collected in a 1.5 mL Eppendorf, 200 μL of chloroform per 1 mL of TriZol was added. The mix was shacked for 15 seconds, then incubated for 2-3 minutes at room temperature. The samples were then centrifuged for 15 minutes at 12.000 g 4°C. At this point, the samples had separated into 3 phases: an upper aqueous phase containing RNA, an interphase containing DNA and an organic phase containing proteins and lipids. 400 μL of the upper phase for each mL of TriZol used (200 μl if starting with 500 μl of TriZol) were transferred into a new tube containing 500 μL of isopropanol/2-propanol. Samples were then vortexed for 30 seconds and incubated at -20°C for 30 mins. After incubation, samples were centrifuged at 12.000 g for 10 mins at 4°C. The supernatant was discarded without disturbing the white gel-like RNA pellet. This was resuspended in 1mL of 75% ethanol, prepared with nuclease-free water. The samples were centrifuged at 8.000 x g for 10 minutes at 4°C. The supernatant was removed and a second ethanol wash performed. The remaining pellet was air dried for 7 minutes to evaporate residual ethanol before being dissolved in 35μL nuclease-free water. Samples were then incubated at 56°C for 5 mins to dissolve RNA and stored at -80°C. RNA quantity was determined by measurement of absorbance at 260nm using a

NanoDrop spectrophotometer. Absorbance 260/280 nm and 260/230 nm ratios were checked to assess presence of non-nucleic acid contaminants. RNA quality was evaluated by 1.5% agarose gel electrophoresis with SYBR SAFE staining, where the presence of 28S and 18S ribosomal RNAs as discrete bands, with minimal smearing indicative of RNA degradation, or high molecular weight products, indicative of DNA contamination, was assessed. In case of genomic DNA contamination, the sample was discarded.

2.2.7 cDNA synthesis

1000 ng of RNA per samples was reverse transcribed into cDNA using High-Capacity cDNA Reverse Transcription Kit by Termo Fisher Scientific according to manufacturer's instruction. 1000 ng of RNA was added to the master mix to complete the mixture given in table 2.1, dH_2O was added to reach a final volume of 20 μL.

Reagent	**Volume per sample**
10X RT Buffer	2 μL
10X Random Primers	2 μL
25X dNTPs	0.8 μL
Multiscribe reverse transcriptase enzyme	1 μL

Table 2.9 complementary DNA (cDNA) synthesis buffer composition.

2.2.8 Quantitative PCR

PowerUp SYBR Green Master Mix and StepOnePlus Real-time PCR System with StepOne Software v2.3 was used for experiments. A 10 μL reaction volume contained 8 μL pre-made qPCR master mix, primers, nuclease-free water, and 2 μL of cDNA. A non-template control was included in each gene assay to detect molecular contamination. All reactions were carried out in triplicate. The thermocycling program was: 20 sec at 95°C, 40 cycles of 95°C for 30 sec and annealing temperature of 60° for 30 sec, then 95°C for 15 sec, 60°C for 1 min and finally 95°C for 15 sec. Relative expression ($2^{-\Delta\Delta CT}$) was calculated

from the cycle threshold (CT) values for each sample and gene of interest. RPLPO was used as housekeeper gene in order to calculate the relative expression. ΔCT value of each gene of interest was calculated according to the following formula:

$$\Delta CT(gene\ of\ interest) = CT(gene\ of\ interest) - CT\ (housekeeping\ gene)$$

Then ΔΔCT is determined by the difference between the single ΔCTs, treated against the internal experimental control. And subsequently using the formula $2^{-\Delta\Delta CT}$ it is possible to calculate the fold change of the gene of interest relative to its expression in the control condition

2.2.9 Type I IFN Reporter HEK293 assay

Hek-Blue IFN-α/β cells were a kind gift from Prof. Andrew Bowie's lab. The cells were cultured for at least 3 passages after thawing in non-selective media (DMEM + 10% FBS, 50 U/mL penicillin, 50 mg/mL streptomycin, and 100 mg/ml normocin). The test media was made up of DMEM, 10% heat-inactivated FBS, 50 U/mL penicillin, 50 mg/mL streptomycin, 100 mg/ml Normocin, 30 mg/mL blasticidin, and 100 mg/mL zeocin. The cells are specifically designed to monitor the activation of JAK-STAT pathway induced by type I Interferon. The cells express a secreted embryonic alkaline phosphatase (SEAP) under the control of the ISG54 promoter, which is an ISG. Upon activation of the JAK-STAT pathway by the presence of type I IFN in the media, SEAP is expressed. IFN levels can be quantitively determined by incubation with QUANTI-blue solution, which contains the SEAP substrate.

20 mL of each sample was added into a flat-bottom 96 well plate in triplicate. A titration curve using a starting concentration of 1000 IU/mL of IFN-β a serial dilution 1:2 was done in triplicate for each plate in order to determine the type I IFN contained in each sample. The range was from 0 IU/mL which was made from test media up to 1000 IU/mL. In each well 180 mL of a HEK-blue suspension (280.000 cells/mL, circa 50.000 cells/well) was added and the plate was incubated overnight at 37°C, 5% CO_2. The following day 20 mL of the HEK-blue conditioned media was transferred into a flat-bottom 96 well plate and 180 mL of QUANTI-blue was added to each well. The plate was incubated at 37°C for

15/30 min and the plate was read at 620 nm wavelength. From this, the levels of type I IFN secreted by stimulated cells could be determined.

2.2.10 ELISA

All ELISAs were carried out according to the manufacturer's instructions. ELISA plates were coated overnight at room temperature with capture antibody (accordingly diluted in PBS, 50 μl/well). The next day, after blocking for 1h at room temperature (1% bovine serum albumin, BSA in PBS, 50 μl/well), diluted cell supernatants (diluted 1:5 in PBS 1% BSA, 50 μl/well) and specific cytokine standard curve were added to each plate in technical duplicate for an overnight at +4°C. The next day, detection antibody (accordingly diluted in PBS 1% BSA, 50 μl/well) was added for 2h at room temperature. Streptavidin-HRP solution (diluted according to the manufacturer's instructions in PBS 1% BSA, 50 μl/well) was added for 20 min, before the last step, consisting in addition of the substrate TMB and stopping solution (1 M H_2SO_4, 25 μl/well). Between each passage ELISA plates were washed 4 times in washing buffer (PBS + 0.1% Tween-20). Absorbance at 450 nm was quantified using a plate reader. Corrected absorbance values were calculated by subtracting the background absorbance (540 nm). Cytokine concentrations were subsequently obtained by extrapolation from a standard curve plotted in Excel.

2.2.11 Western blot

2.2.11.1 Cell lysis and protein denaturation

Supernatants were collected, cells were washed twice with warmed PBS and detached by treatment with trypsin for 10 minutes.

2.2.11.2 SDS-PAGE

Cell lysis and protein solubilization was achieved incubating cell pellets with RIPA buffer supplemented with protease and phosphatase inhibitors for 30 to 60 min in ice. Subsequently the samples were centrifuged at 12.000 g for 15 min 4°C. The supernatant obtained was transferred in new labelled tubes and protein content was determined by

BCA assay. 20 μg of protein for each sample were mixed with SDS-PAGE loading buffer 3X, boiled at 95°C for 5 min and subsequently loaded in the gel.

SDS polyacrylamide gel electrophoresis was used to resolve proteins by molecular weight. 20 μg of proteins were mixed with the 6X loading buffer containing SDS and the reducing agent DTT, to achieve a final concentration of 1% SDS. Samples were boiled at 95°C for 10 mins prior to loading into a 5% stacking gel. The percentage resolving gel depended on the molecular weight of the given protein. Gel compositions are given in table 2.10. The Bio-Rad gel running system was used, whereby the gels were secured in electrodes which were placed into a tetra cell and covered with SDS-PAGE running buffer. Samples were passed through the stacking at 80V, once reached resolving gel, samples were run at 100 V using the molecular weight marker as a reference.

Reagents for two gels	8 % resolving gel	12 % resolving gel	15 % resolving gel	Stacking gel
ultrapure water	9.3 ml	6.6 ml	4.6 ml	5.5 ml
30 % acrylamide	5.3 ml	8 ml	10 ml	1.3 ml
1.5 M Tris pH 8.8	5 ml	5 ml	5 ml	-
1 M Tris pH 6.8	-	-	-	1 ml
10 % SDS	200 µl	200 µl	200 µl	80 µl
10 % APS	200 µl	200 µl	200 µl	80 µl
TEMED	12 µl	8 µl	8 µl	8 µl

Table 2.10 Resolving and stacking gel composition.

2.2.11.3 MAVS aggregation assay

Cellular pellets were resuspended in mitochondrial isolation buffer (as described in Table 2.4) supplemented with protease and phosphatase inhibitors. Cells were lysed on ice by passing through a 20G needle for at least 5 minutes and not more than 10 min, in ice. The cell extract was centrifuged 1.000 g for 5 min 4°C. The supernatant obtained was transferred to a new pre-chilled tube and centrifuged at 10.000 g for 10 min 4°C. The supernatant was transferred to a new tube, containing the cytoplasmatic fraction.

While the pellet is the mitochondria-enriched fraction, it was resuspended in 50 μL of buffer A and its protein content is determined by BCA assay. The samples can be stored at -80°C. For each sample, 30 μg of protein was mixed with 4X of the loading buffer and loaded on a vertical 1.5% agarose gel (1.5% agarose in 1X TAE). After electrophoresis in the running buffer (1x TAE + 0.1% SDS) for 40 min at 100 V on ice, the proteins were transferred on PVDF membrane as described below.

2.2.11.4 Electrophoretic transfer of proteins

The Bio-Rad wet transfer system was used for the electrophoretic transfer of proteins. A gel and membrane sandwich was assembled: a sponge soaked in buffer was placed onto the cathode side of the sandwich cassette, followed by 2 soaked pieces of rectangular filter paper, the gel, a PVDF membrane (activated in methanol for 30 second), 2 pieces of filter paper and a sponge. The cassette was closed and firmly wedged into the transfer cell, which was filled with transfer buffer. The transfer was run in an ice box at 200 mA per box for 2.5 hrs, or at 40 mA overnight.

2.2.11.5 Incubation with antibody and protein visualisation

Following transfer, the PVDF membrane was removed from the transfer cell and incubated in milk powder (5% in TBST) for 1 hour to prevent non-specific antibody binding to the membrane. The membrane was then washed three times for 10 mins each in TBST and incubated in primary antibody (diluted in TBST + 5% BSA and 0.05% sodium azide) rolling overnight at 4°C. The following morning, the membrane was washed three times for 10 mins each in TBST. Prior to visualisation, the membrane was soaked in WesternBright ECL Spray for 2 min. Protein visualisation took place on a ChemiDoc MP Imaging System, and both chemiluminescent and white light images were taken.

2.2.12 Co-immunoprecipitation

HEK293T cells were seeded in 15 cm petri dishes (3 x 10^6 cells/dish, in 20 ml medium) for overnight. The next day cells were transfected with 10 μg/dish for 24h. The following day cells were treated accordingly to the experimental design (in our case with transfected poly I:C 1 μg/ml or lipofectamine as vehicle control for 6h). Media was removed and cells were harvested in PBS, and centrifuged for 5 min at 400 g 4°C and PBS was discarded. The cell pellets were lysed in 400 μl of co-immunoprecipitation lysis buffer for 30 min on ice (aprotinin, PMSF, and sodium orthovanadate were added freshly). During the cell lysis, the solution containing the primary antibody and the protein G-sepharose beads are prepared. In this case, an equal amount of protein G-sepharose beads and Co-IP lysis buffer are added to an eppendorf (e.g. 600 μl), constituting the 50% protein G mixture. This solution can be stored in the fridge for at least one month. After the lysis, the samples were centrifuged for 10 min at 16.000 g. The pellet is composed of membranes and cell debris. 340 μl of lysate is added to 30 μl of 50% protein G mixture, with 2 μg of primary antibody (in our case cMyc since we overexpressed cMyc-tagged PRDX4) and left to roll overnight at 4°C. For the input, 50 μl of lysate is added to 30 μl of 3X loading buffer, boiled for 5 minutes at 95°C and stored at -20°C. The next day, the tubes left to roll overnight, are centrifuged at 1000 g for 3 min. The pellet is composed of the protein G sepharose complexed with the primary antibody. The pellet is washed at least 3 times with Co-IP lysis buffer, adding each time 500 μl of the buffer and centrifuging for 3 minutes 1000 g at 4°C. After the final wash, all supernatant is removed using a long tip, the pellet is resuspended in 30 μl of 3X sample buffer and boiled at 95°C for 5 minutes. The samples are then frozen or analysed by SDS-PAGE in parallel with the input samples.

2.2.13 Gene silencing using pLKO.1 lentiviral system

pLKO.1 is a replication incompetent lentiviral vector used for expression of short-hairpin RNAs. pLKO.1 was introduced into the cells by a lentiviral system. Once introduced, the puromycin resistant marker encoded in pLKO.1 was used for stable selection.

2.2.13.1 Cloning oligos into pLKO.1

Using the RNAi consortium library [187], 21-mers DNA oligos for cloning into pLKO.1 were chosen. The oligos were first resuspended at a final concentration of 20 μM and were incubated for 10 minutes at 70° with the following mix:

- 5 μl forward oligo
- 5 μl reverse oligo
- 5 μl 10X NEB buffer
- 35 μl ddH_2O

The mix was left to reach room temperature overnight. The next day, the pLKO.1 plasmid was digested with AgeI Mix:

- 6 μg of pLKO.1 vector
- 5 μl 10X NEB buffer
- 1 μl AgeI
- ddH_2O to reach a final volume of 50 μl

The mix was incubated at 37°C for 2h. And it was subsequently digested with EcoRI:

- 30 μl of pLKO.1 vector previously digested with AgeI
- 5 μl 10X NEB buffer
- 1 μl EcoRI
- 14 μl ddH_2O

The mix was incubated at 37°C for 2h. At this point, the digested DNA was run on a 0.8 % agarose gel and the 7 kilobases band was cut out and purified from the agarose gel. The AgeI and EcoRI digested pLKO.1 vector was used for ligation with the annealed oligos. A standard T4 ligation was used:

- 2 μl of annealed oligos
- 20 ng of digested pLKO.1 vector
- 2 μl 10X NEB T4 DNA ligase buffer

- 1 μl NEB T4 DNA ligase
- ddH_2O to reach a final volume of 20 μl

The mix was incubated for an overnight at 16°C. 2μl of the ligation mix was used to transform DH5α cells which were plated on an agar LB plate. Colonies were selected with 100 μg/ml of ampicillin overnight at 37°C. 3 different colonies were chosen and amplified by growing in 100 μg/ml ampicillin LB (100 ml) at 37°C in agitation overnight. Bacteria were pelleted and plasmids were recovered through maxiprep. Plasmids were sequenced in order to ensure the correct ligation of the oligos into the pLKO.1 plasmid.

2.2.13.2 Producing lentiviral particles

HEK293T cells were plated in 10 cm^2 plates (3 x 10^6 cells/plate) and left overnight at 37°C 5% CO_2 to attach. The next day, HEK293T cells were transfected with 1 μg of pLKO.1 plasmid containing the oligos, 750 ng of psPAX2 packaging plasmid, and 250 ng pMD2.G envelope plasmid. The following day supernatants were collected and centrifuged at 300 G for 5 minutes to get rid of cell debris. The cleared supernatant was kept at 4°C. The cells were topped with fresh media (DMEM + 10% FBS + 1% pen/strep) and left for 24h at 37°C 5% CO_2. The following day, supernatants were collected, centrifuged at 300 G for 5 minutes to get rid of the cell debris and pulled together with the supernatant collected the previous days. Supernatants were filtered through a 0.45 μm, aliquoted and frozen at -80°C.

2.2.13.3 Infecting target cells with the lentivirus

Cells were plated in a 6 well plate and left to attach overnight at 37°C 5% CO_2. The next day 1 ml of fresh media (containing a final concentration of 8 μg/ml hexadimethrine bromide) and 1 ml of lentiviral particles were added to the cells. The plate was centrifuged at 500 G for 40 minutes in order to spin down the lentiviral particles and help the infection. Cells were left for 48h at 37°C 5% CO_2. Media was replaced and fresh media containing puromycin (5 μg/ml of puromycin for selection in Huh7 cells, 10 μg/ml for selection in HepG2 cells) was used for the selection. One well was non transfected

with the lentivirus and was used as negative control for the selection since cells were not resistant to puromycin. After 48h of incubation with puromycin, cells were expanded and kept in selective media. The knock-down efficiency was by western blot.

2.2.14 Real time cell metabolic analysis with Seahorse XF 96

Mito Stress test was used to determine the OCR and ECAR levels of HepG2 and Huh7 cells. 20.000 or 10.000 cells/well (HepG2 and Huh7 respectively) were plated in a Seahorse 96 well plate and let overnight at 24h at 37°C, 5% CO_2. The next day cells were stimulated for 4 or 24h with transfected poly I:C (1 μg/ml for HepG2 and 5 μg/ml for Huh7 cells). After the stimulation, media was removed and SeahorseXF media was added to the cells (phenol-free DMEM + 10 mM glucose, 2 mM glutamine, and 1 mM pyruvate). The plate was incubated in a 37°C, no-CO_2 incubator for 1h before the assay. Oligomycin (final concentration in the well 2μM), FCCP (final concentration 1 μM) , and Rotenone/Antimycin A (final concentration 1 μM each) were used to determine the different parameters as shown in figure 2.1. The measurements obtained were normalized by number of cells through crystal violet assay. After the assay, media was removed, cells were washed with PBS and fixed with 50 μl/well of paraformaldehyde 2% (diluted in PBS) for 20 min. Each well was washed twice with PBS and 50 μl of 0.1% crystal violet was added for 30 min. Subsequently, wells were washed at least 3 times to remove excess of crystal violet and let to dry overnight. The following day 50 μl of 1% Triton X was added to each well for at least 30 min. The solution from each well of the Seahorse plate was pipetted into a corresponding 96 well plate and the absorbances were read at 595 nm. The obtained values were obtained to normalise the readings from the Seahorse XF and thus took in account possible variations due to the stimulations.

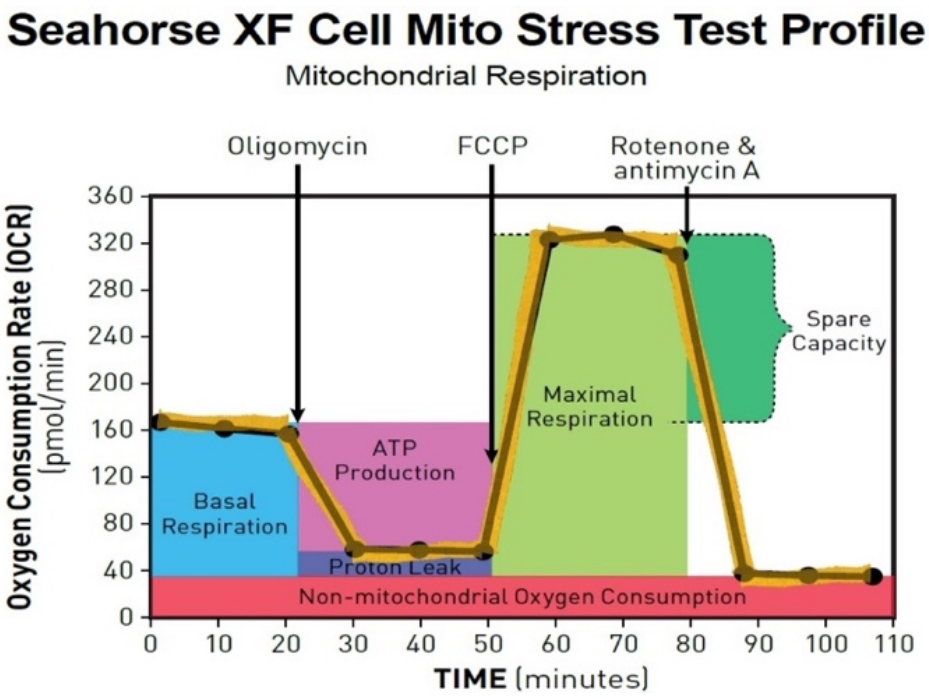

	Experimental Group #1						
	Measurement	Assay Well - A1 OCR (pmol/min)	Assay Well - A2 OCR (pmol/min)	Assay Well - A3 OCR (pmol/min)	Assay Well - A4 OCR (pmol/min)	Average OCR	
Baseline OCR	1	170.02	172.80	169.96	175.99	172.19	
	2	165.36	163.62	167.00	166.42	165.60	
	3	160.50	158.25	159.44	161.75	159.98	<< Last rate measurement before 1st injection
Injection 1 - Oligomycin	4	65.44	53.05	61.53	59.22	59.81	
	5	61.80	49.44	59.62	56.94	56.95	
	6	61.93	49.55	59.06	56.04	56.65	<< Minimum rate measurement after Oligo injection
Injection 2 - FCCP	7	319.58	310.94	312.59	315.98	314.77	
	8	327.95	320.32	325.77	330.73	326.19	<< Maximum rate measurement after FCCP Injection
	9	297.17	292.30	301.35	299.68	297.63	
Injection 3 - Rot/AA	10	51.77	34.62	44.99	39.45	42.71	
	11	49.28	33.24	44.13	39.05	41.42	
	12	47.03	31.80	42.66	39.20	40.17	<< Minimum after Rot/AA Injection (Non-Mitochondrial Oxygen Consumption)

Parameter Value	Equation
Non-mitochondrial Oxygen Consumption	Minimum rate measurement after Rotenone/antimycin A injection
Basal Respiration	(Last rate measurement before first injection) – (Non-Mitochondrial Respiration Rate)
Maximal Respiration	(Maximum rate measurement after FCCP injection) – (Non-Mitochondrial Respiration)
H+ (Proton) Leak	(Minimum rate measurement after Oligomycin injection) – (Non-Mitochondrial Respiration
ATP Production	(Last rate measurement before Oligomycin injection) – (Minimum rate measurement after Oligomycin injection)
Spare Respiratory Capacity	(Maximal Respiration) – (Basal Respiration)
Spare Respiratory Capacity as a %	(Maximal Respiration) / (Basal Respiration) × 100
Acute Response	(Last rate measurement before oligomycin Injection) – (Last rate measurement before acute injection)
Coupling Efficiency	ATP Production Rate) / (Basal Respiration Rate) × 100

Figure 2.1 Mitochondrial stress test using Seahorse XF.

Example of a Mitochondrial stress test (Mitostress test) with a guide for the calculations to determine the different parameters.

2.2.15 Confocal microscopy

Cells were plated on IBIDI 35 μ dishes with a glass bottom of 170 μm height. Cells let to adhere overnight. The net day cells were stimulated accordingly and subsequently stained as described below. Dishes were imaged on Leica SP8 STED microscope using the oil immersion 63x/NA1.4 objective.

2.2.15.1 TMRM staining

After stimulation, cells were washed twice with 37°C warm PBS. Subsequently cells were incubated for 20 minutes with TMRM 200 nM and 1 μg/ml of Hoechst 33342 (for nuclear staining) in PBS with calcium and magnesium. After the staining, cells were washed at least twice in PBS and fresh media containing 5 nM TMRM was added before imaging. The excitation and emission wavelength used were 560 nm and 600 nm respectively.

2.2.15.2 MitoSOX red staining

After stimulation, cells were washed three times with 37°C warm PBS. Subsequently cells were incubated for 20 minutes with MitoSOX red 2.5 μM and 1 μg/ml of Hoechst 33342 (for nuclear staining) in PBS with calcium and magnesium. After the staining, cells were washed at least twice in PBS and fresh media was added before imaging. The excitation and emission wavelength used were 510 nm and 580 nm respectively.

2.2.15.3 Analysis with Cell profiler

Following imaging acquisition, data was analysed using a pipeline in Cell Profiler. The red colour was first converted into a grey scale output image based on the intensity of TMRM or MitoSOX red staining. Mitochondria were identified by the software setting the minimum and maximum diameter of objects in the range of 5 to 100 pixels. Subsequently the values were calculated by the software and used for measuring mitochondrial perimeter and area (for TMRM staining). While intensity of the signal was

used for determining mitochondrial polarization (TMRM staining) or mitochondrial superoxide relative production (MitoSOX red).

2.2.16 Dengue virus production, quantification, and infection

Confluent monolayers of Aedes Albopictus mosquitos cells (C6/36) were infected with dengue virus serotype 2 strain New Guinea C (DENV NGC) at a multiplicity of infection (MOI) of 0.05. The cells were incubated with the virus for 1h in a minimal volume of serum free DMEM, at 28°C 5% CO_2. After incubation, cells were washed once with PBS and DMEM with 2% FBS was added. After 7 days, cell media was collected, centrifuged at 500 g for 5 min. Supernatant was subsequently collected and centrifuged at 2000 g for 8 minutes through an Amicon Ultra-15 centrifuge Filter Unit. The supernatant containing the virus was further concentrated by ultracentrifugation in a sucrose gradient (20% sucrose). The supernatant was ultracentrifuged for 2 hours at 134.000 g, 10°C in a Sorvall WX 100 ultracentrifuge with brake set to 1. The pellet obtained was resuspended in DMEM supplemented with 0.1% BSA, aliquoted and stored at -80°C. Viral titres were determined by infecting Vero monkey kidney cells with a 10-fold serial dilution and analysed by fluorescence activated cell sorting (FACS) 24h post infection. Viral titres were expressed in IU/ml (infection units). Dengue virus production and quantification were done by Dr. Enrico Palermo at Pasteur Institute, Rome.

For viral infection experiments, before infection cells were collected from a spare well and counted in order to calculate the amount of µl needed from the viral stock. Cells were incubated with virus containing DMEM without FBS or pen/strep for 1h at 37°C. Huh7 were infected at a MOI of 5. After 1h of infection, medium was discarded, and cells were incubated with complete medium (DMEM + 10% FBS + 1% pen/strep) for 24h.

2.2.17 In vivo viral infection with LCMV strain 13

Wild type and IFNAR1 knock out C57BL/6J mice were obtained from The Jackson Laboratory. Mice were bred and maintained under specific pathogen-free (SPF)

conditions at the Institute for Molecular Biotechnology of the Austrian Academy of Sciences, Vienna, Austria. Male mice 8 to 12 weeks old were used within the experiments.

Lymphocytic choriomeningitis virus (LCMV) was grown in BHK-21 cells (baby hamster kidney cells) and titre was determined in a focus forming assay using Vero cells. Mice were intravenously infected with 2 x 10^6 focus forming units (FFU) of LCMV. Viral infection was carried by Dr. Henrique Colaço. Livers were collected, snap frozen in liquid nitrogen and stored at -80°C. Subsequently, RNA from liver samples were obtained using TriZol RNA extraction and RT-qPCR was performed by Zsofia Keszei at Centre for Molecular Medicine (Vienna, Austria).

2.2.18 Statistical analysis

Data were expressed as mean ± standard error of mean (S.E.M.). GraphPad Prism v9 was used for statistical analysis. Data were tested for normality to assess whether parametric tests could be applied or not with Shapiro-Wilk test. Then, different tests were applied depending on the experimental design and if the samples were paired or unpaired. P values were calculated using two-tailed Student's t test for pairwise comparisons of variables and one-way analysis of variance (ANOVA) for multiple comparison of variables. Sidak's (parametric) or Dunnett's (non-parametric) multiple comparison test were used as a post-test when performing ANOVA. In each figure the number of independent experiments is indicated with n = number of biological replicates.

Chapter 3: Innate antiviral response in iPSC-derived hepatocytes and human hepatic cell lines

3.1 Abstract

Hepatocytes are targeted by hepatotropic viruses which trigger antiviral activity. This is possible since hepatocytes are equipped with different receptors enabling the detection of pathogens and activation of the specific pathways. PRRs such as TLRs and RLRs are expressed by hepatocytes and are critical for mounting antiviral responses.

Because of the difficulty and elevated costs in obtaining and culturing ex vivo human primary hepatocytes, surrogates systems based on human hepatoma cell lines are widely used. Whether cell lines such as HepG2 and Huh7 reflect the primary hepatocyte function, such as the complex cellular metabolism, is still topic of discussion. iPSC-derived hepatocytes are also used in order to study how hepatocytes respond to viral pathogens. In this chapter we sought to determine which PRRs are used by HepG2, Huh7, and iPSC-derived hepatocytes when stimulated by viral-like RNA ligands dsRNA poly I:C and 5'-triphosphate short-hairpin RNA.

3.2 Introduction

Hepatocytes have widely been studied for their crucial role in modulating the whole-body metabolism [137]. Diet derived macronutrients (carbohydrates, lipids, and amino acids) are absorbed in the GI tract and reach the liver, where they are up taken and processed by hepatocytes. Therefore, the different macromolecules are stored and used by hepatocytes or redistributed to extrahepatic tissues. This process is tightly regulated by hormonal and neuronal signals.

Hepatocytes are also target of several pathogenic viruses, among others hepatitis A-E. Different PRRs are expressed by hepatocytes conferring the ability to mount an antiviral activity when stimulated with the cognate agonists. More specifically RLRs, TLR3, and

PKR have been described to be fundamental in mounting an innate antiviral response to hepatotropic viruses, such as HCV, by binding viral derived immunostimulatory RNA [163, 188, 189].

3.2.1 iPSC-derived hepatocytes as a new model for studying hepatic antiviral response

Different human hepatoma cell lines have been used to study liver function and metabolism *in vitro*. Among these HepG2 and Huh7 are the two most common cell lines [190]. HepG2 is a hepatoblastoma-derived cell line from a 15-years old male [191], while Huh7 is a hepatocellular carcinoma derived from a 57-years old Japanese male [192]. These two cell lines have been extensively used for viral infection models [190]. In particular Huh7 cells, and its subclonal line Huh7.5 (which carries a mutation on DDX58, the RIG-I encoding gene [193]), has been used by different groups as a model for HCV infection [194–196]. Although the two cell lines are still extensively used, since they are cancer cells, they carry limitations in mimicking the complex hepatic metabolism. They present increased glycolysis, decreased oxygen consumption, and downregulated cytochrome P450s expression when compared to PHHs [190, 197]. New human hepatic cellular models have been developed. Among these, iPSC-derived hepatocytes (also indicated as hepatocyte-like cells, HLCs) have been shown to be efficient models for hepatic drug metabolism [198], hepatic steatosis [199], and viral infection [200, 201]. This *in vitro* model can potentially recapitulate PHHs innate immune response more accurately than hepatic cell lines, which present decreased expression in specific TLRs, such as TLR3, when compared to PHHs [157].

3.3 Hypothesis

iPSC-derived hepatocytes, HepG2, and Huh7 cell lines are able to mount an innate antiviral response. Stimulation with immunogenic RNA-based ligands increases the expression of type I and III interferons as well as pro-inflammatory cytokines and ISGs, which are the ultimate effectors of the antiviral activity.

3.4 Aims

- To determine whether the two cell lines, HepG2 and Huh7 cells, respond to viral ligand stimulation by increasing type I and III IFNs, pro-inflammatory cytokines, and ISGs

- To identify which are the main PRRs involved in mounting the antiviral response in the two cell lines.

- To determine whether iPSC-derived hepatocytes upregulate the genes involved in the antiviral activity (interferons and pro-inflammatory genes) upon immunogenic RNA ligands stimulation.

3.5 Results

3.5.1 HepG2 cells activate cytoplasmic PRRs to detect viral-like RNA

In order to determine whether HepG2 respond to viral-like RNA ligands, cells were stimulated for 4 and 24h, mimicking an early response (4h) and a later response (24h). Non-transfected poly I:C was used as TLR3 agonist, transfected poly I:C (T-poly I:C) as MDA5 or PKR ligand, and 5' triphosphate hairpin RNA (3p-hp RNA) as RIG-I ligand. Expression of *IFNB1* (Fig. 3.1 A) and *CXCL10* (Fig. 3.1 B) were increased after 4h of stimulation upon T-poly I:C and 3p-hpRNA, with a dose dependent effect. Transfected poly I:C showed a stronger effect when compared to 3p-hpRNA, while *CXCL10* expression had a greater induction compared to *IFNB1*. At a 24h stimulation we observed an increase in *ISG15* (Fig. 3.1 C) and *MX1* (Fig. 3.1 D), as well as an upregulation of type I IFN levels (Fig. 3.1 E) upon T-poly I:C and 3p-hpRNA stimulations, recapitulating the pattern observed at 4h. While the TLR3 ligand, non-transfected poly I:C, did not induce expression of IFNB1, CXCL10, or ISGs. The results obtained highlight that HepG2 cells mount an innate antiviral response against viral-like RNA through cytoplasmic PRRs, rather than the endosome-located TLR3.

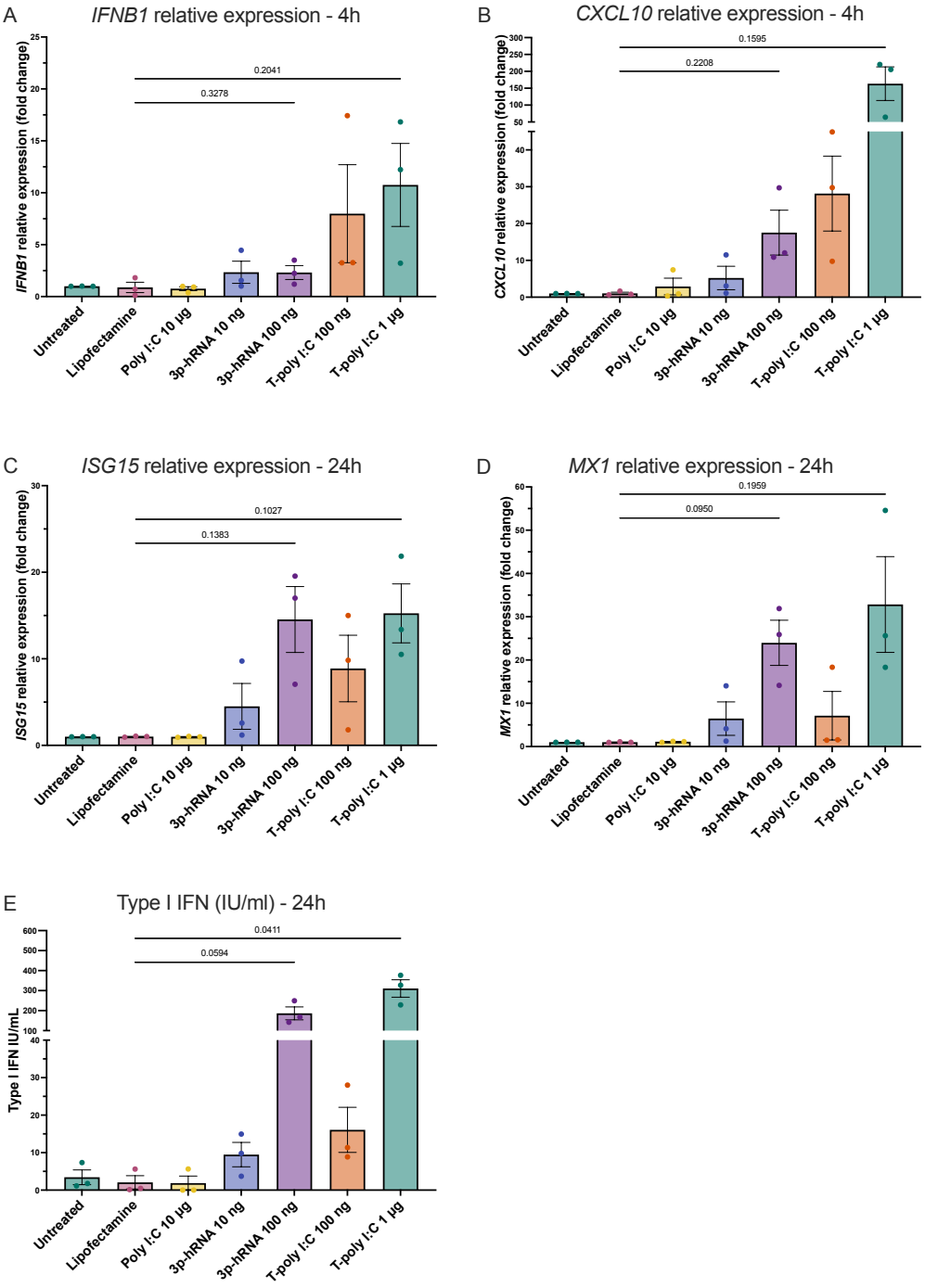

Figure 3.1 Cytoplasmic PRR activation induces antiviral activity in HepG2 cells.

HepG2 cells were stimulated with poly I:C, transfected poly I:C (T-poly I:C) and transfected 3p-hpRNA for 4h and 24h. IFNB1 (A) and CXCL10 (B) gene expression were measured by RT-qPCR after 4h of stimulation while ISG15 (C) and MX1 (D) gene expression were measured by RT-qPCR after 24h of stimulation. Supernatants were collected and type I IFN supernatant level was assessed by HEK-Blue assay (E). Data are mean ± S.E.M. of three independent experiments, p value were calculated using paired one-way ANOVA.

3.5.2 HepG2 cells mount a MAVS-dependent response upon 5'-triphosphate hairpin RNA stimulation

As shown in figure 3.1, HepG2 are able to mount an antiviral response upon the transfected 3p-hpRNA stimulation, which according to literature is a RIG-I specific ligand [43, 202]. We sought to confirm that the response is dependent on the RLR-MAVS pathway. In order to achieve this, we silenced MAVS through a lentiviral system (Fig. 3.2 A). MAVS knock-down resulted in a loss of gene expression of type I and III IFNs (*IFNB1* and *IFNL1*), as well as pro-inflammatory cytokines (CXCL10 and TNF) at 4h (Fig. 3.3) upon transfected 5'-triphosphate hairpin RNA stimulation. IFN-β and IL-29 proteins in the supernatants were also decreased upon a 24h stimulation (Fig. 3.4). Thus, demonstrating that transfected 5'-triphosphate hairpin RNA activates a MAVS-dependent antiviral response.

3.5.3 HepG2 cells upregulate IFN-β upon transfected poly I:C stimulation independently on MAVS

We aimed to identify whether transfected poly I:C, similarly to 3p-hpRNA, activates a MAVS-dependent response in HepG2. Using MAVS KD HepG2 we did not detect any decrease in IFNB1 expression (Fig. 3.5 A), while type III IFNs IFNL1 expression was decreased (Fig. 3.5 B). Furthermore, pro-inflammatory cytokine (CXCL10 and TNF) gene expression was not significantly decreased in MAVS knock-down cells upon transfected poly I:C (Fig. 3.5 C and D).

Similarly to what was observed for IFNB1 gene expression, also IFN-β protein levels were not affected by MAVS silencing at 24h (Fig. 3.6 A). While IL-29 (IFNL1) protein levels were decreased in MAVS knock-down HepG2 cells stimulated with transfected poly I:C (Fig. 3.6 B). These results indicate that transfected poly I:C elicits a MAVS-dependent type III IFN upregulation, but not MAVS-dependent IFN-β upregulation.

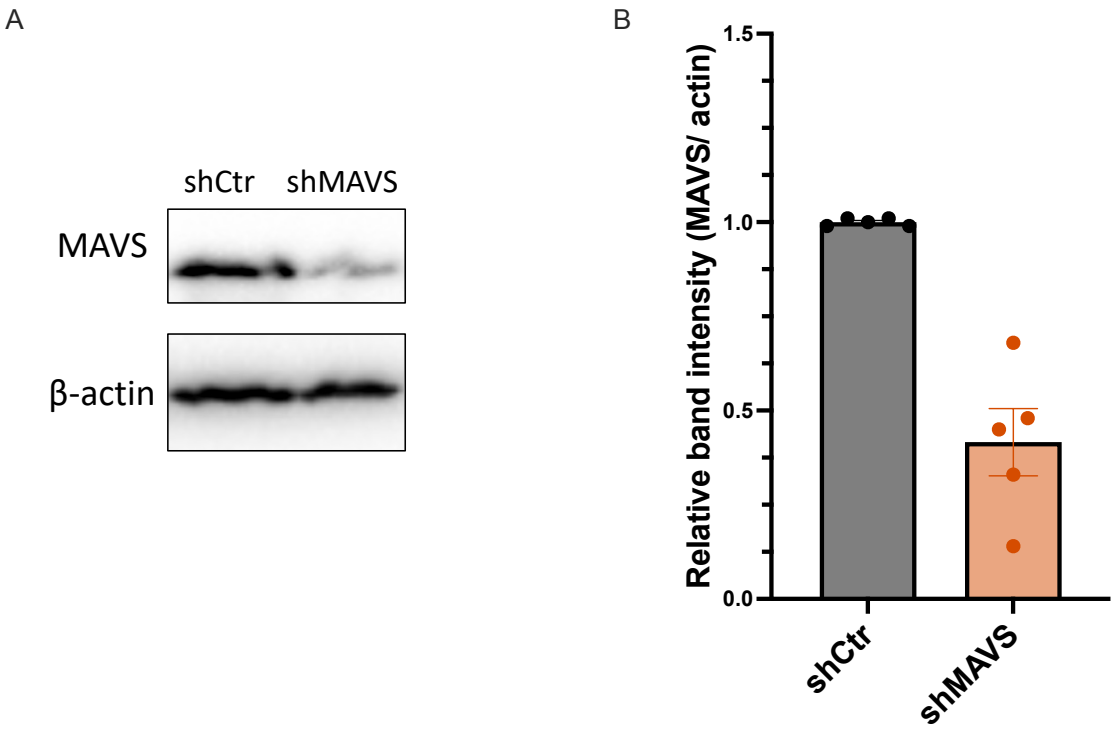

Figure 3.2 MAVS knock-down in HepG2 cells through the pLKO.1 lentiviral system.

Representative immunoblot of MAVS silencing using the pLKO.1 lentiviral system as described in material and methods (A). Relative quantification of the protein level of MAVS through densitometry analysis (B). Data are mean ± S.E.M. of 5 independent experiments.

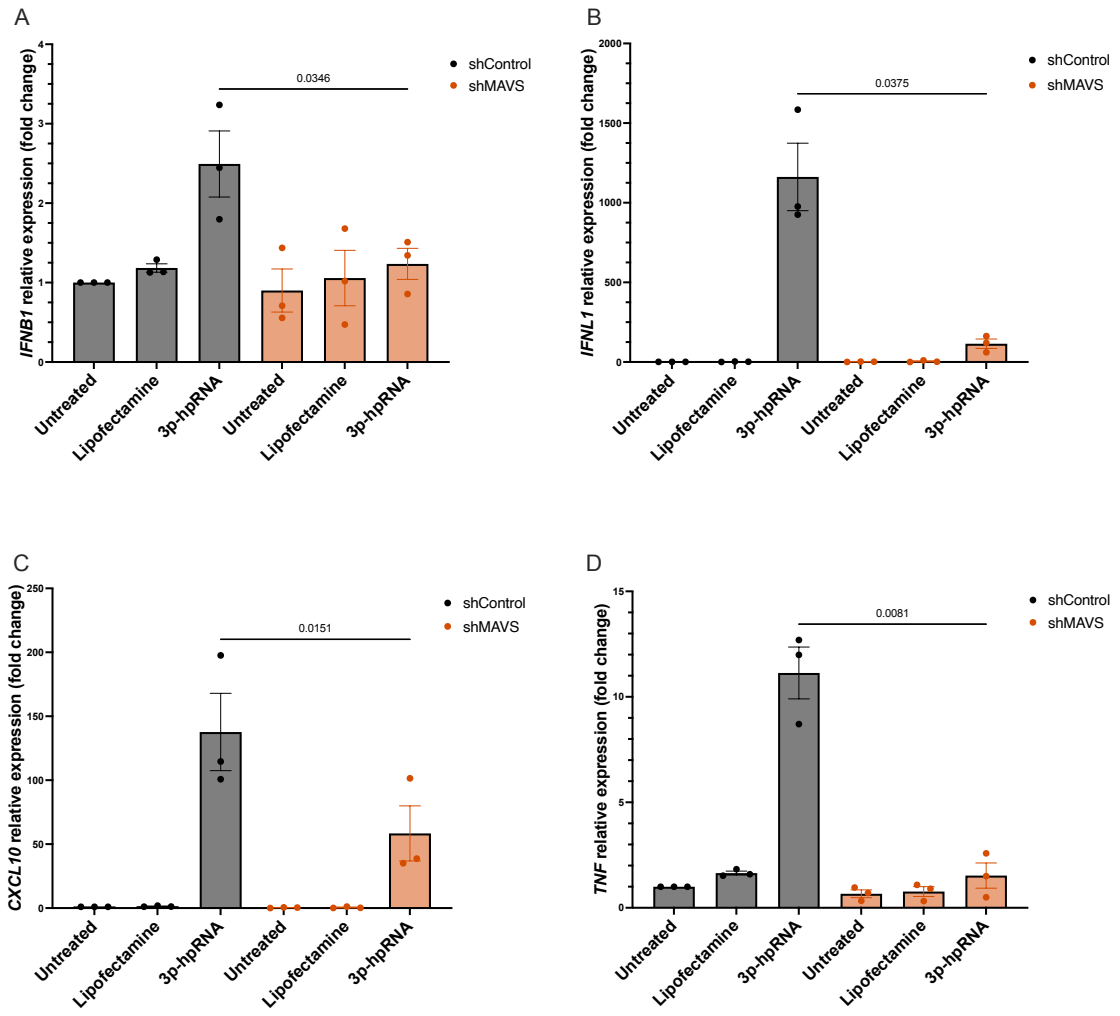

Figure 3.3 HepG2 cells induce type I and III interferon gene expression in a MAVS-dependent response upon 3p-hpRNA stimulation.

ShCtr and shMAVS HepG2 cells were stimulated with 100 ng/ml of transfected 3p-hp RNA for 4h. IFNB1 (A), IFNL1 (B), CXCL10 (C), and TNF (D) expression was measured by RT-qPCR. Data are mean ±S.E.M. of three independent experiments, p value were calculated using paired t-test.

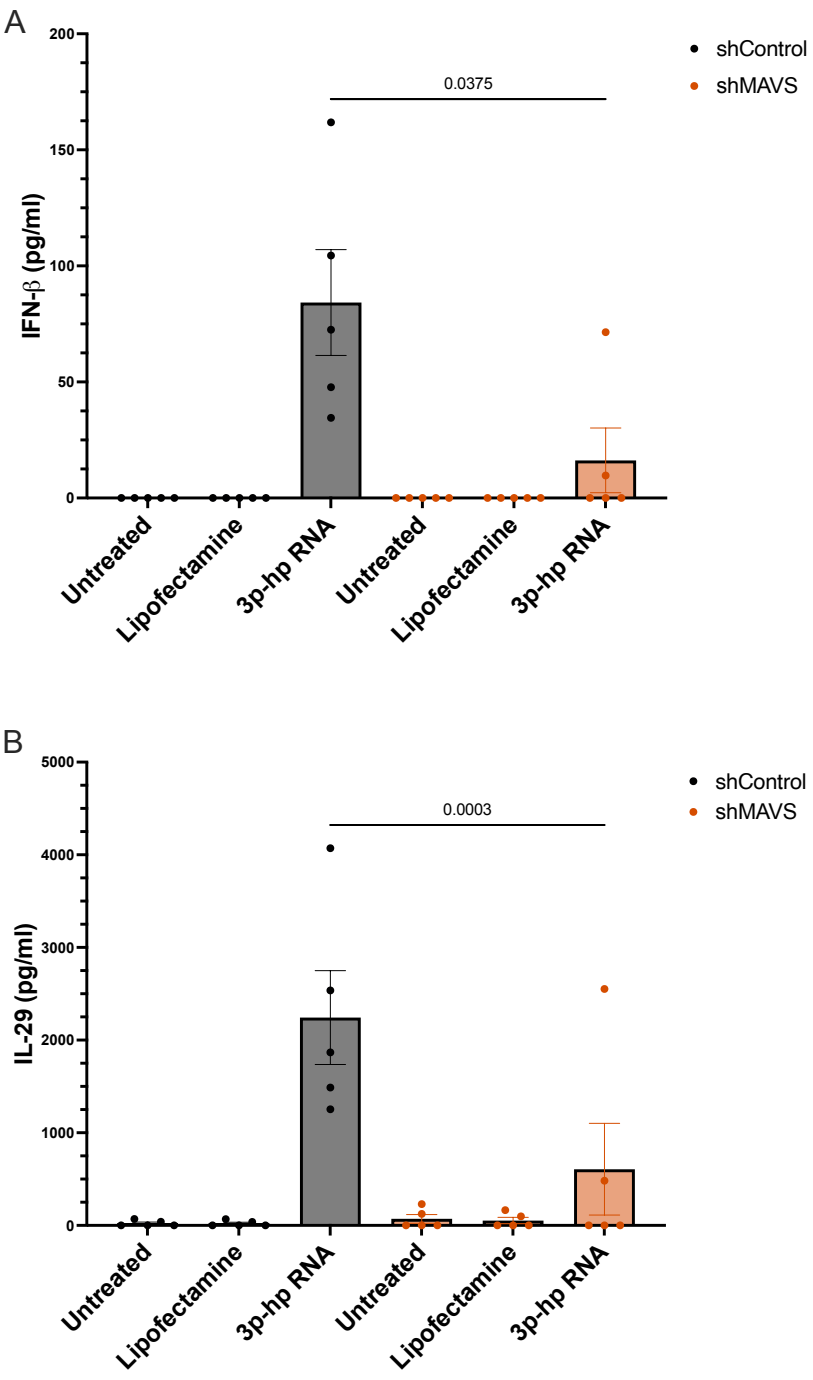

Figure 3.4 HepG2 cells induce type I and III interferon protein expression in a MAVS-dependent response upon 3p-hpRNA stimulation.

ShCtr and shMAVS HepG2 cells were stimulated with 100 ng/ml of transfected 3p-hp RNA for 24h. IFN-β (A) and IL-29 (B) protein levels were measured by ELISA. Data are mean ± S.E.M. of five independent experiments, p value were calculated using paired t-test.

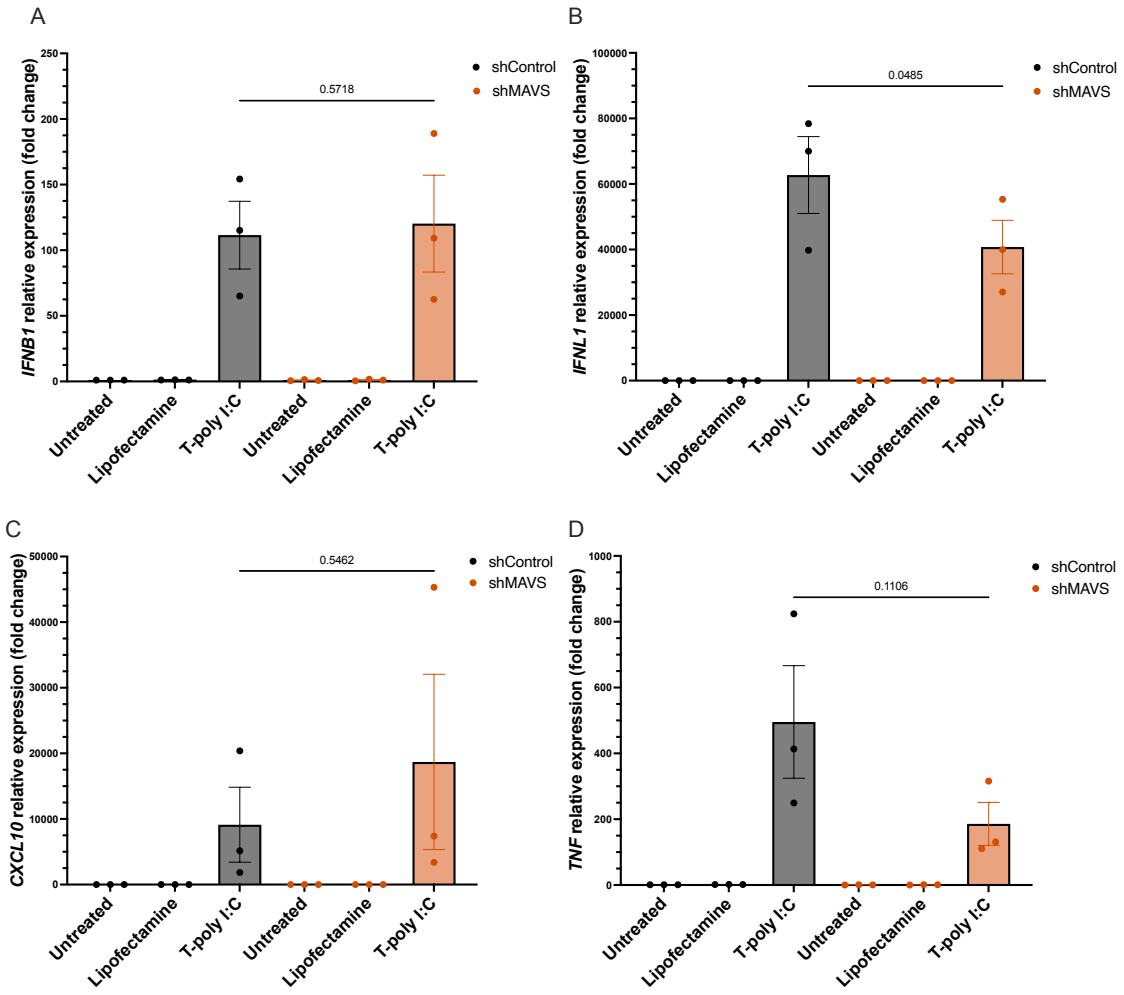

Figure 3.5 HepG2 cells upregulate IFNB1 gene expression in a MAVS independent manner upon transfected poly I:C stimulation.

ShCtr and shMAVS HepG2 cells were stimulated with 1 μg/ml of transfected poly I:C (T-poly I:C) for 4h. IFNB1 (A), IFNL1 (B), CXCL10 (C), and TNF (D) expression was measured by RT-qPCR. Data are mean ± S.E.M. three independent experiments*, p value were calculated using paired t-test.*

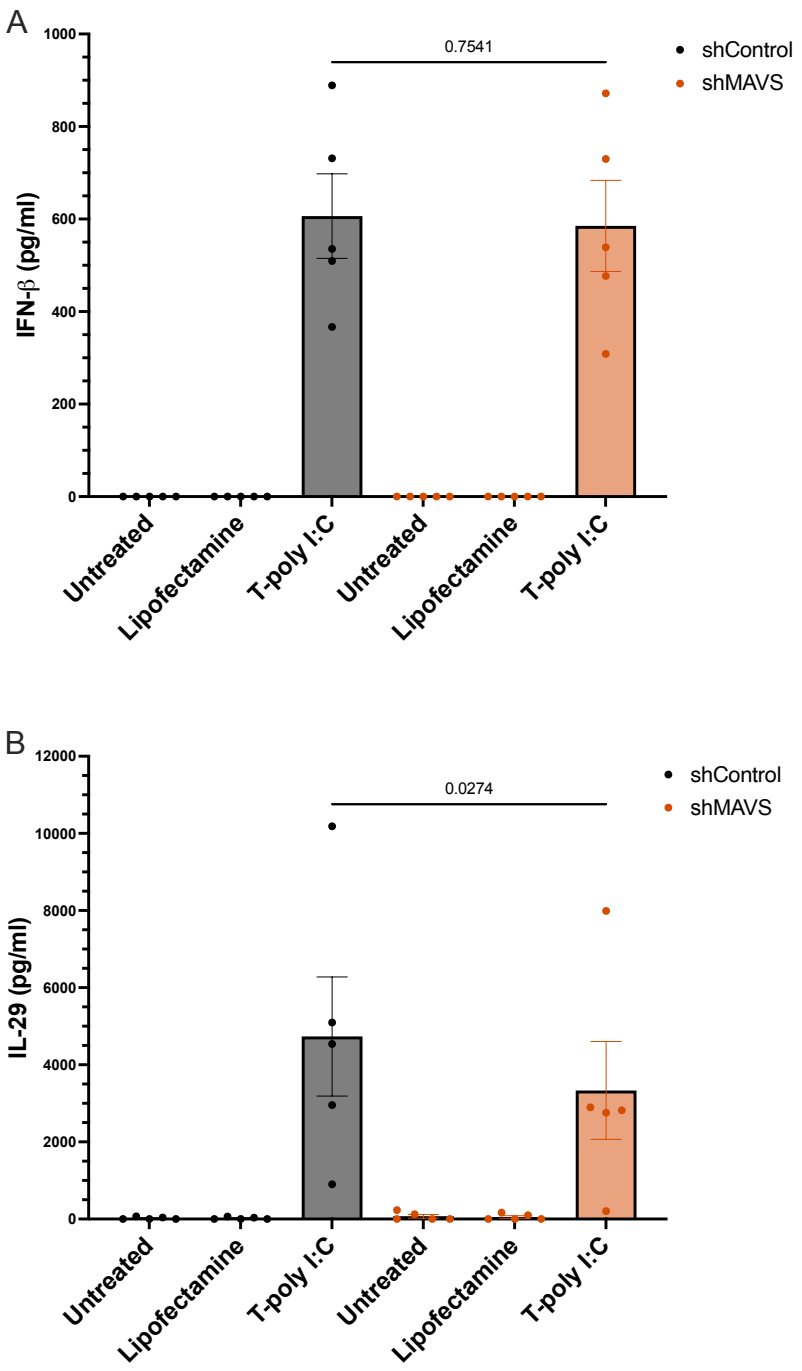

Figure 3.6 HepG2 cells induce IFN-β protein expression in a MAVS-independent manner upon transfected poly I:C.

ShCtr and shMAVS HepG2 cells were stimulated with 1 μg/ml of transfected poly I:C (T-poly I:C) for 24h. IFN-β (A) and IL-29 (B) protein levels were measured by ELISA. Data are mean ± S.E.M. of five independent experiments, p value were calculated using paired t-test.

3.5.4 PKR is required for mounting an innate antiviral response in HepG2 upon RNA-based immunogenic ligands

Since T-poly I:C induces IFNB1 MAVS-independently, we considered the implication of other cytoplasmic PRRs. Among these, the interferon-stimulated genes PKR has been shown to act as a sensor for viral RNA [203]. Using the selective PKR inhibitor C16, we observed a dose-dependent decrease in type I and III interferon expression - *IFNB1* (Fig. 3.7 A) and *IFNL1* (Fig. 3.7 C) expression was downregulated upon 4h stimulation with T-poly I:C. The same pattern was also observed for pro-inflammatory cytokines *CXCL10* and *TNF* (Fig. 3.8 A and C), which were dose-dependent downregulated upon pre-treatment with C16.

We further sought whether also the short hairpin RNA 3p-hpRNA activates a PKR-dependent induction of antiviral genes as well. We noticed that 3p-hpRNA-induced gene expression of IFNs and pro-inflammatory genes was dose-dependent reduced by PKR pre-treatment. In this case we observed exceptions for IFNB1 and TNF, which were not decreased by the PKR inhibitor (Fig. 3.7 B and Fig. 3.8 D).

The experiments carried out in HepG2 cells highlight a phenomena of redundancy. Transfected poly I:C induces both a MAVS-dependent and independent antiviral response in HepG2 as well as a PKR-dependent antiviral response. Moreover, we observed a lack of redundancy in IFNB1 induction, which seemed to be specifically PKR but not MAVS-dependent. On the other hand, IFNL1 was dependent on both MAVS and PKR, highlighting a possible redundancy effect of the two signaling pathways. Further studies inhibiting both MAVS and PKR-dependent antiviral response would also be informative to determine a potential synergistic effect.

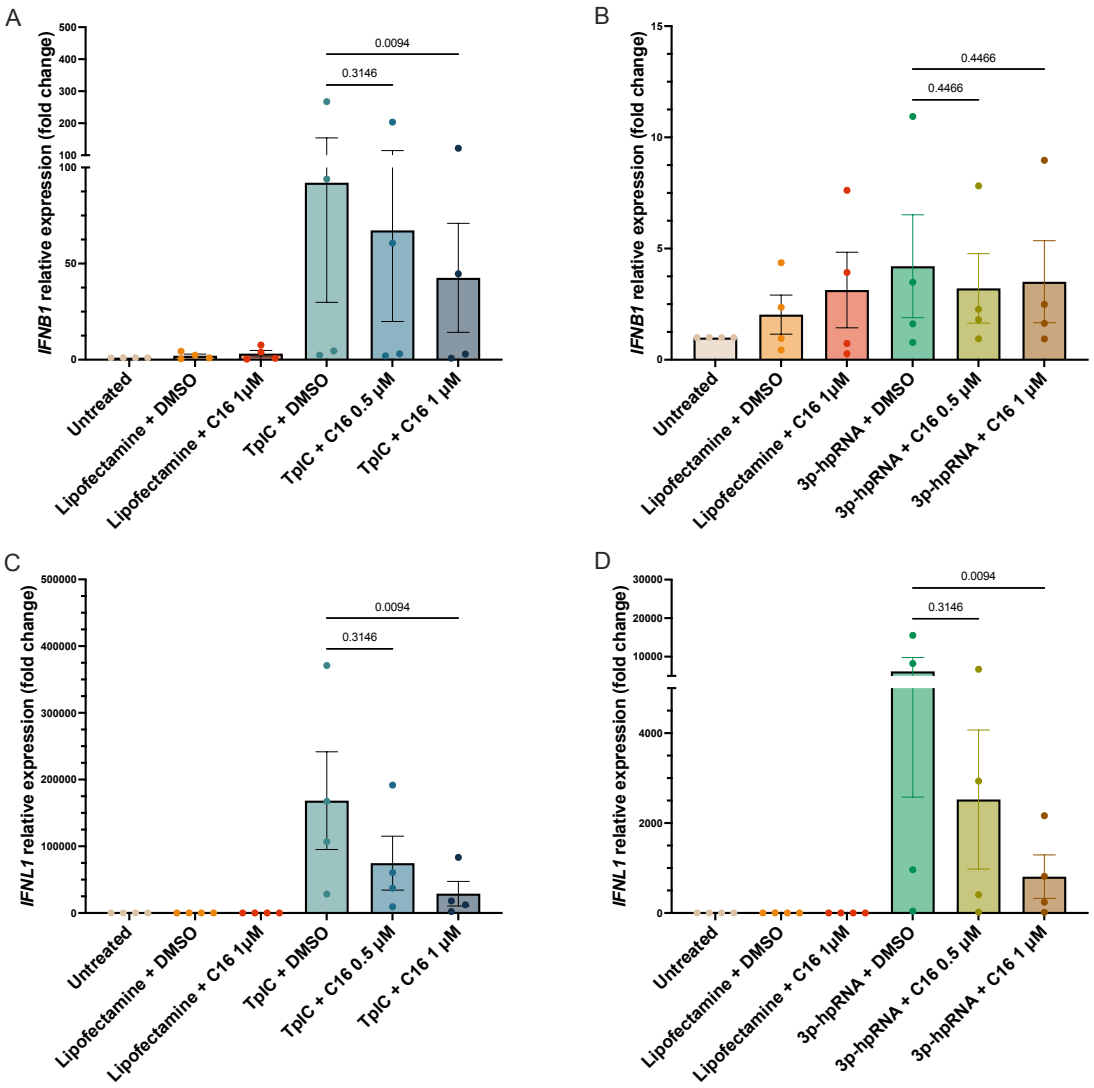

Figure 3.7 PKR is required for inducing type I and III interferon expression upon RNA-based immunogenic ligands in HepG2 cells.

HepG2 cells were pre-treated for 1h with the PKR inhibitor C16 and then stimulated with T-poly I:C or 3p-hpRNA for 4h. Gene expression of IFNB1 (A and B) and IFNL1 (C and D) were analysed by RT-qPCR. Data are mean ± S.E.M. of four independent experiments, p value were calculated using paired one-way ANOVA.

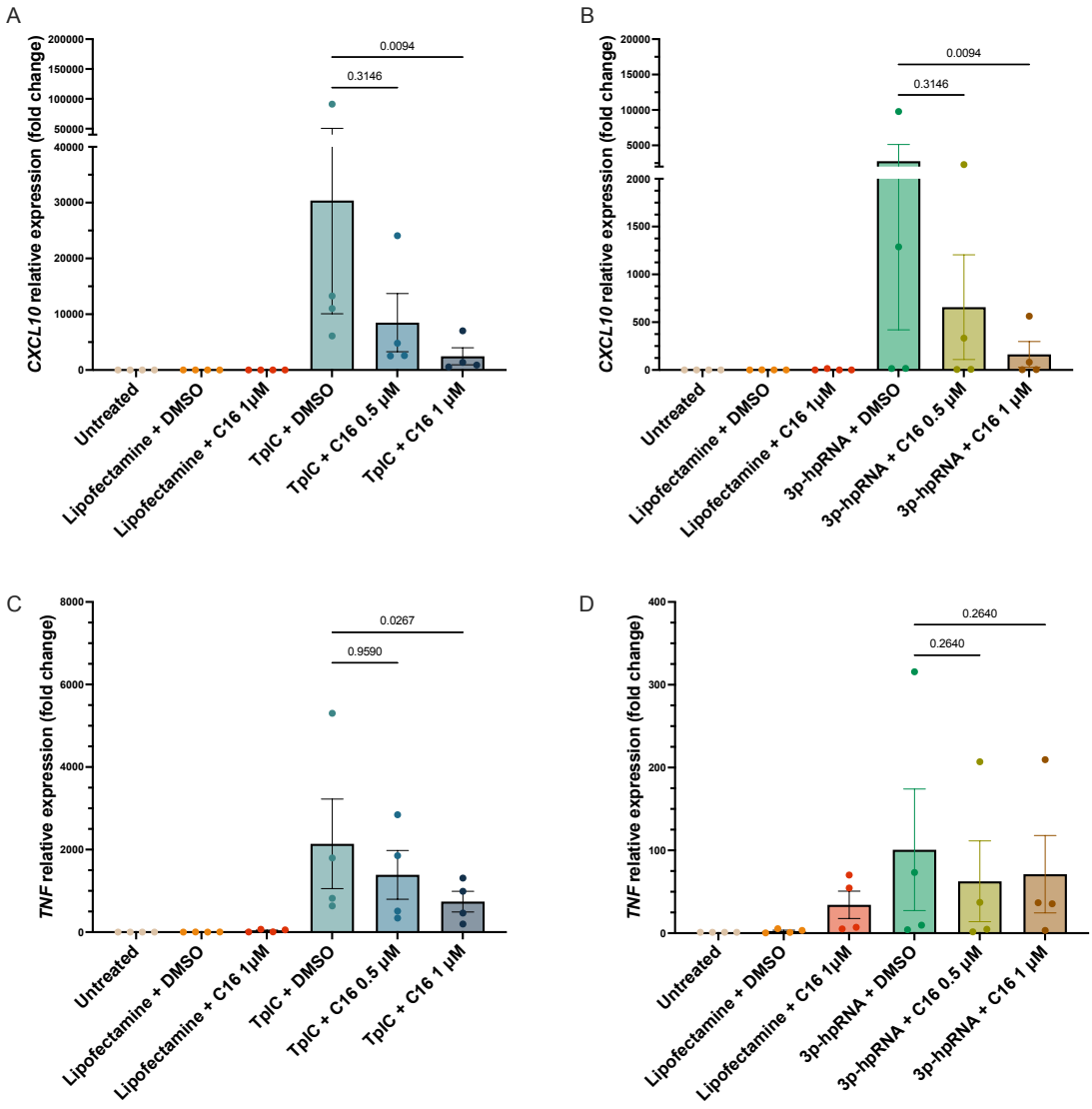

Figure 3.8 PKR is required for inducing pro-inflammatory cytokines expression upon RNA-based immunogenic ligands in HepG2 cells.

HepG2 cells were pre-treated for 1h with the PKR inhibitor C16 and then stimulated with T-poly I:C or 3p-hpRNA for 4h. Gene expression of CXCL10 (A and B) and TNF (C and D) were analysed by RT-qPCR. Data are mean ± S.E.M. of four independent experiments, p value were calculated using paired one-way ANOVA.

3.5.5 Huh7 cells respond to cytoplasmic viral-like RNA PAMPs

We stimulated Huh7 cells with poly I:C as TLR3 ligand, transfected poly I:C (T-poly I:C), and 5' triphosphate hairpin RNA (3p-hp RNA) as cytoplasmic PRRs agonists. After a 24h stimulation, type I IFN level in the supernatants was measured. We observed that, similarly to HepG2 cells (Fig. 3.1), Huh7 increase type I IFN expression upon stimulation with 3p-hpRNA and T-poly I:C (Fig. 3.9). The results showed that also Huh7 rely on cytoplasmic PRRs. Surprisingly Huh7 cells were responsive at higher concentrations of T-poly I:C and 3p-hpRNA compared to HepG2 cells.

3.5.6 Huh7 cells activate a MAVS-dependent response upon dsRNA stimulation

We silenced MAVS expression in Huh7 cells using the same lentiviral system used for HepG2 cells (Fig. 3.10 A) and stimulated the cells with transfected poly I:C or 5'-triphosphate hairpin RNA for 6h. We observed that neither long dsRNA poly I:C or short 5'-triphospahte hairpin RNA did not activate MAVS-dependent pathway since IFNB1 and IFNL1 expression were not altered in the MAVS KD cells (Fig. 3.10 B and C).

We further measured IFN-β and IL-29 protein levels after 24h stimulation with transfected poly I:C or 5'-triphosphate hairpin RNA. We observed that both IFN-β and IL-29 protein levels were reduced in MAVS KD Huh7 cells upon transfected poly I:C stimulation (Fig. 3.11 A and B). These results demonstrate that poly I:C-induced IFNs expression is MAVS-dependent at a later phase (such as 24h).

Interestingly, we could not detect an increase in the IFN-β and IL-29 (IFNL1) protein levels upon the 5'-triphosphate hairpin RNA 3p-hpRNA. This was a surprising result since we observed an increase of 500-fold changes in IFNL1 gene expression upon 5'-triphosphate hairpin RNA stimulation at 6h. Moreover, in a previous experiment (Fig. 3.9), we observed an increase in type I IFN secretion upon 5'-triphosphate hairpin RNA. This might also be due to a greater sensitivity of HEK-blue assay compared to IFN-β ELISA.

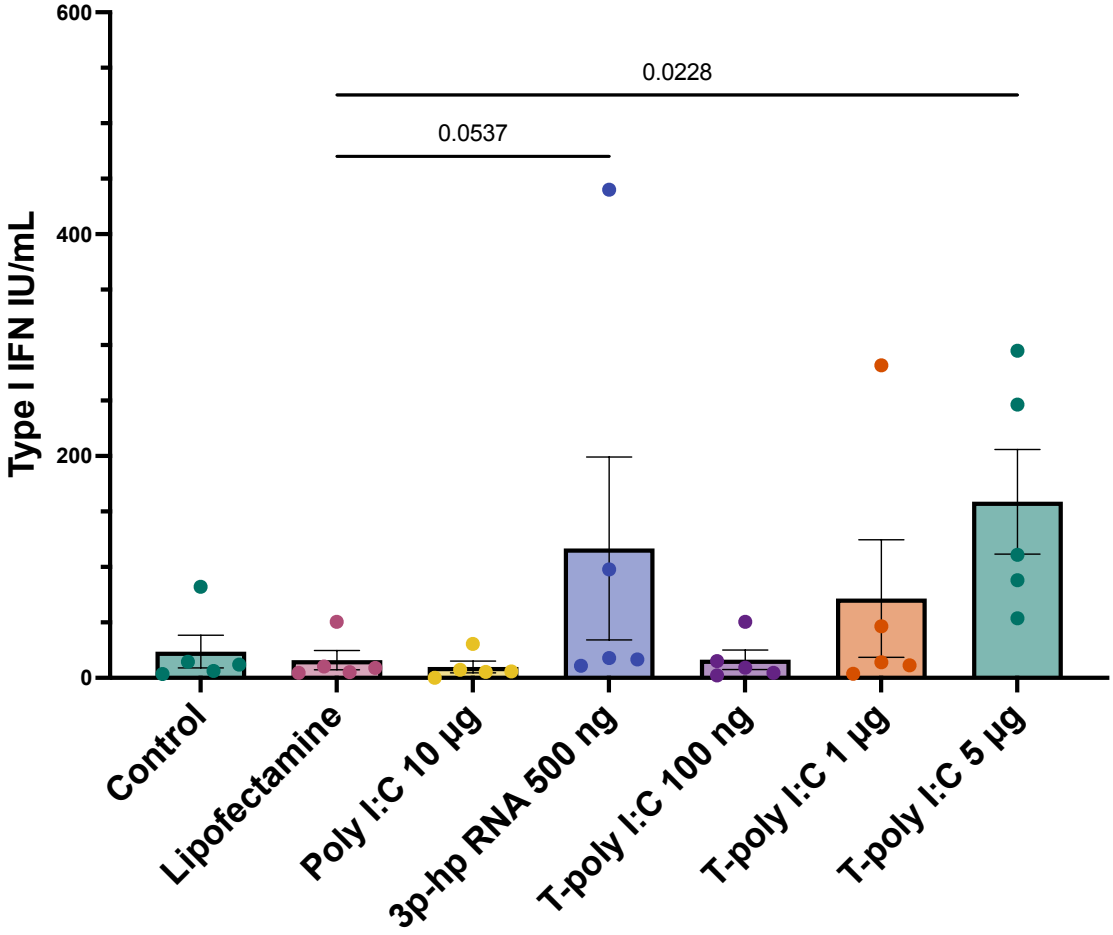

Figure 3.9 Huh7 cells upregulate type I IFN expression upon cytoplasmic PRRs activation.

Huh7 were stimulated for 24h with poly I:C, transfected 3p-hpRNA and transfected poly I:C (T-poly I:C). Supernatants were collected and type I IFN content was measured by HEK-Blue assay. Data are mean ± S.E.M. of five independent experiments, p value were calculated using paired one-way ANOVA.

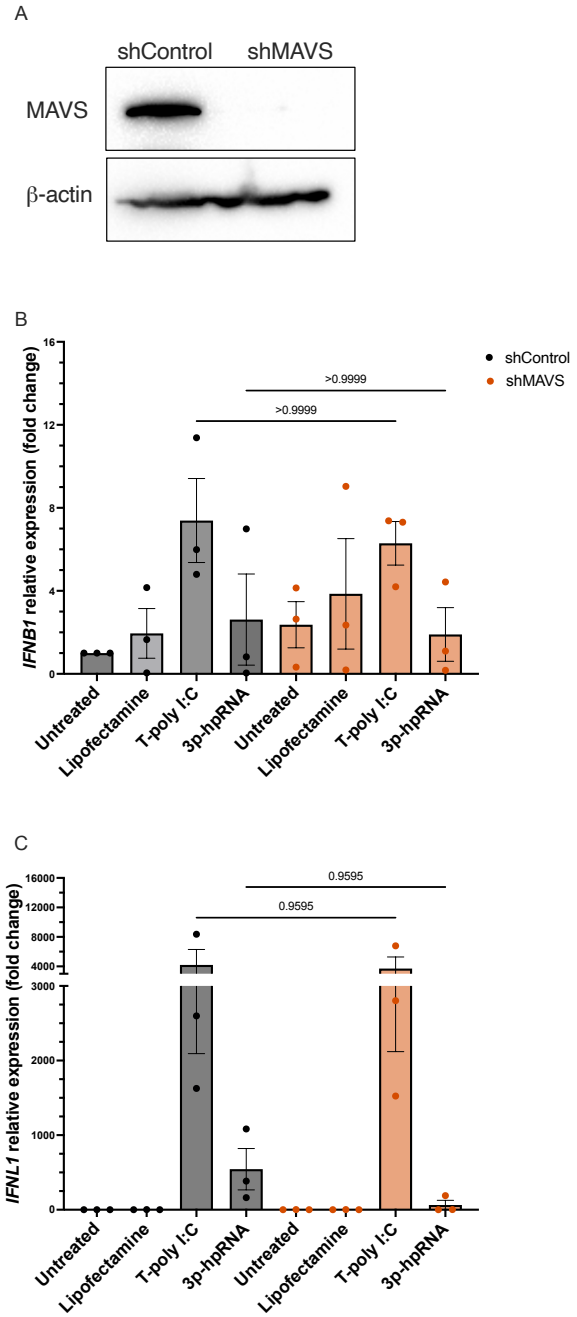

Figure 3.10 Huh7 cells activate a MAVS-dependent response upon short hairpin RNA stimulation.

Representative immunoblot of MAVS silencing in Huh7 cells using the pLKO.1 lentiviral system as described in material and methods (A). ShCtr and shMAVS Huh7 cells were stimulated with 5 μg/ml of transfected poly I:C (T-poly I:C) or 500 ng/ml of 5' triphosphate hairpin RNA (3p-hpRNA) for 6h. IFNB1 (B) and IFNL1 (C) expression was measured by RT-qPCR. Data are mean ±S.E.M. of three independent experiments, p value were calculated using paired one-way ANOVA.

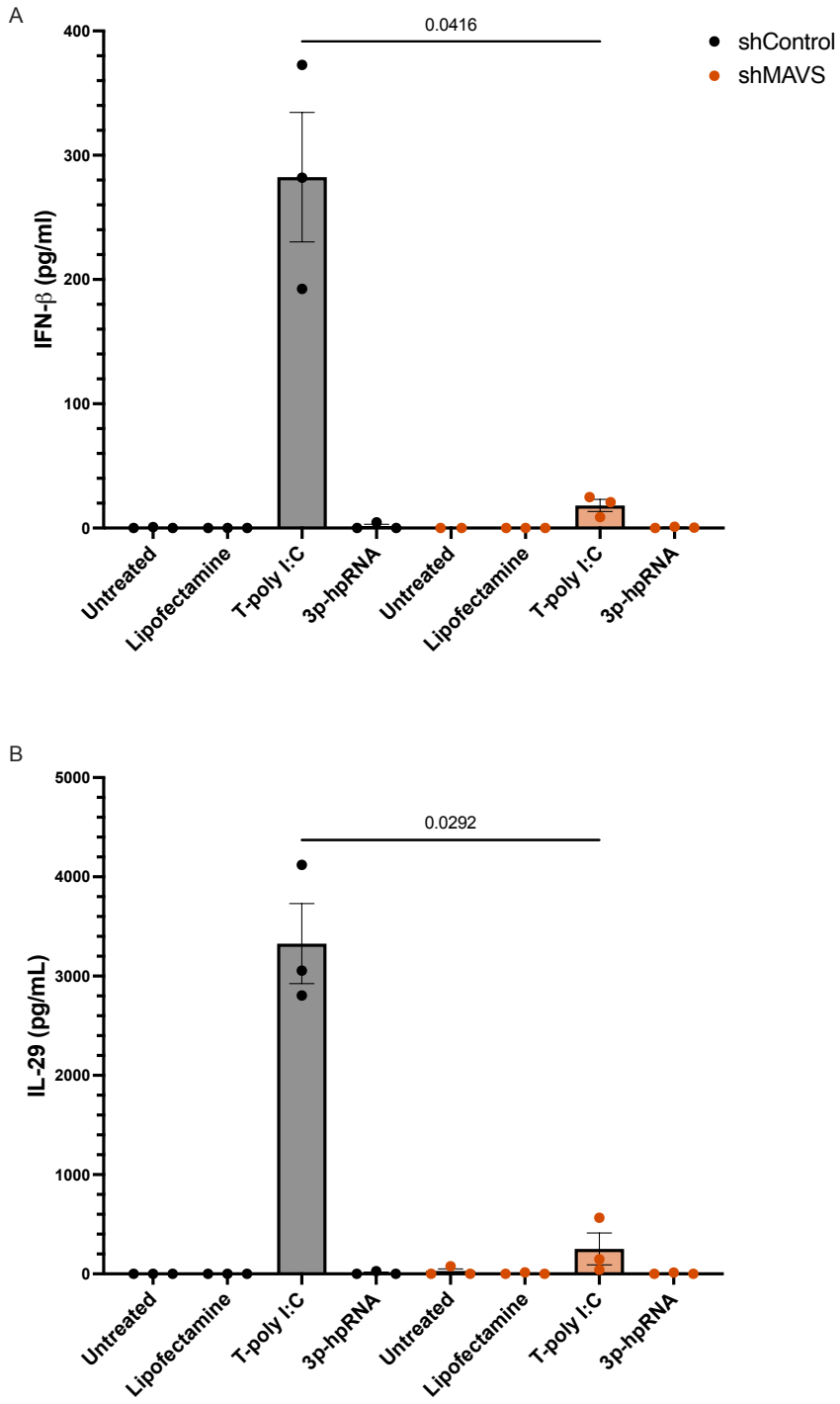

Figure 3.11 Huh7 cells activate a MAVS-dependent antiviral response upon transfected poly I:C stimulation at 24h.

ShControl and shMAVS Huh7 cells were stimulated with 5 μg/ml of transfected poly I:C (T-poly I:C) or 500 ng/ml of 5' triphosphate hairpin RNA (3p-hpRNA) for 24h. IFN-β and IL-29 protein levels were measured ELISA. Data are mean ± S.E.M. of three independent experiments, p value were calculated using paired t-test.

3.5.7 Huh7 cells activate PKR upon RNA-based immunogenic ligands

Since we observed that transfected poly I:C activates an early (6h stimulation) MAVS-independent antiviral response in Huh7 cells (Fig. 3.10), we hypothesised that PKR might be involved in the response. We blocked PKR activation using the specific PKR inhibitor C16, and we noticed a decrease in IFNB1 and IFNL1 expression in transfected poly I:C and 3p-hpRNA stimulations (Fig. 3.12). At 24h we observed the same trend, with a dose dependent decrease of IFN-β and IL-29 protein levels by blocking PKR activation (Fig. 3.13).

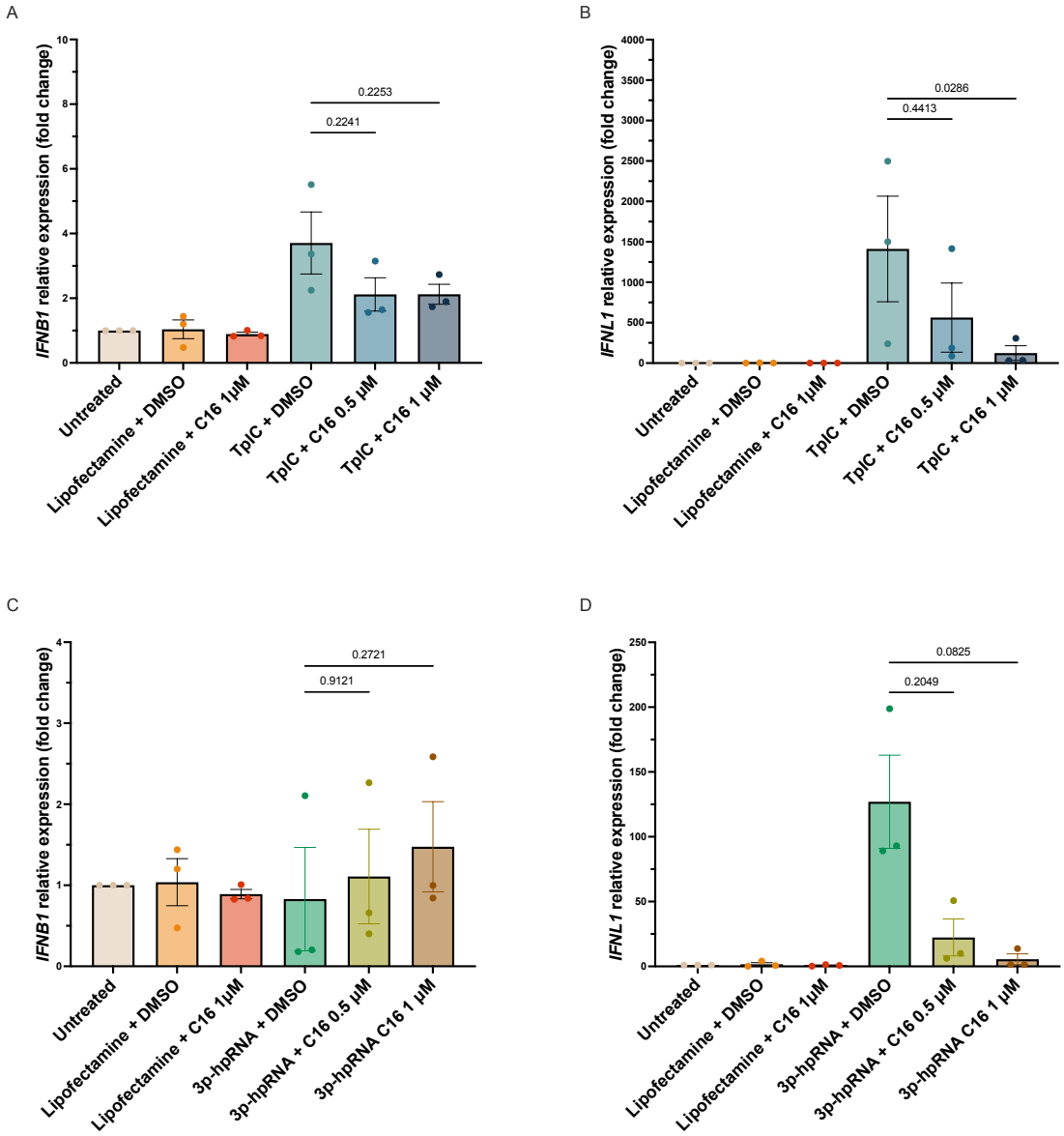

Figure 3.12 Huh7 cells activate PKR upon RNA-based immunogenic ligands.

Huh7 cells were pre-treated for 1h with the PKR inhibitor C16 and then stimulated with 5 µg/ml of transfected poly I:C (T-poly I:C) or 500 ng/ml of 5' triphosphate hairpin RNA (3p-hpRNA) for 6h. Gene expression of IFNL1 (A and B) and IFNL1 (C and D) were analysed by RT-qPCR at 6h after stimulation. Data are mean ± S.E.M. of three independent experiments, p value were calculated using paired one-way ANOVA.

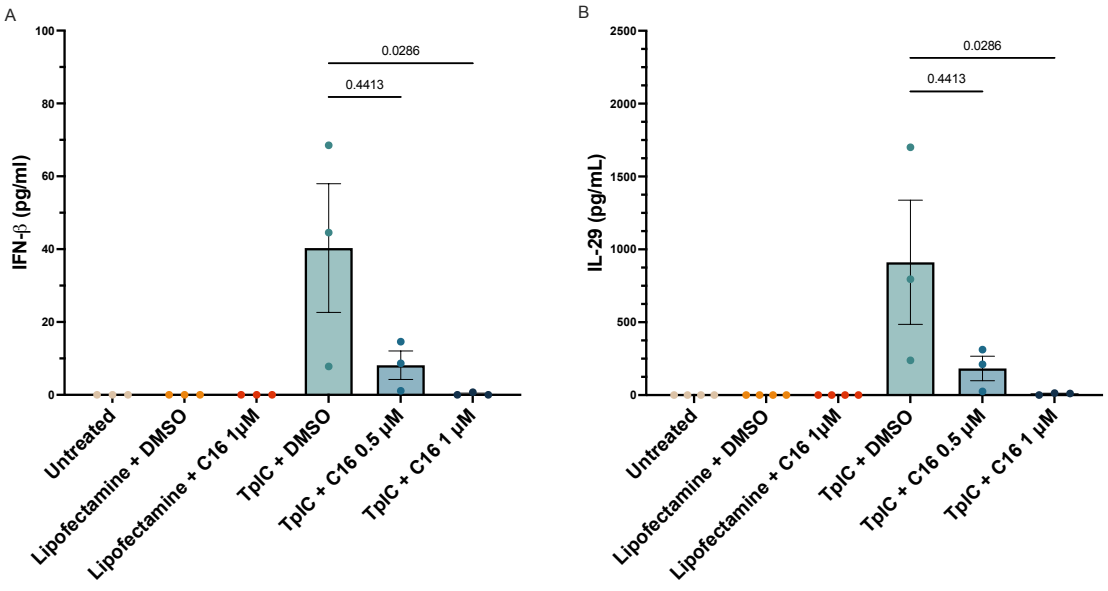

Figure 3.13 PKR inhibition abrogates IFN-β and IL-29 production in Huh7 cells.

Huh7 cells were pre-treated for 1h with the PKR inhibitor C16 and then stimulated with 5 µg/ml of transfected poly I:C (T-poly I:C) 24h. IFN-β (A) and IL-29 (B) protein levels were measured by ELISA after 24h stimulation. Data are mean ± S.E.M. of three independent experiments, p value were calculated using paired one-way ANOVA.

3.5.8 Hepatocyte-like cells produce significant type III interferon, relying on cytoplasmic PRRs for the detection of dsRNA

The third surrogate model used for our studies is the iPSC-derived hepatocytes. Induced pluripotent stem cells were differentiated throughout 4 different stages, pluripotent stem cells, definitive endoderm , hepatic progenitors, and hepatocyte-like cells (HLCs) (Fig. 3.14)[186]. Induced pluripotent stem cells were differentiated through 3 different stages, definitive endoderm, hepatic progenitors, and hepatocyte-like cells (HLCs) [186]. The differentiation process took on average 16 ± 1 days. Cell in the definitive endoderm stage were stained for FOX2A and GATA4. Cells in the hepatic progenitor stage were stained for alpha-fetoprotein (AFP) and hepatic nuclear factor 4-alpha (HNF4A). For the last stage, mature hepatocyte-like cells were stained for albumin and E-cadherin. At every stage, cells were counterstained with DAPI for nuclear DNA.

We sought to determine whether HLCs were able to mount an innate antiviral response upon stimulations with RNA-based viral-like ligands. HLCs were stimulated with TLR3 (non-transfected poly I:C), RIG-I (5' triphosphate hairpin RNA), MDA5 and PKR (transfected poly I:C) agonists for 24h. Upon stimulation with poly I:C, the ligand for TLR3, minimal interferon, either type I or III, was observed. However, stimulation with transfected 5' triphosphate hairpin RNA (3-hpRNA) and transfected poly I:C (T-poly I:C), activating RIG-I, MDA5 and PKR respectively, induced a significant production of the interferons IFNB1 and IFNL1 (Fig. 3.15). Surprisingly, we observed increased *IFNL1* expression (Fig. 3.15 A) but not at a protein level (Fig. 3.15 D) upon stimulation with the vehicle lipofectamine. In this case, we hypothesise that the increased *IFNL1* expression might be due to a slight increase in cellular stress which does not affect the protein levels.

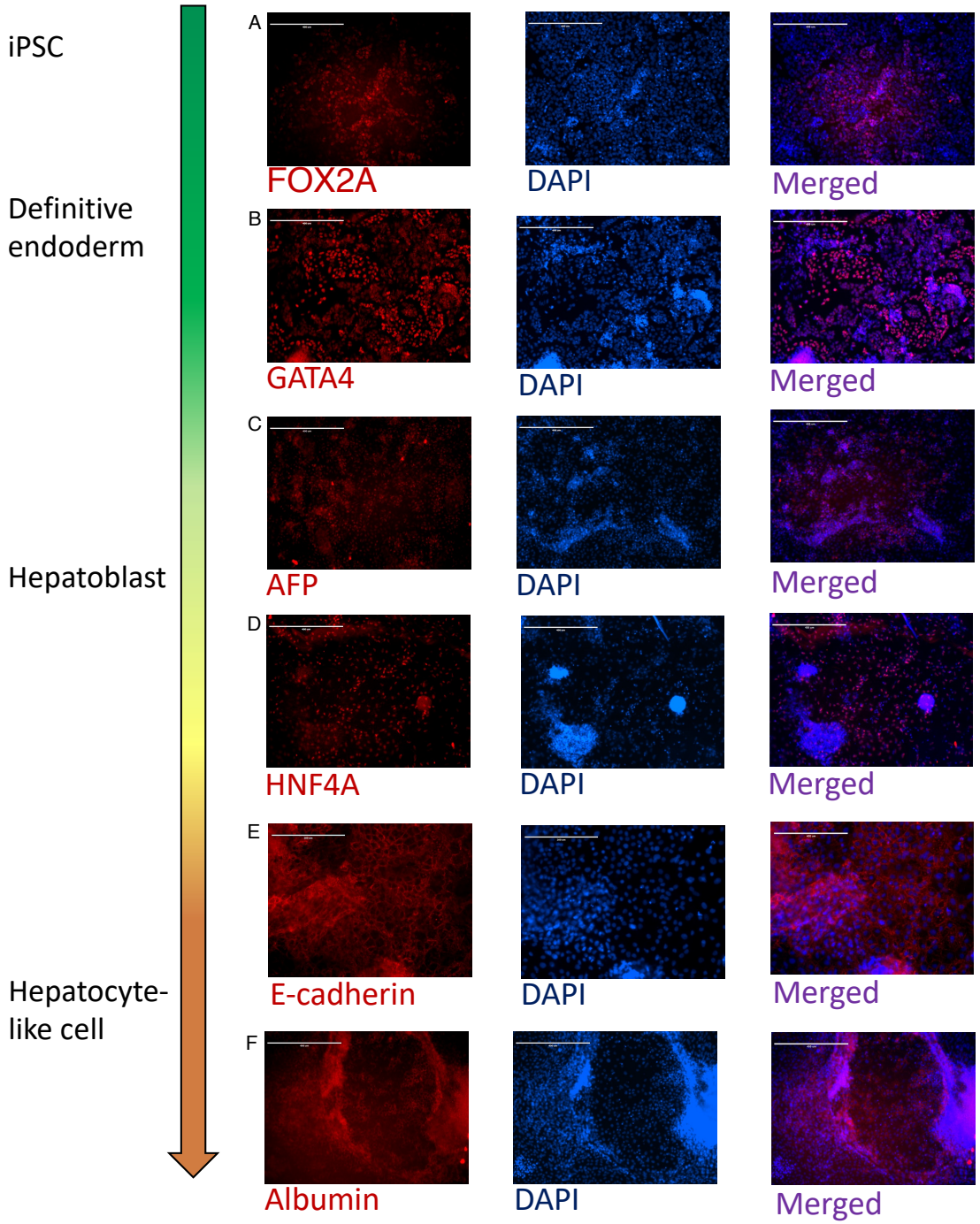

Figure 3.14 Differentiation of iPSCs into hepatocyte-like cells.

iPSC (induced pluripotent stem cells) were differentiated into hepatocyte-like cells (HCLs) through three different stages. Cells were stained for every differentiation stage. (A and B) At the definitive endoderm, cells were stained for FOX2A and GATA4. (C and D) At the

hepatoblast stage, cells were stained for alpha-fetoprotein (AFP) and hepatic nuclear factor 4-a. (E and F) At the last stage, the hepatocytes-like cells (HLCs) were stained for E-cadherin and albumin. Cells were counterstained with DAPI for nuclear DNA.

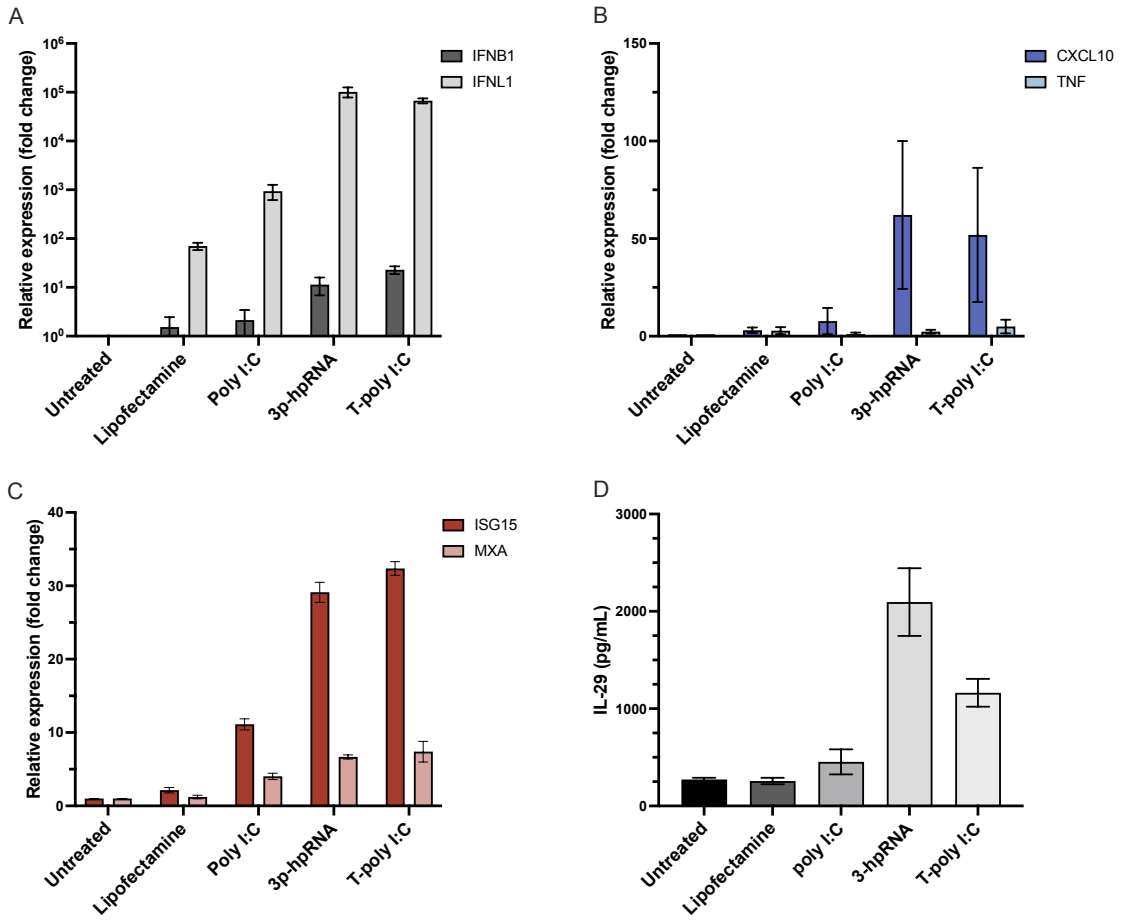

Figure 3.15 Transfected double stranded RNA induces expression of IFNs, pro-inflammatory cytokines and ISGs.

Hepatocyte-like cells were stimulated for 24h with non-transfected poly I:C (25 mg/ml), transfected 5'-triphosphate hairpin RNA (3p-hpRNA) (1 mg/ml), and transfected poly I:C (T-poly I:C) (5 mg/ml). Lipofectamine was used as vehicle control for the transfection. Relative gene expression of IFNs (IFNB1 and IFNL1, A), pro-inflammatory cytokines (CXCL10 and TNF, B), ISGs (ISG15 and MX1, C) were determined by RT-qPCR. IL-29 (IFNL1, D) protein levels were measured by ELISA. Data are mean ± S.E.M. of two independent experiments from one donor.

3.5.9 Time-course study analysis reveals early induction in IFNL1 expression upon dsRNA stimulation in HLCs

We further performed a time course-study with transfected poly I:C stimulation. We observed an early induction at 4h, with an increase in IFNB1 and IFNL1 (Fig. 3.16 A). At the later time points, 8 and 24h after stimulation, we observed a further increase in their expression (Fig. 3.16 C and E). These results matched the IFN-β and IL-29 supernatants protein levels, which peaked at 24h after stimulation (Fig. 3.16 B, D, and F).

We further analysed the gene expression of ISGs and pro-inflammatory cytokines. In this case we also observed a rapid increase in CXCL10 and ISG15 expression already at 4h. While both seem to reach the peak in their expression at 24h (Fig. 3.17).

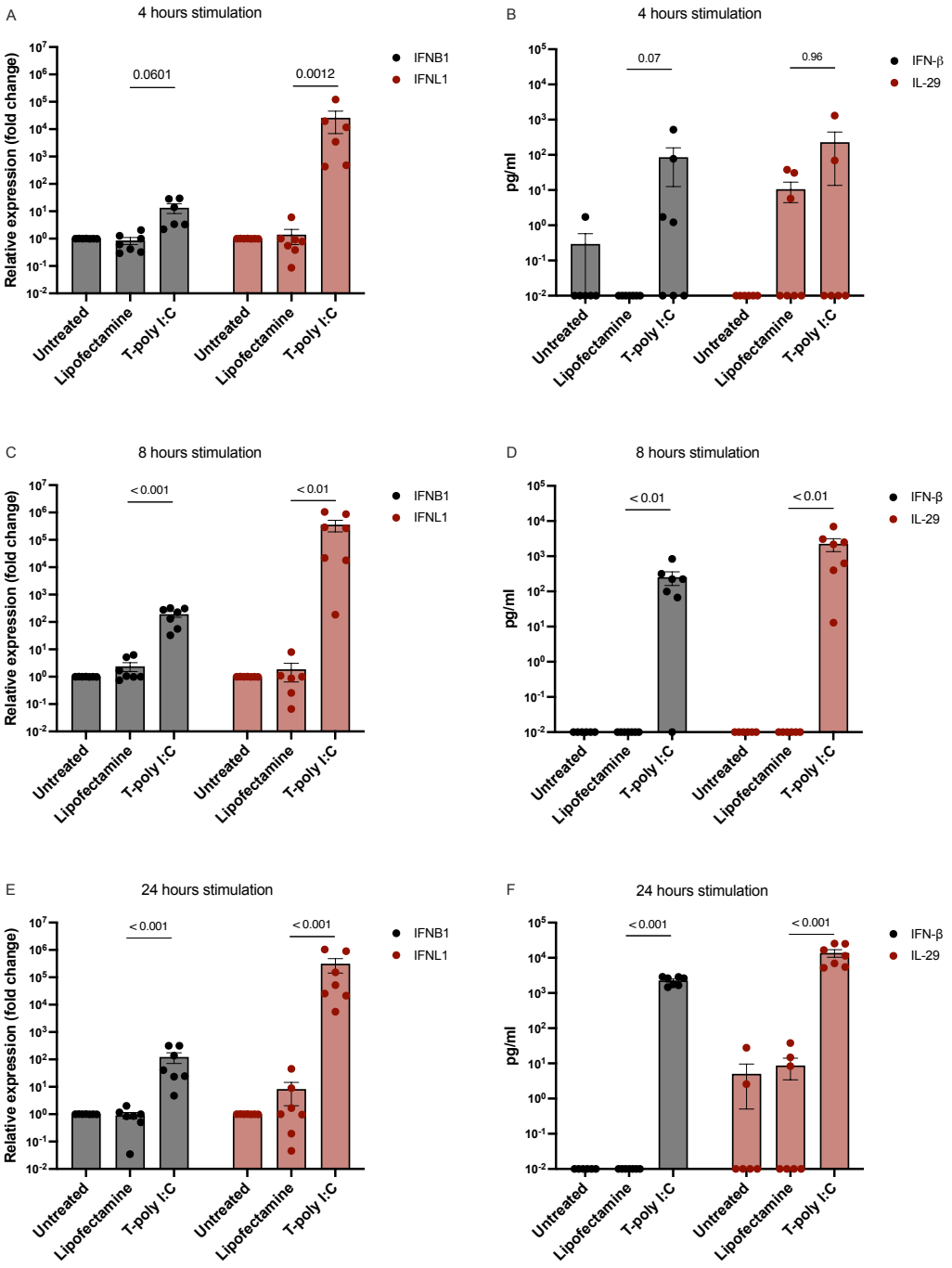

Figure 3.16 IFNB1 and IFNL1 are upregulated upon transfected poly I:C stimulation in iPSC-derived hepatocytes.

Hepatocyte-like cells were stimulated for 4 , 8, and 24h transfected poly I:C (T-poly I:C) (5 mg/ml), lipofectamine was used as vehicle control for the transfection. (A, C, E) IFNB1 and IFNL1 relative gene expression were determined by RT-qPCR. (B, D, F) IFN-b and IL-29 (IFNL1) protein levels were determined by ELISA. Data are mean ± S.E.M. of seven independent experiments from three different donors, p values were calculated using unpaired one-way ANOVA.

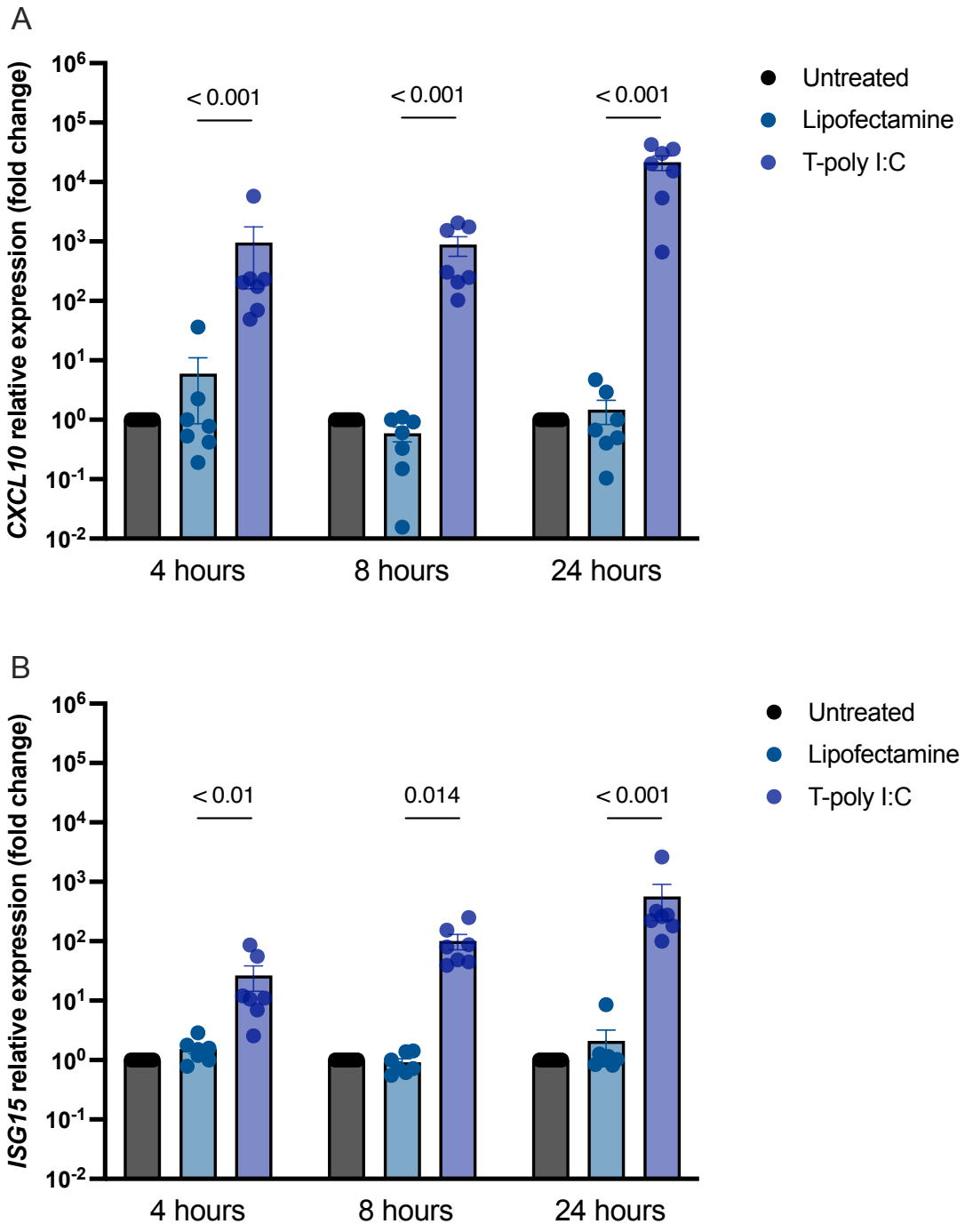

Figure 3.17 ISG15 and CXCL10 expression are upregulated by transfected poly I:C stimulation in iPSC-derived hepatocytes.

Hepatocyte-like cells were stimulated for 4 , 8, and 24h transfected poly I:C (T-poly I:C) (5 µg/ml), lipofectamine was used as vehicle control for the transfection. (A) CXCL10 relative gene expression was determined by RT-qPCR. (B) ISG15 relative gene expression was determined by RT-qPCR. Data are mean ± S.E.M. of seven independent experiments from three different donors, p values were calculated using unpaired one-way ANOVA.

3.6 Discussion

Innate immunity relies on PRRs and their ability to recognise evolutionary conserved pathogen-associated molecular patterns, such as viral DNA and RNA. Every nucleated cell has an intrinsic defence potential depending on their ability to detect invading pathogens via PRRs and activating the downstream signaling. In the present study we aimed to confirm that hepatocytes are able to mount an antiviral innate immune response upon stimulation with viral RNA-based PAMPs.

We utilised three hepatic cellular models, HepG2 cells, Huh7 cells, and human iPSC-derived hepatocytes. In accordance with literature, we observed that HepG2 and Huh7 cells do not respond to poly I:C, which acts as TLR3 agonist [157]. While iPSC-derived hepatocytes showed a slight upregulation of *MX1* and *ISG15* expression, as well as IL-29 protein (encoded by *IFNL1* gene) level upon non-transfected poly I:C. This might be due to an increased expression of TLR3 or adaptor proteins of the signalling pathway in iPSC-derived hepatocytes compared to HepG2 and Huh7 cell lines, similar to what has been observed for PHHs. Although the three different iPSC-derived hepatocyte lines showed significant induction of IFNs, pro-inflammatory cytokines, and ISGs, we also observed intra- and inter-cell line variability in the expression of antiviral genes. Whether this due to differential levels of PRRs or proteins involved in the antiviral signaling has not been investigated yet.

We observed induction of IFNs and pro-inflammatory cytokines upon transfection of poly I:C or 5’ triphosphate hairpin RNA (3p-hpRNA) in the three cellular models. Thus, demonstrating that cytoplasmic PRRs are the main receptors involved in a RNA-dependent innate antiviral response. We also noticed that Huh7 cells induced gene expression of IFNs and pro-inflammatory cytokines at higher concentrations of poly I:C and 3p-hpRNA compared to HepG2 cells. The difference in the responsiveness between the two cell lines might be due to various factors. We hypothesise that this is due to either different transfection efficiencies or basal levels in the expression of the PRRs (RLRs and PKR) or adaptor proteins involved in the antiviral signaling pathways. Further experiments determining the transfection efficiency, for instance using labelled poly I:C,

or measuring the PRRs protein levels in the two cell lines might explain the differences observed.

Although TNF expression was induced in HepG2 cells by stimulation with either 5'-triphosphate hairpin RNA or poly I:C, we could not observe any increase in TNF protein levels, which were undetectable using a commercial ELISA kit. Moreover, there is no evidence in the literature indicating the expression of TNF by hepatocytes [66, 67]. Here we used TNF expression as a read-out for the induction of pro-inflammatory cytokines, but expression of other genes, such as CXCL10, might be a more robust read-out, since CXCL10 is highly expressed by hepatocytes when stimulated with dsRNA as shown in our results and in literature [162].

We investigated which are the PRRs participating in IFNs and pro-inflammatory induction upon dsRNA stimulation. Transfected poly I:C acts as ligand for different PRRs, such as MDA5 and PKR [16, 204], and recently it has been shown to be recognised by NLRP1 and hepatic NLRP6 activating the downstream specific inflammasomes [18, 19]. In this study, we first sought to determine whether HepG2 and Huh7 cells recognise T-poly I:C through RLRs and mediates a MAVS-dependent response. Using MAVS KD HepG2 cells, we observed that transfected poly I:C induces IFNB1 expression independently on MAVS. While type III IFN expression (IFNL1) was MAVS-dependent. Thus, demonstrating that type I and III IFNs are differently regulated in HepG2 cells.

We conducted similar experiments in the Huh7 cell line. In this case, we observed that transfected poly I:C induces gene expression of IFNs independently on MAVS. Surprisingly, at a later phase of the response (24h) IFN-β and IL-29 protein levels were ablated upon MAVS knock-down, suggesting that a MAVS-dependent response might be induced at a latter phase of the response.

We used also a second dsRNA ligand, a 5' triphosphate hairpin RNA (3p-hpRNA) sequence derived from Influenza A virus, known to act as a RIG-I agonist. In this case, both cell lines induced IFNs and pro-inflammatory cytokines dependently on MAVS as in accordance with the literature.

Since transfected poly I:C only partially induced a MAVS-dependent antiviral activity, we hypothesized that the other cytoplasmic receptor, PKR, might be involved. By pharmacologically inhibition of PKR activation, we observed in both the cell lines that IFNs and pro-inflammatory cytokines expression was downregulated upon transfected poly I:C. Furthermore, we observed the same pattern also upon 5'triphosphate hairpin RNA stimulation. The PKR inhibitor C16 has been widely used for studying PKR function and activity [205–207]. However, there is a lack of in vivo studies to completely rule out off target effects. Recent computational analysis showed that C16 might also inhibit the fibroblast growth factor receptor 2 (FGFR2) kinase [208]. Therefore, blocking PKR activation using another approach, such as silencing PKR, would help us to confirm the results observed.

Although poly I:C is a synthetic dsRNA sequence not derived from a viral sequence, it has been widely used as an immunostimulant since it acts as an RNA PAMP, activating TLR3 and cytoplasmic PRRs (among others MDA5 and PKR) [8, 16, 20]. In this chapter, and in significant parts of the work presented in this thesis, we used poly I:C rather than hepatotropic viruses. Hepatotropic viruses, such as HBV and HCV, are known to induce TLR3, PKR, and MDA5-dependent antiviral responses similarly to poly I:C [162–164]. Using poly I:C has allowed us to identify the major PRRs activated by dsRNA in the human hepatic cellular models used in our study and to exclude confounding factors caused by virus-specific immune evasion strategies [188, 209]. Nonetheless, future studies using hepatotropic viral models (such as HBV or HCV) are needed to confirm our observations.

Collectively, our results demonstrate that HepG2 and Huh7 cell lines rely on cytoplasmic PRRs when stimulated with RNA-based PAMPs. The two immunogenic dsRNAs (transfected poly I:C and 3p-hpRNA) used as PAMPs activate both MAVS-dependent and PKR-dependent antiviral activities. Therefore, it is not possible, using the two synthetic PAMPs, to selectively induce a MAVS-dependent or a PKR-dependent antiviral response. Thus, highlighting the complexity and the cross-talk between the different PRRs involved in the innate antiviral response [60].

Since transfected poly I:C showed a greater induction in IFNs and pro-inflammatory cytokines, we used this ligand for the major part of the work presented in this thesis.

We used IFNB1 and IFNL1 gene expression and protein secretion as readouts for the induction of the innate antiviral response. We consistently observed in all three models that IFNL1 induction was stronger than IFNB1. Further investigations focused on type III IFN-dependent antiviral response might their role in the induction of an antiviral state in human hepatocytes.

Chapter 4: Viral sensing alters mitochondrial respiration in human hepatic HepG2 and Huh7 cells

4.1 Abstract

The cellular function of hepatocytes is influenced by their distinct metabolic signature – including homeostatic regulation of glucose, fatty acids and ammonia. However, alterations of hepatic metabolism upon antiviral signalling caused by viral infection remain elusive. Furthermore, the consequences of PRR-induced shifts in hepatic metabolism are greatly unexplored and are focus of this thesis.

In this chapter, using transfected poly I:C as a synthetic viral PAMP stimulant, we sought to determine major metabolic changes in HepG2 and Huh7 human hepatic cell lines. Upon examination, we observed decreased oxygen consumption and mitochondrial membrane polarization, with a concomitant increase in the generation of mitochondrial reactive oxygen species. Moreover, using an antioxidant agent we could modulate the innate antiviral response by decreasing expression of IFNs and pro-inflammatory cytokines. Collectively, the results of this chapter demonstrate that the innate antiviral response in hepatocytes is accompanied by changes in the cellular oxidative state which influences the antiviral potential when manipulated.

4.2 Introduction

On activation, immune cells possess the ability to rapidly alter their cellular metabolism. This phenomenon causes major changes in levels of intracellular metabolites which have moonlighting roles as regulators of cellular function. An informative example includes LPS/Interferon-γ activated macrophages fracturing their conventional Krebs cycle, leading to an accumulation of citrate and succinate and resulting in the subsequent upregulation of compensatory glycolysis. Citrate is used as a substrate in fatty acid synthesis, which is indispensable for membrane biogenesis, needed by antigen-

presenting cells (such as dendritic cells). Succinate has been shown to have pro-inflammatory effects, leading to the stabilisation of transcription factor, hypoxia-inducible factor-1α (HIF-1α), thus inducing IL-1β [101, 111]. Whilst the field of immunometabolism has primarily focused on immune cells, particularly myeloid cells, less is known about cellular metabolism and how it is altered during anti-viral activity in non-immune cells, such as hepatocytes. As previously highlighted, hepatocytes possess unique metabolic activity, being critical regulators of glucose, fatty acids and ammonia homeostasis. Several studies have shown how hepatotropic viruses alter hepatic metabolism in order to achieve persistent infection. For instance, glycolysis and fatty acid biosynthesis are upregulated during hepatitis C infection in order to increase ATP and fatty acid cellular contents required for viral replication [210]. These mechanisms might partly explain the increased incidence of diabetes in chronically infected HCV patients [211].

4.2.1 Type I IFN signalling alters hepatic metabolism

Recent studies are beginning to investigate mechanisms by which hepatocytes induce metabolic alterations while mounting a type I IFN-dependent antiviral response. In a murine model of chronic viral hepatitis, the effects of type I interferons on hepatic amino acid metabolism, such as urea cycle break-down has been inspected. Type I IFN-signalling dependent accumulation of urea cycle metabolite ornithine suppresses viral specific CD8 T cell responses, ameliorating liver pathology [173]. Moreover, type I interferon signalling also caused an imbalance in the cellular oxidative stress, due to decreased antioxidant proteins superoxide dismutase 1 (SOD1) expression [172], perhaps explaining type I IFN-induced cellular damage and consequent hepatic fibrosis during chronic viral infections. Decreased expression of SOD1 has also been observed in chronically infected HCV patients, potentially explaining the increase of hepatic fibrosis development in infected individuals [212, 213]. Yet, how hepatocytes alter their metabolism in response to activation of PRRs responsible for viral PAMPs recognition is still not fully investigated.

4.2.2 Mitochondrial dynamics in antiviral immunity

Mitochondria are dynamic organelles which can divide (fission) or fuse (fusion) with each other, forming smaller or more elongated structures respectively (Fig. 4.1). Mitochondrial fusion and fission are mostly regulated by GTPases localised in the outer mitochondrial membrane [214]. Mitochondrial fission is essential for mitochondrial biogenesis in dividing cells, while mitochondrial fusion has been found critical for cellular energetic homeostasis since mitochondria become more elongated when the cell relies on oxidative phosphorylation [215].

Autophagy is a fundamental cellular mechanism that provides elimination of macromolecules, including nucleic acids, fatty acids, proteins, and organelles to promote homeostasis, differentiation, and cell survival [216]. Also mitochondria can be removed through an autophagic process called mitophagy. Mitophagy has been showed to be intimately linked to mitochondrial fusion and fission, and serve as quality control mechanisms for preserving mitochondria and cellular homeostasis [217, 218]. For instance, it has been shown that irreversible mitochondrial damage by photoirradiation of hepatocytes caused mitochondrial fission and selective segregation of damaged mitochondria which were eliminated by mitophagy [219]. Dysregulations in mitochondrial dynamic and mitophagy cause accumulation of dysfunctional mitochondria, which are at the basis of different pathologies. For instance, mutations in Parkin and PINK1, two proteins involved in mitophagy, lead to early-onset autosomal recessive Parkinson's disease [220, 221].

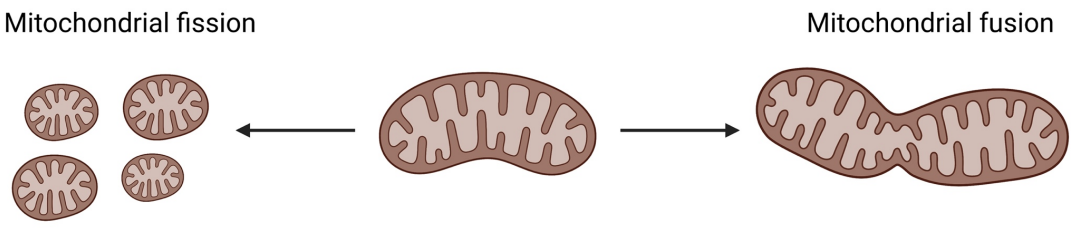

Figure 4.1 Mitochondria are dynamic organelles.

Mitochondria change their structure by diving (fission) or by fusing. These two opposing mechanisms are tightly regulated by GTPases such as mitofusins, which promote mitochondrial fusion, or dynamin-related protein 1 (Drp1) and mitochondrial fission 1 (Fis1), which promote mitochondrial fission.

Since mitochondria are involved in innate antiviral activity, it is not surprising that mitophagy and mitochondrial dynamics influence the outcome of antiviral responses [222]. MAVS, the key player in RLR-dependent antiviral activity, is anchored through its transmembrane domain to mitochondria and is involved in mitochondrial dynamics. Although RLR activation has been shown to promote mitochondrial elongation, the downstream signaling has been shown to be blocked by proteins involved in mitochondrial elongation, such as mitofusin 2 [223, 224]. Whether this is a negative feed-back loop mechanism has not been fully clarified.

Inhibition of mitophagy has been shown to cause accumulation of dysfunctional mitochondria and increased production of reactive oxygen species, which boost MAVS activation, downstream IFNs and pro-inflammatory cytokines expression [133]. MAVS has been also shown to regulate mitophagy. Surprisingly, activated MAVS promotes mitophagy; it limits accumulation of dysfunctional mitochondria and ROS, therefore limiting MAVS-activation itself through a negative feed-back loop [225]. This process is essential for mitochondria homeostasis and regulation of the antiviral response.

Earlier results presented in this thesis demonstrated that the hepatic cell lines HepG2 and Huh7, as well as iPSC-derived hepatocytes respond to transfected poly I:C and 5'-triphosphate hairpin RNA, which act as agonists of cytoplasmic PRRs (PKR and RLRs), by inducing expression of IFNs, pro-inflammatory cytokines, and ISGs. In this chapter, using this synthetic dsRNA poly I:C, we sought to determine whether mounting of an innate antiviral response alters cellular metabolism of hepatocytes, and more specifically mitochondrial activity of HepG2 and Huh7 cells.

4.3 Chapter hypothesis

Double-stranded RNA-induced activation of innate antiviral activity alters the cellular metabolism of HepG2 and Huh7 hepatic cell lines.

4.4 Chapter aims

- To determine whether dsRNA-induced antiviral activity affects glucose metabolism in HepG2 and Huh7 cells.

- To determine how dsRNA stimulation affects the mitochondrial respiration and cellular oxidative stress.

4.5 Results

4.5.1 dsRNA-dependent antiviral activity alters the mitochondrial membrane potential and respiration in HepG2 cells

In order to determine whether activation of the innate antiviral response alters the cellular metabolism in our hepatic models, we measured the oxygen consumption and acidification rate of HepG2 cells upon transfected poly I:C stimulation. In the previous chapter we observed that upon stimulation with transfected poly I:C for 4h, HepG2 cells upregulate gene expression of IFNB1 and CXCL10. Therefore, we hypothesised that this early transcriptional response may be a direct consequence of altered central carbon metabolism needed to amplify the production of antiviral proteins. We stimulated HepG2 cells for 4h and we measured in real time the cellular metabolic profile through mitochondrial stress test. However, we could not detect any change in oxygen consumption rate (OCR) (Fig. 4.2 A) or extracellular acidification rate (ECAR) (Fig. 4.2 B) between the vehicle (lipofectamine) and the transfected poly I:C stimulation.

We further tested the cellular metabolism of HepG2 cells after 24h stimulation with transfected poly I:C. In this case, we observed a decrease in the oxygen consumption rate (OCR) (Fig. 4.3 A) without any significant change in the acidification rate (Fig. 4.3 B). A reduction in basal (Fig. 4.3 C) and maximal respiration (Fig. 4.3 D), as well as ATP production (Fig. 4.3 E) was demonstrated at 24h upon stimulation. These results highlight an antiviral induced alteration in cellular metabolism, with a decrease in mitochondrial-dependent respiration.

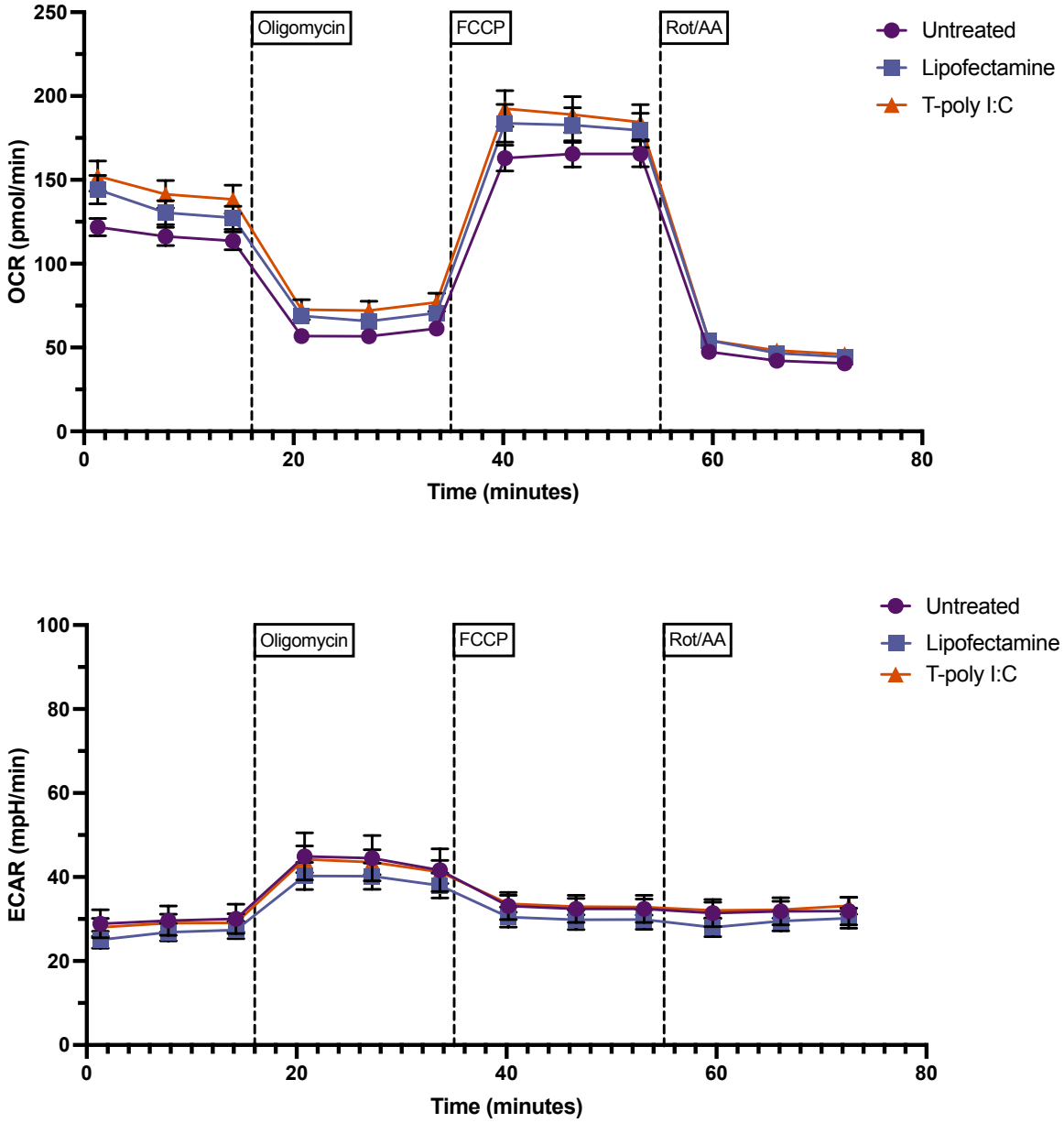

Figure 4.2 HepG2 cells do not alter their cellular respiration upon a short-time period stimulation with dsRNA.

HepG2 cells were stimulated for 4h with transfected poly I:C (T-poly I:C) or the vehicle (lipofectamine). Oxygen consumption rate (OCR) and extracellular acidification rate (ECAR) were measured by Seahorse. Graphs are representative of three independent experiments.

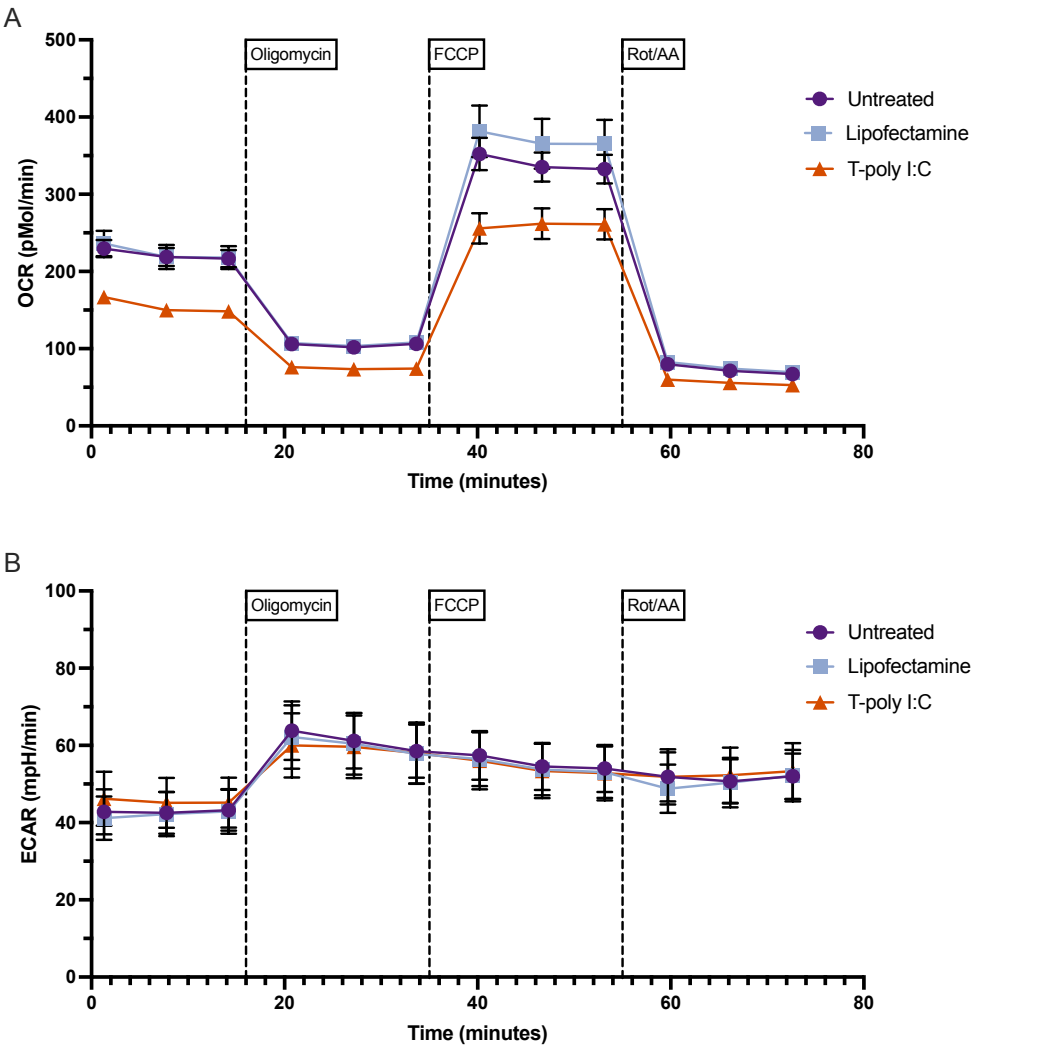
A
Oligomycin
FCCP
Rot/AA
Untreated
Lipofectamine
T-poly I:C
OCR (pMol/min)
Time (minutes)
B
Oligomycin
FCCP
Rot/AA
Untreated
Lipofectamine
T-poly I:C
ECAR (mpH/min)
Time (minutes)

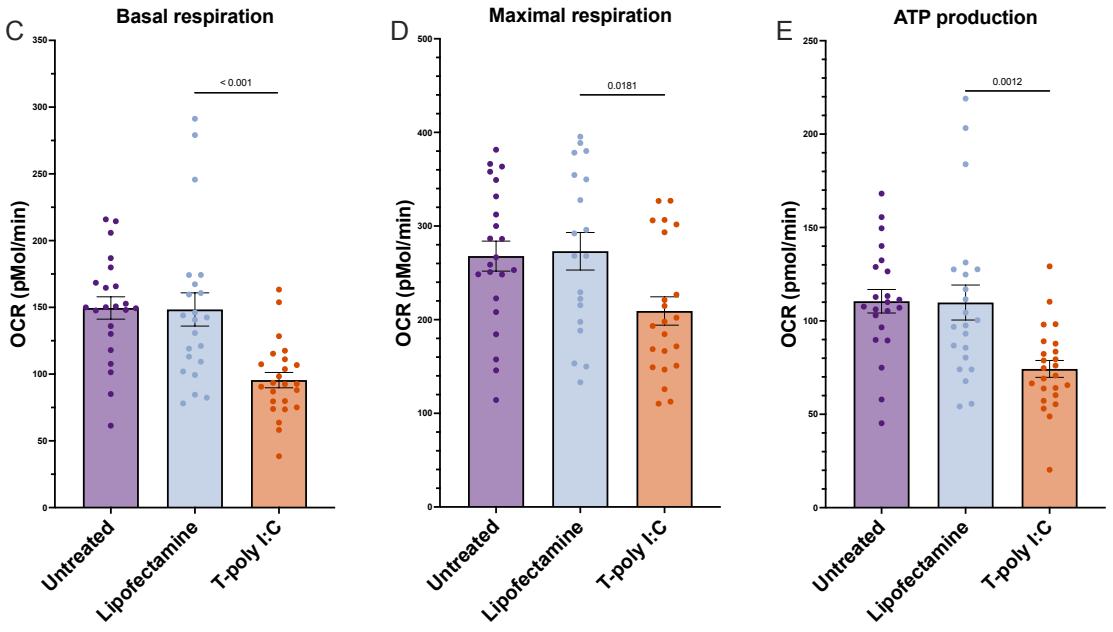
C
Basal respiration
< 0.001
OCR (pMol/min)
Untreated
Lipofectamine
T-poly I:C
D
Maximal respiration
0.0181
OCR (pMol/min)
Untreated
Lipofectamine
T-poly I:C
E
ATP production
0.0012
OCR (pmol/min)
Untreated
Lipofectamine
T-poly I:C

Figure 4.3 Mitochondrial respiration is decreased in HepG2 cells after 24h stimulation with transfected poly I:C.

HepG2 cells were stimulated for 24h with transfected poly I:C (T-poly I:C) or the vehicle (lipofectamine). Oxygen consumption rate (OCR) (A) and extracellular acidification rate (ECAR) (B) were measured by Seahorse. Basal respiration (C), maximal respiration (D), and ATP production (E) were calculated according to protocol. Images A and B are representative of two independent experiments, n = technical replicates from two independent experiments.

4.5.2 HepG2 cells alter the mitochondrial structure and polarization upon transfected poly I:C stimulation

By observing decreased cellular oxygen consumption in response to transfected poly I:C stimulation, we hypothesised that modification of mitochondrial activity may play a central role in the antiviral response of HepG2 cells. Using a specific dye, tetramethyl rhodamine, methyl ester (TMRM), we measured the mitochondrial membrane potential (MMP) and mitochondrial structure. TMRM accumulates in the mitochondrial intermembrane space, with fluorescent intensity dependant on mitochondrial polarization. The greater the mitochondrial polarization (i.e. the more negatively charged the mitochondrial intermembrane space), the greater the fluorescent intensity of TMRM. Since TMRM stains mitochondrial membrane, other parameters such as mitochondrial area and perimeter can be measured. By quantifying mitochondrial perimeter and area, we used the mathematical formula showed in figure 4.4 B to determine the form factor, which indicates a ratio between perimeter and area of the mitochondria. The ratio between the major and minor axes of the mitochondrial structures led us to measure the aspect ratio (Fig. 4.4 C). These two parameters (form factor and aspect ratio) are used as indicative measurements of the mitochondrial structure. A decrease in these two measures indicates that structurally, mitochondria are becoming shorter and more rounded (a process known as mitochondrial fission). While during mitochondrial fusion, when the organelle becomes more elongated, form factor and aspect ratio are increased (Fig. 4.4 A) [218].

A

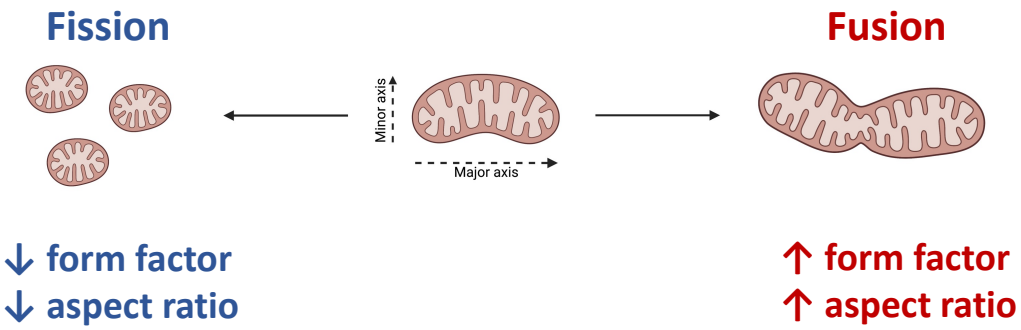

B

$$\text{Form factor} = (\text{Perimeter})^2/(4\pi * \text{Area})$$

C

$$\text{Aspect ratio} = \text{Major axis} / \text{minor axis}$$

Figure 4.4. Calculations of mitochondrial shape parameters.

Mitochondrial shape can be determined by calculating the two parameters form factor and aspect ratio. These two measures can be extrapolated by the two formulas B and C respectively. Increase in form factor and aspect ratio evidences a fusion process, with mitochondria being more elongated. Decrease of form factor and aspect ratio can be seen in mitochondria ongoing through a fission process (A).

We could not detect any change in the mitochondrial membrane polarization at 4h stimulation with transfected poly I:C (Fig. 4.5 A). At this short duration of stimulation, we observed a slight increase in the form factor, without any significant change in the aspect ratio (Fig. 4.5 B and C), thus indicating that the mitochondrial architecture might be affected even at a short time period stimulation without any drastic change in the mitochondrial polarization.

After 24h stimulation with transfected poly I:C, the mitochondrial membrane potential was reduced (Fig. 4.5 D), in concordance with the data obtained through the Seahorse assay, where we observed a decrease in the mitochondrial respiration. Thus, meaning that the mitochondrial activity and respiration is reduced. We also detected an increase in form factor and aspect ratio (Fig. 4.5 E and F). These results might indicate increased mitochondrial fusion process in concomitance with a decrease of mitochondrial respiration.

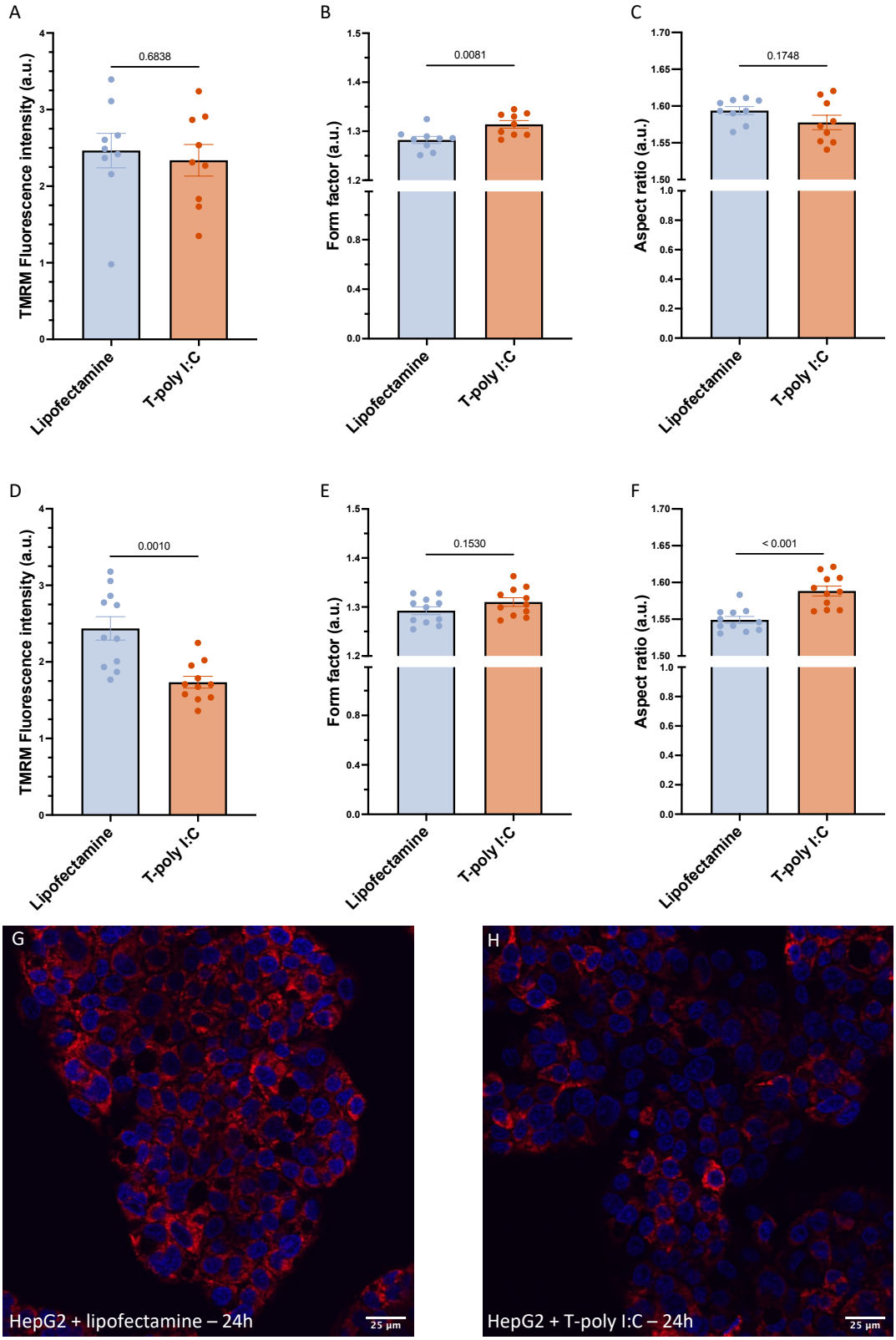
A
TMRM Fluorescence intensity (a.u.)
0.6838
Lipofectamine
T-poly I:C
B
Form factor (a.u.)
0.0081
Lipofectamine
T-poly I:C
C
Aspect ratio (a.u.)
0.1748
Lipofectamine
T-poly I:C
D
TMRM Fluorescence intensity (a.u.)
0.0010
Lipofectamine
T-poly I:C
E
Form factor (a.u.)
0.1530
Lipofectamine
T-poly I:C
F
Aspect ratio (a.u.)
< 0.001
Lipofectamine
T-poly I:C
G
HepG2 + lipofectamine – 24h
25 µm
H
HepG2 + T-poly I:C – 24h
25 µm

Figure 4.5 Mitochondrial structure and polarization are altered in response to transfected poly I:C in HepG2 cells.

HepG2 cells were stimulated for 4h or 24h with transfected poly I:C (T-poly I:C) or vehicle (lipofectamine) and stained with TMRM. Fluorescence intensities, form factor and aspect ratio were determined by analysis with the software Cell Profiler. Data are mean ± SEM, n = technical replicates from three independent experiments. Images G and H are representative of three experiments.

4.5.3 Transfected poly I:C stimulation decreases oxygen consumption rate in Huh7 cells

We next sought to determine whether this decrease in oxygen consumption rate and mitochondrial membrane polarization is cell line specific or if it is a conserved mechanism observable in other hepatic cell lines. We used Huh7 cells as a second hepatic model and stimulated with transfected poly I:C for 24h. We observed a decrease in the oxygen consumption rate and a slight decrease in the acidification rate (Fig. 4.6 A and B). Maximal respiration and ATP production were significantly reduced (Fig. 4.6 D and E). Overall, the data obtained is in concordance with the results observed in HepG2 cells. Conclusively, this indicates that prolonged stimulation with transfected poly I:C decreases the cellular oxygen consumption rate of the two hepatic cell lines used. It is worth noting that lipofectamine (vehicle) affected the cellular metabolism, with a slight increase in the OCR and ECAR, thus highlighting the importance of using proper controls during transfected poly I:C stimulation.

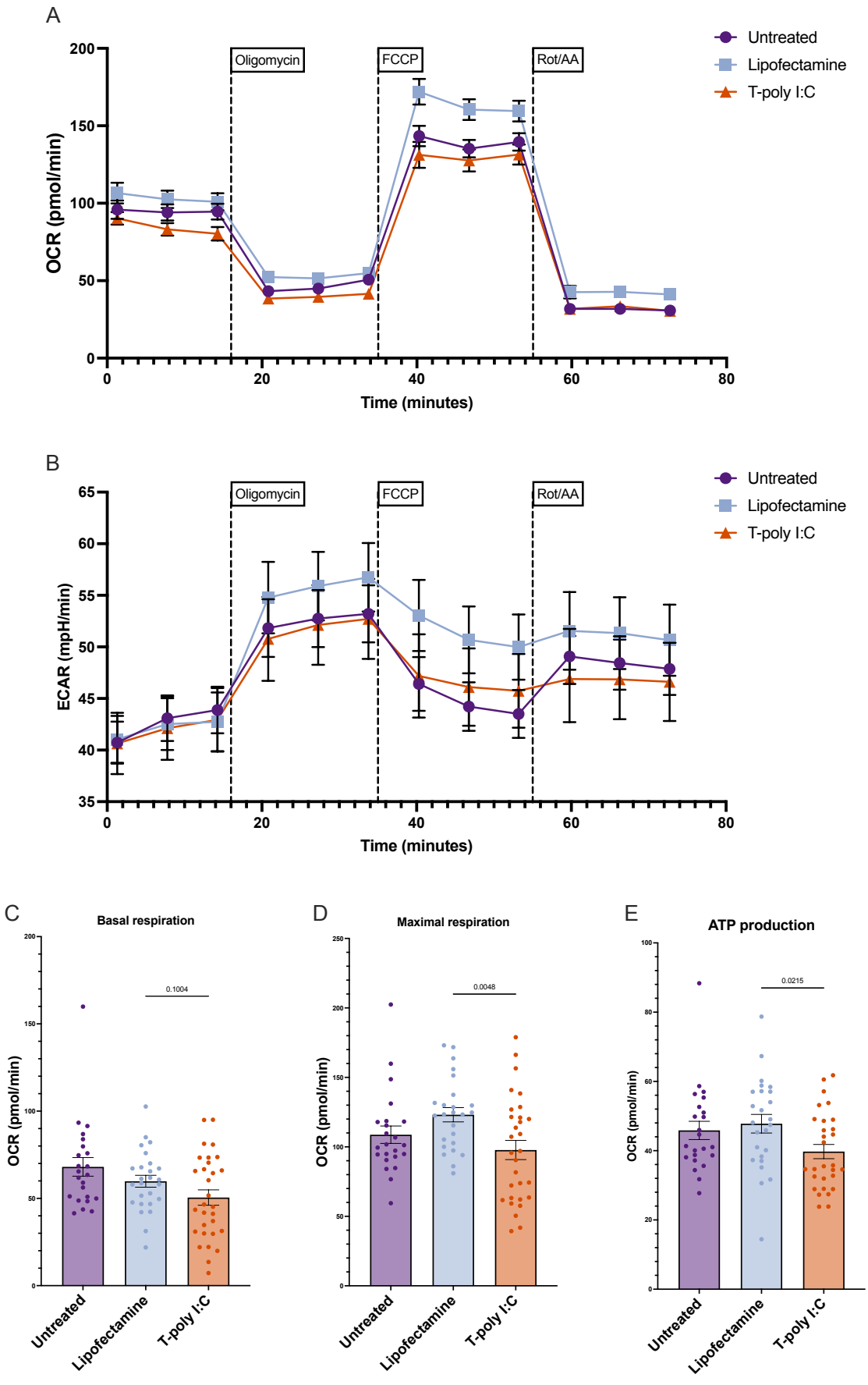
A
Untreated
Lipofectamine
T-poly I:C
Oligomycin
FCCP
Rot/AA
OCR (pmol/min)
Time (minutes)
B
ECAR (mpH/min)
C
Basal respiration
0.1004
D
Maximal respiration
0.0048
E
ATP production
0.0215

Figure 4.6 Transfected poly I:C stimulation decreases oxygen consumption rate in Huh7 cells.

Huh7 cells were stimulated for 24h with transfected poly I:C (T-poly I:C) or the vehicle (lipofectamine). Oxygen consumption rate (OCR) (A) and extracellular acidification rate (ECAR) (B) were measured by Seahorse. Basal respiration (C), maximal respiration (D), and ATP production (E) were calculated according to protocol. Images A and B are representative of two independent experiments, n = technical replicates from two independent experiments.

4.5.4 Transfected poly I:C decreases mitochondrial membrane polarization and boosts mitochondrial reactive oxygen species in Huh7 cells

We further analysed the mitochondrial membrane potential and structure of Huh7 cells stimulated with transfected poly I:C at 4 and 24h. Similarly to what we observed in HepG2 cells, 24h after stimulation, mitochondrial membrane polarization, form factor, and aspect ratio were decreased (Fig. 4.7 D-F). These results indicate decreased mitochondrial activity with changes in mitochondrial shape, becoming shorter and less elongated through the fission process. These results show that, similarly to HepG2 hepatic cells, mitochondrial membrane polarization of Huh7 is also decreased upon a prolonged stimulation (24h) with transfected poly I:C. Interestingly, disparities in mitochondrial shape between the two hepatic cell lines was recorded. Mitochondria within HepG2 cells presented structurally as more fused and elongated (increase in form factor and aspect ratio) when compared to those of Huh7, appearing smaller and more suited for fission. Since we observed a decrease in the oxygen consumption rate and concomitant mitochondrial membrane polarization in Huh7 cells, we hypothesised that transfected poly I:C might affect the oxidative state of the cells. We measured mitochondrial ROS levels after 4h of stimulation (Fig. 4.8 A), and at later time-point (24h) (Fig. 4.8 B), when a decrease in mitochondrial respiration is observed. We observed that at both time points transfected poly I:C slightly increased mitochondrial ROS levels in Huh7 cells.

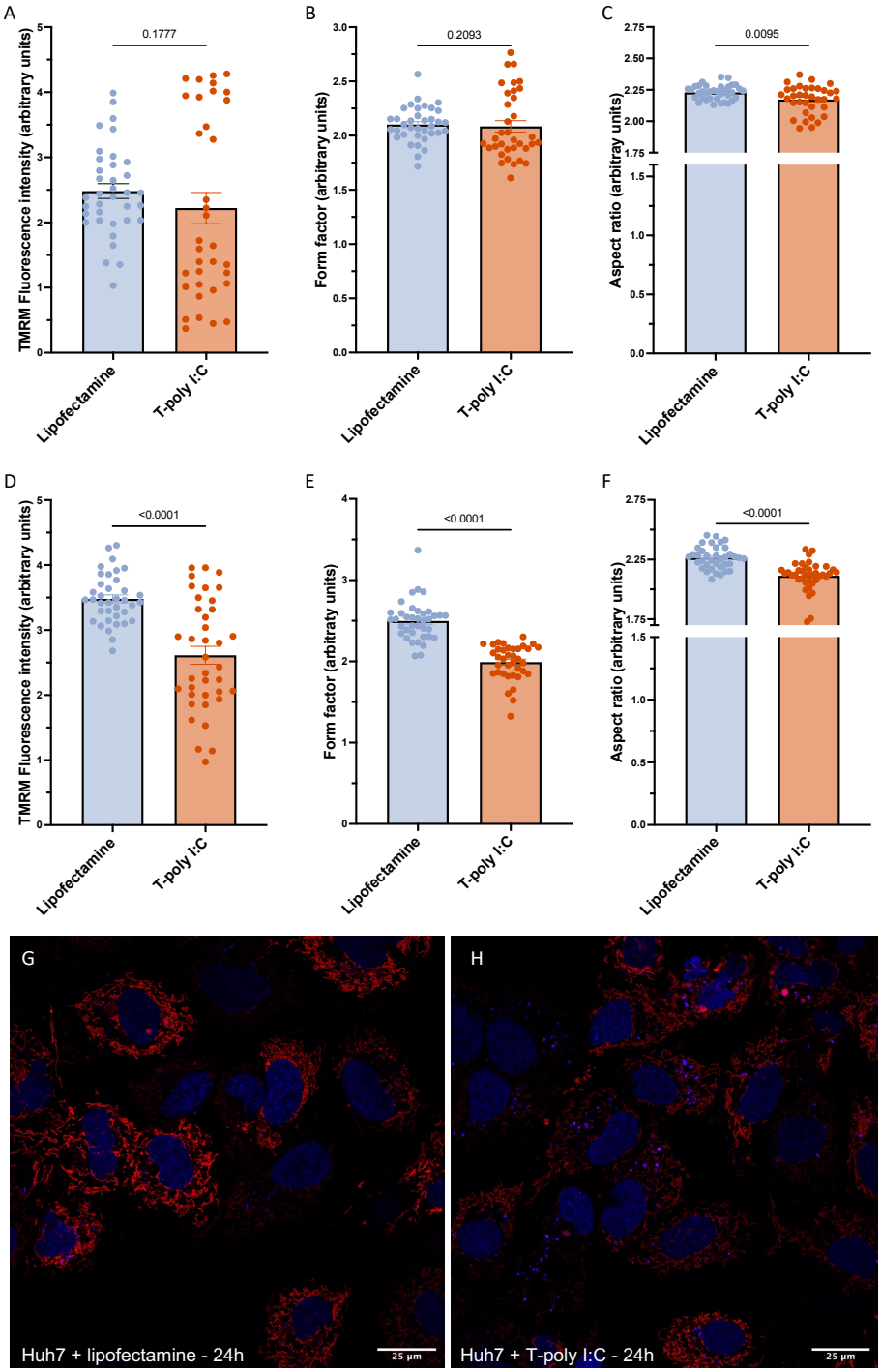

Figure 4.7 Transfected poly I:C stimulation decreases mitochondrial membrane polarization in Huh7 cells.

Huh7 cells were stimulated for 24h with transfected poly I:C (T-poly I:C) or vehicle (lipofectamine) and stained with TMRM. Fluorescence intensities, form factor and aspect ratio were determined by analysis with the software Cell Profiler. Data are mean ± SEM, n = technical replicates from three independent experiments. Images D and E are representative of three independent experiments.

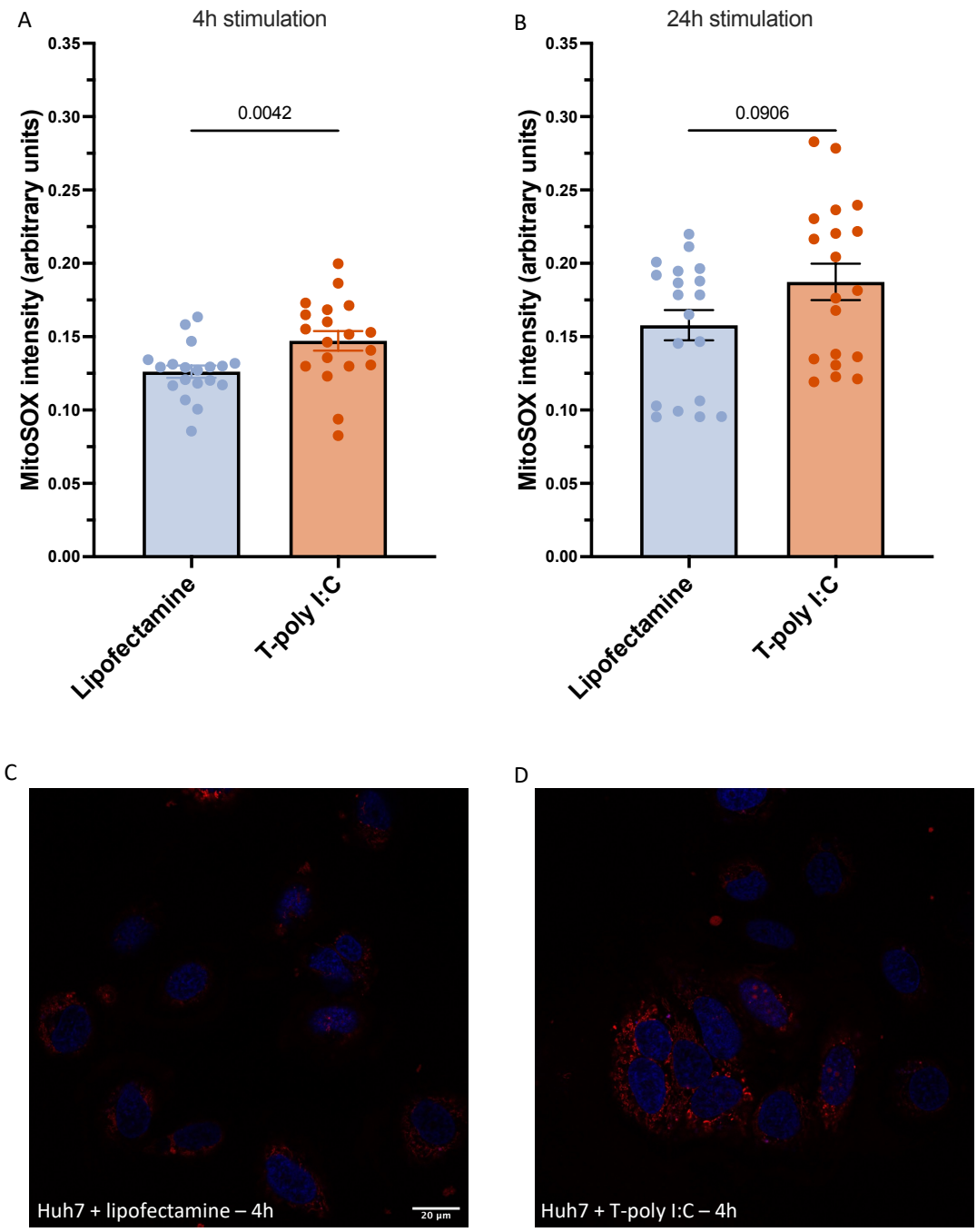

Figure 4.8 Stimulation with transfected poly I:C increases mitochondrial reactive oxygen species in Huh7 cells.

Huh7 cells were stimulated for 4h (A) or 24h (B) with transfected poly I:C (T-poly I:C) or vehicle (lipofectamine) and stained with MitoSOX red. Fluorescence intensity was determined by analysis with the software Cell Profiler. Data are mean ± SEM, n = technical replicates from three independent experiments. Images D and E are representative of three independent experiments.

4.5.5 ROS scavenger N-acetyl cysteine ablates the dsRNA-induced antiviral activity in HepG2 and Huh7 cells

Since we observed that transfected poly I:C stimulation alters the cellular oxidative equilibrium, we next hypothesised that manipulation of the ROS levels might affect the antiviral response. Therefore, we used N-acetyl cysteine (NAC), which is converted in cells to reduced glutathione, a natural ROS scavenger. Pre-treatment with N-acetyl cysteine decreased in a dose-dependent manner IFNL1, CXCL10 and TNF gene expression at 4h (fig. 4.9 A-C), while at 24h type I IFN protein level was reduced in HepG2 cells (Fig. 4.9 D). This observation also remained true for Huh7 cells, where type I IFN and IL-29 protein levels were decreased by NAC pre-treatment prior to transfected poly I:C stimulation (Fig. 4.10 A and B).

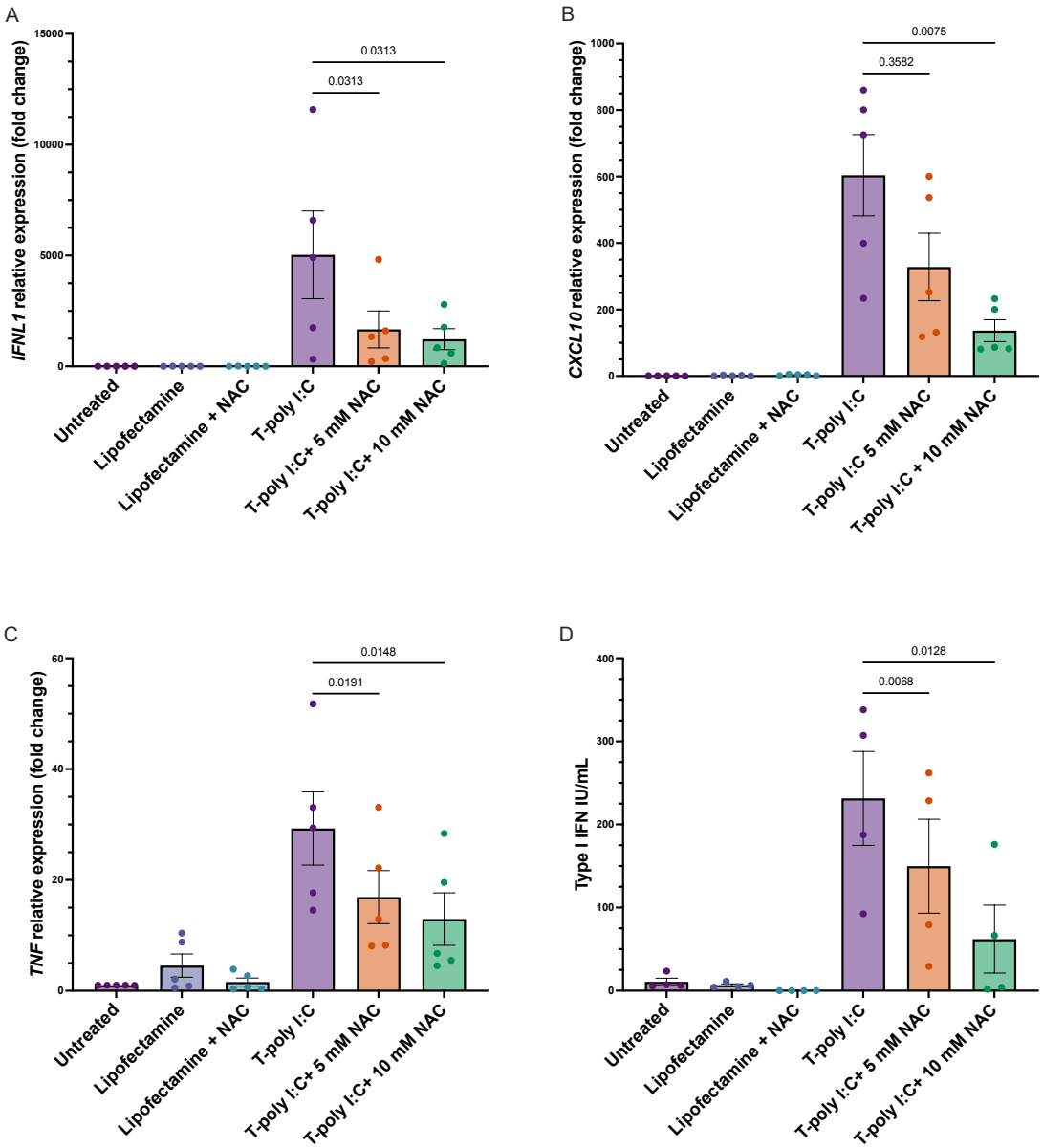

Figure 4.9 ROS scavenger N-acetyl cysteine ablates the dsRNA-induced antiviral response in HepG2 cells.

HepG2 were stimulated for 1h with N-acetyl cysteine (NAC) 5 or 10 nM and subsequently stimulated with transfected poly I:C (T-poly I:C, 1μg/ml) for 4h. Gene expression of IFNL1 (A), CXCL10 (B) and TNF (C) was determined by RT-qPCR. Type I IFN Huh7 (F) levels (D) were determined by HEK-blue assay. Data are mean ± S.E.M. of five (A to C) and four independent experiments, p value were calculated using paired one-way ANOVA.

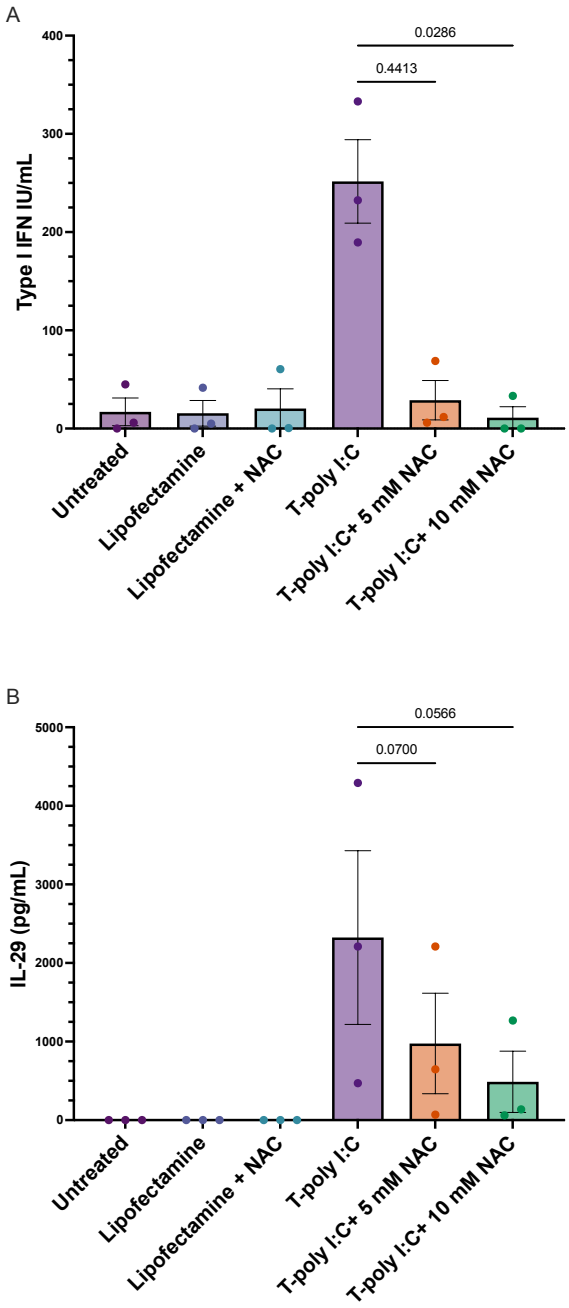

Figure 4.10 ROS scavenger N-acetyl cysteine ablates the dsRNA-induced type I and III interferon secretion.

Huh7 cells were stimulated for 1h with N-acetyl cysteine (NAC) 5 or 10 nM and subsequently stimulated with transfected poly I:C (T-poly I:C, 5 μg/ml) for 24h. Type I IFN (A) and IL-29 protein levels (B) were determined by HEK-blue assay and ELISA respectively. Data are mean ± S.E.M. of three independent experiments, p value were calculated using paired one-way ANOVA.

4.6 Discussion

Unravelling the metabolic features and activity of immune cells expands our knowledge of how the immune system functions and provides novel therapeutic targets and strategies [96]. Since PRRs are not exclusively expressed on immune cells, understanding how cellular metabolism of other cell types (such as epithelial cells and hepatocytes) is linked with innate immune responses would offer additional advantages in developing new therapies, particularly against viruses that infect them.

The previous chapter and results of other researchers have shown that hepatocytes express PRRs and are capable of detecting and responding to viral ligands. In this chapter we aimed to determine whether the two hepatic cell lines, Huh7 and HepG2 used as human hepatic models, alter their metabolism upon stimulation with transfected dsRNA (poly I:C), an activating ligand of cytoplasmic PRRs PKR and RLRs (as shown in the previous chapter). We demonstrated that in both cell lines, the antiviral response induced a decrease in the oxygen consumption rate 24h after stimulation. Surprisingly we did not observe any strong effect on the extracellular acidification rate (ECAR) upon stimulation with poly I:C in neither the two cell lines in contrast to what has been described in other cellular models [107]. In this case we speculate that the absence on variation in ECAR might be due to two different factors. Either hepatocytes have a unique metabolism different from other cell types and the hepatic glycolysis is not affected by poly I:C stimulation, or since the two hepatic cellular models used in the study, being cancer cells and due to Warburg effect, have an enhanced glycolysis which is not perturbated by the stimulation. Further studies using primary human hepatocytes or iPS-derived hepatocytes would help us to unravel which is the case.

We further focused on the mitochondrial activity during the dsRNA sensing. Using a specific dye (TMRM) we noticed a decrease in the membrane mitochondrial polarization after 24h stimulation. While we could detect similar changes at earlier time points such as 4h upon stimulation. Whether this phenotype is due to PRRs activation or to a paracrine/autocrine effect by type I, type III IFNs, or pro-inflammatory cytokines (such

as TNF) signalling is object of further investigations. Employment of IFNAR1 and IFNLR1 KO cells could highlight the possible mechanism behind our observations.

The decreased mitochondrial activity and respiration might be at the basis of a defence mechanism; by downregulating the cellular metabolism, also the viral pathogen might strive in replicating withing the cell, therefore limiting the infection.

Alterations in mitochondrial organisation upon poly I:C transfection were also noted, with those of HepG2 cells displaying a more elongated structure compared to more rounded mitochondria of Huh7 cells. Further research is required to delineate whether these opposing observations are a product of variability between the two cell lines or the possibility of differential antiviral induced mitochondrial activity.

Since we observed downregulation of the mitochondrial respiration upon transfected poly I:C stimulation, we hypothesised that cells might have altered mitochondrial metabolism. We sought to determine whether an increase in the oxidative stress, such as an increase in reactive oxygen species, was observable upon dsRNA stimulation. Reactive oxygen species (ROS) comprehend species derived from molecular oxygen (O_2) that are more reactive than O_2 itself [130]. This group of molecules are produced in different cellular compartments and are involved in several cellular functions as it will be discussed in further detail in chapter 5. Using a specific mitochondrial dye (MitoSOX red), we observed an increase in mitochondrial ROS (mROS) upon transfected poly I:C stimulation at both an early time point (4h) as well as at a later stage (24h).

We further aimed to determine whether a manipulation of ROS levels would affect the antiviral response. In order to achieve this we used N-acetyl cysteine (NAC), a molecule consumed by cells for the generation of the major antioxidant, glutathione. By pre-treating HepG2 and Huh7 cells with NAC, we observed decreased expression of type I and III IFNs, as well as pro-inflammatory cytokines upon transfected poly I:C stimulation. Further research using specific mitochondrial ROS scavengers and mitochondrial-specific oxidants - such as Mito-Tempo and MitoParaquat, respectively - would help us to

determine whether mitochondrial ROS are essential in modulating the innate antiviral activity.

In conclusion, here we showed that activation of RLRs and PKR-mediated innate antiviral activity decreases the cellular respiration of hepatocytes, due to a downregulation of mitochondrial activity. Moreover, we observed a concomitant upregulation of mitochondrial ROS and that modulation of ROS affects the potency of the hepatic antiviral response (Fig. 4.11).

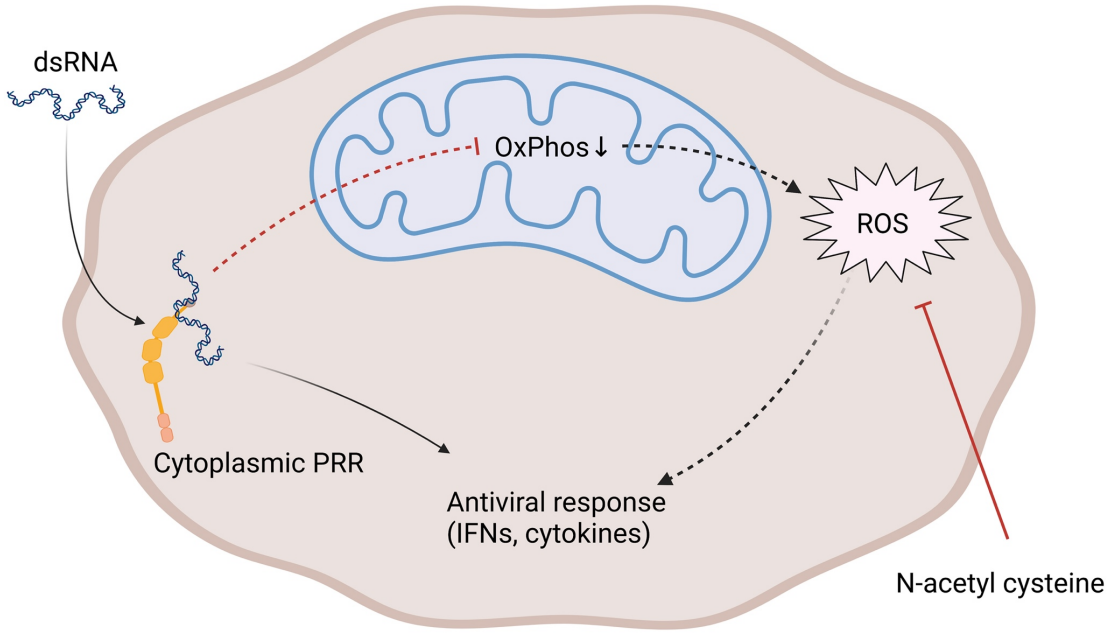

Figure 4.11 Reactive oxygen species modulate the transfected poly I:C-induced antiviral response in human hepatic cell lines HepG2 and Huh7.

The cytoplasmic PRRs (PKR and RLRs) agonist double stranded RNA transfected poly I:C induces decreased oxidative phosphorylation and increased mitochondrial reactive oxygen species. ROS scavengers, such as N-acetyl cysteine, decrease the antiviral response.

Chapter 5: Peroxiredoxin 4 deficiency amplifies the antiviral response to dsRNA

5.1 Abstract

Hepatic viral infection triggers production of type I and type III interferons, followed by induction of genes involved in antiviral activity. Innate antiviral activity is associated with changes in hepatocyte metabolism including a breakdown of the urea cycle and increased type I interferon-dependent oxidative stress.

Having demonstrated increased oxidative stress upon dsRNA stimulation of hepatocytes, in this chapter we focus on identifying antioxidant enzymes that might play roles in regulating innate antiviral activity induced by dsRNA stimulation. We identify the antioxidant peroxiredoxin 4 (PRDX4) as a potential regulator of the innate antiviral response. PRDX4 deficiency increases expression of type I and III interferons upon stimulation with dsRNA or after hepatotropic infection. Furthermore, we observed that PRDX4 knock-down increases mitochondrial antiviral protein (MAVS) activation, involved in the RNA-dependent antiviral response. These findings highlight the role of PRDX4 in the innate antiviral response and suggest potential new therapeutical strategies involving this enzyme.

5.2 Introduction

The term “reactive oxygen species” (ROS) refers to a large family of oxidants derived from O_2 that are more reactive than O_2 itself [130]. ROS are part of a larger family of reactive species, which are named based on the nature of the reactive atom and include reactive oxygen species, reactive nitrogen species (RNS), and reactive sulfur species (RSS). ROS undergo redox (reduction-oxidation) reactions consisting of oxidation of the substrate, which is generally a cellular macromolecule, such as a lipid, protein, carbohydrate, or nucleic acids [226]. ROS can be chemically divided into two groups: free radicals and nonradicals. Molecules containing one or more unpaired electrons are

called free radicals. Nonradical ROS are generated by two free radicals sharing their unpaired electrons. The major cellular ROS of physiological significance are indicated in table 5.1. Among these, superoxide anion ($O_2^{\bullet -}$) and hydrogen peroxide (H_2O_2) have been studied most extensively [227]. While $O_2^{\bullet -}$ is a free radical, H_2O_2 is a nonradical ROS. ROS can act as a secondary messengers involved in signal transduction.

ROS	Chemical formula	Reactivity
Superoxide radical anion	$O_2^{\bullet -}$	• Selectively reactive • Can reduce metals (Fe^{3+}, Cu^{2+}) • Reacts with nitric oxide to generate peroxynitrite • Reacts with other radicals to form hydroperoxides • Can damage enzymes that contain Fe-S clusters
Hydrogen peroxide	H_2O_2	• Reacts slowly with thiols, such as GSH and protein Cys residues
Hydroxyl radical	$^{\bullet}OH$	• Reacts non-specifically with adjacent molecules
Peroxynitrite	$ONOO^-$/ONOOH	• Reactions with thiols and metal • Reaction with CO2 to generate $ONOOOCO_2^-$
Carbonate radical anion	$CO^{\bullet -}$	• Oxidizes guanine in DNA, cysteine, tyrosine and tryptophan
Hypohalous acids (hypoclorus and hypobromus acids)	HOCl and HOBr	• Strong oxidants, mainly react with thiols and methionine

Table 5.1 Common cellular ROS.

Table adapted from [130].

5.2.1 Sources of ROS production

ROS can be derived from endogenous or exogenous sources, including heavy metals, radiation, and xenobiotics. Here we focus on ROS derived from endogenous sources. Within the cell, ROS are produced from molecular oxygen as a product of cellular metabolism. The mitochondrial electron transport chain – in particular Complex I and III – is the major source of ROS, however, other proteins, such as NADPH oxidases (NOXs) [228], the flavoenzyme ERO1 in the endoplasmic reticulum [229], cytochrome P450s [230], xanthine oxidase [231], and nitric oxide synthases [232] also contribute to endogenous ROS levels (table 5.2).

Protein name	**Abbreviation**	**Location**	**Product**
Aldehyde oxidase	AOX1	C	H_2O_2
Amine oxidases	AOFs	M	H_2O_2
D-amino acid oxidase	OXDA	Px	H_2O_2
L-amino acid oxidase	OXLA	L	H_2O_2
Cytochrome P450 3A4	CP3A4	ER	$O_2^{\cdot-}/H_2O_2$
Cytochrome P450 2D6	CP2D6	ER	$O_2^{\cdot-}/H_2O_2$
Cytochrome P450 2E1	CP2E1	ER, M	$O_2^{\cdot-}/H_2O_2$
Cytochrome P450 4A11	CP4AB	ER	$O_2^{\cdot-}/H_2O_2$
ERO1-like protein-α	ERO1A	ER	H_2O_2
ERO1-like protein-β	ERO1B	ER	H_2O_2
Pyridoxine 5'-phosphate oxidase	PNPO	C	H_2O_2
Sulfhydryl oxidase 1 and 2	QSOX1 and 2	G, N, PM, S	H_2O_2
Xanthine dehydrogenase/oxidase	XDH	C, PM, S	H_2O_2
NADPH oxidases (1-3)	NOX1, NOX2, NOX3	PM	$O_2^{\cdot-}$
NADPH oxidase 4	NOX4	ER, PM, N	H_2O_2
NADPH oxidase 5	NOX5	ER	$O_2^{\cdot-}$
Dual oxidase 1	DUOX1	PM	H_2O_2
Dual oxidase 2	DUOX2	PM	H_2O_2

Table 5.2 Major $O_2^{\bullet-}$ and H_2O_2-generating human enzymes.

C, cytoplasm; ER, endoplasmic reticulum; G, Golgi; M, mitochondria; N, nucleus; PM, plasma membrane; Px, peroxisome; S, secreted; R-SH, protein cysteine residue; R-SSG, glutathionylated cysteine residue. Table adapted from [228].

5.2.2 Oxidative stress and ROS scavengers

ROS can act as a secondary messengers involved in signal transduction by oxidising various macromolecules, including those highlighted later in this section. ROS cellular concentrations fluctuate within a specific range – nanomolar for H_2O_2, and picomolar for $O_2^{\bullet-}$ [233] - enabling ROS-dependent cellular signaling, also known as redox signaling. Cellular ROS concentrations are fine-tuned by ROS biogenesis and ROS catabolism. ROS-mediated oxidation of macromolecules such as proteins can provoke a change in their activity. The reaction of ROS with proteins thiol groups provides a mechanism through which cells can sense changes in the redox balance [234]. Antioxidant proteins catabolise ROS to non-reactive oxygen-containing molecules, such as H_2O.

In some situations, where an imbalance between oxidants and antioxidants occurs in favour of the oxidants, the disruption of redox signaling causes molecular and cellular damage [235]. This scenario is known as oxidative stress (Fig. 5.1). Oxidative stress has been shown to be involved in a wide range of pathologies including atherosclerosis, cancer, chronic obstructive pulmonary disease (COPD), Alzheimer disease, chronic liver diseases such as non-alcoholic fatty liver disease (NAFLD), viral hepatitis, and hepatocellular carcinoma [236, 237]. There are two main mechanisms through which oxidative stress contributes to disease. The first involves the oxidation of macromolecules, including lipids, proteins, and nucleic acid, leading to aberrant cell function and eventual cell death or carcinogenesis. The second mechanism is anomalous redox signaling due to excess H_2O_2 and $O_2^{\bullet-}$, therefore provoking aberrant cell functioning [237].

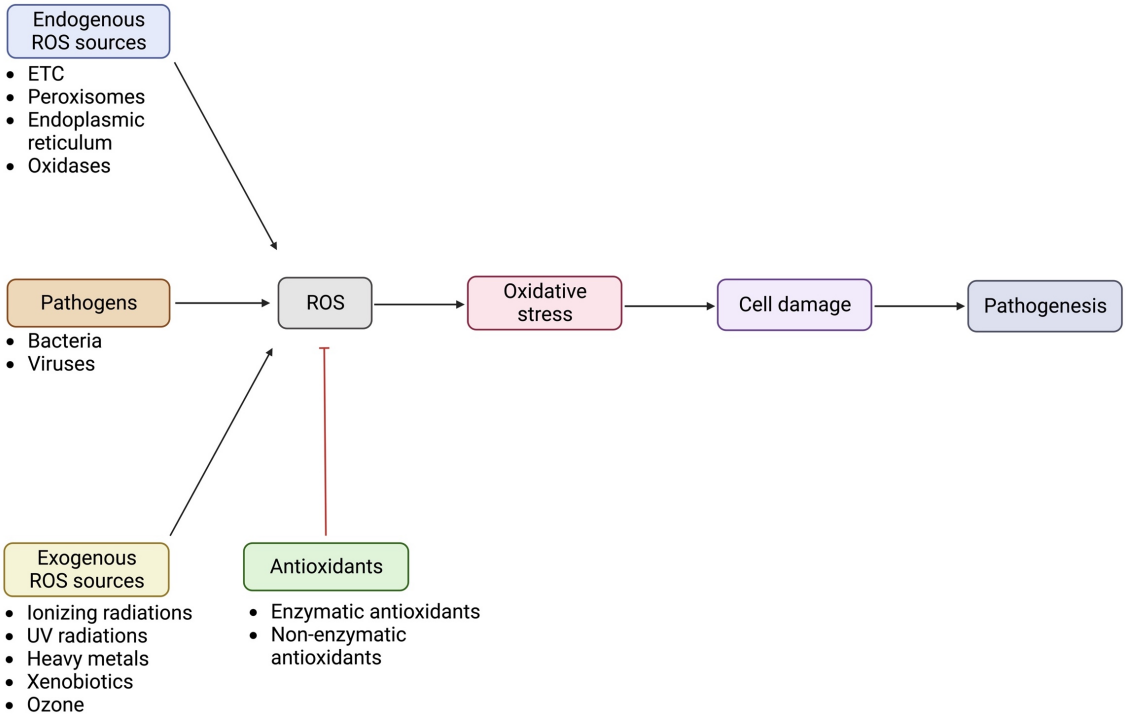

Figure 5.1 Overview of the major ROS sources and ROS-mediated damage.

Figure adapted from [238].

5.2.3 Antioxidant defence

Antioxidant defence can be divided into two categories: enzymatic and non-enzymatic. Since superoxide is the primary ROS produced by various sources – among them Complex I and III of the ETC – its conversion is of primary importance for the balance of the cellular redox state. Superoxide dismutases (SODs) are the main enzymes involved in catalysing the conversion of $O_2^{\bullet -}$ to H_2O_2. H_2O_2 can be scavenged by different enzymes, including thioredoxins, peroxiredoxins, and glutaredoxins (Table 5.3).

Nonenzymatic antioxidants include low-molecular-weight molecules such as the tripeptide glutathione (GSH). GSH is highly abundant in all cell compartments. GSH functions by donating its electrons to H_2O_2 to reduce it into H_2O and O_2, while GSH is oxidised to GSSG. GSH is also a cofactor for several detoxifying enzymes, such as glutathione-S transferases (GSTs), which inactive secondary metabolites by covalently binding GSH molecule to the toxic substrates, such as aldehydes [227]. GSTs, as discussed below are also involved in protein glutathionylation, which act as a post-translational

modification, therefore GSTs and their cofactor, GSH, have a major role in redox signaling.

Protein name	Abbreviation	Location	Product
Catalase	CAT	C	H_2O
Superoxide dismutase 1[Cu–Zn]	SOD1	C, N, M	H_2O_2
Superoxide dismutase 2 [Mn]	SOD2	M	H_2O_2
Extracellular superoxide dismutase [Cu–Zn]	SOD3	PM, S	H_2O_2
Peroxiredoxins 1	PRDX1	C, M	H_2O
Peroxiredoxins 2	PRDX2	C	H_2O
Peroxiredoxins 3	PRDX3	M	H_2O
Peroxiredoxins 4	PRDX4	ER, C, S	H_2O
Peroxiredoxins 5	PRDX5	M	H_2O
Peroxiredoxins 6	PRDX6	C	H_2O
Glutathione-S-transferases	GSTs	C, M, ER, N, PM	R-SH, R-SSG
Glutaredoxins	GLRXs	C, ER, M, N	R-SH, R-SSG
Thioredoxin	TXN	C, N	R-SH
Thioredoxin 2	TXN2	M	R-SH

Table 5.3 Major antioxidant enzymes.

Table adapted from [227] *and* [228].

5.2.4 Peroxiredoxins as transducers H_2O_2-mediated redox signaling

Peroxiredoxins (PRDXs) are a ubiquitous family of small (22 to 30 kDa) cysteine-dependent antioxidant enzymes involved in regulating ROS cellular levels by reducing H_2O_2 molecules (mechanism shown in Fig. 5.2) [239]. Mammalians have six peroxiredoxin, PRDX1 to 6 [240], which contain a conserved cysteine residue which is firstly oxidised by peroxides, designated as “peroxidatic” cysteine (C_P). Peroxiredoxins can be classified by the presence or absence of a second cysteine residue (known as

resolving cysteine, C_R) involved in the reaction. Therefore, PRDXs can be: 2-cysteines (2-Cys), atypical 2-Cys, and 1-Cys PRDXs. 2-Cys PRDXs (from PRDX1 to PRDX4) are homodimeric and contain both C_P and C_R. In 2-Cys PRDXs the thiol group on C_P is oxidised to C_P-SOH, which reacts with the thiol group of C_R contained of the other subunit, forming an intersubunit disulfide (Figure 5.4 A). In atypical 2-Cys PRDX, such as PRDX5, the C_P-SOH reacts with a C_R contained of the same subunit, forming an intra-subunit disulfide bond (Fig. 5.2 B). The difference between 2-Cys and atypical 2-Cys is that in the first case two monomers are involved in the disulfide bond, while in the latter case the disulfide bond is between two cysteines of the same monomer. In 1-Cys PRDXs, such as PRDX6, the C_p-SOH forms disulfide bonds with other proteins or small thiols (Fig. 5.2 C) [241]. The peroxidase activity of PRDXs towards H_2O_2 is critical in preventing the oxidative damage. Moreover, they can also oxidise several substrate proteins. The oxidised PRDXs, either with the sulfenic group (C_p-SOH, in the case of PRDX6) or the disulfide bond (C_p-S-S-C_R), can form intermolecular disulfide bonds with target proteins. Resolution of this disulfide bond results in generation of PRDX reduced cysteine and oxidation of the target protein cysteine, thus modifying the interacting protein (2-Cys PRDX-mediated oxidation mechanism is shown in Fig. 5.2 D) [242]. The oxidised cysteines can be reduced to their initial state by thioredoxins. For instance, PRDX2 has been shown to oxidise STAT3 and inhibit its activation [243], while PRDX1 by oxidising ASK1 activates this kinase and the downstream signaling [244]. In both cases the two peroxiredoxins are firstly oxidised on their cysteines by H_2O_2 and subsequently they can oxidise their targets (Fig. 5.2 D).

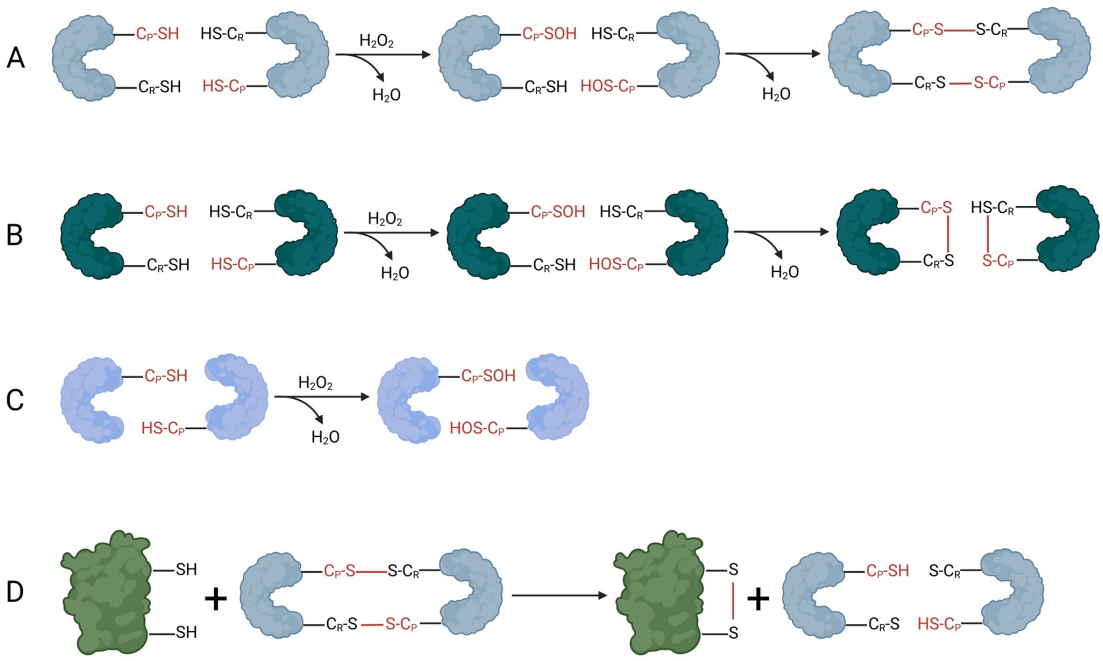

Figure 5.2 Overview of mechanisms of peroxiredoxins for scavenging H_2O_2 and redox signaling.

H_2O_2 scavenging mechanisms in 2-cysteine peroxiredoxins (peroxiredoxin 1 to 4) (A), atypical 2-cysteine peroxiredoxins (peroxiredoxin 5), and 1-cysteine (peroxiredoxin 6) (C). PRDX-mediated oxidation of protein target (in green) cysteine residue with formation of intramolecular disulfide bond (D). Figure adapted from [240] *and* [243].

Because of their dual functions, as scavengers and as redox signaling mediators, PRDXs are involved in several cellular functions and pathologies [245]. Moreover, PRDXs have been shown to be critical in replication and survival of different viruses, including HBV [246]. Peroxiredoxins regulate the life cycle of specific pathogens, not only through modulation of redox homeostasis (which can be pro-viral or anti-viral depending on the virus itself [115, 247]), but also via direct interaction with viral proteins [248]. Viruses can control PRDXs expression in order to enhance viral replication [248]. PRDXs can therefore function as pro- or antiviral proteins depending on the virus (Table 5.4). For instance, in HBV infection, PRDX1 can act as an antiviral protein [246], while in the context of measles infection PRDX1 is required for efficient replication of the virus [249].

Virus	PRDX	Action	Function	Model	Reference
HBV	PRDX1	Antiviral	Facilitates viral RNA degradation	Huh7.5 cell line	[246]
IAV	PRDX1	Proviral	Prevents oxidative damage of viral RNA and proteins	MDCK, A549 cells, MEFs	[250][251]
Measles virus	PRDX1	Proviral	Prevents ROS-induced cell death	HEK293T cells	[249]
RSV	PRDX1 and PRDX4	Proviral	Prevents ROS-induced cell death	A549	[252]

Table 5.4 Peroxiredoxins are involved in the antiviral response.

HBV: Hepatitis B virus; IAV: Influenza a virus; RSV: Respiratory Syncytial virus.

PRDX4 is the only member of the PRDX family found both the cytosol and in the endoplasmic reticulum and that can be secreted. PRDX4 has been shown to be involved in inflammatory processes. PRDX4 was first identified as a regulator of NF-κB activation; PRDX4 overexpression is shown to inhibit TNF-mediated NF-κB phosphorylation in different cell lines, including the HepG2 hepatocyte cell line [253]. PRDX4 acts also as inflammasome negative regulator; it binds to caspase 1 and limits its activation, thus inhibiting IL1-β release [254]. Moreover, PRDX4, by reducing cellular oxidative stress, has been shown to be protective in NAFLD pathogenesis, reducing steatosis and inflammation in murine livers overexpressing PRDX4 [255].

5.2.5 H_2O_2 mediates cellular signalling by modifying target proteins

As mentioned above, ROS-mediated cellular signaling relies on ROS ability to modify proteins, thus influencing their activity. ROS react covalently with an atomic rather than

molecular specificity. H_2O_2 signaling occurs mainly through reversible oxidation of sulphur atoms within cysteine residue thiols groups, while $O_2^{\bullet-}$ oxidises the metal ions complexed in proteins [256, 257]. While $O_2^{\bullet-}$-dependent signaling is not well understood, it is known that cysteine reactivity towards oxidation by H_2O_2 depends on the cellular redox status and the chemical properties of the residue itself.

In this section we will focus on H2O2-mediated signaling, which has been studied more extensively than other mechanisms. The two most important factors determining cysteine thiol group susceptibility towards being modified are the accessibility of the thiol within the three-dimensional protein structure and the reactivity of the cysteine residue (low pK_a) (Fig. 5.3), which is influenced by the surrounding amino acids [258, 259]. The cysteine residue exists in two forms, the thiol and the deprotonated ionized form, the thiolate. In the thiolate form, cysteines are strong nucleophiles that can rapidly undergo redox reactions (Fig. 5.3). The pK_a indicates the pH at which the specific cysteine of a protein is equally present in the thiol and thiolate form. Although the thiol group pK_a of a free cysteine is 8.25, it is perturbed when in a protein structure by the surrounding amino acids, lowering the pK_a and increasing the residue reactivity. For instance, a cysteine in the vicinity of residues providing positive charges (such as arginine, lysine, or histidine) or hydrogen bonding (such as serine, threonine, or tyrosine) stabilise the negative charged thiolate [259]. Proteins involved in several cellular functions have been reported to be regulated by ROS-dependent post translational modifications, from metabolic enzymes (such as GAPDH [260] and PKM2 [261], whose activities are inhibited upon oxidation of specific cysteine residues) to transcriptional factors (such as histone deacetylases) [262].

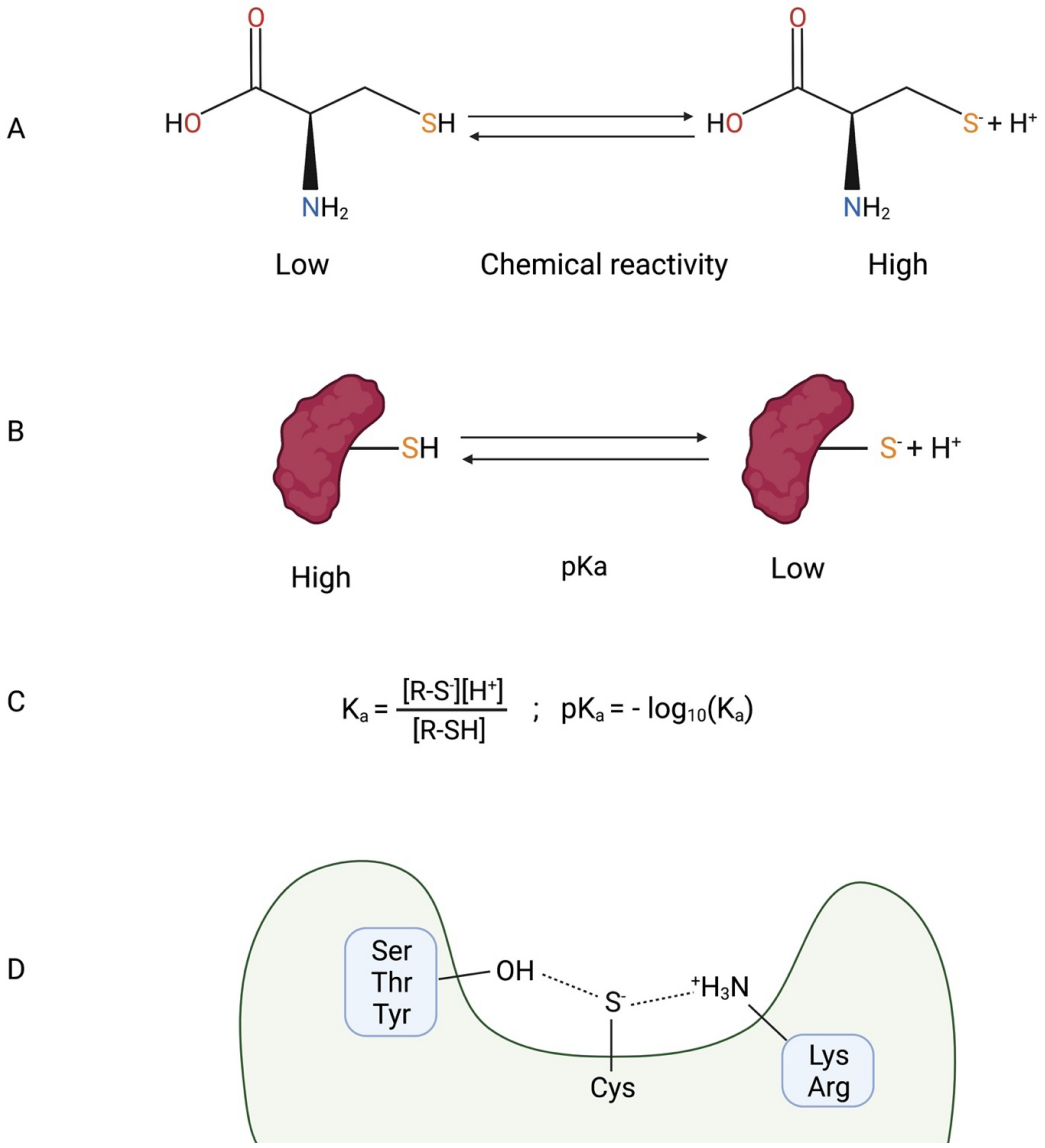

Figure 5.3 Cysteine reactivity influences ROS mediated post translational modifications.

Thiol protonation of the cysteine into thiolate is the major factor determining its reactivity (A). The thiolate group, which is negatively charged, has a stronger nucleophilicity and a low pK_a compared to the thiol group (B and C). The reactivity of a cysteine residue is determined by the three-dimensional structure as well as the surrounding chemical properties. Polar and positively charged amino acids stabilise the thiolate group by hydrogen bounds and ion-ion interactions respectively (D).

Redox reactions of cysteine residues with ROS can lead to different post-translational modifications. Among these modifications, some are reversible, while others such as

addition of sulfinic and sulfonic acids, determine an irreversible modification which is often a hallmark of oxidative stress [234]. Oxidation of the thiolate group within a cysteine residue by H_2O_2 yields sulfenic acid, which, depending on the microenvironment is subject to different fates. Sulfenic acid can be stabilised as observed for human serum albumin [263]. Otherwise, sulfenic acid can react with a protein thiol group forming a disulfide bond (which can be intra- or intermolecular depending whether the reacting cysteine is within the protein or on a second protein), or with GSH forming a protein-S-GSH disulfide (also known as glutathionylation, it is discussed in detail below). In the presence of H_2O_2 excess, therefore during oxidative stress, sulfenic acid can be further oxidised to sulfinic (RSO_2OH) and sulfonic (RSO_3H) acids, which are irreversible modifications (Fig. 5.4).

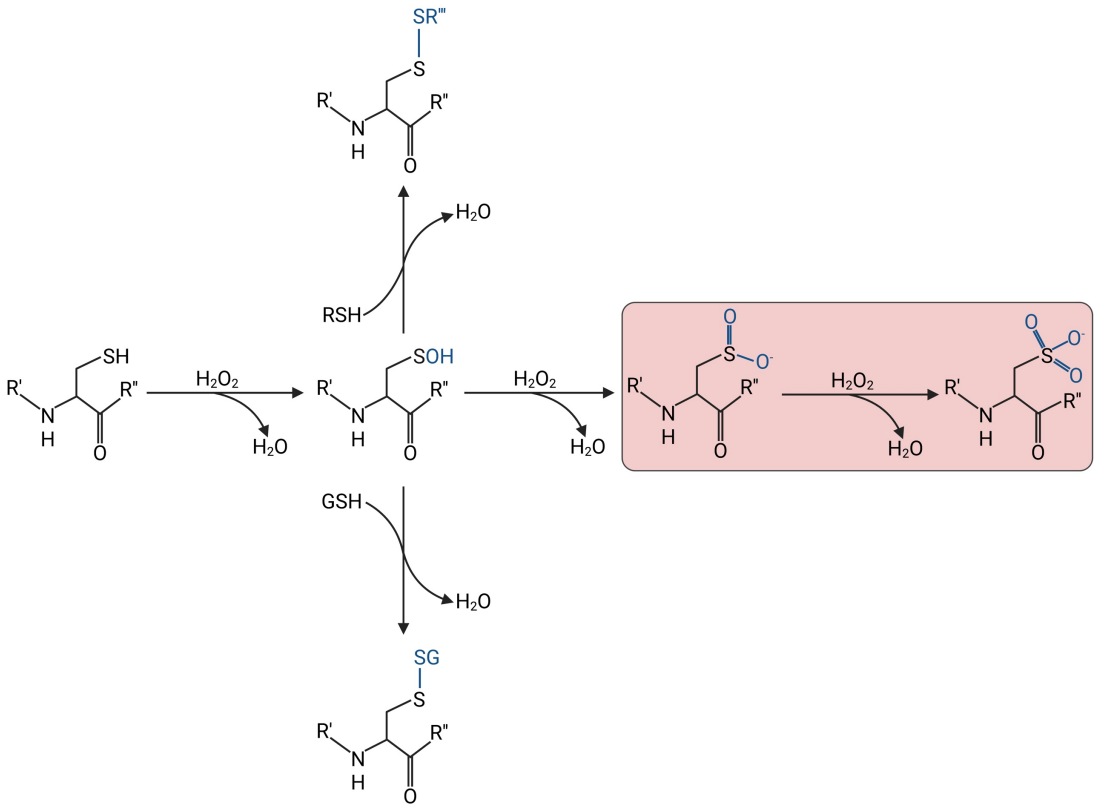

Figure 5.4 Overview of the major thiol modifications caused by H_2O_2.

The first reaction of the thiol group with H_2O_2 generates sulfenic acid (-SOH). Reaction with a second cysteine determines the formation of a disulfide (-S-SR'''). Alternatively,

reaction with glutathione (GSH) yields a glutathione disulfide (-S-SG). While H_2O_2 excess causes the formation of sulfenic acid (-SOO^-), which can be furtherly oxidized to the irreversible sulfonic acid (-$SOOO^-$)(both shown in the red box). Figure adapted from [234].

5.2.6 Glutathionylation as post-translational modification

ROS scavenging by glutathione is one of the most conserved mechanisms across different species [264]. Glutathione (GSH) is a tripeptide formed by glutamate linked through its carboxyl side chain group to cysteine, which is attached to a glycine residue. GSH is the most abundant low-molecular weight thiol and is the major antioxidant molecule within animal cells [264]. In mammalian cells, almost 90% of glutathione is found in cytosol (1 to 10 mM), while around 10% in mitochondria (5 to 10 mM), with small amounts in endoplasmic reticulum and nuclei [258]. Because of the cysteine residue, glutathione can be non-enzymatically oxidised by electrophilic substances, such as ROS and RNS, to glutathione disulfide (GSSG, formed by two glutathione molecules). GSH can be synthetized *de novo* by two reactions, the first catalysed by γ-glutamylcysteine synthase (GCS), and the second by glutathione synthetase. The GSSG formed upon GSH oxidation can be reduced back to GSH by NADPH- or NADH-dependent glutathione reductases [258]. GSH does not only react with ROS and RNS, reducing these reactive molecules, but it can also serve as post-translational modification. GSH can be reversibly conjugated to the thiol group (-SH) of protein cysteinyl residues (PSHs, P stands for protein, while SH is the cysteine thiol group) through a mechanism called S-glutathionylation, which generates S-glutathionylated proteins (PSSGs). Although protein S-glutathionylation is usually increased in response to oxidative or nitrosative stress, it can also occur independently on changes in the cellular redox status [258]. Protein S-glutathionylation is a ubiquitous redox modification which regulates several cell mechanisms, such as energy expenditure, cell death and survival, and calcium homeostasis [265–267]. Numerous *in vitro* studies have shown that redox sensitive cysteine residues can be glutathionylated non-enzymatically; whether this is the case also within cells and at a physiological level is still topic of study [268]. Primarily two classes of enzymes catalyse glutathionylation and deglutathionylation (removal of

glutathione from the cysteine residue) of target proteins, glutathione-S-transferases (GSTs) and glutaredoxins (GRXs) (Fig. 5.5).

To date 22 glutathione-S-transferases have been identified in humans. These enzymes have been studied for their ability to catalyse the conjugation of glutathione to xenobiotic molecules for detoxification processes. GSTs are also able to modify protein reactive cysteine residues by glutathionylation or deglutathionylation, influencing the activity of proteins involved in several mechanisms (Fig. 5.4). An explanatory example is the activation of the NLRP3 inflammasome, which is dependent on the deglutathionylation of the NLRP3 component NEK7 by glutathione-S-transferase omega 1-1 (GSTO1-1) on cysteine 253 [269].

In humans, five glutaredoxins (GLRXs) have been identified, GLRX1, 2, 3, 5, and the microsomal prostaglandin E synthase-2 (PGES-2). They are thiol disulfide oxidoreductases and members of the thioredoxin superfamily [268]. GLRXs catalyse the deglutathionylation, as well as, in oxidative stress conditions, glutathionylation of different target proteins [270]. As GSTs, also GLRXs are involved in several cellular mechanisms. For instance, GLRX1 deglutathionylates the transcriptional factor Sirt1. GLRX1 deficiency causes Sirt1 activity decrease, provoking an unbalanced fatty acid metabolism with accumulation of fatty acids in hepatocytes and a non-alcoholic fatty liver (NAFL) phenotype [271].

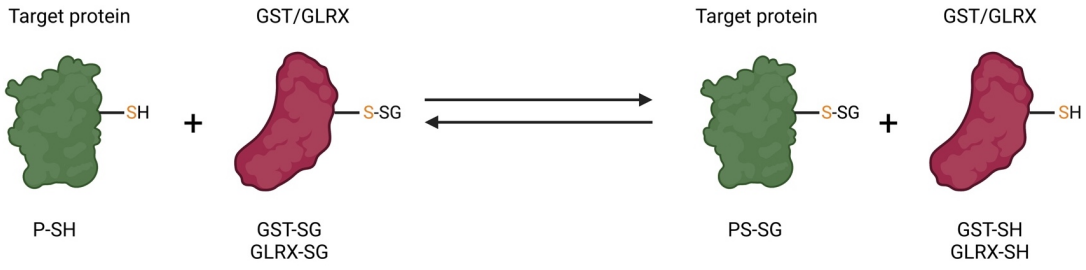

Figure 5.5 Glutathionylation and deglutathionylation mechanisms.

Glutathione-S-transferases and glutaredoxins are the two main classes of protein involved in glutathione-mediated post translational modification, being able to catalyse both glutathionylation and deglutathionylation.

5.2.7 Redox regulation of the antiviral response

Reactive oxygen species play a key role in the immune system, affecting both innate and adaptive responses [272]. Activation of immune cells, such as macrophage polarization towards an M1 phenotype, drastically alters the cellular metabolism [96]. Among the different processes involved in the metabolic switch, macrophages upregulate mitochondrial ROS production needed for an increased phagocytosis [132] and inflammasome activation [273]. ROS increase and alteration of the cellular redox status have been observed also in non-immune cells upon mounting an innate immune response.

Cellular redox status and ROS have been shown to regulate the innate antiviral activity at different levels. Activation of TRAF3 and TRAF6 by DNA viruses is mediated by glutathionylation on specific cysteine residues due to an increase in ROS levels [274]. Also antiviral response against RNA viruses is modulated by the cellular redox status. Accumulation of mitochondrial ROS, caused by inhibiting the mitochondrial electron transport chain or clearance of dysfunctional mitochondria, leads to an enhanced RLR signalling. This causes an upregulation of type I IFNs and pro-inflammatory cytokines production due to an increase in MAVS activation [133]. These results were confirmed also by following studies, showing that MAVS activation (which is characterised by MAVS aggregation) can be triggered viral-independently by pharmacologically increasing mitochondrial ROS levels, while mitochondrial ROS scavengers are able to downregulate MAVS aggregation [109]. These observations are fundamental not only in understanding the link between cellular metabolism and antiviral response, but also for developing new therapeutic strategies against autoimmune pathologies. That is the case for patients affected by systemic lupus erythematosus (SLE), presenting increased type I IFN blood levels due to a spontaneous MAVS aggregation in their peripheral blood lymphocytes. SLE patients also present an increased level of mitochondrial ROS, and *in vitro* treatment with mitochondrial ROS scavengers reduced MAVS aggregation and type I IFN production in patients' blood samples [109]. Whether MAVS activation depends on a ROS-dependent mechanism, such as cysteine residue oxidation or glutathionylation, has not been shown yet. While ROS-mediated signaling is fundamental in innate antiviral

response; as mentioned before, viruses have developed several strategies to hijack cellular redox signaling and exploit oxidative stress. Among others, flaviviruses (such as HCV) replication is enhanced during oxidative stress through oxidation of the viral non-structural protein 5, needed for viral RNA capping [115, 135].

Therefore, redox signaling and oxidative stress are key players in different aspects of cell pathophysiology. In a viral infection scenario oxidative stress and antioxidant systems play a critical role in the antiviral activity and pathogenesis. Unravelling the complex cross-talk among viral infection, antiviral activity, and redox biology provides information for developing new antiviral and anti-inflammatory strategies.

5.3 Hypothesis

Enzymes involved in the cellular redox system such as PRDXs and GRDXs affect the innate antiviral activity of dsRNA-stimulated hepatocytes.

5.4 Aims

1. To determine whether antioxidant enzymes are differentially expressed in the hepatic antiviral response.

2. To study the functions of antioxidant enzymes during the innate hepatic antiviral response.

5.5 Results

5.5.1 Hepatic PRDX4 is downregulated in a in vivo viral infection model

We first sought to determine whether enzymes involved in the cellular redox homeostasis are differentially expressed during hepatic viral infection. We analysed RNA-seq data and corresponding proteomic data from a study conducted on mice infected with chronic lymphocytic choriomeningitis virus (LCMV) [173]. The infection with LCMV clone 13 causes systemic chronic infection that lasts for up to 60 days. According to previous studies, the innate immune response, characterised by type I IFN production, peaks 2 days after infection and decreases over the next 72h; while at 8 days post infection, the viral titres peak, followed by an adaptive immune response [173]. In the following days, viral particles number is reduced due to the adaptive antiviral response (Fig. 5.6 A). Viral infection caused by LCMV clone 13 can persist for a prolonged period of up to 60 days. Therefore, LCMV is widely used as a model to study chronic viral infection and T cell exhaustion. The RNA-seq dataset analysed here is based on liver samples from infected mice at different phases of infection (day 2 = innate phase, day 8 = peak of disease, day 30 = chronic phase, day 60 = resolving phase) [173].

We used a list of 44 annotated genes involved in the antioxidant pathway generated through Molecular Signature Database (MSigDB) [275–277]. When considering all genes, 21 of the antioxidant pathway related genes were differentially expressed genes (DEGs), only 12 were differentially expressed at two or more days. SOD1 was downregulated at both 2 and 8 days post infection as previously described [172]. Two other genes showed a similar pattern to SOD1, methionine sulfoxide reductase A (MSRA) and peroxiredoxin 4 (PRDX4), which were both downregulated at 2 and 8 days post infection (Fig. 5.6 B). MSRA gene expression decrease peaked at 2 days post infection, while the PRDX4 decrease was at 8 days post infection (Fig. 5.6 C and D). We analysed the corresponding proteomic dataset and observed a similar pattern to the RNA-seq dataset (Fig. 5.7 A). In this case, MSRA and PRDX4 protein levels were significantly downregulated at 8 days post infection, with a more significant decrease in PRDX4 (Fig. 5.7 B and C). Because of

these observations, we focused on studying PRDX4 in the context on an innate antiviral response.

We further tested whether PRDX4 decrease is type I IFN signaling-dependent. We infected wild type and IFNAR1 knock-out (KO) mice with LCMV clone 13 for 5 days. PRDX4 was significantly decreased in both WT and IFNAR1 KO infected mice compared to their relative non infected controls, confirming the RNA-seq results. We also observed a basal non-significant increase of PRDX4 expression in the IFNAR1 KO genotype compared to their respective relative controls, not infected and infected (Fig. 5.8).

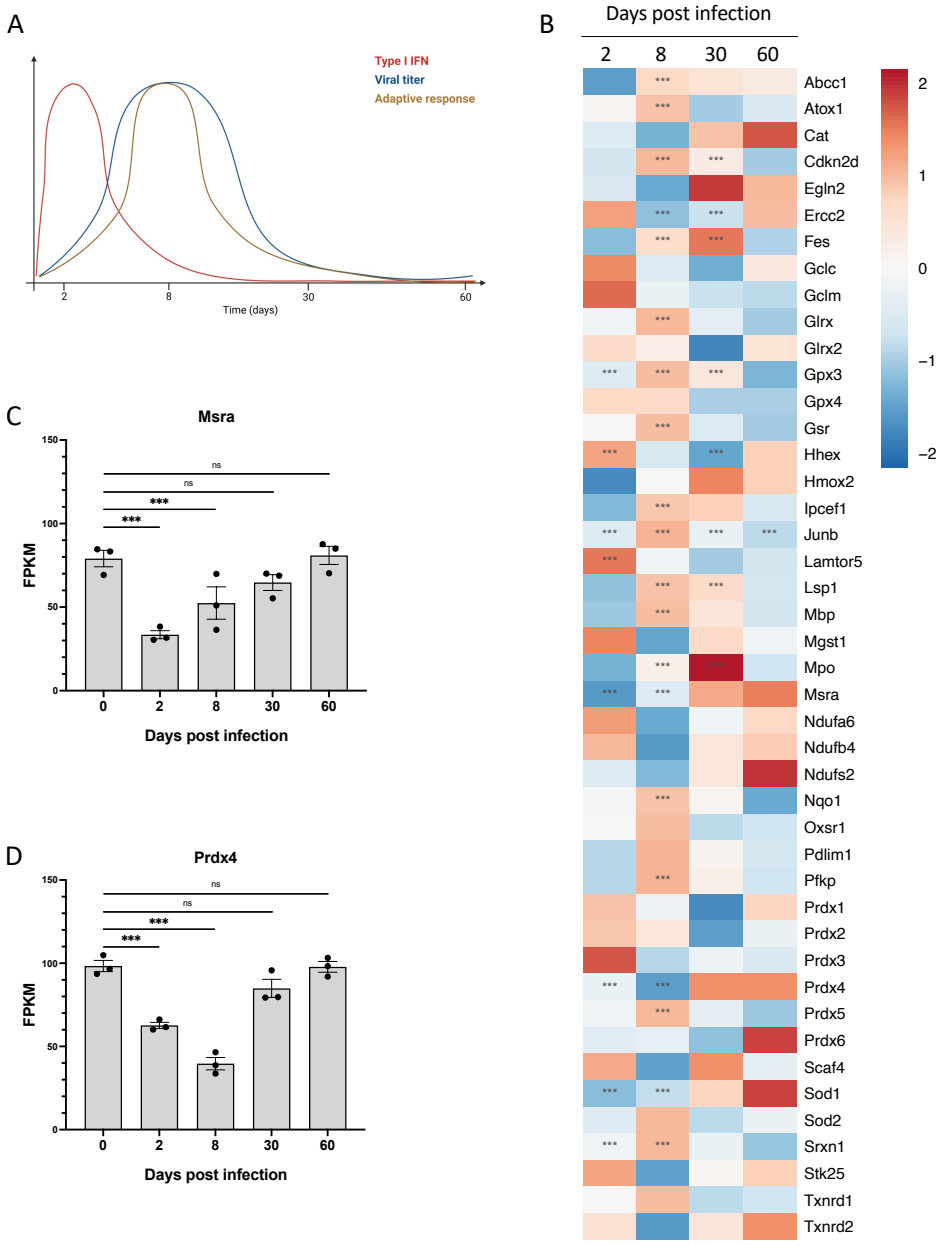

Figure 5.6 Liver expression of the antioxidant enzymes MSRA and PRDX4 is downregulated in mice upon LCMV infection.

Schematic representation of the course of clone 13 LCMV infection in mice (A). LCMV infection is associated with altered expression of genes involved in cellular antioxidant pathways as shown in the heatmap (B). The two antioxidant genes MSRA (C) and PRDX4 were significantly downregulated at both 2 and 8 days upon infection. Data generated and analysed with Dr. Jamie Sugrue's help from a publicly available dataset [173]*. FPKM (fragments per kilobase of transcript per million) values and adjusted p values were calculated according to the protocol as described in* [173] *(* adj p val < 0.05, ** adj p val < 0.01, *** adj p val < 0.001), n = 3 per condition.*

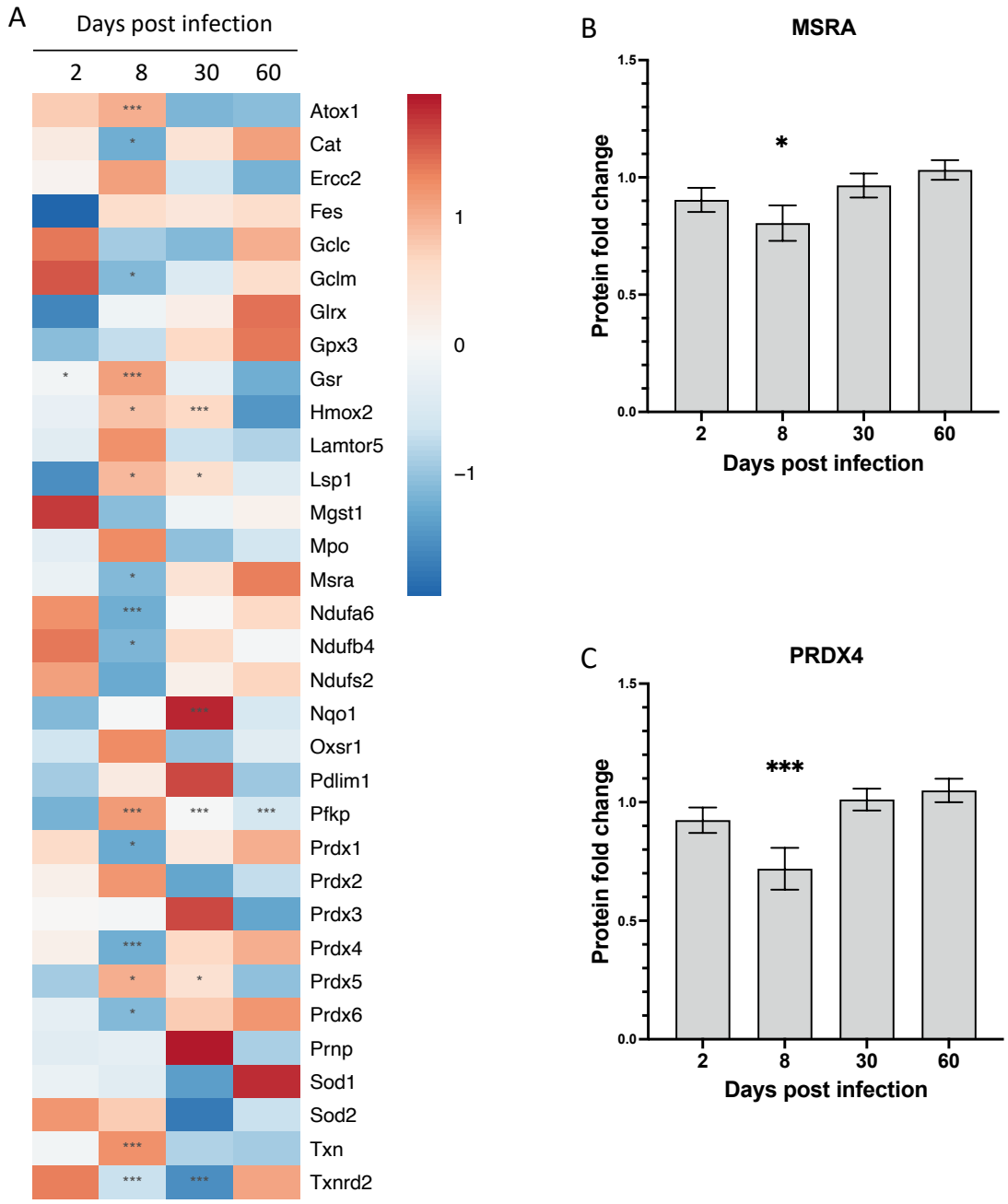

Figure 5.7 MSRA and PRDX4 protein levels are downregulated in LCMV infected mice livers.

Heatmap of antioxidant protein abundance from LCMV-infected mice at different infection stages (A). MSRA (B) and PRDX4 (C) protein fold change compared to infected mice at day 0. Data generated and analysed with Dr. Jamie Sugrue's help from a publicly available dataset [173] *(* adj p val < 0.05, ** adj p val < 0.01, *** adj p val < 0.001), n =.3 per condition.*

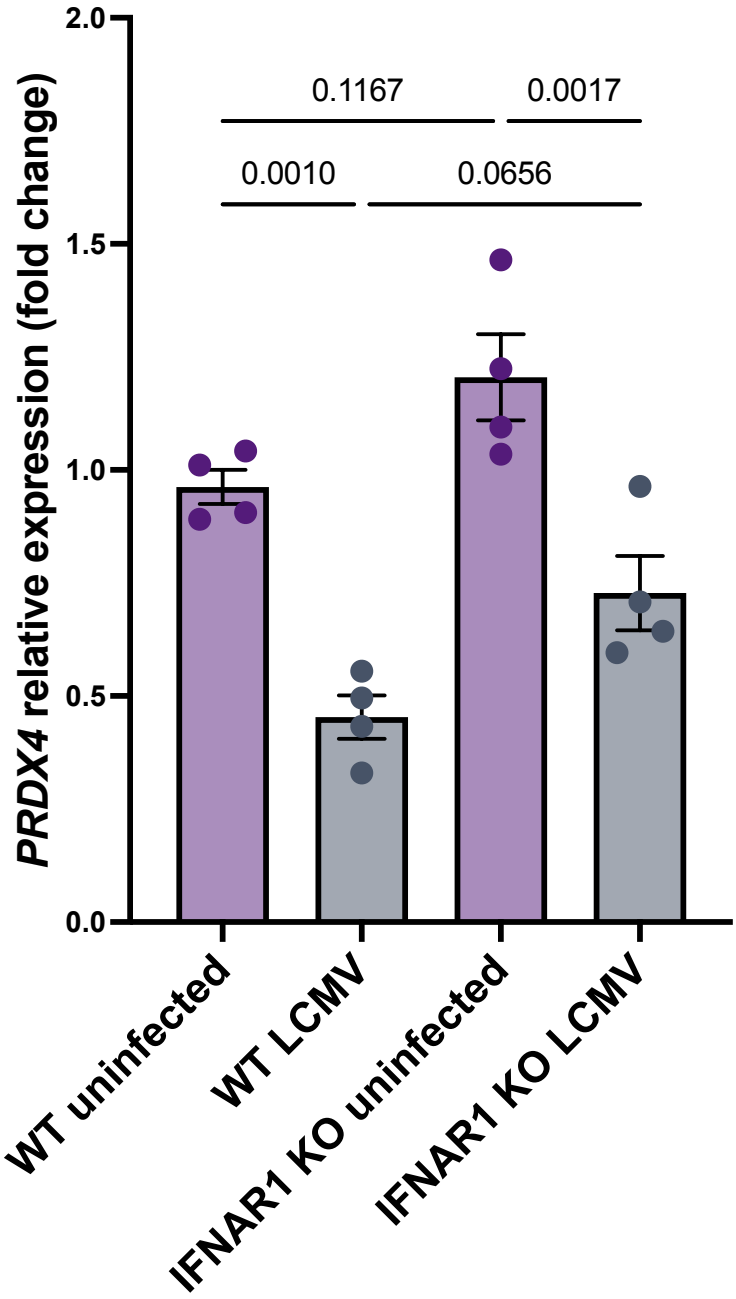

Figure 5.8 PRDX4 expression decreases in LCMV infected wild type and IFNAR1 knock-out mice.

Mice were infected with 2 x 10^6 focus-forming units (FFU) of LCMV strain clone 13 for 5 days. Livers were collected, RNA was extracted and transcribed to cDNA. PRDX4 expression was determined by RT-qPCR, and elongation factor 1-α 1 (EF1α) was used as housekeeping gene. Data are mean $\pm$ S.E.M. of four independent experiments, p value were calculated using one-way ANOVA. Data generated and analysed with Zsofia Keszei in Prof. Andreas Bergthaler's lab.

5.5.3 PRDX4 deficiency increases the innate antiviral response to dsRNA in Huh7 cells

We then sought to determine whether loss of PRDX4 affects the innate antiviral response in our *in vitro* hepatic model. We silenced PRDX4 (Fig. 5.9 A) and stimulated Huh7 cells with transfected poly I:C for 6h. We observed that silencing of PRDX4 showed a trend towards increased CXCL10 expression, but no difference in expression of IFNL1 and IFNB1 at 6h (Fig. 5.9 B, C and D).

This trend was also observed at a later time point. After 24h of stimulation with transfected poly I:C the PRDX4 silencing showed a trend towards increased secretion of IFN-β and IL-29 protein (Fig. 5.10 A and B). Therefore, suggesting that silencing of PRDX4 increases transfected poly I:C-induced antiviral activity.

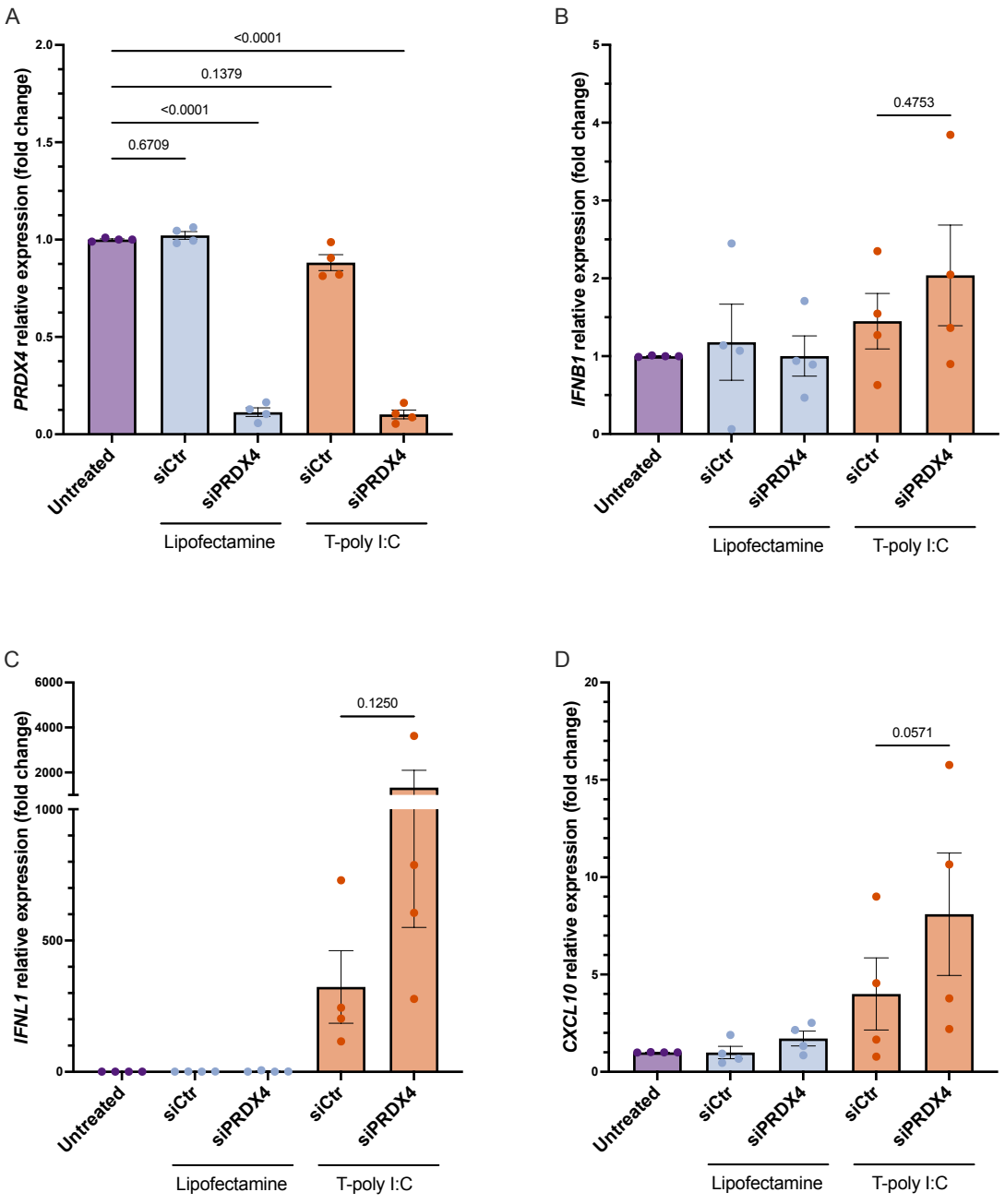

Figure 5.9 PRDX4 silencing increases type III interferon and CXCL10 expression upon transfected poly I:C stimulation in Huh7 cells.

Huh7 cells were silenced with siRNA control or siPRDX4 for 48h before the stimulation. PRDX4 (A), IFNB1 (B), IFNL1 (C), and CXCL10 (D) gene expression after 6h stimulation with transfected poly I:C (T-poly I:C, 5 μg/ml) or the vehicle (lipofectamine) determined by RT-qPCR in silenced control (siCtr) or silenced PRDX4 (siPRDX4) Huh7 cells. Data are mean ± S.E.M. of four independent experiments, p value were calculated using paired t-test or paired one-way ANOVA for multiple comparisons.

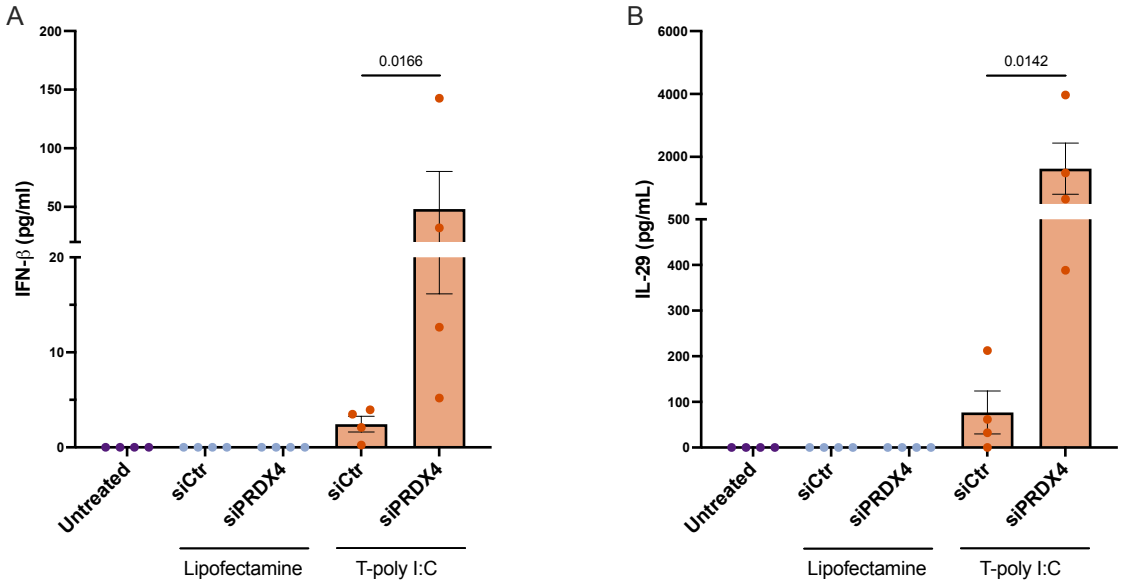

Figure 5.10 PRDX4 silencing increases IFN-β and IL-29 protein levels upon transfected poly I:C stimulation.

Huh7 cells were silenced with siRNA control or siPRDX4 for 48h before the stimulation. IFN-β and IL-29 protein levels after 24h stimulation with transfected poly I:C (T-poly I:C, 5 μg/ml) or vehicle control (lipofectamine) were determined by ELISA in silenced control (siCtr) or silenced PRDX4 (siPRDX4) Huh7 cells. Data are mean ± S.E.M. of four independent experiments, p values were calculated using paired t-test on log10 transformed data.

5.5.4 PRDX4 deficiency increases the innate antiviral response in Dengue virus infected Huh7 cells

We further tested the effect of PRDX4 deficiency in the context of a hepatotropic infection. We infected Huh7 cells with the RNA virus Dengue for 24h at a MOI of 5. We observed an increase in IFNL1, CXCL10, and ISG15 expression, as well as IFN-β protein levels in PRDX4 KD Huh7 cells (Fig. 5.11 A-D). We also measured the viral load by RT-qPCR of the non-structural protein 4A (NS4A) (Fig. 5.11 E). Surprisingly we did not observe a difference in the gene expression of NS4A between the siPRDX4 and siCtr, suggesting no difference in the viral titre between the two conditions. Whether this is due to the fact that PRDX4 KD affects and decreases the ability of clearing the virus or a longer time period is needed by the cells to activate an efficient antiviral response able to clear the virus, has not been investigated yet.

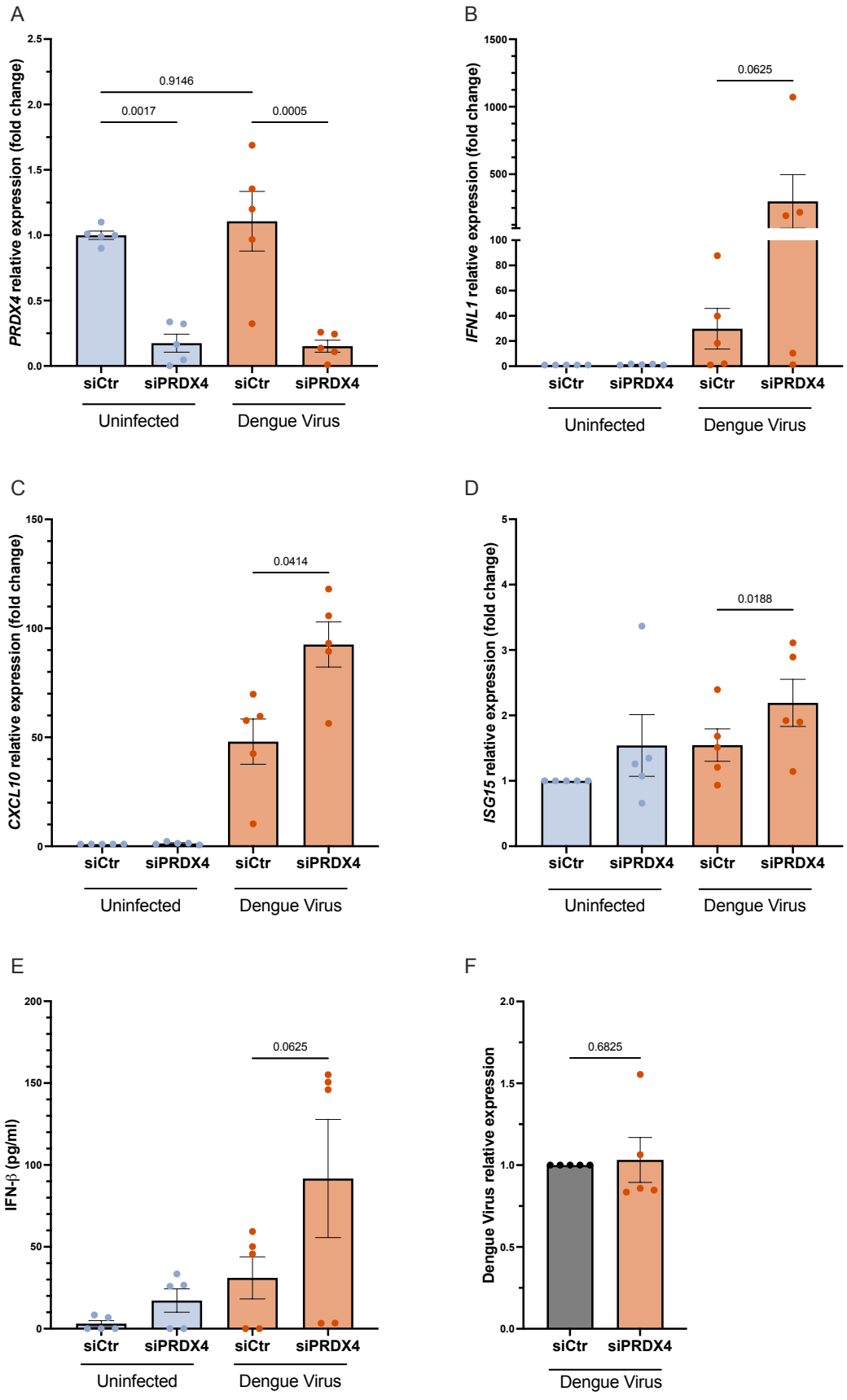
A
PRDX4 relative expression (fold change)
0.9146
0.0017
0.0005
siCtr
siPRDX4
siCtr
siPRDX4
Uninfected
Dengue Virus
B
IFNL1 relative expression (fold change)
0.0625
siCtr
siPRDX4
siCtr
siPRDX4
Uninfected
Dengue Virus
C
CXCL10 relative expression (fold change)
0.0414
siCtr
siPRDX4
siCtr
siPRDX4
Uninfected
Dengue Virus
D
ISG15 relative expression (fold change)
0.0188
siCtr
siPRDX4
siCtr
siPRDX4
Uninfected
Dengue Virus
E
IFN-β (pg/ml)
0.0625
siCtr
siPRDX4
siCtr
siPRDX4
Uninfected
Dengue Virus
F
Dengue Virus relative expression
0.6825
siCtr
siPRDX4
Dengue Virus

Figure 5.11 PRDX4 silencing increases the innate antiviral activity in Dengue virus infected Huh7 cells.

Huh7 cells were silenced with siRNA control or siPRDX4 for 48h before the stimulation. Subsequently, Huh7 cells were infected for 24h with Dengue virus at a MOI of 5. PRDX4 (A), IFNL1 (B), CXCL10 (C), ISG15 (D), and Dengue virus non-structural protein 4A (NS4A) (F) relative gene expression was determined by RT-qPCR, IFN-β protein levels were determined by ELISA (E). Data are mean $\pm$ S.E.M. of five independent experiments, p value were calculated using paired t-test or paired one-way ANOVA for multiple comparisons.

5.5.5 PRDX4 is a potential MAVS interactor

The previous results highlight how PRDX4 play a role in modulating the antiviral response against RNA viruses. Thus, activation of the cytoplasmic PRRs RLRs and PKR and their downstream signaling pathways might be influenced by PRDX4. Whether this mechanism is due to a direct interaction between PRDX4 and proteins involved in the antiviral response has not been elucidated before. By re-analysing a publicly available dataset obtained from a mass-spec data of MAVS interactors [278], we identified six proteins involved in the homeostasis of the cellular oxidative state (Fig. 5.12). These proteins belonged to the class of glutathione-S transferases and peroxiredoxins, and among these PRDX4 was one of the candidates.

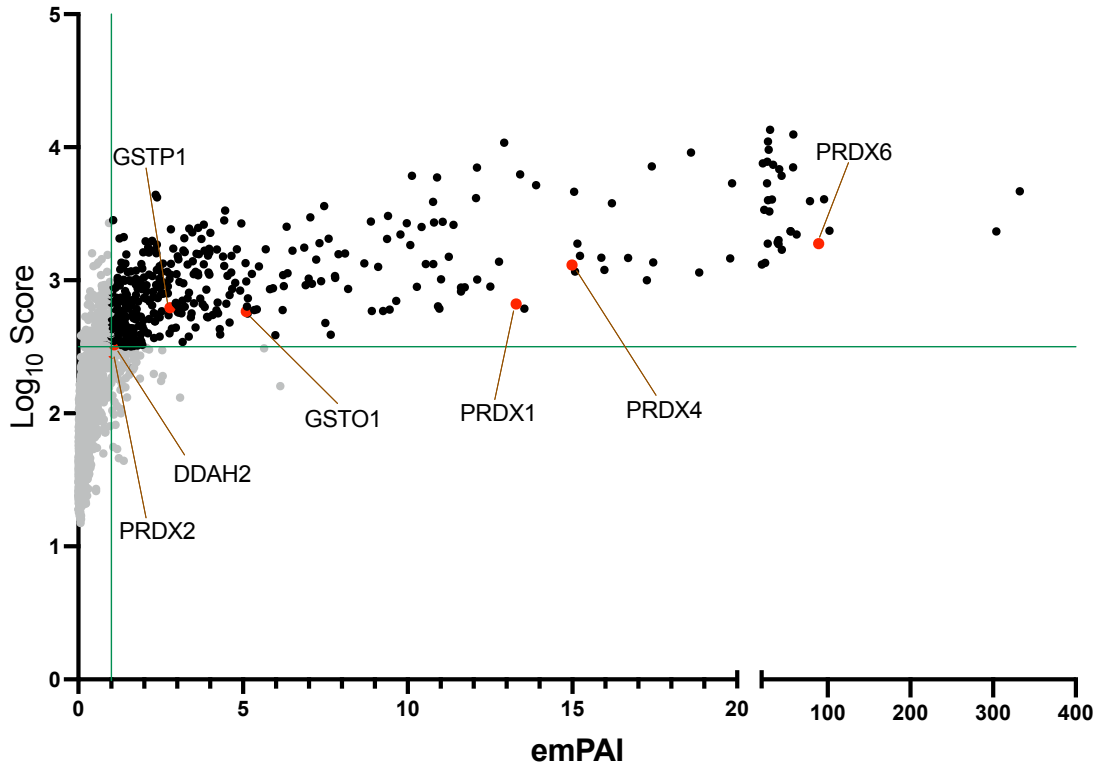

Figure 5.12 PRDX4 is a potential MAVS interactor.

Analysis of mass spec data obtained from MAVS-tagged and immunopreciptation in HEK293T cells [278]*. DDAH2 was used as lower limit for filtering emPAI and the score. emPAI was calculated as* 10^{PAI} *where PAI (Protein Abundancy Index) is the ratio between observed and observable peptides of that specific protein.*

5.5.6 PRDX4 deficiency upregulates the innate antiviral response in HEK293T cells

We used HEK293T cells to test which of the potential MAVS interactors identified in 5.12 might impact the antiviral response. Using siRNAs, we silenced gene expression of the six identified proteins (Fig. 5.13 A) and stimulated HEK293T cells for 8h with transfected poly I:C. We observed that a decrease in PRDX1 and PRDX4 expression caused an increase in IFNB1 and CXCL10 expression (Fig. 5.13 B and C). While TNF expression was significantly increased only upon PRDX4 silencing (Fig. 5.13 D).

We confirmed these results by stimulating for a longer period (16h) with both the dsRNA poly I:C as well as 5' triphosphate hairpin RNA (3p-hpRNA). Also in this case IFNB1, CXCL10, ISG15 expression (Fig. 5.14 A-C), as well as type I IFN protein levels were upregulated upon PRDX4 KD compared to the control (Fig. 5.14 D). PRDX4-deficiency leads to an enhanced antiviral response in both HEK293T cells and Huh7s, suggesting that this phenotype is not cell line specific.

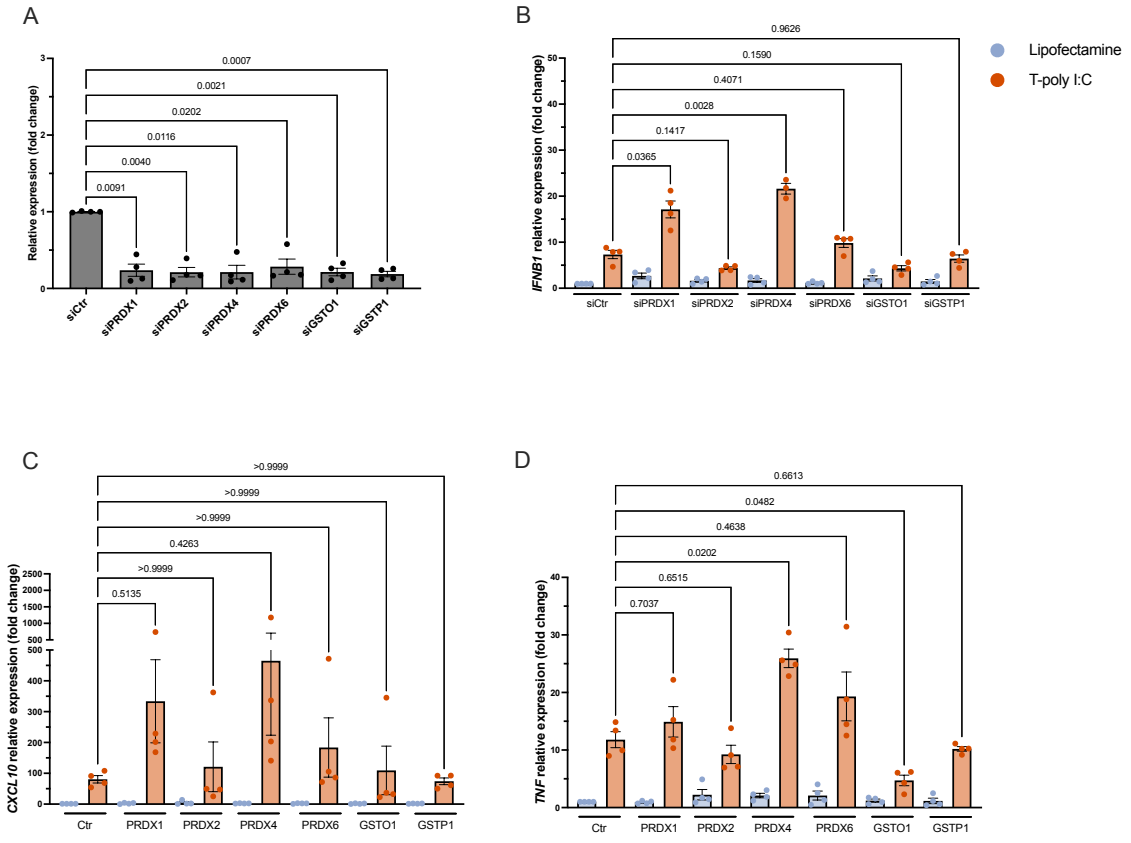

Figure 5.13 PRDX4 silencing upregulates IFNB1 and pro-inflammatory cytokines expression upon transfected poly I:C stimulation in HEK293T cells.

Relative expression of the six silenced genes (PRDX1, PRDX2, PRDX4, PRDX6, GSTO1, GSTP1) determined by RT-qPCR (A). IFNB1 (B) and CXCL10 (C) relative gene expression after 8h treatment with transfected poly I:C (T-poly I:C, 1 μg/ml) and upon 48h silencing of the six different genes. Relative gene expression was determined by RT-qPCR, lipofectamine was used as vehicle control for transfected poly I:C stimulation. Data are mean ± S.E.M of four independent experiments, p value were calculated using paired one-way ANOVA.

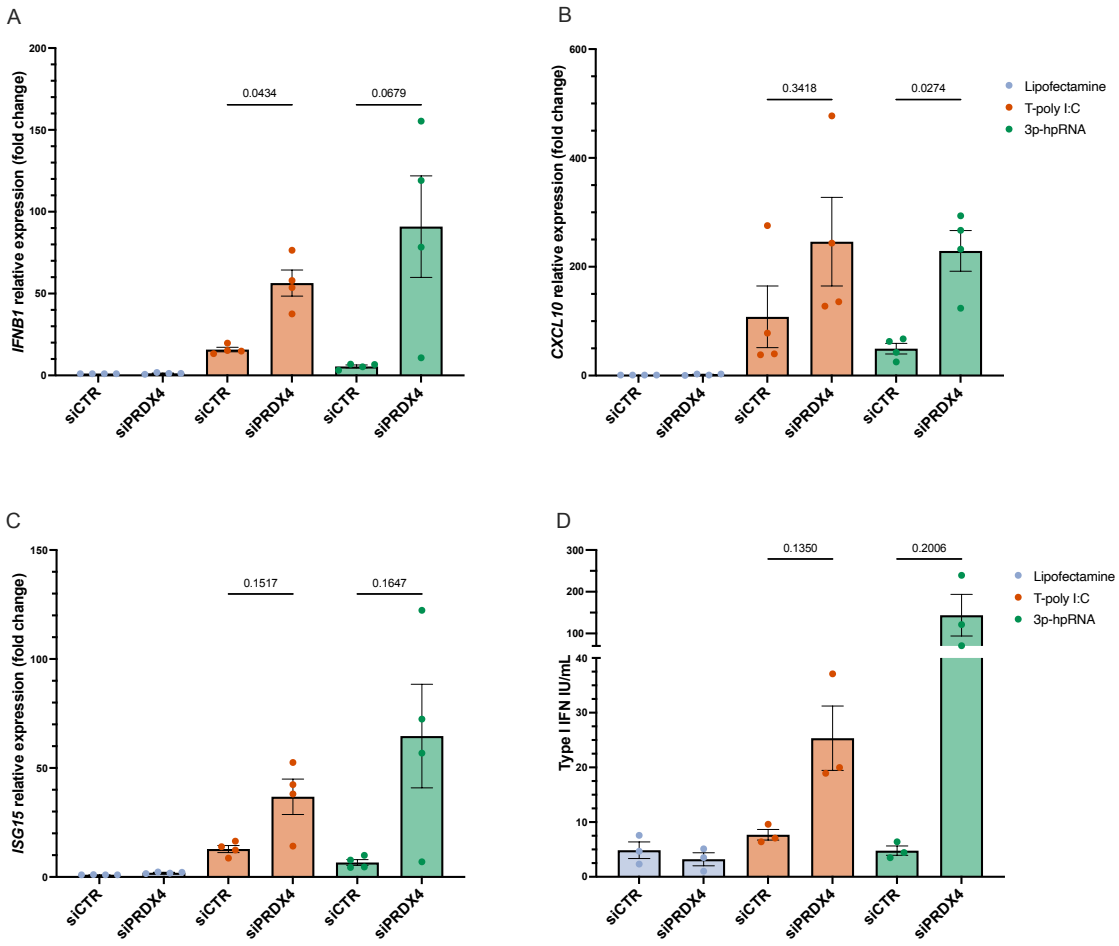

Figure 5.14 PRDX4 silencing upregulates IFN and pro-inflammatory cytokine expression upon dsRNA stimulation in HEK293T cells.

IFNB1 (A), CXCL10 (B), and ISG15 (C) relative expression after 16h stimulation with transfected poly I:C (T-poly I:C, 1 μg/ml), 5'-triphosphate hairpin RNA (3p-hpRNA, 100 ng/ml) or the vehicle (lipofectamine) in control (siCtr) or PRDX4 silenced HEK293T cells. Relative gene expression was determined by RT-qPCR. Supernatants were collected and type I IFN protein levels were measured by HEK-Blue assay (D). Data are mean ± S.E.M. of four (A to C) and three (D) independent experiments , p value were calculated using paired t-test.

5.5.7 MAVS aggregation is increased in PRDX4 KD cells upon dsRNA stimulation

Having found that silencing of PRDX4 is associated with an increased innate antiviral response, we sought to determine the mechanism through which this might occur. As we identified PRDX4 as a putative MAVS-interactor, we determined whether PRDX4 KD is associated with increased MAVS activation upon viral stimulation. Following PRDX4 silencing, we stimulated HEK293T cells with transfected poly I:C and determined MAVS activation by western blot for MAVS aggregation. In this case we observed an increase of MAVS aggregation in PRDX4 KD cells compared to the control (Fig. 5.15 A and B).

Since from the public available dataset analysis, we observed a potential interaction between PRDX4 and MAVS, we sought to determine whether this is the case. To determine whether PRDX4 and MAVS interact directly we used a semi-endogenous immunoprecipitation system. Myc-tagged PRDX4 was overexpressed for 24h in HEK293T cells which were subsequently stimulated with transfected poly I:C. Tagged PRDX4 was immunoprecipitated and MAVS interaction was determined by immunoblot. In this case we could not observe MAVS co-immunoprecipitating with overexpressed PRDX4 (Fig. 5.16). Whether in other conditions, such as a prolonged stimulation, PRDX4 could potentially interact with MAVS has not yet been investigated.

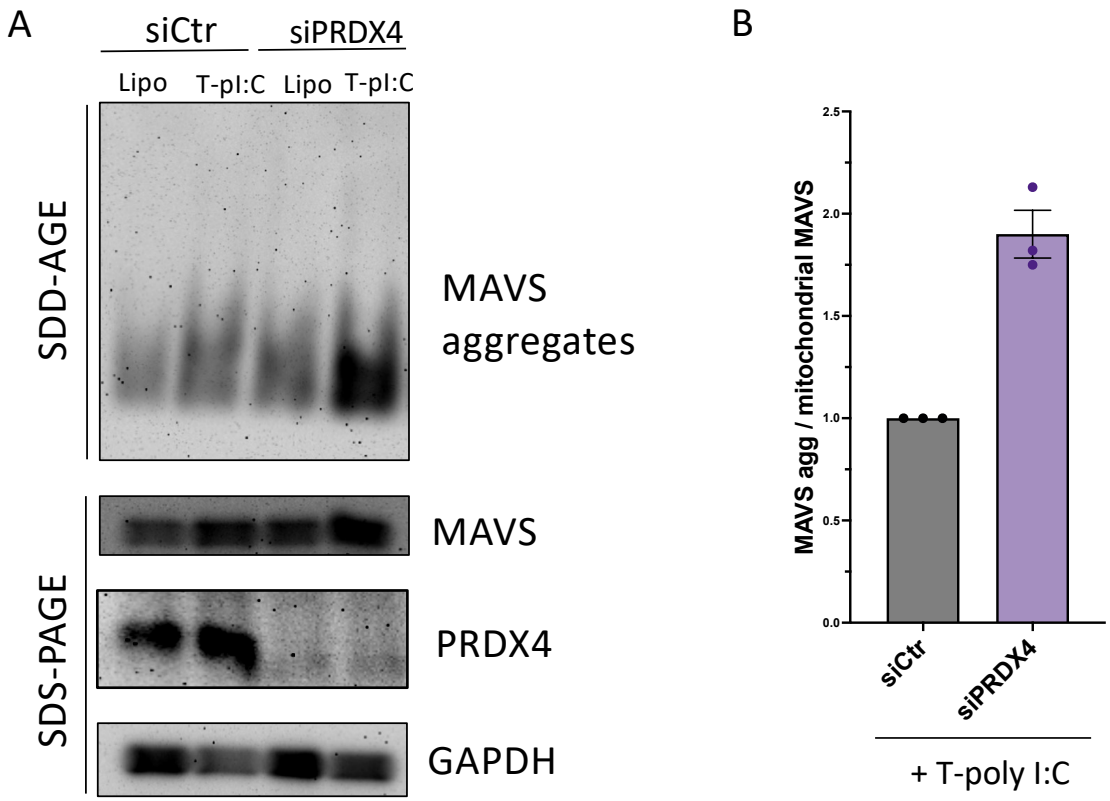

Figure 5.15 PRDX4 deficiency increases MAVS aggregation following stimulation with transfected poly I:C.

Immunoblot of mitochondrial MAVS aggregation upon 4h stimulation with transfected poly I:C (T-pI:C, 1 μg/ml) or vehicle (Lipo, lipofectamine). For MAVS aggregation, the mitochondrial fractions of the different samples were run on a 1.5% agarose gel, while MAVS and GAPDH were used as loading controls for the normalization (A) on an SDS-PAGE as described in materials and methods section. MAVS aggregates were quantified using mitochondrial MAVS as loading control (B). Data are mean ± S.E.M of three independent experiments. Blots are representative of three independent experiments.

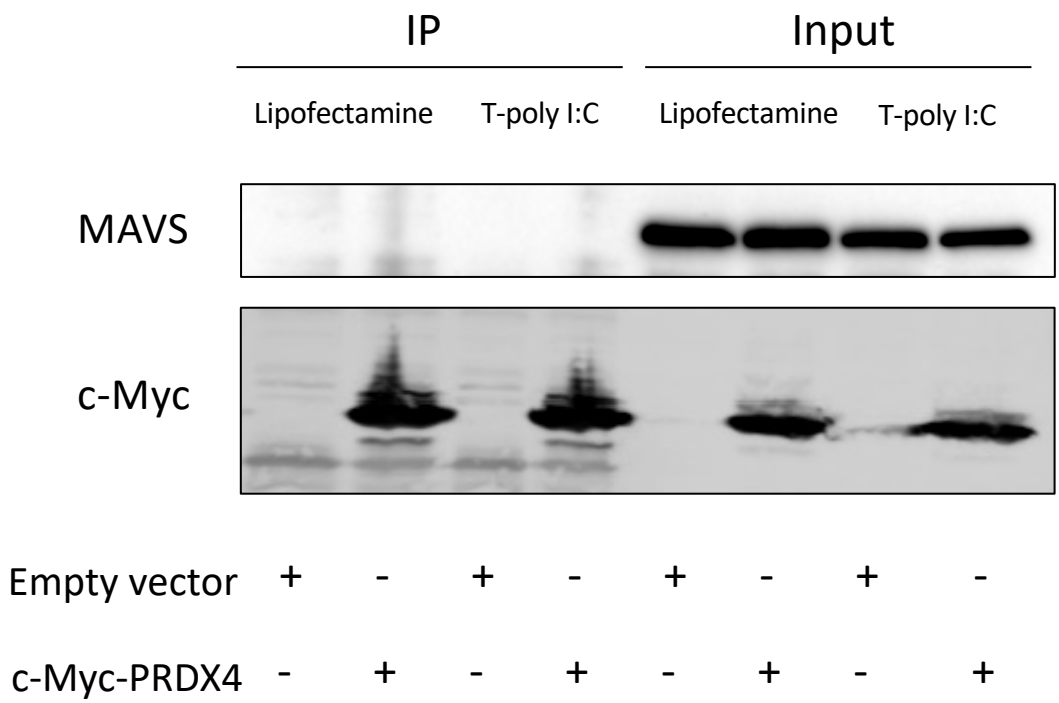

Figure 5.16 MAVS and PRDX4 do not directly interact.

Representative experiment of c-Myc PRDX4 immunoprecipitation and immunoblot of MAVS in HEK293T cell. Cells were transfected with c-Myc PRDX4 plasmid or empty vector as control for 24h and stimulated for 6h with transfected poly I:C (T-poly I:C, 1 μg/ml) or vehicle (lipofectamine) before being collected. Blots are representative of three independent experiments.

5.6 Discussion

Viral infection and innate antiviral activity are associated with major metabolic shifts in hepatocytes [173, 279]. These changes are often virus-specific and difficult to dissect, particularly when one considers that both the host and virus wish to rewire metabolism either to generate an antiviral response, or to facilitate viral replication and immune evasion. Attempting to understand host metabolic requirements during viral infection is therefore difficult. A lack of cellular models that recapitulates the complex hepatic metabolism observed in vivo contributes to this difficulty.

One of the viral models used to study the interplay between viral infection and antiviral response is chronic lymphocytic choriomeningitis virus (LCMV). This virus causes a systemic infection, and a specific clone (clone 13) has been shown to provoke a prolonged infection in mice that can be used as model for studying chronic viral infections. Studies have showed that LCMV-infected mice reprogram their hepatic metabolism by upregulating fatty acid biosynthesis, disrupting the urea cycle, and increasing oxidative stress type I IFN-dependently [172, 173].

In previous results of this thesis, we observed an increase in oxidative stress upon dsRNA stimulation and saw how modulation of the cellular redox status affects the dsRNA-dependent antiviral response. We therefore aimed, in this chapter, to investigate which antioxidant genes are involved in the hepatic antiviral response. By analysing a publicly available dataset, we found peroxiredoxin 4 (PRDX4) to be differentially expressed, at both gene and protein levels, in liver samples from LCMV infected mice. As a previous study in the same model showed that oxidative stress was dependent on type I IFN signaling [172], we sought to determine whether that was also the case in our model. Using IFNAR1 knock-out (KO) mice we observed a slight increase in PRDX4 expression compared to the WT genotype, though this increase was not significant. Moreover, in both genotypes PRDX4 was downregulated upon viral infection, indicating that PRDX4 downregulation during LCMV viral infection is not dependent on type I interferon signalling. Interestingly, PRDX4 downregulation peaked at 8 days post infection, which is in concomitance with adaptive immune response activation and peak of viral titres.

Whether PRDX4 decrease is caused by activation of adaptive immune response or it is a viral intrinsic mechanism is not known. Further experiments using B and T cells depleted mouse strains (e.g. RAG-2 KO mice) and other LCMV strains might be helpful to deconvolute the cause of PRDX4 expression decrease.

We further tested the effect of PRDX4 in dsRNA stimulated hepatocytes. We silenced PRDX4 in Huh7 cells and we observed an increase in type I and III IFNs, as well as pro-inflammatory cytokines. Moreover, a similar pattern was also observed in an hepatotropic viral infection model using Dengue virus, which activates an RLR-dependent antiviral response [280]. Thus, demonstrating that PRDX4 deficiency upregulates the dsRNA and viral infection-induced antiviral response in hepatocytes. Further viral infection models, for instance HBV and HCV which are known to activate RLRs and PKR, might be useful to confirm our results.

We observed that also in other cell types, such as fibroblasts (HEK293T cells), PRDX4 deficiency increases the antiviral response upon stimulation with dsRNA and 5'-triphosphate hairpin RNA, suggesting that the mechanism might be conserved in diverse cell types. Additionally, we saw that PRDX4 deficiency increases MAVS aggregation, which may be the mechanism by which PRDX4 KD increases the antiviral immune response. Previous studies have shown that MAVS aggregation is ROS-dependent [109, 133]. Since PRDX4 is an antioxidant enzyme, we speculate that PRDX4 silencing impairs the cellular redox homeostasis. Therefore ROS upregulation, due to viral infection or dsRNA stimulation, would be enhanced in PRDX4 deficient cells, causing increased MAVS aggregation and downstream activation of the antiviral response. Further studies, such as measuring ROS levels and their origin, whether cytoplasmic, mitochondrial, or both, would provide us with important information.

By analysing proteomic data on MAVS interactors, we identified PRDX4 as a potential MAVS-interacting protein. We hypothesised that PRDX4 might directly interact with MAVS and influence its activation and aggregation. Using a semi-endogenous model, based on PRDX4 overexpression and immunoprecipitation, we could not detect MAVS co-immunoprecipitating with PRDX4. Whether the two proteins – MAVS and PRDX4 –

interact is still subject of study. Further studies are needed in order to confirm the absence of interaction between the two proteins.

Collectively we identified PRDX4 as a novel regulator of the innate antiviral response. Its depletion increases the antiviral response to dsRNA in hepatocytes as well as other cell types. How PRDX4 deficiency upregulates the innate antiviral response is the subject of ongoing research. As PRDX4 is located in the endoplasmic reticulum, a deficiency in PRDX4 may increase endoplasmic reticulum oxidative stress and/or overall cellular oxidative stress and contribute to an increased antiviral immune response.

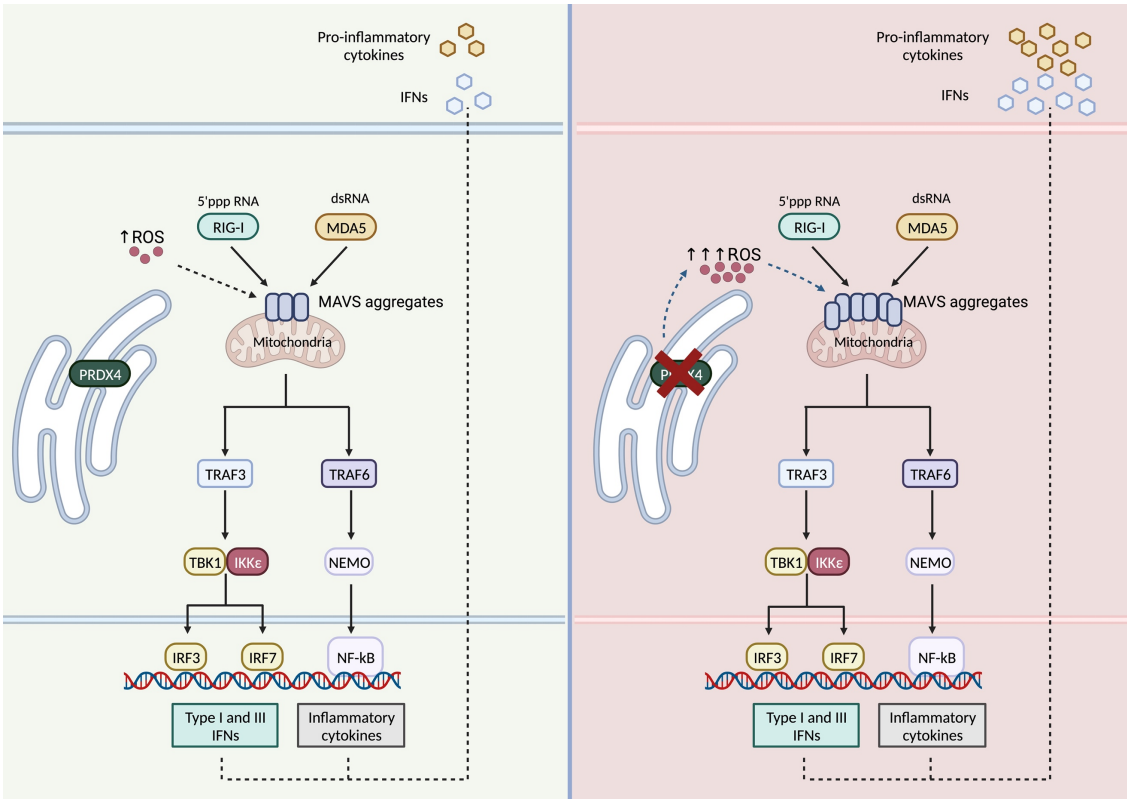

Figure 5.17 Proposed mechanism of PRDX4 deficiency-mediated antiviral response. *Double stranded RNA (dsRNA) and 5'-triphosphate hairpin RNA (3p-hpRNA or 5'pppRNA) increases the innate antiviral response, upregulating interferon and pro-inflammatory cytokine production. Decrease in PRDX4 expression boosts the antiviral response upon the stimulation. ROS-dependent increased MAVS activation and aggregation may contribute to this phenotype.*

6. Final discussion

Metabolism rewiring is crucial for immune cell activation, enabling effective immune responses. Studies in the immunometabolism field are providing critical information for the development of new pharmaceutical strategies [281]. Whether non-immune cells shift also their metabolism has not been fully explored. In this thesis we focus on hepatocytes, which have unique metabolic features due to the fact that they are involved in whole body metabolic homeostasis. Hepatocytes are targets of hepatotropic viruses and, in this scenario, they are able to induce an interferon-based innate antiviral response. Seminal studies have shown that hepatocytes alter their metabolism upon viral infection in a type I IFN-mediated manner [172–174]. Whether activation of PRRs and induction of antiviral activity requires metabolic rewiring is still not clear. This thesis aimed to dissect the role of cellular metabolism in the hepatic innate antiviral response.

We first focused on identifying the PRRs involved in the antiviral response of human hepatocytes upon stimulation with immunogenic double-stranded RNAs – long dsRNA such as poly I:C and short 5'-triphosphate hairpin RNA. We conducted the study on three different cellular models, two human hepatic cell lines (HepG2 and Huh7 cells) and induced-pluripotent stem cell (iPSC)-derived hepatocytes, also known as hepatocyte-like cells (HLCs). We observed that the two hepatic cell lines and HLCs induce expression of IFNs, pro-inflammatory cytokines, and ISGs only by transfection of dsRNA, with poly I:C being the strongest agonist, indicating that cytoplasmic PRRs (RLRs and PKR) are the receptors involved in recognising viral-like dsRNA. Moreover, we observed that IFNL1, which is a type III interferon, is strongly induced at both transcript and protein levels compared to IFNB1. Different studies have highlighted type III IFNs role in protection against viral infections [91, 94]. This is not possible for the liver, since mouse hepatocytes, differently from humans, do not express IFN-λ receptors, thus they do not respond to IFN-λ [85]. Therefore, primary human hepatocyte surrogate models are needed to dissect the differences between the two IFN families. HLCs bring several improvements compared to human hepatic cells lines. For example, they are derived from primary human cells, they are not malignant cells and their genetic background is

preserved and defined. The ability of HLCs to induce type III IFNs, as shown in this thesis, highlights the potential role of this model in studying the innate antiviral response in human hepatocytes.

Since cytosol-delivered (through transfection) immunogenic dsRNA induced antiviral activity in the three cellular models, we speculate that hepatocytes rely on cytosolic PRRs rather than TLR3 for the recognition of dsRNA. Similar observations have been made previously by other groups, showing that TLR3 expression is compromised in Hepg2 and Huh7 cells compared to PHHs [157]. We further investigated which cytosolic PRRs are involved in the antiviral activity. It has been shown that transfected 5' triphosphate hairpin and transfected poly I:C are RIG-I and MDA5 ligands, respectively [43, 46]. RLR-dependent antiviral response depends on MAVS aggregation, which act as signalosome platform. Strikingly, we observed that MAVS knock-down only partially affects IFN induction in transfected poly I:C stimulated HepG2 and Huh7 cells. Thus, we hypothesised that PKR, known to bind dsRNA, might be involved in the mechanism. Pharmacological inhibition of PKR completely abrogated IFN and pro-inflammatory cytokine expression upon both transfected 5' triphosphate hairpin and transfected poly I:C in HepG2 and Huh7 cells. These results demonstrate that PKR, and to some extent RLRs, are involved in inducing antiviral activity in HepG2 and Huh7 cells. It is still unclear whether our observations are fully translatable to primary human hepatocytes (PHHs). Studies have shown that PHHs, but not HepG2 or Huh7 cells, induce IFNs and pro-inflammatory cytokines upon both transfected and non-transfected poly I:C stimulation, the latter being a TLR3 agonist [156, 157]. It is worth noting that non-transfected poly I:C potency is much lower compared to transfected poly I:C in PHHs. This indicates that even though PHHs have some functional TLR signaling, they likely rely mostly on cytosolic receptors. We hypothesise that this might be a mechanism through which hepatocytes keep their tolerogenic ability towards non-pathogenic microbes, while they are able to quickly respond to hepatotropic pathogens [282].

MAVS-mediated antiviral activity is known to cause a decrease in OxPhos and increased mitochondrial membrane polarization in fibroblasts and peripheral blood mononuclear cells [133, 134]. How PKR-dependent antiviral activity affects mitochondria in

hepatocytes has not been investigated yet. Since HepG2 and Huh7 cells primarily activate PKR upon transfected poly I:C stimulation, our results can potentially reveal changes in mitochondrial activity during a PKR-dependent antiviral response. We observed decreased cellular respiration and mitochondrial membrane potential (MMP) after 24h of transfected poly I:C stimulation. According to the literature MAVS-mediated antiviral activity increases MMP, and pharmacological dissipation of MPP reduces MAVS-mediated IFN induction [134, 283]. Therefore, our results highlight a different mechanism where PKR-mediated antiviral response decreases MMP, in contrast to what has been described for MAVS-dependent antiviral activity. It is worth noting that mitochondrial depolarization and decreased OxPhos have been observed at 24 h, but not 4 h stimulation with transfected poly I:C in both HepG2 and Huh7. From these results it is hard to discern whether the mitochondrial changes are due to prolonged PRRs activation or are dependent on downstream PRR-mediated signaling processes, such as IFN signaling. In this instance, dissecting the major signaling pathways – for instance inhibiting IFN signaling through a pharmacological or genetic approach - would help to unravel the mechanism responsible for our observations.

Reactive oxygen species (ROS) are implicated in many cellular mechanisms, including innate antiviral activity [115]. ROS are predominantly produced during OxPhos by electron leaking – mostly from complex I and complex III – which are accepted by oxygen molecules, therefore forming $O_2^{\bullet -}$ and H_2O_2 [129]. Mitochondrial ROS (mROS) have been described to be upregulated in MAVS-dependent antiviral activity in fibroblasts and PBMCs [134]. Whether this is the case in hepatocytes during innate antiviral activity is still unclear. Here, we measured increased mROS upon transfected poly I:C in both an earlier phase (such as 4h) and at a later time point (24h), indicating that MAVS and PKR-dependent antiviral activity increases mROS in hepatic cellular models. PKR is essential in cellular responses to different stimuli, including endoplasmic reticulum stress, oxidative stress, and exogenous dsRNA recognition [57]. Therefore, we hypothesised that modulation of cellular ROS content, would impact the PKR-mediated antiviral activity. Using N-acetyl cysteine (which is an antioxidant molecule), type I and III IFNs as well as pro-inflammatory cytokines expression was decreased, suggesting that cellular redox status impacts hepatocyte antiviral activity.

While at physiological concentrations, ROS are involved in several cellular processes through their ability to serve as secondary messenger molecules, at increased and pathophysiological levels, they damage cell macromolecules by oxidising the latter [227]. Cells have developed different and redundant antioxidant mechanisms to protect themselves against oxidative stress. Malfunctioning in the cellular antioxidant system leads to inappropriate ROS accumulation with subsequent oxidative stress and cellular damage. This scenario has been described in different pathologies, such as chronic HCV [284, 285]. In this case, HCV-induced oxidative stress is presumably among the causes of liver inflammation and subsequent fibrosis [286]. HCV infection does not only increase hepatic ROS concentration, but it has been also shown to decrease expression of enzymes involved in scavenging ROS, among others SOD1 [213]. Whether SOD1 downregulation is due to HCV-mediated strategy or to an endogenous mechanism is still not clear. Although in a chronic hepatitis mouse model (LCMV clone 13 infection) recapitulating chronic HCV, SOD1 decrease has been found to be type I IFN-dependent, indicating SOD1 protection towards IFN-mediated oxidative stress [172]. Through a bioinformatic approach, we identified several antioxidant protein coding genes being differentially expressed upon hepatic viral infection in mice (LCMV clone 13 infection)[173]. Among these, peroxiredoxin 4 (PRDX4) was downregulated at both gene and protein levels. We confirmed PRDX4 downregulation upon viral infection by RT-qPCR in a mouse model of LCMV clone 13 infection. We further observed that, differently to what has been shown for SOD1 [172], PRDX4 downregulation is type I IFN-signaling independent. It is worth mentioning the decrease of PRDX4 expression reached its … at day 8 post infection. At this time point (between 6 and 12 days post infection), according to LCMV clone 13 infection model, the adaptive immune response and viral titres reach their peak. Therefore, PRDX4 downregulation might be caused by either adaptive immunity or the virus itself hijacking the antioxidant system. Further experiments using RAG-2 knock out mice, which do not have mature B and T cells, might elucidate whether PRDX4 downregulation is adaptive response-dependent.

We aimed to assess PRDX4 effect on hepatic antiviral activity. By silencing PRDX4 in Huh7 cells, type I and III IFNs, as well as pro-inflammatory cytokine expression were increased

upon stimulation with dsRNA (transfected poly I:C). These results were confirmed also in an *in vitro* hepatotropic viral infection using Dengue virus (DENV), where we observed increases in IFN, pro-inflammatory cytokine, and ISG expression. Surprisingly, although PRDX4 silencing increased antiviral activity, we did not observe a change in DENV titres 24h post infection. This might be because of two different reasons. First, we carried out the infection only for 24h; at longer periods, increased IFNs and ISGs in PRDX4 KD cells might control more efficiently the viral infection compared to the control. Secondly, PRDX4 is an antioxidant protein and it has been reported that its deficiency increases cellular ROS levels upon viral infection [252]. DENV, being a Flaviviridae, expresses the non-structural protein 4 A (NS4A) (the capping enzyme) which is activated by oxidation of a methionine residue. Therefore, PRDX4 silencing which increases cellular ROS and induces oxidative stress might be beneficial for DENV replication itself by activation of NS4A.

We observed that also other cell types, such as the embryonic kidney cells HEK293T, increase IFNs and ISGs expression upon PRDX4 silencing and transfected poly I:C stimulation. These results might indicate that the mechanism through which PRDX4 limits antiviral activity is conserved in different cell types and tissues. Extending our work by using other cell types and primary cells would confirm our observations and highlight the fact that PRDX4-mediated increased antiviral activity is not hepatocyte specific.

PRDX4 localises in different cellular compartments, and uniquely to other peroxiredoxins, it has been found also in the endoplasmic reticulum (ER), where it acts as H_2O_2 scavenger. PRDX4 is crucial in governing ER redox homeostasis and ER stress [287]. A recent study has shown that PRDX4 localization within the organelle is dynamic, and during ER stress this protein is localised at the mitochondria-associated membranes (MAMs) interface, where it interacts with several proteins involved in linking ER and mitochondrial activities [288]. Interestingly, MAVS has been shown to be localised on the MAMs to form signaling synapses during RLR-mediated antiviral response [48]. Thus, we hypothesised that PRDX4 might affect MAVS activation. In this case, we found an increase in MAVS aggregation upon PRDX4 silencing, which might explain the upregulated antiviral activity observed. We further tested whether MAVS and PRDX4

directly interact. Meta analysis of putative MAVS interactors identified PRDX4 as a possible candidate, but in our experimental set up, we could not identify direct interaction between the two proteins. We do not exclude a possible interaction between MAVS and PRDX4; further investigations considering different time points as well as using appropriate experimental set ups (such as alkylating reagents that block cysteines free thiols) will help testing our hypothesis.

Different studies have already linked antioxidant enzymes, especially peroxiredoxins, with the immune response and inflammation [254, 289]. Moreover, antioxidant enzymes have also been shown to directly regulate the activation of transcriptional factors involved in innate immunity [290, 291]. Whether this is also the case for PRDX4 has not been investigated yet. Since we observed increased MAVS activation in silenced PRDX4 cells, we expect that also the downstream transcriptional factors activation, in particular IRF3 and NF-kB, would be increased. Further work analysing IRF3 and NF-kB phosphorylation would confirm the data obtained in this thesis. As mentioned in 5.6, we speculate that PRDX4 silencing increases ROS levels upon dsRNA stimulation compared to the silenced control. Mitochondrial activity, such as mitochondrial respiration and mitochondrial membrane polarization, has been linked with MAVS activation and downstream expression of IFNs [109, 133, 283]. Whether PRDX4 deficiency influences mitochondrial metabolism and activity, for instance increasing mitochondrial polarization and therefore mitochondrial ROS, could explain the increased MAVS aggregation and downstream antiviral activity. Future work investigating the relationship between PRDX4 and mitochondria would provide new insights into the molecular mechanism.

6.1 Limitations of this study

As mentioned above, hepatic metabolism rewiring is now a subject of major interest. In particular, different studies have investigated how type I IFN signaling reprograms hepatic metabolism using *in vivo* models of chronic hepatitis. But studies of the cross-talk between the early antiviral activities and their consequences on hepatic metabolism are not complete. This lack of information might be due in part to the absence of an *in*

vitro model that fully recapitulates the complex hepatic metabolism observed in vivo. In our experimental set up, we used the two human hepatic cell lines Huh7 and HepG2. Being transformed cells, both these cell lines have an altered metabolism compared to primary hepatocytes. According to a study, HepG2 and Huh7 hepatic cell lines have 89 and 115 mutations, respectively, compared to PHHs [292]. Mutations mostly occurred in genes involved in controlling cell cycle, survival, and proliferation, conferring the cancer phenotype. Different mitogen-activated protein kinases (MAPKs), which are involved in also controlling the cellular metabolism, were found mutated in the two cell lines, thus it is not surprising that other studies highlighted the metabolic differences between HepG2 and Huh7 cell lines and primary human hepatocytes (PHHs) [292]. Also genes involved in fatty acid synthesis and detoxification processes (cytochrome P450s, aldehyde dehydrogenases), which are also involved in ROS metabolism, present mutations in HepG2 and Huh7 cells lines [293, 294]. Thus, the results obtained by using the two cell lines might be only partially reflecting the sophisticated hepatic metabolism. Further investigations using other cellular models, such as iPSC-derived hepatocytes, might be needed to develop and test our hypothesis. Nevertheless, we are confident that we have identified a novel link between the cellular antioxidant systems involving the antioxidant enzyme PRDX4 and the hepatocyte innate antiviral activity.

6.2 Future directions

The results presented in this thesis has generated new lines of research for our group and has formed the basis for future research in innate antiviral immunometabolism field.

We identified PKR as a key player in binding dsRNA and activating a downstream antiviral response in hepatocytes. PKR is not only involved in antiviral activity; but it has been also described as a sensor of cellular stress and, more recently, of metabolic homeostasis [295]. In a context of metabolic disorder, such as obesity, PKR has been shown to be constitutively activated and detrimental for cellular homeostasis. Mice exposed to high fat diet have been shown to have increased expression of TNF, IRF7, ISG15, and OAS1 due to PKR activation in adipocytes and liver. Moreover, PKR can be activated by fatty acids causing a subsequent phosphorylation of insulin receptor substrate 1 (IRS1), thus

inducing insulin resistance, which is at the basis of type II diabetes [295]. Different studies have found that the prevalence of type II diabetes among HCV patients ranges from 7 to 43% [296–299]. These observations have been often linked to HCV-induced metabolic switch, such as increase in glycolysis and lipid biosynthesis [279]. HCV-derived dsRNA is sensed by different PRRs, among these also PKR [300], whether and how PKR is involved in HCV-related type II diabetes and metabolic disorders is still unknown. A first *in vitro* approach using HLCs, which sustain HCV infection [201, 301] and, as we observed in our results, respond to dsRNA, might set the basis for better understanding HCV pathophysiology and its effects on hepatocyte metabolism.

PRDX4 was firstly identified and described as negative regulator of NF-κB activation in 1997 [253]. Since then, it has been discovered to be involved in several pathologies, such as NAFLD and cancer [255, 302]. PRDX4 overexpression has been identified in several human cancers, often correlating with decreased survival rate [302]. A recent study investigated PRDX4 role in pancreatic adenocarcinoma, showing that PRDX4 silencing increases oxidative damage and cell death, therefore increasing the ability of clearing malignant cells in *in vivo* models [303]. Specifically, PRDX4 has been shown to protect pancreatic adenocarcinomas from H_2O_2-induced stress. On the other hand, genetic depletion of PRDX4 increased oxidative stress-mediated single and double stranded DNA breaks [303]. More recently, the same research group gathered preliminary data showing that PRDX4 deficiency activates IFN-based antiviral activity in pancreatic adenocarcinoma cells mediated through recognition of self-damaged DNA by cGAS-STING [304]. Opposite to what has been described in pancreatic adenocarcinoma, in our experiments, “steady-state” PRDX4-silenced cells not stimulated with transfected dsRNA did not induce any significant increase in IFN or pro-inflammatory cytokine expression. In contrast, the stimulation with transfected dsRNA caused a higher antiviral activity in PRDX4 silenced cells compared to the control.

Several studies have highlighted that cellular stress due to PRR activation or pathogen infection causes leakage of nuclear and mitochondrial DNA and RNA (mtDNA and mtRNA), which activate cellular PRRs and induce subsequent innate immune activity. DNA and RNA viruses, such as herpesviruses and Influenza virus, promote mitochondrial

stress and mtDNA release in the cytosol, where it acts as ligand for the DNA sensor cGAS, activating a downstream STING-dependent IFN-based antiviral response [305, 306]. Also PRR activation can trigger IFN-dependent antiviral responses due to recognition of self-nucleic acids; LPS stimulation induces a rewiring in the macrophage mitochondrial metabolism which causes leakage of mtRNA that activates RLRs and TLR7 [112]. While mtDNA and mtRNA have been extensively shown to act as immunostimulatory molecules, only recently nuclear DNA has been described to act similarly, triggering cytosolic PRRs – including cGAS-STING. Nuclear DNA-mediated activation of STING has been described in norovirus infections [307] and also as a result of anticancer treatments, which cause DNA damage and leakage in the cytosolic compartment [308].

PRDX4 has antioxidant functions and is involved in regulating the ER stress as described above. The increase in IFNs and pro-inflammatory cytokines observed in PRDX4 KD cells might be due to increased cellular stress. In this scenario we do not exclude the possibility of host-derived DAMPs, in particular DNA and RNA, that might function in a forward positive feed-back fashion. Further work in our laboratory will shed light on the molecular mechanism.

In conclusion, here we found that innate antiviral activity in hepatocytes majorly relies on cytosolic PRRs. Activation of the antiviral activity affects cellular metabolism, causing increased ROS production. Among the different enzymes involved in ROS metabolism, we identified PRDX4, which is decreased in a *in vivo* infection model, to be critical in limiting the antiviral activity. These findings may lay the foundations for future studies centred on deconvoluting the cross-talk between antiviral response and redox signaling, which can potentially lead to development of novel antiviral therapies.

References

1. Iwasaki A, Medzhitov R (2015) Control of adaptive immunity by the innate immune system. Nat Immunol 16:343–353
2. Marshall JS, Warrington R, Watson W, Kim HL (2018) An introduction to immunology and immunopathology. Allergy, Asthma Clin Immunol 14:49
3. Li D, Wu M (2021) Pattern recognition receptors in health and diseases. Signal Transduct Target Ther 6:291
4. Krausgruber T, Fortelny N, Fife-Gernedl V, et al (2020) Structural cells are key regulators of organ-specific immune responses. Nature 583:296–302
5. Takeuchi O, Akira S (2010) Pattern Recognition Receptors and Inflammation. Cell 140:805–820
6. Lien E, Sellati TJ, Yoshimura A, et al (1999) Toll-like Receptor 2 Functions as a Pattern Recognition Receptor for Diverse Bacterial Products. J Biol Chem 274:33419–33425
7. Takeuchi O, Sato S, Horiuchi T, Hoshino K, Takeda K, Dong Z, Modlin RL, Akira S (2002) Cutting Edge: Role of Toll-Like Receptor 1 in Mediating Immune Response to Microbial Lipoproteins. J Immunol 169:10–14
8. Alexopoulou L, Holt AC, Medzhitov R, Flavell RA (2001) Recognition of double-stranded RNA and activation of NF-κB by Toll-like receptor 3. Nature 413:732–738
9. Poltorak A, He X, Smirnova I, et al (1998) Defective LPS Signaling in C3H/HeJ and C57BL/10ScCr Mice: Mutations in Tlr4 Gene. Science (80-) 282:2085–2088
10. Hoshino K, Takeuchi O, Kawai T, Sanjo H, Ogawa T, Takeda Y, Takeda K, Akira S (1999) Cutting Edge: Toll-Like Receptor 4 (TLR4)-Deficient Mice Are Hyporesponsive to Lipopolysaccharide: Evidence for TLR4 as the Lps Gene Product. J Immunol 162:3749–3752
11. Heil F, Hemmi H, Hochrein H, Ampenberger F, Kirschning C, Akira S, Lipford G, Wagner H, Bauer S (2004) Species-Specific Recognition of Single-Stranded RNA via Toll-like Receptor 7 and 8. Science (80-) 303:1526–1529
12. Diebold SS, Kaisho T, Hemmi H, Akira S, Reis e Sousa C (2004) Innate Antiviral

Responses by Means of TLR7-Mediated Recognition of Single-Stranded RNA. Science (80-) 303:1529–1531

13. Forsbach A, Nemorin J-G, Montino C, et al (2008) Identification of RNA Sequence Motifs Stimulating Sequence-Specific TLR8-Dependent Immune Responses. J Immunol 180:3729–3738
14. Hemmi H, Takeuchi O, Kawai T, et al (2000) A Toll-like receptor recognizes bacterial DNA. Nature 408:740–745
15. Yoneyama M, Kikuchi M, Natsukawa T, Shinobu N, Imaizumi T, Miyagishi M, Taira K, Akira S, Fujita T (2004) The RNA helicase RIG-I has an essential function in double-stranded RNA-induced innate antiviral responses. Nat Immunol 5:730–737
16. Gitlin L, Barchet W, Gilfillan S, Cella M, Beutler B, Flavell RA, Diamond MS, Colonna M (2006) Essential role of mda-5 in type I IFN responses to polyriboinosinic:polyribocytidylic acid and encephalomyocarditis picornavirus. Proc Natl Acad Sci 103:8459–8464
17. Sabbah A, Chang TH, Harnack R, Frohlich V, Tominaga K, Dube PH, Xiang Y, Bose S (2009) Activation of innate immune antiviral responses by Nod2. Nat Immunol 10:1073–1080
18. Bauernfried S, Scherr MJ, Pichlmair A, Duderstadt KE, Hornung V (2021) Human NLRP1 is a sensor for double-stranded RNA. Science (80-). https://doi.org/10.1126/science.abd0811
19. Shen C, Li R, Negro R, et al (2021) Phase separation drives RNA virus-induced activation of the NLRP6 inflammasome. Cell 184:5759-5774.e20
20. Su Q, Wang S, Baltzis D, Qu L-K, Wong AH-T, Koromilas AE (2006) Tyrosine phosphorylation acts as a molecular switch to full-scale activation of the eIF2α RNA-dependent protein kinase. Proc Natl Acad Sci 103:63–68
21. Hornung V, Ablasser A, Charrel-Dennis M, Bauernfeind F, Horvath G, Caffrey DR, Latz E, Fitzgerald KA (2009) AIM2 recognizes cytosolic dsDNA and forms a caspase-1-activating inflammasome with ASC. Nature 458:514–518
22. Unterholzner L, Keating SE, Baran M, et al (2010) IFI16 is an innate immune sensor for intracellular DNA. Nat Immunol 11:997–1004
23. Takaoka A, Wang Z, Choi MK, et al (2007) DAI (DLM-1/ZBP1) is a cytosolic DNA

sensor and an activator of innate immune response. Nature 448:501–505

24. Zhang Z, Yuan B, Bao M, Lu N, Kim T, Liu Y-J (2011) The helicase DDX41 senses intracellular DNA mediated by the adaptor STING in dendritic cells. Nat Immunol 12:959–965
25. Sun L, Wu J, Du F, Chen X, Chen ZJ (2013) Cyclic GMP-AMP Synthase Is a Cytosolic DNA Sensor That Activates the Type I Interferon Pathway. Science (80-) 339:786–791
26. Lemaitre B, Nicolas E, Michaut L, Reichhart J-M, Hoffmann JA (1996) The Dorsoventral Regulatory Gene Cassette spätzle/Toll/cactus Controls the Potent Antifungal Response in Drosophila Adults. Cell 86:973–983
27. Medzhitov R, Preston-Hurlburt P, Janeway CA (1997) A human homologue of the Drosophila Toll protein signals activation of adaptive immunity. Nature 388:394–397
28. Rock FL, Hardiman G, Timans JC, Kastelein RA, Bazan JF (1998) A family of human receptors structurally related to Drosophila Toll. Proc Natl Acad Sci 95:588–593
29. Botos I, Segal DM, Davies DR (2011) The Structural Biology of Toll-like Receptors. Structure 19:447–459
30. O'Neill LAJ, Bowie AG (2007) The family of five: TIR-domain-containing adaptors in Toll-like receptor signalling. Nat Rev Immunol 7:353–364
31. Kagan JC, Su T, Horng T, Chow A, Akira S, Medzhitov R (2008) TRAM couples endocytosis of Toll-like receptor 4 to the induction of interferon-β. Nat Immunol 9:361–368
32. Carty M, Goodbody R, Schröder M, Stack J, Moynagh PN, Bowie AG (2006) The human adaptor SARM negatively regulates adaptor protein TRIF–dependent Toll-like receptor signaling. Nat Immunol 7:1074–1081
33. Halajian EA, LeBlanc E V., Gee K, Colpitts CC (2022) Activation of TLR4 by viral glycoproteins: A double-edged sword? Front Microbiol. https://doi.org/10.3389/fmicb.2022.1007081
34. Zhao Y, Kuang M, Li J, et al (2021) SARS-CoV-2 spike protein interacts with and activates TLR41. Cell Res 31:818–820
35. Zheng M, Karki R, Williams EP, Yang D, Fitzpatrick E, Vogel P, Jonsson CB,

Kanneganti T-D (2021) TLR2 senses the SARS-CoV-2 envelope protein to produce inflammatory cytokines. Nat Immunol 22:829–838

36. Lester SN, Li K (2014) Toll-Like Receptors in Antiviral Innate Immunity. J Mol Biol 426:1246–1264
37. Gorden KB, Gorski KS, Gibson SJ, Kedl RM, Kieper WC, Qiu X, Tomai MA, Alkan SS, Vasilakos JP (2005) Synthetic TLR Agonists Reveal Functional Differences between Human TLR7 and TLR8. J Immunol 174:1259–1268
38. Rehwinkel J, Gack MU (2020) RIG-I-like receptors: their regulation and roles in RNA sensing. Nat Rev Immunol 20:537–551
39. Rothenfusser S, Goutagny N, DiPerna G, Gong M, Monks BG, Schoenemeyer A, Yamamoto M, Akira S, Fitzgerald KA (2005) The RNA Helicase Lgp2 Inhibits TLR-Independent Sensing of Viral Replication by Retinoic Acid-Inducible Gene-I. J Immunol 175:5260–5268
40. Uchikawa E, Lethier M, Malet H, Brunel J, Gerlier D, Cusack S (2016) Structural Analysis of dsRNA Binding to Anti-viral Pattern Recognition Receptors LGP2 and MDA5. Mol Cell 62:586–602
41. Venkataraman T, Valdes M, Elsby R, Kakuta S, Caceres G, Saijo S, Iwakura Y, Barber GN (2007) Loss of DExD/H Box RNA Helicase LGP2 Manifests Disparate Antiviral Responses. J Immunol 178:6444–6455
42. Kowalinski E, Lunardi T, McCarthy AA, Louber J, Brunel J, Grigorov B, Gerlier D, Cusack S (2011) Structural Basis for the Activation of Innate Immune Pattern-Recognition Receptor RIG-I by Viral RNA. Cell 147:423–435
43. Hornung V, Ellegast J, Kim S, et al (2006) 5’-Triphosphate RNA Is the Ligand for RIG-I. Science (80-) 314:994–997
44. Pichlmair A, Schulz O, Tan CP, Näslund TI, Liljeström P, Weber F, Reis e Sousa C (2006) RIG-I-Mediated Antiviral Responses to Single-Stranded RNA Bearing 5’-Phosphates. Science (80-) 314:997–1001
45. Schuberth-Wagner C, Ludwig J, Bruder AK, et al (2015) A Conserved Histidine in the RNA Sensor RIG-I Controls Immune Tolerance to N1-2’O-Methylated Self RNA. Immunity 43:41–51
46. Kato H, Takeuchi O, Mikamo-Satoh E, Hirai R, Kawai T, Matsushita K, Hiiragi A, Dermody TS, Fujita T, Akira S (2008) Length-dependent recognition of double-

stranded ribonucleic acids by retinoic acid–inducible gene-I and melanoma differentiation–associated gene 5. J Exp Med 205:1601–1610

47. Dias Junior AG, Sampaio NG, Rehwinkel J (2019) A Balancing Act: MDA5 in Antiviral Immunity and Autoinflammation. Trends Microbiol 27:75–85
48. Horner SM, Liu HM, Park HS, Briley J, Gale M (2011) Mitochondrial-associated endoplasmic reticulum membranes (MAM) form innate immune synapses and are targeted by hepatitis C virus. Proc Natl Acad Sci 108:14590–14595
49. Dixit E, Boulant S, Zhang Y, et al (2010) Peroxisomes Are Signaling Platforms for Antiviral Innate Immunity. Cell 141:668–681
50. Hou F, Sun L, Zheng H, Skaug B, Jiang Q-X, Chen ZJ (2011) MAVS Forms Functional Prion-like Aggregates to Activate and Propagate Antiviral Innate Immune Response. Cell 146:448–461
51. Liu S, Chen J, Cai X, Wu J, Chen X, Wu Y-T, Sun L, Chen ZJ (2013) MAVS recruits multiple ubiquitin E3 ligases to activate antiviral signaling cascades. Elife. https://doi.org/10.7554/eLife.00785
52. Refolo G, Vescovo T, Piacentini M, Fimia GM, Ciccosanti F (2020) Mitochondrial Interactome: A Focus on Antiviral Signaling Pathways. Front Cell Dev Biol. https://doi.org/10.3389/fcell.2020.00008
53. Kim YK, Shin J-S, Nahm MH (2016) NOD-Like Receptors in Infection, Immunity, and Diseases. Yonsei Med J 57:5
54. Chen L, Cao S, Lin Z, He S, Zuo J (2021) NOD-like receptors in autoimmune diseases. Acta Pharmacol Sin 42:1742–1756
55. KUHEN KL, SAMUEL CE (1997) Isolation of the Interferon-Inducible RNA-Dependent Protein KinasePkrPromoter and Identification of a Novel DNA Element within the 5′-Flanking Region of Human and MousePkrGenes. Virology 227:119–130
56. Meurs E, Chong K, Galabru J, Thomas NSB, Kerr IM, Williams BRG, Hovanessian AG (1990) Molecular cloning and characterization of the human double-stranded RNA-activated protein kinase induced by interferon. Cell 62:379–390
57. García MA, Meurs EF, Esteban M (2007) The dsRNA protein kinase PKR: Virus and cell control. Biochimie 89:799–811
58. Gal-Ben-Ari S, Barrera I, Ehrlich M, Rosenblum K (2019) PKR: A Kinase to

Remember. Front Mol Neurosci. https://doi.org/10.3389/fnmol.2018.00480
59. Paludan SR, Bowie AG (2013) Immune Sensing of DNA. Immunity 38:870–880
60. Guy C, Bowie AG (2022) Recent insights into innate immune nucleic acid sensing during viral infection. Curr Opin Immunol 78:102250
61. Jiang Z, Wei F, Zhang Y, et al (2021) IFI16 directly senses viral RNA and enhances RIG-I transcription and activation to restrict influenza virus infection. Nat Microbiol 6:932–945
62. Schleimer RP, Kato A, Kern R, Kuperman D, Avila PC (2007) Epithelium: At the interface of innate and adaptive immune responses. J Allergy Clin Immunol 120:1279–1284
63. Leiva-Juárez MM, Kolls JK, Evans SE (2018) Lung epithelial cells: therapeutically inducible effectors of antimicrobial defense. Mucosal Immunol 11:21–34
64. Price AE, Shamardani K, Lugo KA, Deguine J, Roberts AW, Lee BL, Barton GM (2018) A Map of Toll-like Receptor Expression in the Intestinal Epithelium Reveals Distinct Spatial, Cell Type-Specific, and Temporal Patterns. Immunity 49:560-575.e6
65. Loo Y-M, Gale M (2011) Immune Signaling by RIG-I-like Receptors. Immunity 34:680–692
66. Uhlén M, Fagerberg L, Hallström BM, et al (2015) Tissue-based map of the human proteome. Science (80-). https://doi.org/10.1126/science.1260419
67. Thul PJ, Åkesson L, Wiking M, et al (2017) A subcellular map of the human proteome. Science (80-). https://doi.org/10.1126/science.aal3321
68. (1957) Virus interference. I. The interferon. Proc R Soc London Ser B - Biol Sci 147:258–267
69. Mesev E V., LeDesma RA, Ploss A (2019) Decoding type I and III interferon signalling during viral infection. Nat Microbiol 4:914–924
70. Hu X, Ivashkiv LB (2009) Cross-regulation of Signaling Pathways by Interferon-γ: Implications for Immune Responses and Autoimmune Diseases. Immunity 31:539–550
71. Ivashkiv LB (2018) IFNγ: signalling, epigenetics and roles in immunity, metabolism, disease and cancer immunotherapy. Nat Rev Immunol 18:545–558
72. Prokunina-Olsson L, Muchmore B, Tang W, et al (2013) A variant upstream of

IFNL3 (IL28B) creating a new interferon gene IFNL4 is associated with impaired clearance of hepatitis C virus. Nat Genet 45:164–171

73. Teijaro JR (2016) Type I interferons in viral control and immune regulation. Curr Opin Virol 16:31–40
74. Stevenson NJ, Bourke NM, Ryan EJ, Binder M, Fanning L, Johnston JA, Hegarty JE, Long A, O'Farrelly C (2013) Hepatitis C virus targets the interferon-α JAK/STAT pathway by promoting proteasomal degradation in immune cells and hepatocytes. FEBS Lett 587:1571–1578
75. Ivashkiv LB, Donlin LT (2014) Regulation of type I interferon responses. Nat Rev Immunol 14:36–49
76. Thomas C, Moraga I, Levin D, et al (2011) Structural Linkage between Ligand Discrimination and Receptor Activation by Type I Interferons. Cell 146:621–632
77. Schreiber G (2017) The molecular basis for differential type I interferon signaling. J Biol Chem 292:7285–7294
78. Kotenko S V., Gallagher G, Baurin V V., Lewis-Antes A, Shen M, Shah NK, Langer JA, Sheikh F, Dickensheets H, Donnelly RP (2003) IFN-λs mediate antiviral protection through a distinct class II cytokine receptor complex. Nat Immunol 4:69–77
79. Sheppard P, Kindsvogel W, Xu W, et al (2003) IL-28, IL-29 and their class II cytokine receptor IL-28R. Nat Immunol 4:63–68
80. Yin Z, Dai J, Deng J, et al (2012) Type III IFNs Are Produced by and Stimulate Human Plasmacytoid Dendritic Cells. J Immunol 189:2735–2745
81. Sommereyns C, Paul S, Staeheli P, Michiels T (2008) IFN-Lambda (IFN-λ) Is Expressed in a Tissue-Dependent Fashion and Primarily Acts on Epithelial Cells In Vivo. PLoS Pathog 4:e1000017
82. Lazear HM, Schoggins JW, Diamond MS (2019) Shared and Distinct Functions of Type I and Type III Interferons. Immunity 50:907–923
83. Koltsida O, Hausding M, Stavropoulos A, et al (2011) IL-28A (IFN-λ2) modulates lung DC function to promote Th1 immune skewing and suppress allergic airway disease. EMBO Mol Med 3:348–361
84. Hermant P, Demarez C, Mahlakõiv T, Staeheli P, Meuleman P, Michiels T (2014) Human but Not Mouse Hepatocytes Respond to Interferon-Lambda In Vivo.

PLoS One 9:e87906

85. Mordstein M, Kochs G, Dumoutier L, Renauld J-C, Paludan SR, Klucher K, Staeheli P (2008) Interferon-λ Contributes to Innate Immunity of Mice against Influenza A Virus but Not against Hepatotropic Viruses. PLoS Pathog 4:e1000151
86. Crotta S, Davidson S, Mahlakoiv T, Desmet CJ, Buckwalter MR, Albert ML, Staeheli P, Wack A (2013) Type I and Type III Interferons Drive Redundant Amplification Loops to Induce a Transcriptional Signature in Influenza-Infected Airway Epithelia. PLoS Pathog 9:e1003773
87. Odendall C, Dixit E, Stavru F, Bierne H, Franz KM, Durbin AF, Boulant S, Gehrke L, Cossart P, Kagan JC (2014) Diverse intracellular pathogens activate type III interferon expression from peroxisomes. Nat Immunol 15:717–726
88. Caine EA, Scheaffer SM, Arora N, Zaitsev K, Artyomov MN, Coyne CB, Moley KH, Diamond MS (2019) Interferon lambda protects the female reproductive tract against Zika virus infection. Nat Commun 10:280
89. Marcello T, Grakoui A, Barba–Spaeth G, Machlin ES, Kotenko S V., Macdonald MR, Rice CM (2006) Interferons α and λ Inhibit Hepatitis C Virus Replication With Distinct Signal Transduction and Gene Regulation Kinetics. Gastroenterology 131:1887–1898
90. Jilg N, Lin W, Hong J, et al (2014) Kinetic differences in the induction of interferon stimulated genes by interferon-α and interleukin 28B are altered by infection with hepatitis C virus. Hepatology 59:1250–1261
91. Galani IE, Triantafyllia V, Eleminiadou E-E, et al (2017) Interferon-λ Mediates Non-redundant Front-Line Antiviral Protection against Influenza Virus Infection without Compromising Host Fitness. Immunity 46:875-890.e6
92. François-Newton V, Magno de Freitas Almeida G, Payelle-Brogard B, Monneron D, Pichard-Garcia L, Piehler J, Pellegrini S, Uzé G (2011) USP18-Based Negative Feedback Control Is Induced by Type I and Type III Interferons and Specifically Inactivates Interferon α Response. PLoS One 6:e22200
93. Andreakos E, Zanoni I, Galani IE (2019) Lambda interferons come to light: dual function cytokines mediating antiviral immunity and damage control. Curr Opin Immunol 56:67–75
94. Mahlakõiv T, Hernandez P, Gronke K, Diefenbach A, Staeheli P (2015) Leukocyte-

Derived IFN-α/β and Epithelial IFN-λ Constitute a Compartmentalized Mucosal Defense System that Restricts Enteric Virus Infections. PLOS Pathog 11:e1004782

95. Warburg O, Gawehn K, Geissler A-W (1958) Stoffwechsel der weißen Blutzellen. Zeitschrift für Naturforsch B 13:515–516
96. O'Neill LAJ, Kishton RJ, Rathmell J (2016) A guide to immunometabolism for immunologists. Nat Rev Immunol 16:553–565
97. Makowski L, Chaib M, Rathmell JC (2020) Immunometabolism: From basic mechanisms to translation. Immunol Rev 295:5–14
98. Lercher A, Baazim H, Bergthaler A (2020) Systemic Immunometabolism: Challenges and Opportunities. Immunity 53:496–509
99. Rodríguez-Prados J-C, Través PG, Cuenca J, Rico D, Aragonés J, Martín-Sanz P, Cascante M, Boscá L (2010) Substrate Fate in Activated Macrophages: A Comparison between Innate, Classic, and Alternative Activation. J Immunol 185:605–614
100. Jha AK, Huang SC-C, Sergushichev A, et al (2015) Network Integration of Parallel Metabolic and Transcriptional Data Reveals Metabolic Modules that Regulate Macrophage Polarization. Immunity 42:419–430
101. Tannahill GM, Curtis AM, Adamik J, et al (2013) Succinate is an inflammatory signal that induces IL-1β through HIF-1α. Nature 496:238–242
102. Michelucci A, Cordes T, Ghelfi J, et al (2013) Immune-responsive gene 1 protein links metabolism to immunity by catalyzing itaconic acid production. Proc Natl Acad Sci 110:7820–7825
103. Mills EL, Ryan DG, Prag HA, et al (2018) Itaconate is an anti-inflammatory metabolite that activates Nrf2 via alkylation of KEAP1. Nature 556:113–117
104. Sánchez-García FJ, Pérez-Hernández CA, Rodríguez-Murillo M, Moreno-Altamirano MMB (2021) The Role of Tricarboxylic Acid Cycle Metabolites in Viral Infections. Front Cell Infect Microbiol. https://doi.org/10.3389/fcimb.2021.725043
105. Syed GH, Amako Y, Siddiqui A (2010) Hepatitis C virus hijacks host lipid metabolism. Trends Endocrinol Metab 21:33–40
106. Everts B, Amiel E, Huang SC-C, et al (2014) TLR-driven early glycolytic

reprogramming via the kinases TBK1-IKKε supports the anabolic demands of dendritic cell activation. Nat Immunol 15:323–332

107. Zhang W, Wang G, Xu ZG, et al (2019) Lactate Is a Natural Suppressor of RLR Signaling by Targeting MAVS. Cell 178:176-189.e15
108. Stoolman JS, Chandel NS (2019) Glucose Metabolism Linked to Antiviral Responses. Cell 178:10–11
109. Buskiewicz IA, Montgomery T, Yasewicz EC, et al (2016) Reactive oxygen species induce virus-independent MAVS oligomerization in systemic lupus erythematosus. Sci Signal 9:ra115–ra115
110. Subramanian N, Natarajan K, Clatworthy MR, Wang Z, Germain RN (2013) The Adaptor MAVS Promotes NLRP3 Mitochondrial Localization and Inflammasome Activation. Cell 153:348–361
111. Mills EL, Kelly B, Logan A, et al (2016) Succinate Dehydrogenase Supports Metabolic Repurposing of Mitochondria to Drive Inflammatory Macrophages. Cell 167:457-470.e13
112. Hooftman A, Peace CG, Ryan DG, et al (2023) Macrophage fumarate hydratase restrains mtRNA-mediated interferon production. Nature 615:490–498
113. Zecchini V, Paupe V, Herranz-Montoya I, et al (2023) Fumarate induces vesicular release of mtDNA to drive innate immunity. Nature 615:499–506
114. Saraste M (1999) Oxidative Phosphorylation at the fin de siècle. Science (80-) 283:1488–1493
115. Foo J, Bellot G, Pervaiz S, Alonso S (2022) Mitochondria-mediated oxidative stress during viral infection. Trends Microbiol 30:679–692
116. Rowland AA, Voeltz GK (2012) Endoplasmic reticulum–mitochondria contacts: function of the junction. Nat Rev Mol Cell Biol 13:607–615
117. Marchi S, Patergnani S, Pinton P (2014) The endoplasmic reticulum–mitochondria connection: One touch, multiple functions. Biochim Biophys Acta - Bioenerg 1837:461–469
118. Martínez-Reyes I, Chandel NS (2020) Mitochondrial TCA cycle metabolites control physiology and disease. Nat Commun 11:102
119. Williams NC, O'Neill LAJ (2018) A Role for the Krebs Cycle Intermediate Citrate in Metabolic Reprogramming in Innate Immunity and Inflammation. Front

Immunol. https://doi.org/10.3389/fimmu.2018.00141

120. O'Neill LAJ, Artyomov MN (2019) Itaconate: the poster child of metabolic reprogramming in macrophage function. Nat Rev Immunol 19:273–281
121. Infantino V, Iacobazzi V, Menga A, Avantaggiati ML, Palmieri F (2014) A key role of the mitochondrial citrate carrier (SLC25A1) in TNFα- and IFNγ-triggered inflammation. Biochim Biophys Acta - Gene Regul Mech 1839:1217–1225
122. Tummers B, Goedemans R, Pelascini LPL, Jordanova ES, van Esch EMG, Meyers C, Melief CJM, Boer JM, van der Burg SH (2015) The interferon-related developmental regulator 1 is used by human papillomavirus to suppress NFκB activation. Nat Commun 6:6537
123. Rubic T, Lametschwandtner G, Jost S, et al (2008) Triggering the succinate receptor GPR91 on dendritic cells enhances immunity. Nat Immunol 9:1261–1269
124. Xiao Y, Chen X, Wang Z, Quan J, Zhao X, Tang H, Wu H, Di Q, Wu Z, Chen W (2022) Succinate Is a Natural Suppressor of Antiviral Immune Response by Targeting MAVS. Front Immunol. https://doi.org/10.3389/fimmu.2022.816378
125. Hooftman A, Angiari S, Hester S, et al (2020) The Immunomodulatory Metabolite Itaconate Modifies NLRP3 and Inhibits Inflammasome Activation. Cell Metab 32:468-478.e7
126. Sohail A, Iqbal AA, Sahini N, et al (2022) Itaconate and derivatives reduce interferon responses and inflammation in influenza A virus infection. PLOS Pathog 18:e1010219
127. Daniels BP, Kofman SB, Smith JR, et al (2019) The Nucleotide Sensor ZBP1 and Kinase RIPK3 Induce the Enzyme IRG1 to Promote an Antiviral Metabolic State in Neurons. Immunity 50:64-76.e4
128. Chaban Y, Boekema EJ, Dudkina N V. (2014) Structures of mitochondrial oxidative phosphorylation supercomplexes and mechanisms for their stabilisation. Biochim Biophys Acta - Bioenerg 1837:418–426
129. Murphy MP (2009) How mitochondria produce reactive oxygen species. Biochem J 417:1–13
130. Murphy MP, Bayir H, Belousov V, et al (2022) Guidelines for measuring reactive oxygen species and oxidative damage in cells and in vivo. Nat Metab 4:651–662

131. Chouchani ET, Pell VR, Gaude E, et al (2014) Ischaemic accumulation of succinate controls reperfusion injury through mitochondrial ROS. Nature 515:431–435
132. West AP, Brodsky IE, Rahner C, Woo DK, Erdjument-Bromage H, Tempst P, Walsh MC, Choi Y, Shadel GS, Ghosh S (2011) TLR signalling augments macrophage bactericidal activity through mitochondrial ROS. Nature 472:476–480
133. Tal MC, Sasai M, Lee HK, Yordy B, Shadel GS, Iwasaki A (2009) Absence of autophagy results in reactive oxygen species-dependent amplification of RLR signaling. Proc Natl Acad Sci 106:2770–2775
134. Buskiewicz IA, Montgomery T, Yasewicz EC, et al (2016) Reactive oxygen species induce virus-independent MAVS oligomerization in systemic lupus erythematosus. Sci Signal. https://doi.org/10.1126/scisignal.aaf1933
135. Gullberg RC, Jordan Steel J, Moon SL, Soltani E, Geiss BJ (2015) Oxidative stress influences positive strand RNA virus genome synthesis and capping. Virology 475:219–229
136. Trefts E, Gannon M, Wasserman DH (2017) The liver. Curr Biol 27:R1147–R1151
137. Rui L (2014) Energy metabolism in the liver. Compr Physiol. https://doi.org/10.1002/cphy.c130024
138. Ringelhan M, Pfister D, O'Connor T, Pikarsky E, Heikenwalder M (2018) The immunology of hepatocellular carcinoma. Nat Immunol 19:222–232
139. Lumsden AB, Henderson JM, Kutner MH (1988) Endotoxin levels measured by a chromogenic assay in portal, hepatic and peripheral venous blood in patients with cirrhosis. Hepatology 8:232–236
140. Uhrig A, Banafsche R, Kremer M, Hegenbarth S, Hamann A, Neurath M, Gerken G, Limmer A, Knolle PA (2005) Development and functional consequences of LPS tolerance in sinusoidal endothelial cells of the liver. J Leukoc Biol 77:626–633
141. Crispe IN (2009) The Liver as a Lymphoid Organ. Annu Rev Immunol 27:147–163
142. Crispe IN (2014) Immune tolerance in liver disease. Hepatology 60:2109–2117
143. Robinson MW, Harmon C, O'Farrelly C (2016) Liver immunology and its role in inflammation and homeostasis. Cell Mol Immunol 13:267–276
144. Jameson G, Harmon C, Santiago RM, Houlihan DD, Gallagher TK, Lynch L,

Robinson MW, O'Farrelly C (2022) Human Hepatic CD56bright NK Cells Display a Tissue-Resident Transcriptional Profile and Enhanced Ability to Kill Allogenic CD8+ T Cells. Front Immunol. https://doi.org/10.3389/fimmu.2022.921212

145. Bertolino P, Trescol-Biémont M-C, Rabourdin-Combe C (1998) Hepatocytes induce functional activation of naive CD8+ T lymphocytes but fail to promote survival. Eur J Immunol 28:221–236
146. Thomson AW, Knolle PA (2010) Antigen-presenting cell function in the tolerogenic liver environment. Nat Rev Immunol 10:753–766
147. Horst AK, Neumann K, Diehl L, Tiegs G (2016) Modulation of liver tolerance by conventional and nonconventional antigen-presenting cells and regulatory immune cells. Cell Mol Immunol 13:277–292
148. Zhou Z, Xu MJ, Gao B (2016) Hepatocytes: A key cell type for innate immunity. Cell Mol Immunol 13:301–315
149. Gruys E, Toussaint MJM, Niewold TA, Koopmans SJ (2005) Acute phase reaction and acute phase proteins. J Zhejiang Univ B 6:1045–1056
150. Gauldie J, Richards C, Harnish D, Lansdorp P, Baumann H (1987) Interferon beta 2/B-cell stimulatory factor type 2 shares identity with monocyte-derived hepatocyte-stimulating factor and regulates the major acute phase protein response in liver cells. Proc Natl Acad Sci 84:7251–7255
151. Gabay C, Kushner I (1999) Acute-Phase Proteins and Other Systemic Responses to Inflammation. N Engl J Med 340:448–454
152. Krausgruber T, Fortelny N, Fife-Gernedl V, et al (2020) Structural cells are key regulators of organ-specific immune responses. Nature 583:296–302
153. Dustin LB, Bartolini B, Capobianchi MR, Pistello M (2016) Hepatitis C virus: life cycle in cells, infection and host response, and analysis of molecular markers influencing the outcome of infection and response to therapy. Clin Microbiol Infect 22:826–832
154. Sugrue JA, Bourke NM, O'Farrelly C (2021) Type I Interferon and the Spectrum of Susceptibility to Viral Infection and Autoimmune Disease: A Shared Genomic Signature . Front. Immunol. 12:
155. Zhang L, Xiang W, Wang G, et al (2016) Interferon β (IFN-β) Production during the Double-stranded RNA (dsRNA) Response in Hepatocytes Involves

Coordinated and Feedforward Signaling through Toll-like Receptor 3 (TLR3), RNA-dependent Protein Kinase (PKR), Inducible Nitric Oxide Synthase (iNOS),. J Biol Chem 291:15093–15107

156. Li K, Li NL, Wei D, Pfeffer SR, Fan M, Pfeffer LM (2012) Activation of chemokine and inflammatory cytokine response in hepatitis C virus-infected hepatocytes depends on toll-like receptor 3 sensing of hepatitis C virus double-stranded RNA intermediates. Hepatology 55:666–675
157. Li K, Chen Z, Kato N, Gale M, Lemon SM (2005) Distinct Poly(I-C) and Virus-activated Signaling Pathways Leading to Interferon-β Production in Hepatocytes. J Biol Chem 280:16739–16747
158. Wang N, Liang Y, Devaraj S, Wang J, Lemon SM, Li K (2009) Toll-Like Receptor 3 Mediates Establishment of an Antiviral State against Hepatitis C Virus in Hepatoma Cells. J Virol. https://doi.org/10.1128/jvi.01125-09
159. Lee J, Wu CCN, Lee KJ, et al (2006) Activation of anti-hepatitis C virus responses via Toll-like receptor 7. Proc Natl Acad Sci 103:1828–1833
160. Beauclair G, Streicher F, Chazal M, et al (2020) Retinoic Acid Inducible Gene I and Protein Kinase R, but Not Stress Granules, Mediate the Proinflammatory Response to Yellow Fever Virus. J Virol. https://doi.org/10.1128/JVI.00403-20
161. Brisse M, Ly H (2019) Comparative Structure and Function Analysis of the RIG-I-Like Receptors: RIG-I and MDA5. Front Immunol. https://doi.org/10.3389/fimmu.2019.01586
162. Sato S, Li K, Kameyama T, et al (2015) The RNA Sensor RIG-I Dually Functions as an Innate Sensor and Direct Antiviral Factor for Hepatitis B Virus. Immunity 42:123–132
163. Saito T, Owen DM, Jiang F, Marcotrigiano J, Gale M (2008) Innate immunity induced by composition-dependent RIG-I recognition of hepatitis C virus RNA. Nature 454:523–527
164. Cao X, Ding Q, Lu J, Tao W, Huang B, Zhao Y, Niu J, Liu Y-J, Zhong J (2015) MDA5 plays a critical role in interferon response during hepatitis C virus infection. J Hepatol 62:771–778
165. Liang Y, Cao X, Ding Q, Zhao Y, He Z, Zhong J (2018) Hepatitis C virus NS4B induces the degradation of TRIF to inhibit TLR3-mediated interferon signaling

pathway. PLOS Pathog 14:e1007075

166. Li X-D, Sun L, Seth RB, Pineda G, Chen ZJ (2005) Hepatitis C virus protease NS3/4A cleaves mitochondrial antiviral signaling protein off the mitochondria to evade innate immunity. Proc Natl Acad Sci 102:17717–17722

167. Zhao H-J, Hu Y-F, Han Q-J, Zhang J (2022) Innate and adaptive immune escape mechanisms of hepatitis B virus. World J Gastroenterol 28:881–896

168. Yu S, Chen J, Wu M, Chen H, Kato N, Yuan Z (2010) Hepatitis B virus polymerase inhibits RIG-I- and Toll-like receptor 3-mediated beta interferon induction in human hepatocytes through interference with interferon regulatory factor 3 activation and dampening of the interaction between TBK1/IKKε and DDX3. J Gen Virol 91:2080–2090

169. Fischer L, Lucendo-villarin B, Hay DC, O'farrelly C (2020) Human PSC-derived hepatocytes express low levels of viral pathogen recognition receptors, but are capable of mounting an effective innate immune response. Int J Mol Sci. https://doi.org/10.3390/ijms21113831

170. Lee J, Tian Y, Chan ST, Kim JY, Cho C, Ou JJ (2015) TNF-α Induced by Hepatitis C Virus via TLR7 and TLR8 in Hepatocytes Supports Interferon Signaling via an Autocrine Mechanism. PLOS Pathog 11:e1004937

171. Pflugheber J, Fredericksen B, Sumpter R, Wang C, Ware F, Sodora DL, Gale M (2002) Regulation of PKR and IRF-1 during hepatitis C virus RNA replication. Proc Natl Acad Sci 99:4650–4655

172. Bhattacharya A, Hegazy AN, Deigendesch N, et al (2015) Superoxide Dismutase 1 Protects Hepatocytes from Type I Interferon-Driven Oxidative Damage. Immunity 43:974–986

173. Lercher A, Bhattacharya A, Popa AM, et al (2019) Type I Interferon Signaling Disrupts the Hepatic Urea Cycle and Alters Systemic Metabolism to Suppress T Cell Function. Immunity. https://doi.org/10.1016/j.immuni.2019.10.014

174. Lercher A, Popa AM, Viczenczova C, Kosack L, Klavins K, Agerer B, Opitz CA, Lanz T V., Platten M, Bergthaler A (2020) Hepatocyte-intrinsic type I interferon signaling reprograms metabolism and reveals a novel compensatory mechanism of the tryptophan-kynurenine pathway in viral hepatitis. PLOS Pathog 16:e1008973

175. Zhou L, He R, Fang P, et al (2021) Hepatitis B virus rigs the cellular metabolome to avoid innate immune recognition. Nat Commun 12:98
176. Nordlie RC, Foster JD, Lange AJ (1999) REGULATION OF GLUCOSE PRODUCTION BY THE LIVER. Annu Rev Nutr 19:379–406
177. Petersen MC, Vatner DF, Shulman GI (2017) Regulation of hepatic glucose metabolism in health and disease. Nat Rev Endocrinol 13:572–587
178. Moore MC, Coate KC, Winnick JJ, An Z, Cherrington AD (2012) Regulation of Hepatic Glucose Uptake and Storage In Vivo. Adv Nutr 3:286–294
179. Karim S (2012) Hepatic expression and cellular distribution of the glucose transporter family. World J Gastroenterol 18:6771
180. Zhou L, He R, Fang P, et al (2021) Hepatitis B virus rigs the cellular metabolome to avoid innate immune recognition. Nat Commun 12:1–13
181. Wu Y-H, Yang Y, Chen C-H, Hsiao C-J, Li T-N, Liao K-J, Watashi K, Chen B-S, Wang LH-C (2021) Aerobic glycolysis supports hepatitis B virus protein synthesis through interaction between viral surface antigen and pyruvate kinase isoform M2. PLOS Pathog 17:e1008866
182. Liu B, Fang M, He Z, Cui D, Jia S, Lin X, Xu X, Zhou T, Liu W (2015) Hepatitis B virus stimulates G6PD expression through HBx-mediated Nrf2 activation. Cell Death Dis 6:e1980–e1980
183. Allonso D, Andrade IS, Conde JN, Coelho DR, Rocha DCP, da Silva ML, Ventura GT, Silva EM, Mohana-Borges R (2015) Dengue Virus NS1 Protein Modulates Cellular Energy Metabolism by Increasing Glyceraldehyde-3-Phosphate Dehydrogenase Activity. J Virol 89:11871–11883
184. Ramière C, Rodriguez J, Enache LS, Lotteau V, André P, Diaz O (2014) Activity of Hexokinase Is Increased by Its Interaction with Hepatitis C Virus Protein NS5A. J Virol 88:3246–3254
185. Freshney RI (2011) Culture of Animal Cells: A Manual of Basic Technique and Specialized Applications, 6th ed. https://doi.org/10.1002/9780470649367
186. Cameron K, Tan R, Schmidt-Heck W, et al (2015) Recombinant Laminins Drive the Differentiation and Self-Organization of hESC-Derived Hepatocytes. Stem Cell Reports 5:1250–1262
187. Moffat J, Grueneberg DA, Yang X, et al (2006) A Lentiviral RNAi Library for

Human and Mouse Genes Applied to an Arrayed Viral High-Content Screen. Cell 124:1283–1298

188. Li K, Foy E, Ferreon JC, Nakamura M, Ferreon ACM, Ikeda M, Ray SC, Gale M, Lemon SM (2005) Immune evasion by hepatitis C virus NS3/4A protease-mediated cleavage of the Toll-like receptor 3 adaptor protein TRIF. Proc Natl Acad Sci 102:2992–2997
189. Gale MJ, Korth MJ, Tang NM, Tan S-L, Hopkins DA, Dever TE, Polyak SJ, Gretch DR, Katze MG (1997) Evidence That Hepatitis C Virus Resistance to Interferon Is Mediated through Repression of the PKR Protein Kinase by the Nonstructural 5A Protein. Virology 230:217–227
190. Arzumanian VA, Kiseleva OI, Poverennaya E V. (2021) The Curious Case of the HepG2 Cell Line: 40 Years of Expertise. Int J Mol Sci 22:13135
191. López-Terrada D, Cheung SW, Finegold MJ, Knowles BB (2009) Hep G2 is a hepatoblastoma-derived cell line. Hum Pathol 40:1512–1515
192. Nakabayashi H, Taketa K, Miyano K, Yamane T, Sato J (1982) Growth of human hepatoma cells lines with differentiated functions in chemically defined medium. Cancer Res 42:3858–63
193. Sumpter R, Loo Y-M, Foy E, Li K, Yoneyama M, Fujita T, Lemon SM, Gale M (2005) Regulating Intracellular Antiviral Defense and Permissiveness to Hepatitis C Virus RNA Replication through a Cellular RNA Helicase, RIG-I. J Virol 79:2689–2699
194. Lohmann V, Körner F, Koch J-O, Herian U, Theilmann L, Bartenschlager R (1999) Replication of Subgenomic Hepatitis C Virus RNAs in a Hepatoma Cell Line. Science (80-) 285:110–113
195. Blight KJ, McKeating JA, Rice CM (2002) Highly Permissive Cell Lines for Subgenomic and Genomic Hepatitis C Virus RNA Replication. J Virol 76:13001–13014
196. Zhong J, Gastaminza P, Cheng G, Kapadia S, Kato T, Burton DR, Wieland SF, Uprichard SL, Wakita T, Chisari F V. (2005) Robust hepatitis C virus infection in vitro. Proc Natl Acad Sci 102:9294–9299
197. Huang Q, Tan Y, Yin P, Ye G, Gao P, Lu X, Wang H, Xu G (2013) Metabolic Characterization of Hepatocellular Carcinoma Using Nontargeted Tissue

Metabolomics. Cancer Res 73:4992–5002

198. Meseguer-Ripolles J, Lucendo-Villarin B, Tucker C, et al (2021) Dimethyl fumarate reduces hepatocyte senescence following paracetamol exposure. iScience 24:102552

199. Sinton MC, Meseguer-Ripolles J, Lucendo-Villarin B, et al (2021) A human pluripotent stem cell model for the analysis of metabolic dysfunction in hepatic steatosis. iScience 24:101931

200. Schwartz RE, Trehan K, Andrus L, Sheahan TP, Ploss A, Duncan SA, Rice CM, Bhatia SN (2012) Modeling hepatitis C virus infection using human induced pluripotent stem cells. Proc Natl Acad Sci 109:2544–2548

201. Carpentier A, Sheldon J, Vondran FWR, Brown RJP, Pietschmann T (2020) Efficient acute and chronic infection of stem cell-derived hepatocytes by hepatitis C virus. Gut. https://doi.org/10.1136/gutjnl-2019-319354

202. Liu G, Park H-S, Pyo H-M, Liu Q, Zhou Y (2015) Influenza A Virus Panhandle Structure Is Directly Involved in RIG-I Activation and Interferon Induction. J Virol 89:6067–6079

203. García MA, Gil J, Ventoso I, Guerra S, Domingo E, Rivas C, Esteban M (2006) Impact of Protein Kinase PKR in Cell Biology: from Antiviral to Antiproliferative Action. Microbiol Mol Biol Rev 70:1032–1060

204. Zamanian-Daryoush M, Mogensen TH, DiDonato JA, Williams BRG (2000) NF-κB Activation by Double-Stranded-RNA-Activated Protein Kinase (PKR) Is Mediated through NF-κB-Inducing Kinase and IκB Kinase. Mol Cell Biol 20:1278–1290

205. Farabaugh KT, Majumder M, Guan B-J, et al (2017) Protein Kinase R Mediates the Inflammatory Response Induced by Hyperosmotic Stress. Mol Cell Biol. https://doi.org/10.1128/MCB.00521-16

206. Ingrand S, Barrier L, Lafay-Chebassier C, Fauconneau B, Page G, Hugon J (2007) The oxindole/imidazole derivative C16 reduces in vivo brain PKR activation. FEBS Lett 581:4473–4478

207. Page G, Rioux Bilan A, Ingrand S, Lafay-Chebassier C, Pain S, Perault Pochat MC, Bouras C, Bayer T, Hugon J (2006) Activated double-stranded RNA-dependent protein kinase and neuronal death in models of Alzheimer's disease. Neuroscience 139:1343–1354

208. Lo Y-C, Liu T, Morrissey KM, Kakiuchi-Kiyota S, Johnson AR, Broccatelli F, Zhong Y, Joshi A, Altman RB (2019) Computational analysis of kinase inhibitor selectivity using structural knowledge. Bioinformatics 35:235–242
209. Gale M, Blakely CM, Kwieciszewski B, Tan S-L, Dossett M, Tang NM, Korth MJ, Polyak SJ, Gretch DR, Katze MG (1998) Control of PKR Protein Kinase by Hepatitis C Virus Nonstructural 5A Protein: Molecular Mechanisms of Kinase Regulation. Mol Cell Biol 18:5208–5218
210. Heim MH, Thimme R (2014) Innate and adaptive immune responses in HCV infections. J Hepatol 61:S14–S25
211. Lonardo A, Adinolfi LE, Loria P, Carulli N, Ruggiero G, Day CP (2004) Steatosis and hepatitis C virus: Mechanisms and significance for hepatic and extrahepatic disease. Gastroenterology 126:586–597
212. Diamond DL, Krasnoselsky AL, Burnum KE, et al (2012) Proteome and computational analyses reveal new insights into the mechanisms of hepatitis C virus-mediated liver disease posttransplantation. Hepatology 56:28–38
213. Levent G, Ali A, Ahmet A, Polat EC, Aytaç Ç, Ayşe E, Ahmet S (2006) Oxidative stress and antioxidant defense in patients with chronic hepatitis C patients before and after pegylated interferon alfa-2b plus ribavirin therapy. J Transl Med 4:25
214. Youle RJ, van der Bliek AM (2012) Mitochondrial Fission, Fusion, and Stress. Science (80-) 337:1062–1065
215. Rossignol R, Gilkerson R, Aggeler R, Yamagata K, Remington SJ, Capaldi RA (2004) Energy Substrate Modulates Mitochondrial Structure and Oxidative Capacity in Cancer Cells. Cancer Res 64:985–993
216. Aman Y, Schmauck-Medina T, Hansen M, et al (2021) Autophagy in healthy aging and disease. Nat Aging 1:634–650
217. Twig G, Elorza A, Molina AJA, et al (2008) Fission and selective fusion govern mitochondrial segregation and elimination by autophagy. EMBO J 27:433–446
218. Westermann B (2010) Mitochondrial fusion and fission in cell life and death. Nat Rev Mol Cell Biol 11:872–884
219. Kim I, Lemasters JJ (2011) Mitophagy Selectively Degrades Individual Damaged Mitochondria After Photoirradiation. Antioxid Redox Signal 14:1919–1928

220. Kitada T, Asakawa S, Hattori N, Matsumine H, Yamamura Y, Minoshima S, Yokochi M, Mizuno Y, Shimizu N (1998) Mutations in the parkin gene cause autosomal recessive juvenile parkinsonism. Nature 392:605–608
221. Valente EM, Abou-Sleiman PM, Caputo V, et al (2004) Hereditary Early-Onset Parkinson's Disease Caused by Mutations in PINK1. Science (80-) 304:1158–1160
222. Kim S-J, Ahn D-G, Syed GH, Siddiqui A (2018) The essential role of mitochondrial dynamics in antiviral immunity. Mitochondrion 41:21–27
223. Castanier C, Garcin D, Vazquez A, Arnoult D (2010) Mitochondrial dynamics regulate the RIG-I-like receptor antiviral pathway. EMBO Rep 11:133–138
224. Yasukawa K, Oshiumi H, Takeda M, Ishihara N, Yanagi Y, Seya T, Kawabata S, Koshiba T (2009) Mitofusin 2 Inhibits Mitochondrial Antiviral Signaling. Sci Signal. https://doi.org/10.1126/scisignal.2000287
225. Sun X, Sun L, Zhao Y, Li Y, Lin W, Chen D, Sun Q (2016) MAVS maintains mitochondrial homeostasis via autophagy. Cell Discov 2:16024
226. Sies H, Belousov V V., Chandel NS, Davies MJ, Jones DP, Mann GE, Murphy MP, Yamamoto M, Winterbourn C (2022) Defining roles of specific reactive oxygen species (ROS) in cell biology and physiology. Nat Rev Mol Cell Biol 23:499–515
227. Birben E, Sahiner UM, Sackesen C, Erzurum S, Kalayci O (2012) Oxidative Stress and Antioxidant Defense. World Allergy Organ J 5:9–19
228. Sies H, Jones DP (2020) Reactive oxygen species (ROS) as pleiotropic physiological signalling agents. Nat Rev Mol Cell Biol 21:363–383
229. Pollard MG, Travers KJ, Weissman JS (1998) Ero1p: A Novel and Ubiquitous Protein with an Essential Role in Oxidative Protein Folding in the Endoplasmic Reticulum. Mol Cell 1:171–182
230. Veith A, Moorthy B (2018) Role of cytochrome P450s in the generation and metabolism of reactive oxygen species. Curr Opin Toxicol 7:44–51
231. Okamoto K, Matsumoto K, Hille R, Eger BT, Pai EF, Nishino T (2004) The crystal structure of xanthine oxidoreductase during catalysis: Implications for reaction mechanism and enzyme inhibition. Proc Natl Acad Sci 101:7931–7936
232. Forstermann U, Sessa WC (2012) Nitric oxide synthases: regulation and function. Eur Heart J 33:829–837

233. Chance B, Sies H, Boveris A (1979) Hydroperoxide metabolism in mammalian organs. Physiol Rev 59:527–605
234. Paulsen CE, Carroll KS (2013) Cysteine-Mediated Redox Signaling: Chemistry, Biology, and Tools for Discovery. Chem Rev 113:4633–4679
235. Sies H, Berndt C, Jones DP (2017) Oxidative Stress. Annu Rev Biochem 86:715–748
236. Friedman SL, Neuschwander-Tetri BA, Rinella M, Sanyal AJ (2018) Mechanisms of NAFLD development and therapeutic strategies. Nat Med 24:908–922
237. Forman HJ, Zhang H (2021) Targeting oxidative stress in disease: promise and limitations of antioxidant therapy. Nat Rev Drug Discov 20:689–709
238. Sharifi-Rad M, Anil Kumar N V., Zucca P, et al (2020) Lifestyle, Oxidative Stress, and Antioxidants: Back and Forth in the Pathophysiology of Chronic Diseases. Front Physiol. https://doi.org/10.3389/fphys.2020.00694
239. van Dam L, Pagès-Gallego M, Polderman PE, van Es RM, Burgering BMT, Vos HR, Dansen TB (2021) The Human 2-Cys Peroxiredoxins form Widespread, Cysteine-Dependent- and Isoform-Specific Protein-Protein Interactions. Antioxidants 10:627
240. Rhee SG, Woo HA, Kil IS, Bae SH (2012) Peroxiredoxin Functions as a Peroxidase and a Regulator and Sensor of Local Peroxides. J Biol Chem 287:4403–4410
241. Fisher AB (2011) Peroxiredoxin 6: A Bifunctional Enzyme with Glutathione Peroxidase and Phospholipase A 2 Activities. Antioxid Redox Signal 15:831–844
242. (2016) Overview on Peroxiredoxin. Mol Cells 39:1–5
243. Sobotta MC, Liou W, Stöcker S, Talwar D, Oehler M, Ruppert T, Scharf AND, Dick TP (2015) Peroxiredoxin-2 and STAT3 form a redox relay for H2O2 signaling. Nat Chem Biol 11:64–70
244. Jarvis RM, Hughes SM, Ledgerwood EC (2012) Peroxiredoxin 1 functions as a signal peroxidase to receive, transduce, and transmit peroxide signals in mammalian cells. Free Radic Biol Med 53:1522–1530
245. Park MH, Jo M, Kim YR, Lee C-K, Hong JT (2016) Roles of peroxiredoxins in cancer, neurodegenerative diseases and inflammatory diseases. Pharmacol Ther 163:1–23
246. Deng L, Gan X, Ito M, et al (2019) Peroxiredoxin 1, a Novel HBx-Interacting

Protein, Interacts with Exosome Component 5 and Negatively Regulates Hepatitis B Virus (HBV) Propagation through Degradation of HBV RNA. J Virol. https://doi.org/10.1128/JVI.02203-18

247. Schwarz KB (1996) Oxidative stress during viral infection: A review. Free Radic Biol Med 21:641–649
248. Karpenko IL, Valuev-Elliston VT, Ivanova ON, Smirnova OA, Ivanov A V. (2021) Peroxiredoxins—The Underrated Actors during Virus-Induced Oxidative Stress. Antioxidants 10:977
249. Watanabe A, Yoneda M, Ikeda F, Sugai A, Sato H, Kai C (2011) Peroxiredoxin 1 Is Required for Efficient Transcription and Replication of Measles Virus. J Virol 85:2247–2253
250. Liu C, Zhang A, Guo J, Yang J, Zhou H, Chen H, Jin M (2012) Identification of Human Host Proteins Contributing to H5N1 Influenza Virus Propagation by Membrane Proteomics. J Proteome Res 11:5396–5405
251. Dai X, Li N, Roller RJ (2018) Peroxiredoxin 1 protein interacts with influenza virus ribonucleoproteins and is required for efficient virus replication. Vaccine 36:4540–4547
252. Jamaluddin M, Wiktorowicz JE, Soman K V., Boldogh I, Forbus JD, Spratt H, Garofalo RP, Brasier AR (2010) Role of Peroxiredoxin 1 and Peroxiredoxin 4 in Protection of Respiratory Syncytial Virus-Induced Cysteinyl Oxidation of Nuclear Cytoskeletal Proteins. J Virol 84:9533–9545
253. Jin D-Y, Chae HZ, Rhee SG, Jeang K-T (1997) Regulatory Role for a Novel Human Thioredoxin Peroxidase in NF-κB Activation. J Biol Chem 272:30952–30961
254. Lipinski S, Pfeuffer S, Arnold P, et al (2019) Prdx4 limits caspase-1 activation and restricts inflammasome-mediated signaling by extracellular vesicles. EMBO J. https://doi.org/10.15252/embj.2018101266
255. Nabeshima A, Yamada S, Guo X, et al (2013) Peroxiredoxin 4 Protects Against Nonalcoholic Steatohepatitis and Type 2 Diabetes in a Nongenetic Mouse Model. Antioxid Redox Signal 19:1983–1998
256. Forman HJ, Maiorino M, Ursini F (2010) Signaling Functions of Reactive Oxygen Species. Biochemistry 49:835–842
257. R. Buettner G (2011) Superoxide Dismutase in Redox Biology: The Roles of

Superoxide and Hydrogen Peroxide. Anticancer Agents Med Chem 11:341–346

258. Dalle-Donne I, Rossi R, Colombo G, Giustarini D, Milzani A (2009) Protein S-glutathionylation: a regulatory device from bacteria to humans. Trends Biochem Sci 34:85–96

259. Matsui R, Ferran B, Oh A, Croteau D, Shao D, Han J, Pimentel DR, Bachschmid MM (2020) Redox Regulation via Glutaredoxin-1 and Protein S - Glutathionylation. Antioxid Redox Signal 32:677–700

260. Talwar D, Miller CG, Grossmann J, et al (2023) The GAPDH redox switch safeguards reductive capacity and enables survival of stressed tumour cells. Nat Metab. https://doi.org/10.1038/s42255-023-00781-3

261. Anastasiou D, Poulogiannis G, Asara JM, et al (2011) Inhibition of Pyruvate Kinase M2 by Reactive Oxygen Species Contributes to Cellular Antioxidant Responses. Science (80-) 334:1278–1283

262. Nathan C, Cunningham-Bussel A (2013) Beyond oxidative stress: an immunologist's guide to reactive oxygen species. Nat Rev Immunol 13:349–361

263. Carballal S, Alvarez B, Turell L, Botti H, Freeman BA, Radi R (2007) Sulfenic acid in human serum albumin. Amino Acids 32:543–551

264. Wu G, Lupton JR, Turner ND, Fang Y-Z, Yang S (2004) Glutathione Metabolism and Its Implications for Health. J Nutr 134:489–492

265. Beer SM, Taylor ER, Brown SE, Dahm CC, Costa NJ, Runswick MJ, Murphy MP (2004) Glutaredoxin 2 Catalyzes the Reversible Oxidation and Glutathionylation of Mitochondrial Membrane Thiol Proteins. J Biol Chem 279:47939–47951

266. Mailloux RJ (2020) Protein S-glutathionylation reactions as a global inhibitor of cell metabolism for the desensitization of hydrogen peroxide signals. Redox Biol 32:101472

267. Lermant, Murdoch (2019) Cysteine Glutathionylation Acts as a Redox Switch in Endothelial Cells. Antioxidants 8:315

268. Xiong Y, Uys JD, Tew KD, Townsend DM (2011) S-Glutathionylation: From Molecular Mechanisms to Health Outcomes. Antioxid Redox Signal 15:233–270

269. Hughes MM, Hooftman A, Angiari S, et al (2019) Glutathione Transferase Omega-1 Regulates NLRP3 Inflammasome Activation through NEK7 Deglutathionylation. Cell Rep 29:151-161.e5

270. Mustafa Rizvi SH, Shao D, Tsukahara Y, Pimentel DR, Weisbrod RM, Hamburg NM, McComb ME, Matsui R, Bachschmid MM (2021) Oxidized GAPDH transfers S-glutathionylation to a nuclear protein Sirtuin-1 leading to apoptosis. Free Radic Biol Med 174:73–83
271. Shao D, Han J, Hou X, et al (2017) Glutaredoxin-1 Deficiency Causes Fatty Liver and Dyslipidemia by Inhibiting Sirtuin-1. Antioxid Redox Signal 27:313–327
272. Morris G, Gevezova M, Sarafian V, Maes M (2022) Redox regulation of the immune response. Cell Mol Immunol 19:1079–1101
273. Zhou R, Yazdi AS, Menu P, Tschopp J (2011) A role for mitochondria in NLRP3 inflammasome activation. Nature 469:221–225
274. Gonzalez-Dosal R, Horan KA, Rahbek SH, Ichijo H, Chen ZJ, Mieyal JJ, Hartmann R, Paludan SR (2011) HSV Infection Induces Production of ROS, which Potentiate Signaling from Pattern Recognition Receptors: Role for S-glutathionylation of TRAF3 and 6. PLoS Pathog 7:e1002250
275. Subramanian A, Tamayo P, Mootha VK, et al (2005) Gene set enrichment analysis: A knowledge-based approach for interpreting genome-wide expression profiles. Proc Natl Acad Sci 102:15545–15550
276. Liberzon A, Subramanian A, Pinchback R, Thorvaldsdóttir H, Tamayo P, Mesirov JP (2011) Molecular signatures database (MSigDB) 3.0. Bioinformatics 27:1739–1740
277. Liberzon A, Birger C, Thorvaldsdóttir H, Ghandi M, Mesirov JP, Tamayo P (2015) The Molecular Signatures Database Hallmark Gene Set Collection. Cell Syst 1:417–425
278. Huang S, Li Z, Wu Z, Liu C, Yu M, Wen M, Zhang L, Wang X (2021) DDAH2 suppresses RLR-MAVS–mediated innate antiviral immunity by stimulating nitric oxide–activated, Drp1-induced mitochondrial fission. Sci Signal. https://doi.org/10.1126/scisignal.abc7931
279. Sularea VM, Sugrue JA, O'Farrelly C (2023) Innate antiviral immunity and immunometabolism in hepatocytes. Curr Opin Immunol 80:102267
280. Nasirudeen AMA, Wong HH, Thien P, Xu S, Lam K-P, Liu DX (2011) RIG-I, MDA5 and TLR3 Synergistically Play an Important Role in Restriction of Dengue Virus Infection. PLoS Negl Trop Dis 5:e926

281. Pålsson-McDermott EM, O'Neill LAJ (2020) Targeting immunometabolism as an anti-inflammatory strategy. Cell Res 30:300–314
282. Horner SM, Gale M (2013) Regulation of hepatic innate immunity by hepatitis C virus. Nat Med 19:879–888
283. Koshiba T, Yasukawa K, Yanagi Y, Kawabata S (2011) Mitochondrial Membrane Potential Is Required for MAVS-Mediated Antiviral Signaling. Sci Signal. https://doi.org/10.1126/scisignal.2001147
284. De Maria N, Colantonl A, Fagiuoli S, Liu G-J, Rogers BK, Farinati F, Van Thiel DH, Floyd RA (1996) Association between reactive oxygen species and disease activity in chronic hepatitis C. Free Radic Biol Med 21:291–295
285. Valgimigli M, Valgimigli L, Trerè D, Gaiani S, Pedulli GF, Gramantieri L, Bolondi L (2002) Oxidative Stress EPR Measurement in Human Liver by Radical-probe Technique. Correlation with Etiology, Histology and Cell Proliferation. Free Radic Res 36:939–948
286. Ivanov A, Bartosch B, Smirnova O, Isaguliants M, Kochetkov S (2013) HCV and Oxidative Stress in the Liver. Viruses 5:439–469
287. Elko EA, Manuel AM, White S, Zito E, van der Vliet A, Anathy V, Janssen-Heininger YMW (2021) Oxidation of peroxiredoxin-4 induces oligomerization and promotes interaction with proteins governing protein folding and endoplasmic reticulum stress. J Biol Chem 296:100665
288. Bassot A, Chen J, Takahashi-Yamashiro K, et al (2023) The endoplasmic reticulum kinase PERK interacts with the oxidoreductase ERO1 to metabolically adapt mitochondria. Cell Rep 42:111899
289. Rao Z, Wang S, Wang J (2017) Peroxiredoxin 4 inhibits IL-1β-induced chondrocyte apoptosis via PI3K/AKT signaling. Biomed Pharmacother 90:414–420
290. Jones JT, Qian X, van der Velden JLJ, et al (2016) Glutathione S-transferase pi modulates NF-κB activation and pro-inflammatory responses in lung epithelial cells. Redox Biol 8:375–382
291. Reynaert NL, van der Vliet A, Guala AS, et al (2006) Dynamic redox control of NF-κB through glutaredoxin-regulated S-glutathionylation of inhibitory κB kinase β. Proc Natl Acad Sci 103:13086–13091

292. Zhao Y, Chen Y, Hu Y, Wang J, Xie X, He G, Chen H, Shao Q, Zeng H, Zhang H (2018) Genomic alterations across six hepatocellular carcinoma cell lines by panel-based sequencing. Transl Cancer Res 7:231–239
293. Guo L, Dial S, Shi L, Branham W, Liu J, Fang J-L, Green B, Deng H, Kaput J, Ning B (2011) Similarities and Differences in the Expression of Drug-Metabolizing Enzymes between Human Hepatic Cell Lines and Primary Human Hepatocytes. Drug Metab Dispos 39:528–538
294. Huggett ZJ, Smith A, De Vivo N, Gomez D, Jethwa P, Brameld JM, Bennett A, Salter AM (2022) A Comparison of Primary Human Hepatocytes and Hepatoma Cell Lines to Model the Effects of Fatty Acids, Fructose and Glucose on Liver Cell Lipid Accumulation. Nutrients 15:40
295. Nakamura T, Furuhashi M, Li P, Cao H, Tuncman G, Sonenberg N, Gorgun CZ, Hotamisligil GS (2010) Double-Stranded RNA-Dependent Protein Kinase Links Pathogen Sensing with Stress and Metabolic Homeostasis. Cell 140:338–348
296. Rao H, Wei L, Li H, et al (2015) Prevalence of abnormal glycometabolism in treatment-naive patients with hepatitis C virus infection in a Chinese Han population. J Gastroenterol Hepatol 30:1049–1056
297. Kwon SY, Kim SS, Kwon OS, et al (2005) Prognostic significance of glycaemic control in patients with HBV and HCV-related cirrhosis and diabetes mellitus. Diabet Med 22:1530–1535
298. Antonelli A (2014) Hepatitis C virus infection and type 1 and type 2 diabetes mellitus. World J Diabetes 5:586
299. Ambachew S, Eshetie S, Geremew D, Endalamaw A, Melku M (2019) Prevalence of type 2 diabetes mellitus among hepatitis C virus-infected patients: a protocol for systematic review and meta-analysis. Syst Rev 8:60
300. Delhem N, Sabile A, Gajardo R, Podevin P, Abadie A, Blaton MA, Kremsdorf D, Beretta L, Brechot C (2001) Activation of the interferon-inducible protein kinase PKR by Hepatocellular carcinoma derived-Hepatitis C virus core protein. Oncogene 20:5836–5845
301. Wu X, Robotham JM, Lee E, Dalton S, Kneteman NM, Gilbert DM, Tang H (2012) Productive Hepatitis C Virus Infection of Stem Cell-Derived Hepatocytes Reveals a Critical Transition to Viral Permissiveness during Differentiation. PLoS Pathog

8:e1002617

302. Jia W, Chen P, Cheng Y (2019) PRDX4 and Its Roles in Various Cancers. Technol Cancer Res Treat 18:153303381986431

303. Jain P, Dvorkin-Gheva A, Mollen E, et al (2021) NOX4 links metabolic regulation in pancreatic cancer to endoplasmic reticulum redox vulnerability and dependence on PRDX4. Sci Adv. https://doi.org/10.1126/sciadv.abf7114

304. Malbeteau L, Jain P, Harding S, Wouters B, Koritzinsky M (2022) Abstract 124: PRDX4 links ER-specific redox vulnerability to innate immunity in pancreatic cancer. Cancer Res 82:124–124

305. West AP, Khoury-Hanold W, Staron M, et al (2015) Mitochondrial DNA stress primes the antiviral innate immune response. Nature 520:553–557

306. Moriyama M, Koshiba T, Ichinohe T (2019) Influenza A virus M2 protein triggers mitochondrial DNA-mediated antiviral immune responses. Nat Commun 10:4624

307. Jahun AS, Sorgeloos F, Chaudhry Y, Arthur SE, Hosmillo M, Georgana I, Izuagbe R, Goodfellow IG (2023) Leaked genomic and mitochondrial DNA contribute to the host response to noroviruses in a STING-dependent manner. Cell Rep 42:112179

308. Dunphy G, Flannery SM, Almine JF, Connolly DJ, Paulus C, Jønsson KL, Jakobsen MR, Nevels MM, Bowie AG, Unterholzner L (2018) Non-canonical Activation of the DNA Sensing Adaptor STING by ATM and IFI16 Mediates NF-κB Signaling after Nuclear DNA Damage. Mol Cell 71:745-760.e5